Targeting the tumour extracellular environment through rational modification of the SNX class of HSP90 inhibitors

A thesis submitted in fulfilment of the academic requirements for the
Degree of Doctor of Philosophy

School of Chemistry and Physics
College of Agriculture, Engineering and Science (Pietermaritzburg)

Gciniwe Sindiswa Mathenjwa

Supervisor: **Prof. Matthew P. Akerman**
Co-supervisor: **Prof. Clinton G. L. Veale (UCT)**
Prof. Moira L. Bode (WITS)

DECLARATION

I declare that the work presented in this thesis was carried out exclusively by me under the supervision of Prof. Matthew P. Akerman, Prof. Clinton G. L. Veale and Prof. Moira L. Bode. It is being submitted for the degree of Doctor of Philosophy in Chemistry in the University of KwaZulu-Natal, Pietermaritzburg. It has not been submitted before for any degree or examination in any other University.

Signed.....  .....

Gciniwe Sindiswa Mathenjwa

I hereby certify that this statement is correct

Signed.....

Prof. Matthew P. Akerman (**Supervisor**)

Signed.....

Prof. Clinton G. L. Veale (**Co-supervisor**)

Signed.....

Prof. Moira L. Bode (**Co-supervisor**)

ABSTRACT

HSP90 remains a valuable target for cancer therapy. Unfortunately, targeting intracellular HSP90 has proven not to be a viable chemotherapeutic approach. Compensatory HSR induction and HSP70 overexpression are the main limitations of this approach. A growing body of evidence suggests that targeting the extracellular environment would be of advantage and devoid of the drawbacks observed with intracellular HSP90 inhibition. As a result, the development of extracellular HSP90 inhibitors represents a novel opportunity for cancer therapeutics. In view of this hypothesis, we aimed to design and synthesise extracellular inhibitors and to assay these compounds against HSP90. To develop extracellular HSP90 inhibitors, cell-impermeable analogues of the well-developed benzamide HSP90 inhibitor (**SNX 2112**) were designed, synthesised and biologically evaluated. The desired target compounds were synthesized using developed methodology, as well as modified methodology.

In Chapter 3 we compared and evaluated a variety of reported synthetic methods to deliver the analogues of **SNX 2112**. Interested in a general procedure for the synthesis of our analogues, we initially attempted to afford both the methyl and the trifluoromethyl containing analogues *via* a β-triketone mediated procedure. Despite the success observed with the methyl analogues, the instability of a trifluoromethyl containing β-triketone, deemed this procedure not feasible for this class of compounds. Our continued effort towards a general procedure led to the investigation of a tosylhydrazone mediated tetrahydroindazolone condensation; unexpectedly attempts to synthesise the methyl containing analogues *via* this procedure led to a 1—5 nitrogen to carbon tosyl migration, which was further investigated for varying substrates, and these results are explained in detail in this thesis. It then became apparent that each of the reported methods had its merits and shortcomings, there was no one best method, rather the synthetic approach was mainly determined by the C-3 substituent.

The key intermediates were then converted into the desired targeted compounds by tethering the HSP90 pharmacophore to flexible alkyl groups, attached to polar sulfonate and phosphonate

functionalities. Hypothetically, introduction of polar alkyl groups, would inhibit cell penetration thus limiting them to the extracellular environment.

Based on the goals of our study we were interested in three biological evaluations; to confirm that our modified compounds were still capable of inhibiting HSP90s ATPase activity, to evaluate if our modifications reduced intracellular HSP90 activity, whether they stimulated the pro-oncogenic HSR, and to evaluate their cytotoxicity. Preliminary biological assessment of our compounds was consistent with our hypothesis. Here we showed that our compounds did not inhibit intracellular HSP90, and did not stimulate HSP70 expression, a marker of induction of the compensatory HSR. Furthermore, our analogues displayed cytotoxicity in the nanomolar range against the *HeLa* cell line. These preliminary data support the feasibility of targeting extracellular HSP90 as a novel anticancer strategy.

This thesis is dedicated to my lovely parents, Mr Khuzwayo Enock & Mrs Dudu Christina Mathenjwa.

I hope that this achievement will fulfill the dream you had envisioned for me.

Ngiyabonga boMgabadzeli.

To my daughter, Nkanyezi, I dedicate this to you as a symbol of hard work and dedication. Always remember that all things are possible. I love you.

ACKNOWLEDGMENTS

To Prof. Clinton Veale, thank you for patiently mentoring me in every step of my doctoral journey. For me to see this finish line is due, in no small part, to your constant support and encouragement. I am humbled by your confidence in my abilities and promise to continue always doing my best work. Thank you for believing in me and lighting up my career path.

To Prof. Moira Bode, many thanks for your invaluable intellectual contribution. Also, thank you for introducing me to Prof. Clinton Veale whose passion for science and students' growth has undoubtedly played a significant role in my development as a young scientist.

I would like to thank Prof. Matthew Akerman for his advice and support, particularly during the last months of this project.

To Prof. Charles de Koning, a significant part of the reason I am here today is because you had the amazing ability of springing my passion for Chemistry during those 3rd year organic chemistry lectures. Thank you for seeing something in me that I hadn't seen in myself.

I would like to thank Prof. Adrienne Edkins from Rhodes University for the extensive biological testing of my synthesised compounds.

Many thanks to the technical and support staff who have generously assisted me throughout this project: Mr Craig Grimmer for his NMR expertise, Mr Leigh Hunter for the XRD analysis, and Mr Shawn Ball for technical assistance. I'd also like to extend my gratitude to Prof. Maritjie Stander from Stellenbosch University for the HRMS analysis.

At times doing a PhD felt like a sinking ship, but many thanks to my research group and colleagues for constantly reminding me that we are all in this together, and that one day we will see the finish line.

Thank you to the National Research Fund and the UKZN FLAGSHIP for funding; and thank you to the University of KwaZulu-Natal for providing the facilities to do my research.

To my God-given family, the UKZN-P Methodist Student Society: Mark 12:31 instructs us to “love your neighbour as yourself” and my time with you has been nothing, but a true reflection of that. Thank you.

To all my friends, thank you for always holding space for me. Thank you for listening to my constant nagging and still manage to encourage me to carry on.

To all my sisters; Samke, Lindy, Kuhle, Lah and Mfuyo, I cannot express how much your presence keeps me going, I love you and thank you! To my younger sisters, nieces and nephews, may this serve as constant encouragement for you to follow your dreams.

To my dad, nothing in this world compares to your love, care, and support. I know God loves me because He gave me you as a father. Your words of encouragement and constant reassurance have carried me to this point. INkosi ikubusise njalo, ngiyabonga Mgabadzeli.

To my mom, ngiyabonga mama for all your unimaginable sacrifices, you have constantly carried me in your arms. Your prayers have sustained me thus far. May God continue to bless and keep you always.

To my forever love, iNkanyezi yami: I missed all your “firsts”; your first crawl, your first step, your first word; all of them. It was for us. I love you baby and this thesis is dedicated to you.

Last but not least, all glory to The Lord Jesus Christ for giving me the strength to endure not escape…“not by might nor by power, but by my Spirit,” says the LORD Almighty.

TABLE OF CONTENTS

LIST OF ABBREVIATIONS

17-AAG	17-allylamino-17-desmethoxygeldanamycin
ADP	adenosine diphosphate
ATP	adenosine triphosphate
AHA1	ATPase homologue 1
DCM	dichloromethane
DDRs	discoidin domain receptors
DIPEA	diisopropylethylamine
17-DMAG	17-dimethylaminoethylamino-17-demethoxygeldanamycin
DMAP	4-dimethylamino-pyridine
DME	dimethoxyethane
DMEM	Dulbecco's Modified Eagle's Medium
DMF	*N*,*N*-dimethylformamide
DMSO	dimethyl sulfoxide
DPPF	1,1'-bis(diphenylphosphino)ferrocene
ECM	extracellular matrix
EDCI	1-ethyl-3-(3-dimethylaminopropyl)carbodiimide
EGCG	epigallocatechin-3-gallate
eHSP90	extracellular HSP90
ER	endoplasmic reticulum

F-5	fragment-5
FBS	fetal bovine serum
FDA	food and drug administration
Grp94	94-kDa glucose-regulated protein
HDF	human dermal fibroblasts
HDMEC	human dermal microvascular endothelial cells
HK	human keratinocyte
HMBC	heteronuclear multiple bond correlation
HRESMS	high resolution electrospray mass spectrometry
HRMS	high resolution mass spectroscopy
HSFs	heat shock transcription factors
HSPs	heat shock proteins
HSQC	heteronuclear single quantum correlation
HSR	heat shock response
HOBt	hydroxybenzotriazole
HOP	HSP70/HSP90 organizing protein
HIF-1α	hypoxia-inducible factor-1alpha
IR	infrared
LRP-1	lipoprotein receptor-related protein-1
MMP	matrix metalloproteinase

m/z	mass to charge ratio
NHS	*N*-hydroxysuccinimide
NMR	nuclear magnetic resonance
PEG	polyethylene glycol
PPI	protein-protein interactions
ppm	parts per million
PSA	pencillin-streptomycin-amphotericin
R_f	retardation factor
ROS	reactive oxygen species
r.t.	room temperature
SAR	structure-activity relationship
SDS-PAGE	sodium dodecyl sulphate – polyacrylamide gel electrophoresis
TEA	triethylamine
THF	tetrahydrofuran
TPR	tetratricopeptide-containing repeats
TLC	thin layer chromatography
TME	tumour microenvironment
Trap1	tumour necrosis factor receptor-associated protein 1
UPR	unfolded protein response
UPRmt	mitochondrial UPR

UV	ultraviolet

LIST OF SCHEMES

LIST OF FIGURES

LIST OF TABLES

PUBLICATIONS AND CONFERENCE CONTRIBUTIONS

Publication

Mathenjwa, G. S.; Akerman, M. P.; Bode, M.; Veale, C., *Synlett* **2022**, *33*, 1907-1912.

Flash oral presentation

Gciniwe S. Mathenjwa, Targeting the tumour extracellular environment through rational modification of the SNX class of HSP90 inhibitors. The 44th South African Chemical Institute's (SACI) National Convention 2023 – Stellenbosch University, Stellenbosch – South Africa, 8th – 13th January 2023.

Poster presentations

Gciniwe S. Mathenjwa, Matthew P. Akerman, Adrienne L. Edkins, Moira L. Bode, Clinton G.L. Veale, Targeting the tumour extracellular environment through rational modification of the SNX class of HSP90 inhibitors. The 44th South African Chemical Institute's (SACI) National Convention 2023 – Stellenbosch University, Stellenbosch – South Africa, 8th – 13th January 2023.

Gciniwe S. Mathenjwa, Moira L. Bode, Clinton G.L. Veale, Protein degradation over protein inhibition: HSP90 PROTACs as novel cancer therapeutics. The South African Chemical Institute (SACI) Frank Warren 2019 – Alpine Health, Drakensberg - South Africa, 7th – 11th July 2019.

1. CHAPTER 1: INTRODUCTION

While the post-genome era has allowed for the identification and validation, of numerous new drug targets, this vastly expanded insight, has not translated into a steady pipeline of clinically efficacious drugs.[1] This is in part due to the heterogeneity factors underpinning a disease, as well the as the limited druggable space explored through the current target-receptor model.

The traditional model of drug discovery typically screens libraries of 'drug-like' molecules against intracellular biological targets, where compounds are optimised to access these targets. However, the intracellular space only account for a subsection of biologically relevant chemical space.

The chaperone proteins represent a promising class of anti-cancer targets, essential for myriad intra- and extracellular functions, and are considered promising anti-cancer targets. However, their utility has mostly been confined to targeting the intracellular environment.

Accordingly, this thesis will describe our efforts to expand the scope of chaperone inhibition, through the rational modification of HSP90 inhibitors into extracellular inhibitors.

1.1. Cell stress and survival mechanisms: A brief introduction

Cells grow and function optimally under 'normal' physiological conditions. However, stressful conditions such as heat shock, hypoxia and nutrient imbalance affect the distinct cell functions and there are various defence mechanisms through which cells respond to stress. One such method is the activation of survival pathways that assist the cell to defend against and recover from the stress induced damage. The heat shock response (HSR), also known as the cellular stress response, and the unfolded protein response (UPR) are the main pro-survival pathways of the cell.[1-3] Notably, these pathways are specific to the subcellular localization. The UPR is activated by the environmental

stressors experienced in the endoplasmic reticulum (ER) and the mitochondria;[4] while the HSR has overlapping roles in cytoplasmic and ER stress responses. [4-6]

The ER proteome consists of properly folded transmembrane proteins and ensures proper processing of proteins entering the secretory pathway.[5] Hypoxic stress leads to energy deficiency which disturbs the ER homeostasis leading to the accumulation of misfolded and unfolded proteins.[4, 5] Subsequent activation of the UPR signalling pathways restores the ER homeostasis, thus preventing stress-induced apoptosis.[5] Hypoxia-induced ER stress is often implicated in diseases such as Alzheimer's and diabetes.[4, 5]

The mitochondrial proteome regulates the cell's metabolic pathways essential for the synthesis of ATP, amino acids, lipids and nucleic acids.[7, 8] Hypoxia-induced mitochondrial dysfunction leads to ATP deficiency, which could subsequently result in cell death. As a result, the cellular response to hypoxic conditions is the stimulation of the mitochondrial UPR (UPRmt), which activates multiple pathways required for adaptation and cell survival.[6-9] Defective mitochondrial functions are implicated in diseases such as, schizophrenia, anxiety and bipolar disorders.[10]

Similarly, cells subjected to elevated temperatures accumulate misfolded proteins, which in turn triggers the activation of the HSR for cell survival. The HSR is a physiological process characteristic of many organisms including animals, bacteria, fungi and plants. The HSR is a highly conserved survival pathway through which cells maintain homeostasis and protect themselves against various biological, chemical and physical environmental stressors.[11, 12] The expression of genes by HSR is regulated by heat shock transcription factors (HSFs), with HSF1 being the most commonly investigated, which regulate the expression of heat shock proteins.[2, 12, 13]

1.2. Heat shock proteins (HSPs): biological roles and functionality

Heat shock proteins (HSPs) are cellular defence proteins that are expressed as part of the HSR as a result of cellular stress.[12, 14] HSP27, HSP40, HSP70, HSP90, and HSP110 are some of the major cytosolic HSP families. These HSP families were named and classified according to their molecular weights; for

example, 90 kilo Dalton HSP is known as HSP90.[1, 14, 15] Initially, HSPs were identified as overexpressed proteins in cells exposed to a variety of stressors most notably heat shock.[1] There is, however, evidence that under normal physiological conditions HSPs also play significant housekeeping roles including, protein folding, stability and function of client proteins, and they play a significant role in maintaining cellular proteostasis by ensuring that client proteins are maintained in a functional conformation.[1, 12, 14, 16] For example, HSP70 was reported to ensure the translocation of newly synthesised proteins from the cytoplasm to the mitochondria.[17] Therefore, it is important to note that several members of HSPs are overexpressed and serve significant roles in unstressed cells. As previously mentioned, environmental stressors such as heat shock lead to the accumulation of misfolded proteins and ultimately the loss of their function.[17, 18] This dysfunction activates the HSR, and consequently the expression of HSPs.[19] The distinct HSP families then act in a complementary fashion to prevent aggregation of the misfolded proteins, refolding them, and consequently promoting cell survival.[14, 18] Broadly speaking, HSPs mediate critical biological functions under disease, stressful and physiological conditions.

Most HSPs are involved in various regulatory pathways and behave as molecular chaperones for other client proteins; they play a significant role in maintaining cellular proteostasis by integrating the fundamental processes of protein folding and degradation.[14, 16] Interaction of HSPs with client proteins facilitates the proper folding of the target proteins, their assembly into protein complexes, and/or their translocation into organelles.[14, 16] Some members of the HSP family, i.e. HSP40, act as co-chaperones, which are required by chaperone proteins, for regulatory purposes. For example, over 20 co-chaperones have been reported for the HSP90 family, the co-chaperones fine tune its function and adapt it to the different stages of the HSP90 molecular chaperone cycle.[13, 14]

1.3. HSPs association with cancer

The significant involvement of HSPs in the growth and progression of many tumour types has been extensively discussed in literature.[20-22] It has been reported that various cancers constitutively express

high levels of HSPs. For example HSP27, HSP70 and HSP90 have been shown to be overexpressed in various cancer types such as breast, prostate, lung and melanoma.[20-23] In addition, cancer cells have been shown to engage the HSR during their growth and reproduction; leading to the overexpression and constitutive activation of HSF1 in many cancers.[11, 12, 15] The expression of HSF1 has been shown to be crucial in the oncogenic network for the growth and survival of cancer cells.[15, 23-25] While gene knock out experiments have shown that its loss in normal healthy cells has a negligible effect,[11] several studies have established that tumour cells become dependent on HSPs and their regulators such as HSF1 for their survival.[11, 21]

Much of the research into the function of HSPs in cancer has focused on their intracellular roles.[15, 23, 24] HSPs are known to function intracellularly in an ATP dependant manner, where they operate in response to folding stresses that arise during the different stages of cancer proliferation.[15, 23-25] Within cancer cells there is a substantially increased expression and accumulation of pro-oncogenic proteins, many of which are mutated.[11, 13, 15] This necessitates increased intracellular concentrations of HSPs, to facilitate correct protein folding and cellular survival.[15, 23-25] Accordingly, HSPs have been extensively investigated as potential molecular targets for cancer therapy, with HSP90 being the main focus of cancer therapeutics.[12, 21, 24]

1.4. HSP90 classification, structure, and mode of action

1.4.1. HSP90 classification and structure

A mammalian cell consists of four major HSP90 homologs, HSP90α, HSP90β, 94-kDa glucose-regulated protein (Grp94) and tumour necrosis factor receptor-associated protein 1 (Trap1) which can be classified according to their subcellular localization and their regulation (**Figure 1.1**).[26, 27] Additionally, various cellular stressors such as heat, irradiation, reactive oxygen species and hypoxia have been reported to lead to the secretion of HSP90α and HSP90β from the cell. Secreted HSP90α resides outside the cell and is generally known as extracellular HSP90 (eHSP90).[27, 28]

The stress-inducible HSP90α form and the constitutive HSP90β form are the two main mammalian isoforms.[29] HSP90α and HSP90β are highly homologous, sharing 86% amino acid identity and are mostly located in the cytoplasm and the nucleus.[27, 30] These two cytoplasmic forms are ubiquitously expressed in all nucleated cells and exist in a 2:1 ratio of HSP90α to HSP90β.[31] Grp94 is located in the endoplasmic reticulum and Trap1 is found in the mitochondrial matrix.[26, 27]

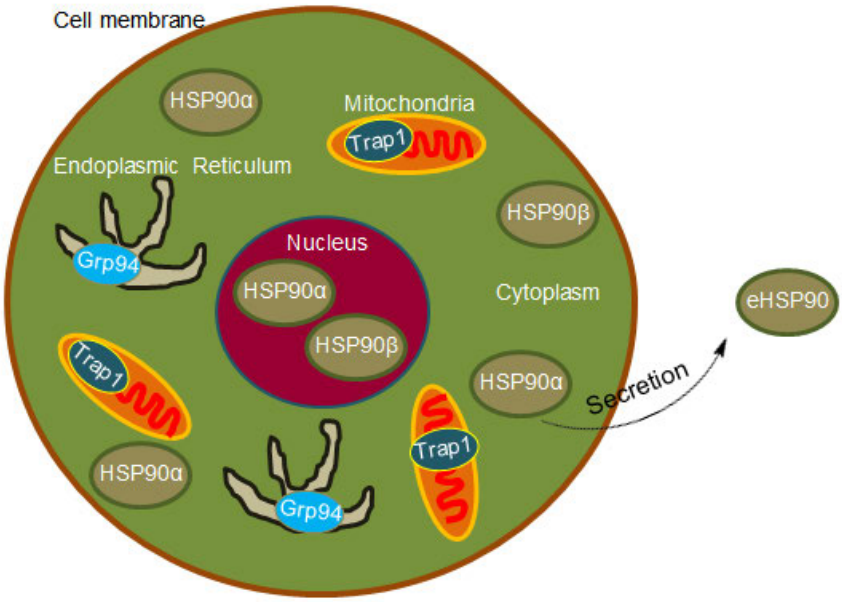

Figure 1.1: A representation of organelle specific localization of each of the four HSP90 isoforms, including eHSP90.[27] HSP90α and HSP90β are localized in the cytoplasm and nucleus. Grp94 resides in the endoplasmic reticulum, and Trap1 is found in the mitochondria. Secreted HSP90α is found outside the cell, and it is known as extracellular HSP90 (eHSP90). This diagram was redrawn based on that published by Seo *et al*..[27]

As previously stated, HSP90α and HSP90β are the two main isoforms of mammalian HSP90; and very often HSP90 is used to refer to both of these cytoplasmic isoforms, unless stated otherwise.[1, 29] HSP90 is a highly conserved molecular chaperone that exists as a homodimer with each monomer consisting of three main domains; the *N*-terminal domain (N), the middle domain (M) and the *C*-terminal domain (C). In eukaryotes, the N-terminal and the middle domain are connected by a charged linker (**Figure 1.2**).[29, 32]

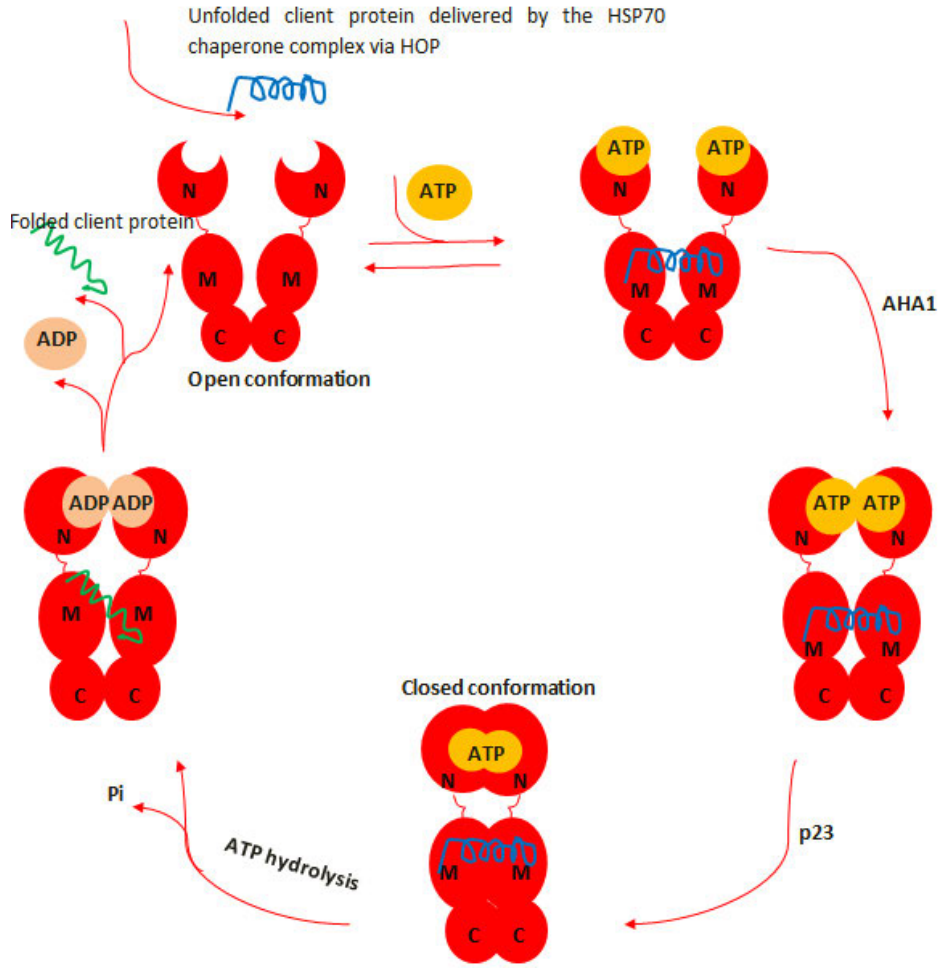

Figure 1.2: Schematic representation of the HSP90 chaperone cycle. Partially folded client proteins are loaded to the HSP90 chaperone cycle through the HSP70 chaperone complex *via* HOP. Upon ATP binding, AHA1 accelerates the ATPase activity of HSP90 bringing the two *N*-termini close to each other (ATP bound state). The ATP bound state "closed conformation" is then stabilized by p23, increasing the contact time between HSP90 and the client proteins, even after ATP hydrolysis. ATP hydrolysis leads to the ADP bound state, which upon the release of ADP, phosphate products and the mature client protein reforms the open conformation. This diagram was redrawn based on that published by Pearl *et al*..[32]

The N-terminal, sometimes known as the nucleotide-binding site, contains an ATP binding site. Hence, it is responsible for HSP90 ATPase activity critical for chaperone function and client protein binding. Most notably, as will be discussed later, HSP90 targeted cancer therapeutics have mainly focussed on the development of ATP competitive inhibitors which bind in the *N*-terminal, thus disrupting HSP90 chaperone activity.[29, 33]

The middle domain is reported to play a significant role in modulating ATP hydrolysis through binding the γ-phosphate of ATP bound in the N-terminal. Additionally, this domain is responsible for client protein binding and interaction.[34, 35]

Lastly, the *C*-terminal is essential for HSP90 dimerization. Interestingly, the *C*-terminal contains a distinct ATP binding pocket which exhibits different ligand specificities from the *N*-terminal nucleotide binding site.[14, 36] Unlike the *N*-terminal nucleotide which specifically binds adenosine nucleotides containing an intact adenine ring, the *C*-terminal nucleotide shows less specificity with the ability to bind both purine and pyrimidine nucleotides.[36] This variability suggests that the function of HSP90 can be disrupted through the development of different classes of HSP90 inhibitors, i.e., *N*-terminal and *C*-terminal targeted drugs.[24, 29] Another characteristic feature of the *C*-terminal is the presence of the highly conserved MEEVD motif which binds tetratricopeptide-containing repeats (TPR)-domain containing co-chaperones like the HSP70/HSP90 organizing protein (HOP).[37]

The fundamental differences between intracellular and extracellular HSP90 are in their cellular locations and the structural domain used to perform various biological functions.[16, 28] Firstly, as suggested by their names, one is located inside and the other is located outside the cell, respectively.[16, 27, 28] Secondly, the former has three essential domains for its effectiveness; the N-terminal for ATPase activity, the middle domain for client protein binding and the *C*-terminal for dimerization binding (**Figure 1.2**).[16, 32] The latter uses a 115 amino acids peptide known as the fragment-5 (F-5) region, located between the charged linker and the middle domain (M) to promote cell motility.[13, 16, 31] Thirdly, while intracellular HSP90 functions as a molecular chaperone, extracellular HSP90 functions as a pro-motility factor.[13, 16]

Extracellular HSP90 interacts with various cell surface receptors to mediate critical functions in wound healing and cancer progression.[38, 39] In particular, Cheng *et al*. provided evidence that extracellular HSP90 plays an essential role in wound healing through the critical interaction of the F-5 fragment with the lipoprotein receptor-related protein 1 (LRP-1) receptor.[39] During their studies, they

performed a parallel experiment where they treated acute and diabetic wounds on mice with F-5 and the FDA-approved growth factor therapy, becaplermin gel (PDGF-BB). The F-5 treated wounds healed much faster than the ones treated with PDGF-BB. The recruitment/migration of epidermal and dermal cells into the wound bed is an essential process for wound healing; and the three major skin cell types are HKs, HDFs, and HDMECs. The wound healing agents exert their activity through binding with receptors found in the three major cell types. Only HDFs expressed the PDGF-BB specific receptor, thus PDGF-BB wound healing activity was affected by the inability to migrate the other essential skin cells. In contrast, HKs, HDFs, and HDMECs all express LRP-1, which is a promotility receptor for extracellular HSP90. Consequently, the superior wound healing activity of the F-5 fragment was due to the ability to recruit the three major skin cells through an interaction with LRP-1. This study highlighted the importance of the interaction between extracellular HSP90, particularly the F-5 fragment, and LRP-1 in wound healing.[39] Important to note is that the F-5 fragment was found to be the optimum peptide length for this function, retaining the same activity as the 732-amino-acid full length extracellular HSP90, and superior to other peptide fragments.[31, 39] Similarly, the same phenomenon was observed for cancer progression, the F-5 fragment was reported to play a critical role in breast cancer cell invasion.[31, 38]

1.4.2. HSP90 mode of action

As discussed above, HSP90 exists as a homodimer with each monomer consisting of the *N*-terminal, middle and *C*-terminal structural domains. The HSP90 homodimers can exist in the ADP-bound or the ATP-bound conformation (**Figure 1.2**). In the ADP-bound conformation the two *N*-termini are separated in what is referred to as the "open conformation" to capture client proteins. Client proteins are then delivered to HSP90 by the HSP70 chaperone complex through following the formation of a ternary complex with HOP**.**[32, 37] ATP binding then results in the formation of the *N*-termini dimerized "closed" conformation.[2, 32] A range of co-chaperones play an essential role in regulating the HSP90 ATPase cycle; for example, the activator of HSP90 ATPase homologue 1 (AHA1), stimulates the formation of the closed conformation and accelerates the overall rate of the chaperone cycle.[1, 14, 32]

The "twisted" closed conformation is then stabilized by the p23 co-chaperone.[2, 32] ATP hydrolysis leads to the formation of the ADP bound conformation, which subsequently releases ADP, phosphate products and the correctly folded client protein, reforming the open conformation ready to capture another partially folded client protein.[2, 14, 32] As previously mentioned, intracellular *N*-terminal HSP90 inhibitors exert their function by competitively occupying the ATP binding cleft, thus inhibiting the ATPase activity necessary for the HSP90 chaperone cycle.[24, 40] The *C*-terminal inhibitors induce HSP90 client protein degradation by interfering with the *C*-terminal dimerization domain, which in turn blocks ATP binding and hydrolysis necessary for HSP90 chaperone function, thus preventing proper folding and maturation of the substrates.[40-42]

1.5. Intracellular HSP90 inhibition

1.5.1. HSP90 inhibitors targeting the ATP binding site of the *N*-terminal

The reduction of HSP90 function in cancer cells by inhibitory compounds prevents appropriate folding of proteins into their active conformations thus leading to the loss of activity of a wide array of pro-oncogenic proteins. This inhibition results in decreased tumour cell growth and ultimately death, thus substantial research has focussed on HSP90 as a promising target for cancer treatment.[15, 23, 24, 43] The initial strategy towards HSP90 inhibition was to design compounds that would bind in the *N*-terminal ATP binding site with higher affinity than the natural substrate, hence disrupting the chaperone cycle. The inhibition of HSP90 ATPase activity, and therefore its ability to cycle between the ADP and ATP bound conformations disrupts the proper folding and stabilization of oncogenic client proteins.[24, 43, 44] The misfolded client proteins are then recruited by E3-ubiquitin ligases leading to their proteasome-mediated degradation.[24, 43, 44]

The benzoquinone ansamycin, resorcinol analogues and purine derivatives are some of the HSP90 inhibitors that have been investigated.[43, 44] The first class of HSP90 inhibitors, the benzoquinone ansamycins (**Figure 1.3**), was discovered in 1994 and is represented by geldanamycin (**1.1**). Compound

1.1 is a natural antibiotic that was first isolated from *Streptomyces hygroscopicus,* and was the first HSP90 inhibitor reported to have antitumour potential.[24, 43-45] Compound **1.1** is an ATP competitive inhibitor; preventing ADP/ATP binding, and the subsequent ATP hydrolysis, essential for the HSP90 chaperone cycle. Consequently, HSP90 is inhibited from carrying out its molecular chaperone function.[12, 24, 46] This results in client protein degradation through the ubiquitin–proteasome pathway.[24] Compound **1.1** was reported to have potent anti-cancer activities in preclinical *in vivo* studies, however, its poor solubility, partial *in vivo* instability and the high hepatotoxicity observed in animal models hindered its development.[24, 43-45] Structural variations of **1.1** led to the development of 17-allylamino-17-desmethoxygeldanamycin (17-AAG) (**1.2**).[24, 43-45]

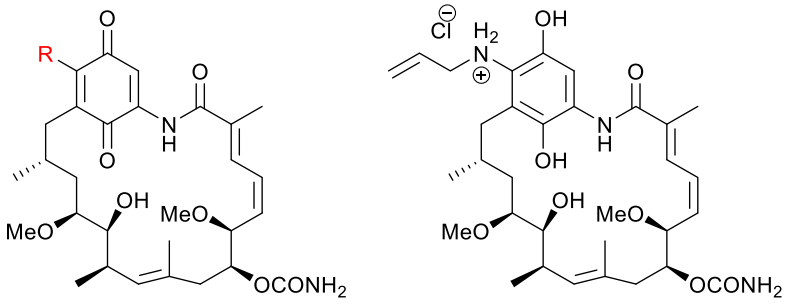

1.1 Geldanamycin R=OCH_3
1.2 17-AAG R=$NHCH_2CHCH_2$
1.3 17-DMAG R=$NHCH_2CH_2N(CH_3)_2$

1.4 IPI-504

Figure 1.3: Benzoquinone ansamycin class of HSP90 inhibitors.[43]

Compound **1.2** maintained similar anti-cancer activity to **1.1** with improved toxicological properties and it was the first HSP90 inhibitor to enter clinical trials.[24, 43-45] Compound **1.2** provided proof-of-concept for HSP90 inhibition as a valid anti-cancer strategy in humans. Despite the observed cancer efficacy with **1.2** in phase I/II clinical trials, its development was discontinued; mainly due to poor hydrophilic solubility, instability in solution, low oral bioavailability and patent concerns.[24, 43-45] Further structural variations were applied to circumvent these drawbacks leading to the development of 17-dimethylaminoethylamino-17-demethoxygeldanamycin (17-DMAG) (**1.3**), however, hepatotoxicity

remained a limiting factor for this class of inhibitors.[13-16] The hepatotoxicity was identified to be due to the quinone ring, with efforts to overcome this drawback leading to the development of 17-allylamino-17-demethoxygeldanamycinhydroquinone hydrochloride (IPI-504) (**1.4**).[24, 43-45, 47] Compound **1.4** is an oral analogue of **1.2**, which is a water-soluble hydroquinone hydrochloride salt formed by the reduction of **1.2** with sodium dithionite and the subsequent conversion to its hydrochloride salt.[24, 48] Moreover, **1.4** (hydroquinone) and **1.2** (quinone) have been reported to exist in an oxidoreductase catalysed-redox equilibrium *in vivo*, and were further confirmed to have similar pharmacokinetic profiles,[49] suggesting that both **1.2** and **1.4** collectively contribute to the observed antitumour activity.[48, 49] Sydor *et al*. further reported that **1.4** was slightly more potent and thus more essential *in vivo*.[49] Although **1.4** was the most promising HSP90 inhibitor from the ansamycin class, its development was halted during its phase III clinical trials.[44] This was mainly due to safety concerns, observed mortality rates of patients and the interconversion of **1.4** with **1.2** *in vivo*.[44] Overall, the ansamycin class provided proof-of-concept for inhibiting HSP90 in cancer; however, hepatotoxicity and other toxic effects limited their therapeutic benefit.

An alternative class of ATP competitive HSP90 inhibitors studied were the resorcinol derivatives, represented by radicicol (**1.5**) (**Figure 1.4**).[24, 43-45, 47]

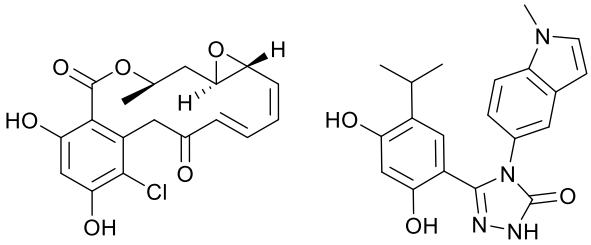

1.5 Radicicol **1.6** Ganetespib

Figure 1.4: Resorcinol class of HSP90 inhibitors.[43]

Compound **1.5** is also a natural antibiotic that was initially isolated from the fungus *Monocillium nordinii* and *Monosporium bonorden*.[43, 44, 50] Compound **1.5** was reported to demonstrate anticancer activity *in vitro* but not *in vivo*, its major obstacle was chemical and metabolic instability due to its

reactive epoxide and the 1,6-dienone moieties which are highly reactive towards nucleophiles in the body of the animal.[24, 43, 44, 51] However, structure-activity relationship (SAR) studies revealed that its resorcinol core was crucial for binding; hence, it provided the chemical basis for the development of several derivatives, which overcame some liabilities associated with **1.5** including ganetespib (**1.6**). Poor activity during clinical trials stalled further development of this class.[24, 43, 44] Neither compound class gave rise to any small molecules that were FDA-approved for patient use. These natural products have, however, played a significant role in the identification of lead compounds.

Novel synthetic small molecules were then developed and investigated to overcome the limitations observed with the natural product classes discussed above. Purine based derivatives, designed to mimic the endogenous ATP ligand, was the first group to be explored; compounds such as PU-H71 (**1.7**), BIIB021 (**1.8**), MPC-3100 (**1.9**) and CUDC-305 (**1.10**) were advanced to clinical evaluation (**Figure 1.5**).[24, 43-45] Major improvements such as overcoming multi-drug resistance, favourable hydrophilic solubility, oral bioavailability, and metabolic stability were observed with this class of HSP90 inhibitors.[43, 45]

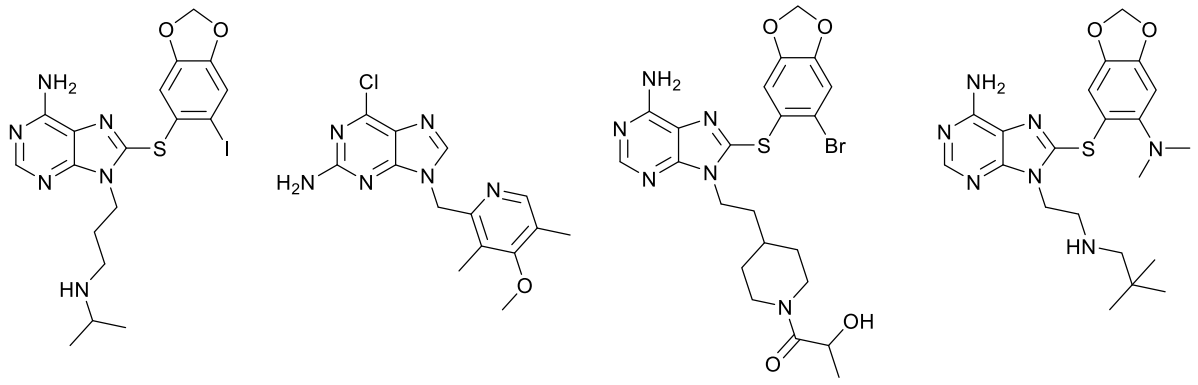

1.7 PU-H71 **1.8** BIIB021 **1.9** MPC-3100 **1.10** CUDC-305

Figure 1.5: Purine-based class of HSP90 inhibitors.[43, 44]

Dihydroindazolone derivatives was another novel class of synthetic inhibitors developed (**Figure 1.6**). In a study done by Huang *et al.,* SNX-2112 (**1.11**), SNX-5422 (**1.12**), compound **1.13** and **1.14** displayed potent anti-proliferative activity against various cancer cell lines.[24, 43-45, 47, 52] Compounds **1.11** and **1.13**

were equally potent, while substituting the indolone moiety of **1.13** with 3-methylindazolone afforded a less potent derivative (**1.14**, **Figure 1.6**).[52] Compound **1.11** displayed excellent activity *in vitro* with greater potency than **1.2** and **1.3**,[52] however, oral bioavailability and solubility limited further evaluations of this compound.[24] Its orally bioavailable pro-drug, SNX-5422 (**1.12**) was selected for clinical evaluation and it displayed *in vivo* potency; however, the development of both compounds was halted due to ocular toxicity and the potential of irreversible retinal damage observed in early clinical trials.[24, 43, 44, 53] Most notably, these compounds had a strong binding affinity for HSP90 over its immediate family members, Grp94 and Trap1.[52] Furthermore, the binding mode and structural information of selected analogues in the *N*-terminal were evaluated and provided a valuable basis for further developments.[26, 52]

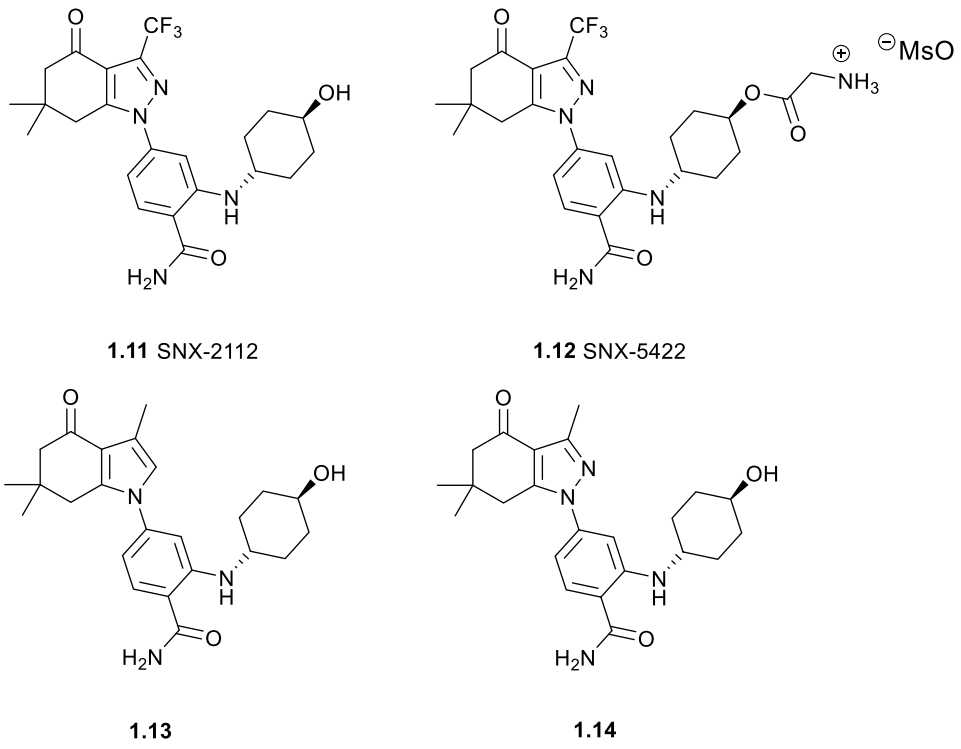

Figure 1.6: Dihydroindazolone class of HSP90 inhibitors.[52]

Other *N*-terminal targeting HSP90 inhibitors developed were DS-2248 (**1.15**) and XL-888 (**1.16**).[24, 44, 53] The structure of **1.15** has not been disclosed and that of **1.16** is shown below (**Figure 1.7**).[26, 53]

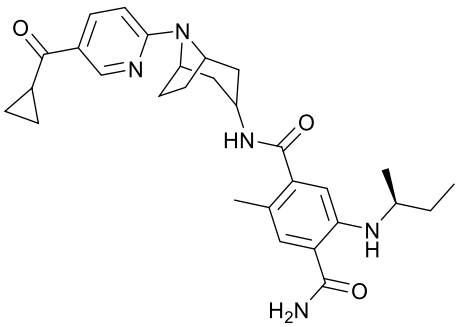

1.16 XL-888

Figure 1.7: The structure of an *N*-terminal HSP90 inhibitor XL-888 (**1.16**)

To date, there are no FDA approved HSP90 inhibitors, despite their promising activities. The major drawback with HSP90 inhibitors targeting the *N*-terminal domain is that inhibition of ATP binding induces the pro-survival HSR leading to the transcriptional activation of HSP70 and its subsequent over expression.[10,13-20] This up-regulation results in HSP70 facilitating the appropriate folding of HSP90 client proteins thus compensating for HSP90 inhibition. Furthermore, HSP70 upregulation was reported to inhibit apoptosis signalling. Other challenges such as hepatotoxicity and ocular toxicity have dampened enthusiasm towards the development of these inhibitors.[24, 43-45, 52-54] However, given the promise of wholesale shutdown of cellular chaperone function in the treatment of cancer, several alternative strategies to inhibit HSP90 function through alternate means which do not induce the HSR have been investigated.

1.5.2. HSP90 inhibitors targeting the *C*-terminal

A distinct ATP binding pocket has been identified in the *C*-terminal of HSP90 (**Figure 1.2**). Importantly, some researchers have reported that inhibition of the *C*-terminal does not induce the HSR, hypothesising that inhibiting HSP function is still a viable cancer target.[55] During recent years several promising lead molecules with potent antiproliferative activity against multiple cancer cell lines have been identified.

Novobiocin (**1.17**), a natural antibiotic, was the first *C*-terminal HSP90 inhibitor identified (**Figure 1.8**).[43, 45, 56] Structurally, **1.17** can be separated into three components; the noviose sugar (blue), the

coumarin core (black) and the benzamide side chain (red). Originally known as a gyrase inhibitor, it was found to be a potential anticancer agent through binding in the region overlapping the *C*-terminal dimerization domain of HSP90, disrupting the HSP90-HSP70 and the HSP90-p23 client protein interaction, which consequently inhibits the ATP-mediated dimerization and ATP hydrolysis essential for the folding and maturation of client proteins.[42, 56-58] Compound **1.17** was reported to interfere with the interaction between the HSP90 complex and its co-chaperones, p23 and HSP70. When evaluated against the SkBr3 cell lines, novobiocin resulted in the degradation of several HSP90 client proteins; however, it displayed poor antiproliferative activity.[26, 56, 57] In an attempt to improve the poor HSP90 inhibition activity a SAR investigation was carried out where the three separate domains of **1.17** were varied.

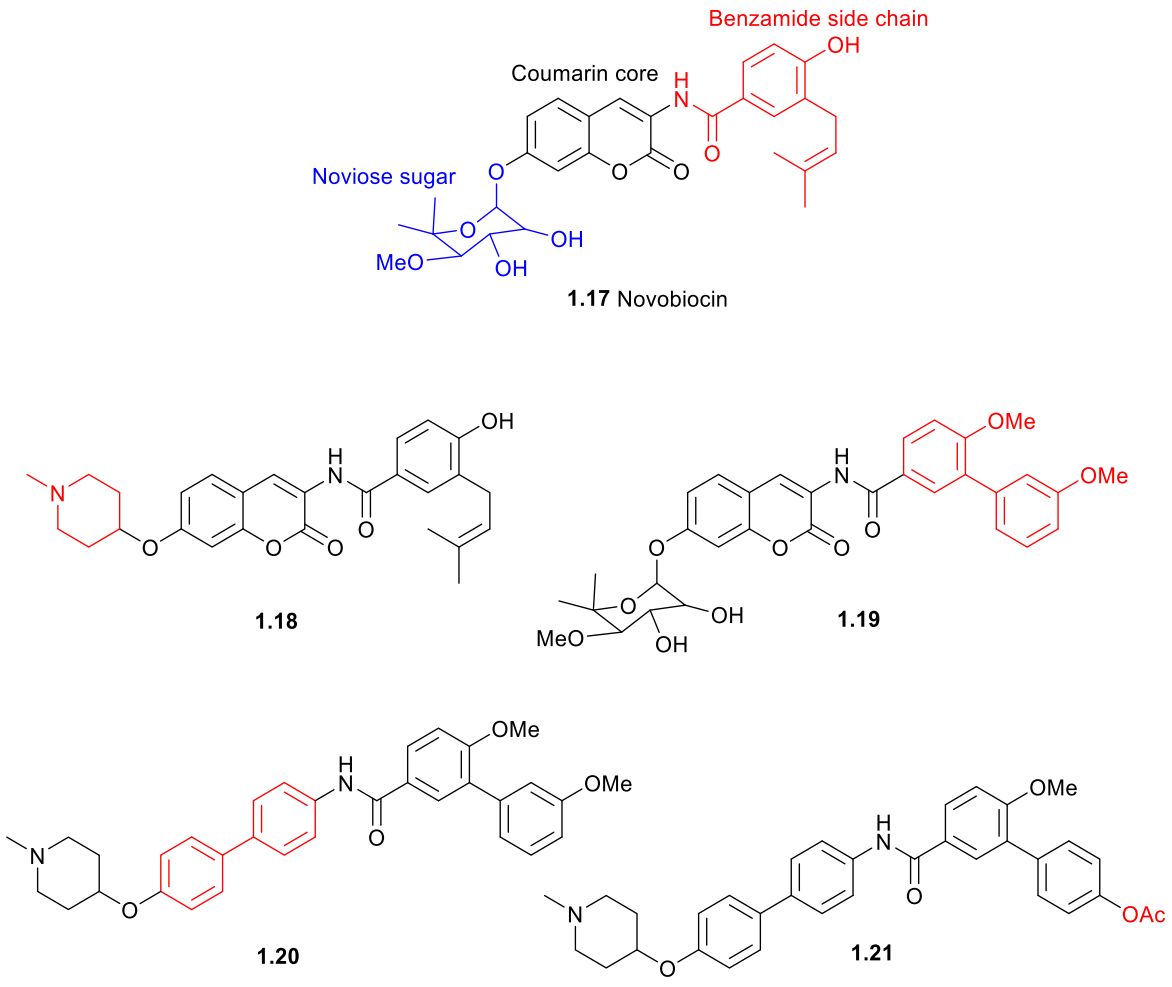

Figure 1.8: *C*-terminal HSP90 inhibitors originating from Novobiocin.[26, 57, 59]

Structural modifications on the benzamide side chain revealed its importance for the inhibitory activity. The noviose sugar was identified as having a major contribution to solubility and efficacy, however, its substitution with ionizable amines led to the development of analogues with improved inhibitory activity.[26, 57] As a result, compounds such as **1.18** and **1.19** were developed and displayed improved antiproliferative activity against various cancer cell lines.[57] Initially, the coumarin moiety was thought to be a key structural element for HSP90 inhibition. However, a study performed by Donnelly *et al.* investigating the effect of different substitutions on the coumarin ring found that while the coumarin ring was not critical for antiproliferative activity, it was necessary for the correct orientation of the sugar moiety and the benzamide side chain in the ATP binding pocket.[56] This prompted a search of optimal ring systems to bridge the noviose and benzamide functionalities.

Provided with that information, Zhao *et al.* then designed and synthesized a small library of compounds where the coumarin ring was substituted with a biphenyl ring.[59] These compounds were found to have improved anticancer activity when compared to their coumarin analogues. As a result of this investigation, compounds such as **1.20 and 1.21** were developed, which displayed activity in the mid nanomolar range against various cancer cell lines.[59] Most importantly, the novobiocin analogues displayed improved antiproliferative activity which did not induce the HSR.[53, 54, 57, 59]

Another class of *C*-terminal targeting HSP90 inhibitors originated from deguelin (**1.22**) (**Figure 1.9**).[26, 60] Compound **1.22**, a natural rotenoid isolated from *Mundulea sericei*, was reported to be a *C*-terminal ATP-competitive compound disrupting the HSP90 chaperone cycle.[26, 60] Its binding led to destabilization of HSP90 client proteins such as HIF-1 consequently reducing tumour growth in xenograft models of various human cancers.[60] Subsequent SAR studies revealed the more flexible compounds such as **1.23** and **1.24** which exhibited potent cell growth inhibition and lower cytotoxicity against normal cells compared to **1.22**.[26, 60] Recently, a novel derivative of deguelin, SL-145 **1.25** displayed potent anti-tumour and anti-metastatic activity without inducing the pro-survival HSR.[55]

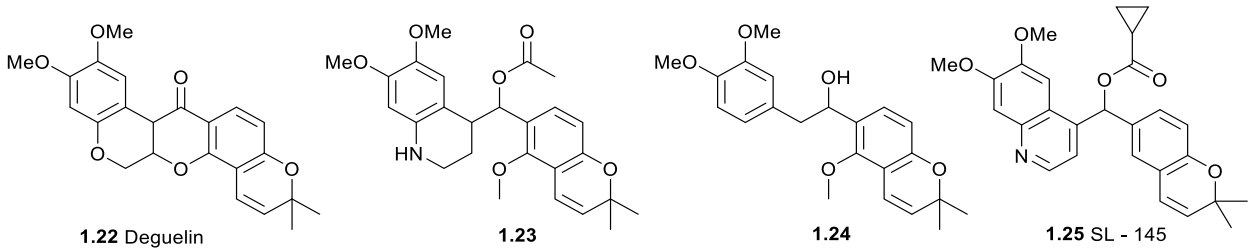

Figure 1.9: *C*-terminal HSP90 inhibitors originating from deguelin (1.22).[26, 55]

A green tea extract, epigallocatechin-3-gallate (EGCG) (**1.26**), represents a different class of *C*-terminal HSP90 inhibitors (**Figure 1.10**).[26, 45] Treatment of pancreatic cancer cells with **1.26** disrupted HSP90 interaction with various client proteins such as Akt, HER-2, Raf-1, Cdk4, and pErk and decreased the levels of these clients, leading to reduced cell proliferation.[26] Structural variations led to the development of compound **1.27** which displayed improved antiproliferative activity.[26]

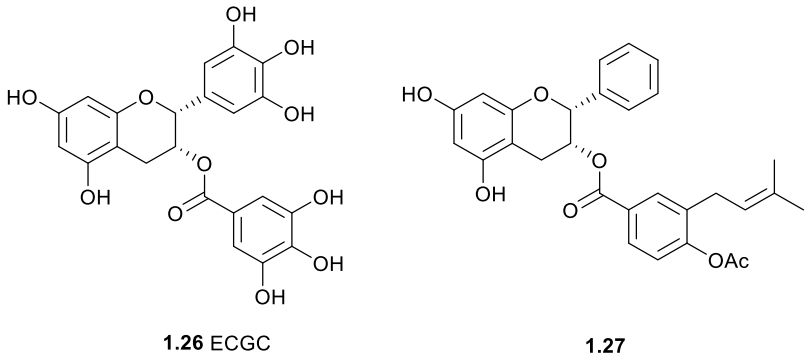

Figure 1.10: *C*-terminal HSP90 inhibitors originating from epigallocatechin-3-gallate (EGCG) (**1.26**).[26]

Other identified inhibitors targeting the HSP90 *C*-terminal were derrubone (**1.28**)[45] and silybin (**1.29**); and their respective analogues, **1.30** and **1.31** (**Figure 1.11**).[26] To this end, inhibition of the ATP-binding site of the *C*-terminal remains a promising anti-cancer strategy. The developed compounds displayed antiproliferative activity without inducing HSR.[45, 53, 57] Further developments of potent *C*-terminal inhibitors will require advanced structural information of its ATP binding site. Additionally, the binding mode of the inhibitors will have to be well-understood.

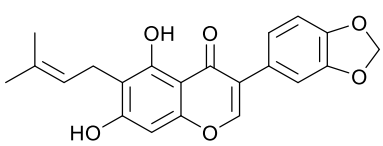

1.28 Derrubone

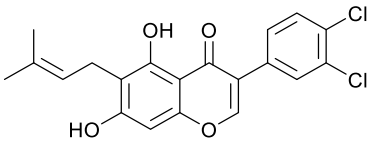

1.30

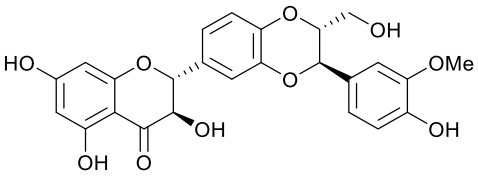

1.29 Silybin

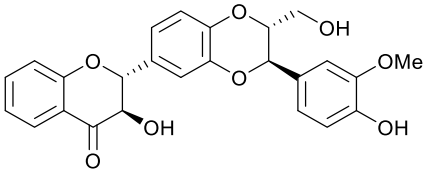

1.31

Figure 1.11: Derrubone (**1.28**) and silybin (**1.29**) derivatives of *C*-terminal HSP90 inhibitors.[26]

1.5.3. HSP90 inhibitors targeting protein-protein interactions

The HSP90 chaperone cycle is facilitated by a series of co-chaperones, including HOP, Cdc37, AHA1 and p23 (**Figure 1.2**), and the disruption of protein-protein interactions (PPI) between HSP90 and these co-chaperones has emerged as an alternative therapeutic strategy towards HSP90 inhibition.[26, 61-63] The disruption of these PPIs results in an incomplete HSP90 chaperone cycle, which subsequently leads to premature oncogenic client protein degradation.[61-63]

The first intermediate complex of the HSP90 chaperone cycle consists of HSP90 and HOP. HOP is a bridging co-chaperone that facilitates client protein folding and maturation through mediating the transfer of partially folded client proteins from HSP70 to HSP90. HOP consists of three TPR domains, TPR1, TPR2A and TPR2B; which are essential for organizing the HSP90-HOP-HSP70 ternary complex (**Figure 1.12**).[32] TPR domains are helical coiled structures formed by loosely conserved 34 amino acids. Crystallographic and biochemical studies have revealed that both HSP70 and HSP90 bind to HOP in a similar nucleotide-dependent manner through the IEEVD and MEEVD motifs found in their C-terminal, respectively. The distinct upstream sequences of the EEVD motifs of the two chaperones allows the TPR domains to be selective; the TPR1 domain selectively binds to HSP70 through the GSGPTIEEVD motif, while the TPR2A domain selectively binds to HSP90 through the DDTSRMEEVD motif.[32]

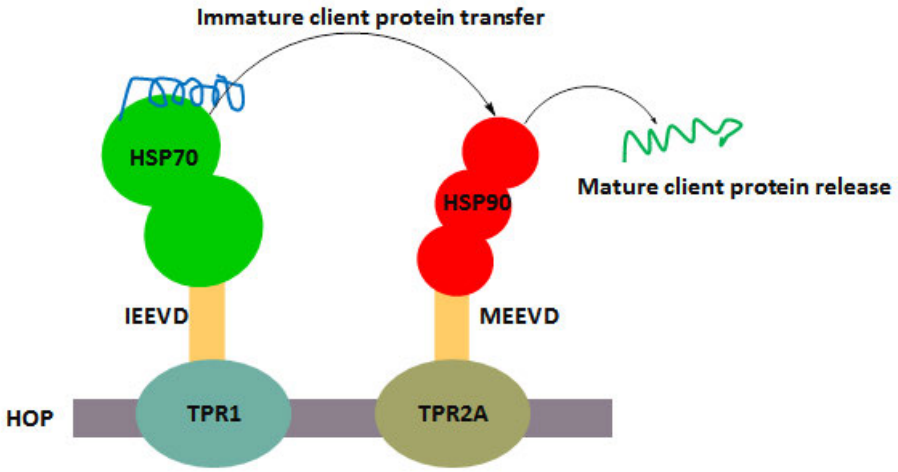

Figure 1.12: The HSP90-HOP-HSP70 ternary complex. Partially folded client proteins are transferred from HSP70to HSP90 through the bridging co-chaperone, HOP. HOP's TPR1 domain selectively binds the IEEVD region of HSP70's *C*-terminal, while the TPR2A domain selectively binds the MEEVD region of HSP90's *C*-terminal. This diagram was redrawn based on that published by Li *et al*..[26]

Inhibiting the interaction between HSP90 and the TPR2A domain of HOP prevents the progression of the chaperone cycle, hence disrupting the HSP90-HOP-HSP70 client protein folding system, subsequently leading to client protein degradation. Various groups have reported designed TPR domains targeted against HSP90-HOP PPI. The first reported TPR domain mimic was CTPR390+.[63] CTPR390+ is a TPR mimic that was reported to have a high binding affinity for the MEEVD region on HSP90's C-terminal in comparison to the native TPR2A domain of HOP. Moreover, CTPR390+ was found to be highly selective for HSP90's MEEVD region over HSP70's IEEVD region.[45, 63] The effect of CTPR390+ was tested using BT474 breast cancer cells, where it disrupted the HSP90-HOP PPI, as a result the HSP90-HOP-HSP70 ternary complex did not form. CTPR390+ displayed antiproliferative activity against the breast cancer cells, correlated to the reduced levels of HSP90-depedent HER-2.[45, 63]

In 2008 six compounds containing a pyrimidotriazinedione structural core were discovered (**Figure 1.13**, **1.32 – 1.37**) as potential HSP90-HOP PPI inhibitors.[61, 62] These compounds competitively bind to the C-terminal of HSP90, thus inhibiting the interaction between the HSP90 and the TPR2A domain. The evaluation of these compounds *in vitro* against the BT474 and SKBR3 cell lines resulted in reduced levels of the oncogene HER2 in a HSP90-dependent manner.[61, 62] The downregulation of oncogene HER2 is significant since it is involved in critical cellular functions that stimulate tumour cell growth, proliferation and survival.

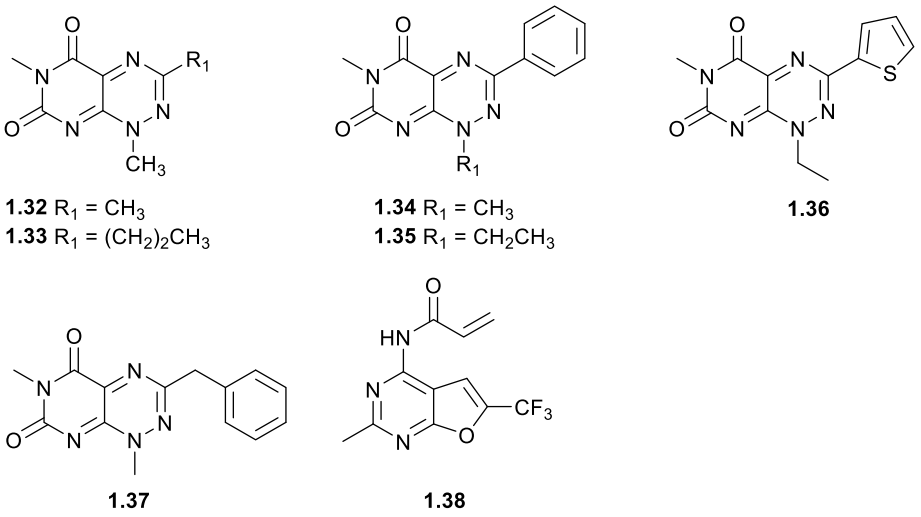

Figure 1.13: Inhibitors targeting HSP90-HOP protein-protein interactions (PPI).[26, 62]

Subsequently, compound **1.33** displayed moderate antiproliferative activity against a series of breast cancer cell lines, including the MDA-MB-231 (IC_{50} = 2.00 µM) and MDA-MB-468 (IC_{50} = 1.75 µM) TNBC cell lines. The specificity of **1.33** was also determined using cell viability assays where it was confirmed that the disruption of HSP90-HOP PPI was at least partially responsible for the observed inhibitory effect of **1.33**.[61, 62] Most notably, these compounds did not induce the pro-survival HSR making them more desirable than the *N*-terminal inhibitors.[26, 45] In 2016, a pyrimidine containing HSP90-HOP PPI inhibitor was discovered (**1.38**, **Figure 1.13**).[26, 64] Rather than directly disrupting the HSP90-HOP interface, **1.38** exerts its inhibitory effects through thiol oxidation of HSP90's cysteine residues using its α,β-unsaturated moiety, hence preventing the formation of the HSP90-HOP-HSP70 ternary

complex leading to client protein proteasomal degradation.[26, 61, 64] Reduced levels of HSP90-dependent client proteins (Bcr-Ab1, Raf-1, Akt and Cdk6) and an increase in HSP70 expression were observed with SKBR3, A431, MCF-7 and SNU-5 cell lines.[26, 45, 61]

Cdc37 is another HSP90 co-chaperone that is currently being targeted for cancer therapeutics. Cdc37 recruits protein kinases to the HSP90 chaperone cycle. Thus, inhibition of HSP90-Cdc37 PPI provides an alternative strategy for kinase driven cancer therapeutics.[61, 62] Additionally, targeting HSP90-AHA1 PPI has also emerged as a potential strategy to inhibit HSP90 activity.[61, 62] Despite the complexity associated with this novel strategy, disrupting interactions between HSP90 and its co-chaperones represents a feasible way for HSP90 inhibition.

1.5.4. Limitations of intracellular HSP90 inhibitors and future perspectives

As discussed above, none of the developed intracellular HSP90 inhibitors have been FDA approved. Despite the promising preclinical results of the distinct classes of *N*-terminal targeted inhibitors, these compounds display various drawbacks during clinical trials, halting their further clinical advancement. In particular, the therapeutic window of *N*-terminal ATP-competitive inhibitors is limited by the activation of the compensatory HSR, triggering the over-expression of HSP70 and other HSPs which facilitate tumour cell rescue, desensitizing them to HSP90 inhibition.[12, 65] Broadly, ocular toxicity, hepatotoxicity, activation of the pro-survival HSR at concentration levels required for client protein degradation and drug resistance are some of the observed limitations with this class of HSP90 inhibitors.[53, 66, 67] Hence, there are continued research efforts towards the development of alternative strategies towards HSP90 inhibition.

Alternatively, researchers have reported that *C*-terminal targeted HSP90 inhibitors provide a potent alternative strategy for cancer therapeutics devoid of the major challenges observed with N-terminal inhibitors.[57] As discussed in section **1.5.2**, a variety of *C*-terminal HSP90 inhibitors have been investigated for cancer treatment and were reported to inhibit HSP90 molecular chaperone function without inducing the HSR.[53, 65] This is a developing area of research with a promising therapeutic

potential for HSP90 inhibition in cancer treatment. Furthermore, the discussion in **1.5.3** highlights the potential of disrupting HSP90-co-chaperone interactions for effective client protein degradation. However, an in-depth understanding of the biology of HSP90 and its co-chaperones is crucial when it comes to novel approaches for targeting HSP90 for cancer therapeutics.[30, 44]

Most notably, due to the lack of well-defined differences between the cytoplasmic HSP90 isoforms, contemporary hypothesis suggests that current HSP90 inhibitors exert their anticancer activity by multitargeting the intracellular and extracellular HSP90. Thus, phenotypic responses to HSP90 inhibition, may be due to their extracellular HSP90 inhibitory function.[30, 68, 69] This therefore suggests that extracellular HSP90 might be the effective target for the developed drugs.[30, 69] Somewhat ironically, contemporary drug design seeks to optimise 'drug-like' properties which typically improve cell permeability, and as a result, restrict access to the extracellular space.

1.6. Extracellular inhibition

Cancer therapeutics have traditionally focused on directly targeting the tumour cell, however, it has become apparent that the tumour microenvironment (TME) is also a potential target.[70, 71] The TME complex structure is made up of, blood vessels, cytokines, distinct cell types such as fibroblasts, immune cells, endothelial cells, adipocytes; and the extracellular matrix (ECM).[71, 72]

1.6.1. The extracellular matrix (ECM)

The ECM is a highly dynamic three-dimensional network, encompassing cells within tissues, composed of secreted proteins such as HSPs, proteoglycans, hyaluronans, collagens, elastins, laminins, fibronectin and matricellular proteins.[71, 73] The ECM is not only structurally important for the TME complex, but it also regulates cellular events at a molecular level that in turn control cell behaviour.[74] Interactions between the ECM components with specific receptors leads to signal transduction into the intracellular environment, generating control of the cytoskeleton, survival, differentiation and gene expression. The three major ECM receptors are integrins, discoidin domain receptors (DDRs) and

CD44.[71, 73] Interaction of the ECM with integrins triggers intracellular signalling which regulates various processes such cell proliferation, invasion, migration, and survival. The cell's biological processes are influenced by both the chemical and physical properties of the ECM and these properties are altered in tumour cells.[73, 74]

Interestingly, extensive alterations are observed in the ECM composition during wound healing and cancer progression.[31, 39] This includes an upregulation of the secreted proteins, which ultimately leads to cancer development and promotes high metastatic ability of tumours. Moreover, ECM alterations are not only limited to cancer cells, with various diseases exhibiting the same phenomenon.[75-81] As a result, ECM-targeted therapeutics provide a potential strategy for the treatment of a variety of human diseases such as asthma,[82] arthritis,[83] and hypertension.[84] For drug development, a better understanding of disease associated ECM composition and related cellular responses is required.[71] Furthermore, differentiation between disease-causing ECM changes and disease-induced ECM changes is necessary for drug development.[75]

Since ECM interactions play a significant role in cancer cell survival and behaviour, the development of ECM-targeted inhibitors presents a promising approach for cancer therapeutics. ECM inhibition can be achieved by either directly targeting the ECM components or by targeting the synthesis, degradation or signalling of the ECM.[75] For example, various tumours have been shown to overexpress HSP90 contributing to a microenvironment that promotes the growth and metastasis of tumour cells.[75]

1.6.2. Extracellular HSP90

Various tumours such as breast, prostate and colon have been reported to constitutively secrete HSP90α.[31, 85] Alternatively, the discovery of the role of extracellular HSP90 in cancer progression has offered an alternative strategy for cancer therapeutics.[85]

Although HSP90 was originally reported to be exclusively intracellular to normal cells, cancer cells and other cells of the TME, it has become apparent that HSP90 also has biological properties in the ECM

which are independent of its chaperone functions.[27, 53, 66] For example, in tumour cells secreted HSP90 plays a significant role in tissue invasion and metastasis, whereas normal cells secrete HSP90 mainly for tissue repair.[66, 85] The observation that HSP90 has multiple cellular locations and more than one cellular function led to its designation as a "moonlighting protein". Moonlighting proteins are proteins capable of being secreted outside the cell and interact with different cell types to activate different signalling pathways that stimulate a range of biological effects.[13]

Extracellular HSP90 has been reported to interact with multiple neighbouring cell-surface client proteins, such as matrix metalloproteinases (MMP-2 and MMP-9), the LDL receptor-related protein-1 (LRP-1), HER-2 tyrosine kinase receptor, LOX1, SREC-I and FEEL-1.[27, 85] Interaction of extracellular HSP90 with these surface receptors has been shown to play a critical role in cancer progression and ultimately metastasis.[86] For example, several groups have reported that extracellular HSP90 binds and activates MMP-2, enhancing tumour cells migration and invasion of neighbouring tissues.[27, 85] Furthermore, extracellular HSP90 has been shown to promote cancer cell migration/motility through interaction with LRP-1.[31, 67]

1.6.3. Extracellular HSP90 inhibition

Traditionally, cancer therapeutics targeting HSP90 have focused on its intracellular functions as the centre of *in vitro* and *in vivo* investigations.[27, 66] Despite early promise, intracellular HSP90-targeted cancer therapeutics have displayed various challenges, resulting in their limited progress through clinical trials. These include complexity associated with low selectivity between HSP90 isoforms i.e., HSP90α, HSP90β, and extracellular HSP90.[26, 30, 86]

Similarly, to the intracellular environment, environmental stress signals such as hypoxia, heat, ultraviolet (UV) light, reactive oxygen species (ROS) and inflammatory cytokines, stimulate the HSR. This in turn results in the secretion of HSP90α and HSP90β.[31, 67] Hypoxia-inducible factor-1alpha (HIF-1α) has been identified as a key regulator of HSP90α secretion with HIF-1α overexpression observed in approximately 40% of human tumours.[67] Environmental stresses induce HSP90α to migrate into the

intraluminal vesicles called exosomes and are subsequently released to the extracellular space via the exosome protein secretory pathway.[31, 67] Following the open questions posed by Picard *et al*. highlighting the lack of intensive understanding as to why tumour cells are more sensitive to HSP90 inhibitors and why these inhibitors are selective to certain cancers;[87] Li *et al*. suggested that since the main difference between tumour and normal cells is HSP90 secretion, tumour cells are more sensitive to HSP90 inhibitors due to their interactions with extracellular HSP90, and thus HSP90 inhibitors are selectively targeted to cancer cells that constitutively secrete HSP90.[30] This implied that directly targeting extracellular HSP90 presents a more selective cancer therapeutic strategy with fewer toxicities.[30, 86] Furthermore, recent data suggest that the efficacy of HSP90 inhibitors is at least partially linked to inhibition of its extracellular roles, and has thus been identified as a potential target for novel cancer therapeutics.[30, 69]

Different strategies have been developed for targeting extracellular HSP90, with monoclonal antibodies and small molecule inhibitors being the most documented.[27] Monoclonal antibodies are commonly targeted at secreted proteins and cell-surface-bound proteins of the ECM, where they exert their therapeutic activity *via* different mechanisms. One such mechanism is the disruption of target-ligand interactions thus impairing the signalling pathways required for tumour cell survival.[88] As previously stated, MMP2 is an extracellular HSP90 client protein reported to be overexpressed and active in numerous human cancers; and the interaction of HSP90 with MMP2 is reported to promote cancer cell invasion and metastasis in MDAMB45 breast cancer cell lines.[85] Stellas *et al*. provided evidence that disrupting the interaction between extracellular HSP90 and the MMP2 client protein inhibits the invasiveness of MDA-MB-45 breast cancer cells.[89] The monoclonal antibody, 4C5 was found to inhibit tumour cell invasion *in vitro* by disrupting the interaction between extracellular HSP90 and MMP2; thus inhibiting the maturation of MMP2, which is required for tumour cell invasion. Furthermore, mAb 4C5 was found to prevent the formation of metastatic tumour cell deposits *in vivo*.[89]

Dong *et al.*[90] conducted a study where they reported that the triple negative breast cancer cell line, MDA-MB-231, secreted HSP90α to survive hypoxia-induced apoptosis, and its direct inhibition led to enhanced tumour cell death.[90] During their investigation, increased levels of hypoxia-induced cell death was observed with HSP90α-knockout cells as compared to their native counterparts. Interestingly, they reported that the depletion of extracellular HSP90, and not intracellular HSP90, resulted in the increased hypoxia-triggered cell death. Furthermore, the direct inhibition of extracellular HSP90 using 1G6-D7, a cell-impermeable monoclonal antibody targeted at the F-5 fragment, blocked tumour cell invasion.[31, 90, 91] As previously mentioned, LRP-1 is a critical client protein for extracellular HSP90, promoting tumour cell survival under hypoxia. 1G6-D7 exerted its activity by downregulating LRP-1, thus, subsequently inhibiting the function of extracellular HSP90 on tumour formation and growth.[31, 91] This data further suggests that extracellular HSP90 is critical for tumour cell survival, thus, it is a viable pharmacological target for cancer therapeutics. Hence, there is continued interest towards the development of cell-impermeable HSP90 inhibitors which should not affect the *N*-terminal ATPase chaperone functions which normally results in cytotoxicity.[27, 86, 92]

Unlike monoclonal antibodies which are specific for the ECM, small molecule inhibitors can effectively target both extracellular and intracellular proteins. Classical medicinal chemistry optimisation strategies aim for physicochemical properties, which tend to enhance cellular penetration, which in this specific context would reduce efficacy of HSP90 inhibitors. Alteration of small molecule inhibitors to disproportionality remain in the extracellular environment, is commonly afforded through the introduction of polar moieties to the scaffold, with the aim of inhibiting cell-permeability, whilst retaining the functional groups essential for target binding at the active site.

Eustace *et al*. performed a surface targeted proteomic screen to determine proteins implicated in tumour progression and this study identified extracellular HSP90 as an essential component for tumour invasion in fibrosarcoma and breast cancer cell lines.[85] MMP2 is a cell-surface receptor characteristic of tumour invasion and metastasis.[85, 93] Extracellular HSP90 regulates MMP2 pro-

invasive activity, thus its inhibition directly affects MMP2 activity, resulting in the loss of invasiveness.[85] Interestingly, inhibition of extracellular HSP90 using a cell-impermeable analogue of **1.1** (solid-phase immobilized geldanamycin derivative), decreased tumour cell invasiveness without interfering with the intracellular HSP90 functions.[85] This further validated the critical involvement of extracellular HSP90 in tumour progression, and further identified a new target for cancer treatment. Furthermore, selective inhibition of extracellular HSP90 presented a novel therapeutic strategy with the potential of overcoming challenges experienced with intracellular HSP90 inhibitors.[85]

Tsutsumi *et al.* modified the dimethyl amino group of the intracellular HSP90 inhibitor **1.3** to a polar *N*-oxide (coloured in red) to get the cell-impermeable HSP90 inhibitor DMAG-*N*-Oxide (**1.39**, **Figure 1.14**).[27, 30, 92] Compound **1.39** displayed potent anti-invasive activity in various cancer cells, inhibiting tumour cell migration and invasion *in vitro*. *In vivo*, **1.39** displayed anti-metastatic activity in the murine melanoma model, significantly suppressing lung colonization of the cells in mice.[27, 67] Compound **1.39** spared the intracellular functions of HSP90, *i.e.* the expression levels of HSP90 client proteins such as Akt and Raf-1 were not reduced.[27, 30]

STA-12-7191 (**1.40**), a biotinylated analogue of **1.6**, is another reported extracellular HSP90 inhibitor.[27] Similar to **1.39**, **1.40** did not affect the intracellular functions of HSP90, as confirmed by the poor activity in HER-2 degradation. Compound **1.40** displayed anti-metastatic activity in MDA-MB-231 and A172 GBM cancer cell lines, inhibiting migration due to its ability to bind extracellular HSP90.[27] Most interestingly this novel strategy has been reported to not induce the HSR. Moreover, inhibiting extracellular HSP90 could potentially overcome toxicities observed with intracellular HSP90 inhibitors, as they have been reported to be due to the disruption of normal, critical intracellular functions.[94]

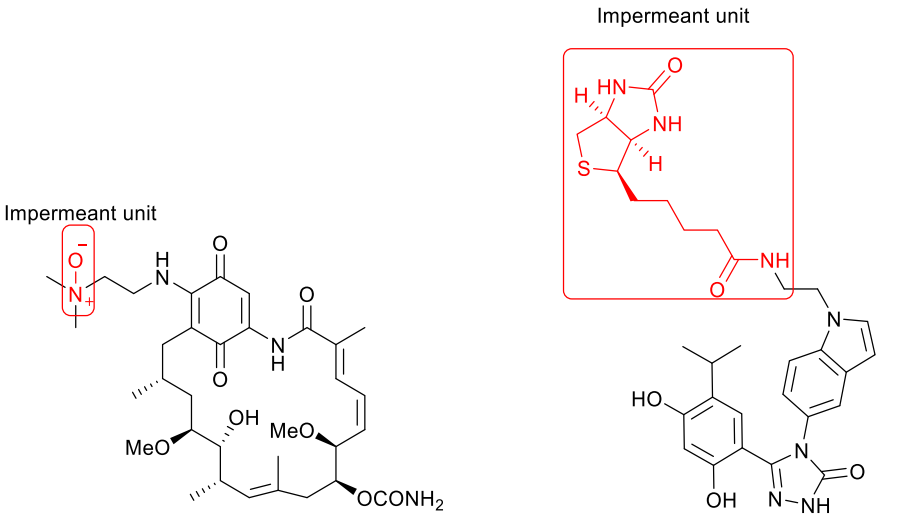

1.39 DMAG-N-Oxide

1.40 STA-12-7191

Figure 1.14: Cell-impermeable HSP90 inhibitors. Compound **1.39** is a polar analogue of DMAG (**1.3**), while **1.40** is a biotinylated analogue of Ganetespib (**1.6**).[27]

Further evidence for the involvement of extracellular HSP90 in metastatic progression, hence the significance of its inhibition for cancer therapeutics, was demonstrated by Hughes *et al.*[54] and Barrott *et al*.[95] in their related studies. A chemoproteomic profiling of HSP90 done by Hughes *et al.* focused on the development of a HSP90 selective affinity resin with a cleavable linker using a known potent and selective HSP90 inhibitor **1.14** discovered by Huang *et al*..[52, 54] Significantly, this study revealed that tethering at position 3' of **1.14** with a polyethylene glycol (PEG) related 19-atom linker (**1.41**, **Figure 1.15**) increased the binding specificity of the compound towards HSP90 over Grp94 and Trap-1.[54, 95] In their subsequent work, HSP90 inhibitors tethered at the same position to fluorophores selectively targeted and captured extracellular HSP90, and they were used to detect breast cancer malignancies through non-invasive imaging.[54, 95]

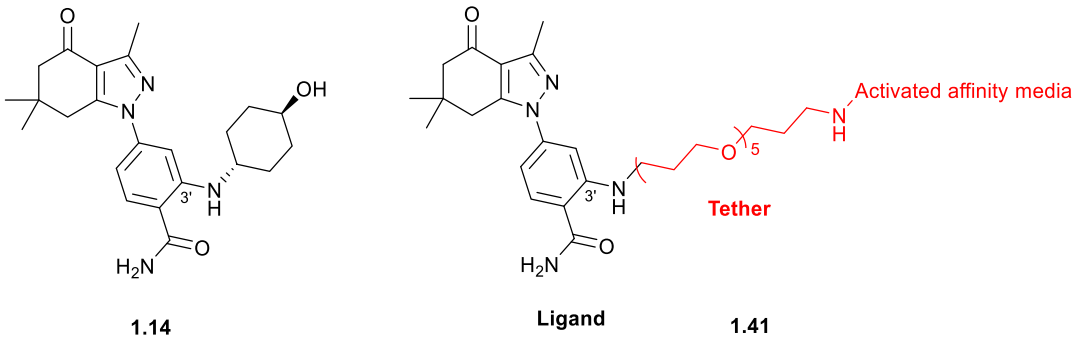

Figure 1.15: Structure of affinity resin **1.41** developed for the selective recovery of HSP90. Resin **1.41** was prepared by tethering HSP90 inhibitor **1.14** at position 3' with a polyethylene glycol related cleavable linker.

Collectively, these studies highlighted the essential role extracellular HSP90 plays in cancer progression and the viability of its inhibition using cell-impermeable compounds, which would subsequently result in the degradation of its oncogenic client proteins. Ultimately, as will be discussed in the next section, this knowledge provided the critical basis of this project. As previously mentioned, unintentional inhibition of extracellular HSP90 has been hypothesised to be the main mode of action of the developed HSP90 inhibitors. Thus, the current hypothesis is that cancer patients could benefit from inhibitors which selectively target extracellular HSP90.[95] Important to note is that this is still an unclear developing area of research, and intensive research is still required to fully understand the function and role of extracellular HSP90 in cancer progression.

1.7. Aims of the project

While inhibition of the HSP90 has promise for the development of cancer therapies, the pro-survival HSR induction and various toxicities observed with intracellular *N*-terminal HSP90 inhibitors have greatly limited their clinical development. Extracellular inhibition has emerged as an alternative strategy for the expansion of druggable chemical space, devoid of many of the limitations associated with traditional drug discovery. It is believed that intracellular HSP90 inhibitors first encounter extracellular HSP90 prior to penetrating into the cell to perform their inhibitory functions. The introduction of polar alkyl chains has been shown to be a valid method preventing active compounds from penetrating the cell membrane, thus relegating them to the extracellular matrix.

The study done by Hughes *et al*. provided the basis for this project, where it revealed that tethering at position 3' of **1.14** with a polyethylene glycol (PEG) related 19-atom linker increased the binding specificity of the compound towards HSP90 over Grp94 and Trap-1.[54] In addition, their compound libraries provide a position for chemical modification of compound **1.14**, which does not disrupt HSP90 binding.

On that basis, it is proposed that the introduction of polar alkyl chains such as sulphonic acid (**1.42** and **1.43**) and phosphonic acid (**1.44** and **1.45**) at the indicated positions of **1.11** and **1.14**, respectively, would result in cell-impermeable HSP90 inhibitors (**Figure 1.16**).

The aim of the work described in this thesis is to adapt well characterised HSP90 inhibitors **1.11** and **1.14** in order to develop extracellular HSP90 inhibitors to exploit the therapeutic potential of HSP0 inhibition, whilst circumventing the shortfalls discussed in the previous sections. This will provide an alternative strategy for novel HSP90-targeted cancer therapeutics, as well as provide new insight into changes to cellular processes as a result of extracellular HSP90 inhibition of intracellular degradation.

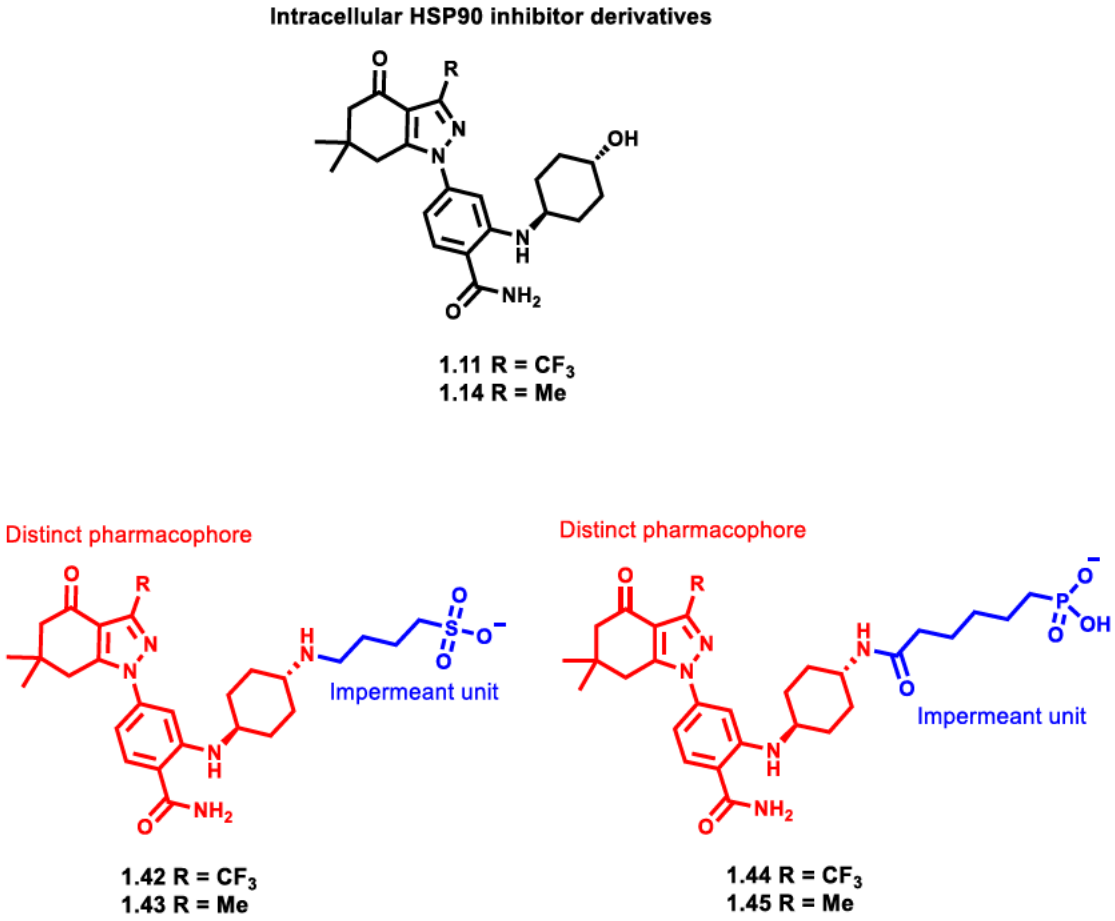

Figure 1.16: Chemical structures representative of the desired extracellular HSP90 inhibitors.

2. CHAPTER 2: REVIEW OF PREVIOUS SYNTHETIC METHODS

2.1. Synthetic planning

We reasoned that the desired extracellular inhibitors **2.1** - **2.4** could be divided into two distinct regions namely the HSP90 inhibitory pharmacophore and the cell entry inhibitory moiety (**Scheme 2.1**). To this end, our first 'retrosynthetic' disconnect was placed between these two regions. While HSP90 inhibitors **1.11** and **1.14**, feature a 4-aminocyclohexan-1-ol moiety, Taldone *et al.* showed that a nitrogen is tolerated in this position, with their superior nucleophilicity making them more synthetically tractable.[96] Accordingly, based on the reactivity of the free amine compounds **2.5** and **2.6**, as well as the commercial availability of a 4-bromobutane-1-sulfonic acid (**2.7**) and 6-phosphonohexanoic acid (**2.8**), we envisioned generating compounds **2.1** and **2.2** through nucleophilic substitution of the alkyl halide (**2.7**), and compounds **2.3** and **2.4**, through amide formation, with the acid (**2.8**) respectively.

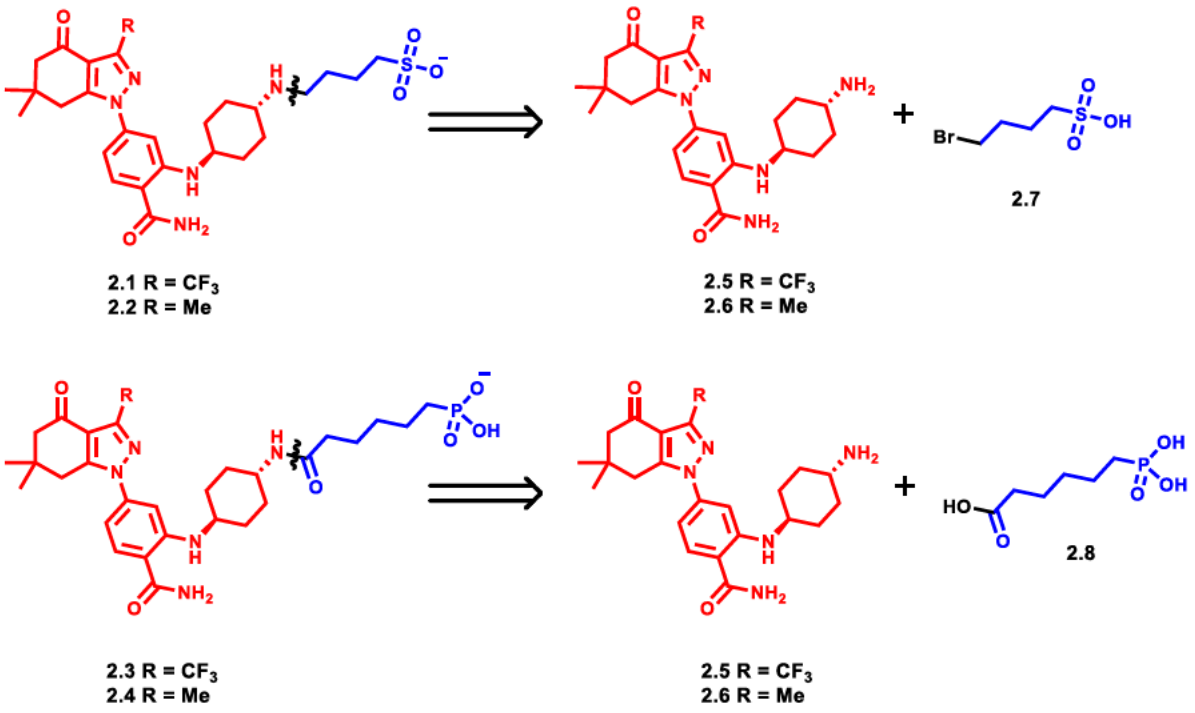

Scheme 2.1: Distinct pharmacophore (red) and cell-entry inhibitor region (blue) of the extracellular inhibitors, showing putative retrosynthetic break

2.1.1. Overview of the synthesis of HSP90 inhibitor tetrahydroindazolones

Several synthetic procedures toward the SNX class of HSP90 inhibitors have been published,[52, 54, 96-98] all of which take advantage of previously reported methodology. Broadly speaking, and as touched upon in **Figure 2.1**, this requires the synthesis of a tetrahydroindazolone ring and the incorporation of a phenyl region, which is suitably functionalised to facilitate the incorporation of the aminocylohexane containing side chain. These reported methods have inherent advantages and disadvantages with respect to the number of synthetic steps, complexity of each step, and regioselectivity. Therefore, while our chosen scaffold for modification differs slightly from the reported **SNX-2112** the numerous similarities render them important considerations for the synthesis of our target compounds. These individual methods will be discussed below, and critically evaluated at the end of this chapter

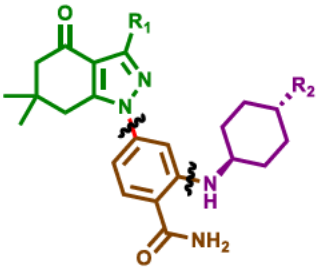

2.5 $R_1 = CF_3$, $R_2 = NH_2$
2.6 $R_1 = Me$, $R_2 = NH_2$
SNX-2112 $R_1 = CF_3$, $R_2 = OH$

Figure 2.1: The main areas for modification of **SNX-2112** towards our desired HSP90 inhibitory pharmacophore. Similar to the previously reported procedure, the two synthetic breaks would be derived from a suitably functionalized benzonitrile and the R_1 substituent could either be a trifluoromethyl or a methyl group. Dissimilarly, our target compounds consist of an amine functional group as the R_2 substituent, and not the hydroxyl group of **SNX-2112**.

2.1.1.1. Indazolone ring synthesis

Indazolones and related indazoles are considered privileged scaffolds in medicinal chemistry, and feature in several biologically active compounds.[52, 97, 99, 100] As such, various procedures have been investigated for their synthesis.[52, 54, 98-101]

In order to carry out their in-depth structural assessment study, Claramunt *et al.* required access to several tetrahydroindazolones (**2.9** – **2.12**, **Scheme 2.2**). Compounds **2.9** and **2.10**, which did not feature a C-3 substituent, were generated in two steps from either 1,3-cyclohexanedione (**2.13**) or dimedone (**2.14**), *via* the dimethylaminomethylenes **2.15** and **2.16**. The key cyclization step occurred with hydrazine hydrate in the presence of acetic acid in butanol.[99] Alteration of the starting material to a 2-acetyldimedone derivative **2.17** and **2.18**, facilitated the introduction of a methyl at the indazolone C-3 position, with the nitrogen atoms again being incorporated *via* hydrazine hydrate mediated cyclization to afford **2.11** and **2.12**. While in this instance, the cyclization step occurred in tetrahydrofuran (THF), in the absence of additional acid, several other methods have reported the same transformation in ethanol.[98, 102, 103] While 2-acetyldimedone derivatives, **2.17** and **2.18** are sporadically available from local vendors, there are several reported synthetic procedures for the selective acetylation of dimedone, which will be discussed later in this thesis.

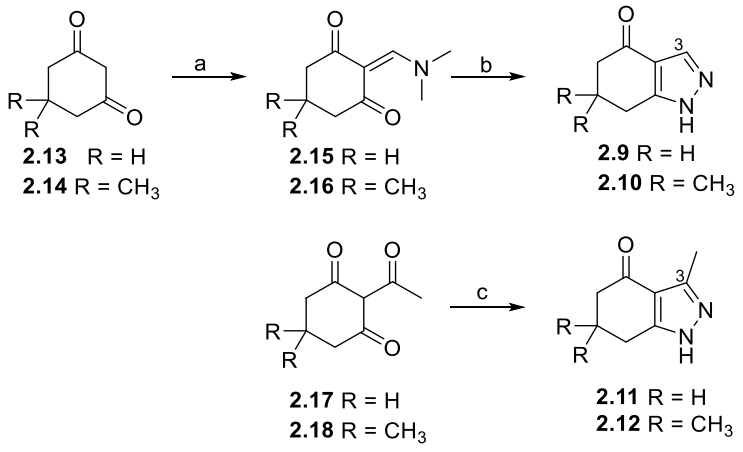

Scheme 2.2: Tetrahydroindazolone condensation as reported by Claramunt *et al*.[99]

Reagents and conditions: a) $HC(OCH_3)_2N(CH_3)_2$, reflux, 1 h; b) H_2NNH_2, *n*-BuOH, AcOH, reflux, 4 h; c) H_2NNH_2, THF, reflux, 2 h

In a similar approach, compound **2.12** was generated as a by-product, from solid phase peptide synthesis, where 2-acetyldimedone **2.18** served as an amine protecting group (**Scheme 2.3 step a**), and could be removed with hydrazine in *N*,*N*-dimethylformamide (DMF) (**step b**).[104]

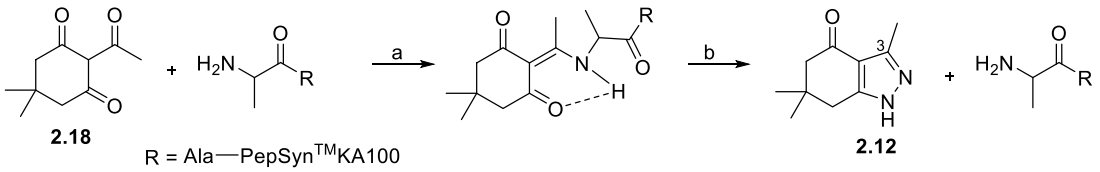

Scheme 2.3: Bycroft *et al*.'s tetrahydroindazolone condensation during peptide synthesis[104]

Reagents and conditions: b) 2.0% v/v hydrazine, DMF, 3 min.

Anderson-McKay *et al.* reported a study aimed at synthesizing **2.19** *via* a molybdenum hexacarbonyl promoted ring opening of isoxazole **2.20** (**Scheme 2.4**). Surprisingly, this reaction led to the formation of a mixture of unexpected products, which included our compound of interest **2.12**. The reaction of **2.18** with hydroxylamine over two steps afforded **2.20**, **Scheme 2.4(a)**, which was subsequently treated with molybdenum hexacarbonyl in the presence of water and acetonitrile to afford the corresponding intermediate **2.19**.

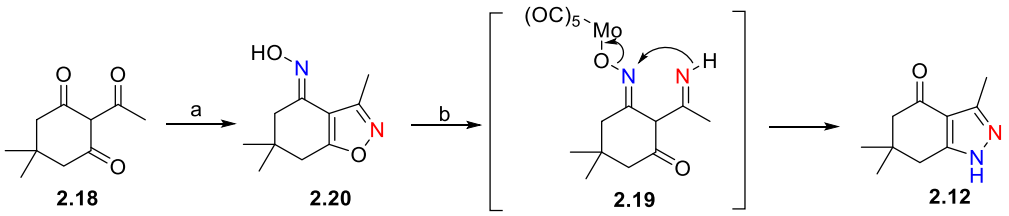

Scheme 2.4: Anderson-McKay *et al.*'s isoxazole mediated tetrahydroindazolone condensation[105]

Reagents and conditions: a) NH_2OH, Benzene; b) $Mo(OC)_6$, $MeCN/H_2O$, reflux, 2 h

The proposed mechanism for formation of **2.12** involves the complexation of molybdenum hexacarbonyl with the oxime oxygen atom to promote the reductive N-O bond cleavage of **2.19**, and

the intramolecular cyclisation *via* the nucleophilic attack of the oxime nitrogen atom by the imine nitrogen atom to yield **2.12**.[105]

Following a slight alteration of the approaches followed by Claramunt *et al*., *N*-phenyl substituted tetrahydroindazolones were synthesised by the cyclization of dimethylaminomethylene (**2.16**)[100] or 2-acetyldimedone (**2.18**)[101] with 1-phenylhydrazine under acidic conditions to afford the corresponding tetrahydroindazolones **2.21** and **2.22**, respectively (**Scheme 2.5**).

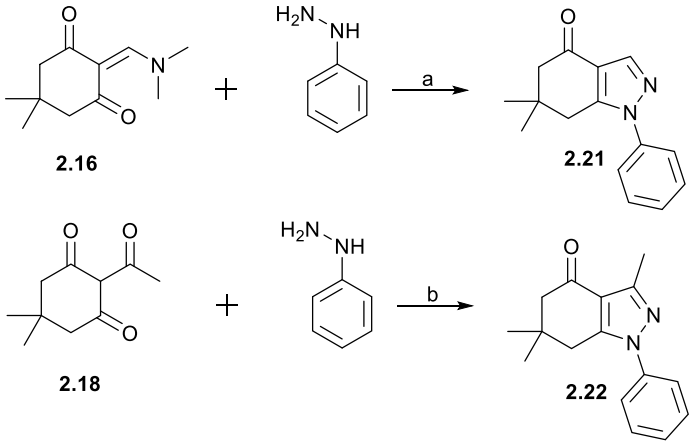

Scheme 2.5: Synthesis of *N*-phenyl substituted tetrahydroindazolones

Reagents and conditions: a) BuOH, AcOH, reflux, 2h[100]; b) EtOH, conc. HCl, r.t., overnight[101]

Due to the desire to install a trifluoromethyl moiety at the C-3 position of indazolone (**2.23**), as well as reported instability of the putative 2-trifluoroacetyl dimedone, Huang *et al.* developed a method, starting with unsubstituted dimedone **2.14**, where the requisite nitrogen atoms were introduced in the form of a tosylhydrazide in refluxing toluene to give **2.24**. This was followed by a one pot, two step, trifluoro acetylation, cyclisation and detosylation to generate the desired trifluoromethylated tetrahydroindazolone (**2.23**, **Scheme 2.6**).[52]

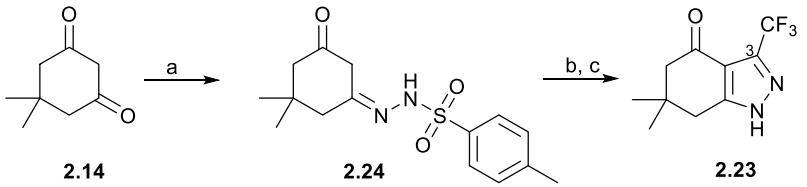

Scheme 2.6: Tosyl hydrazone mediated tetrahydroindazolone condensation[52]

Reagents and conditions: a) $TsNH_2NH_2$, cat. *p*-TsOH, toluene, reflux; b) $(CF_3CO)_2O$, THF, TEA, 55 °C, 2 h; c) NaOH, MeOH, H_2O, r.t., 3 h

2.1.1.2. Synthesis of tetrahydroindazolone containing HSP90 inhibitors

Access to the tetrahydroindazolone class of HSP90 inhibitors has seen several related but slightly divergent synthetic methodologies being employed. The following section will briefly describe them, and will be followed by a critical analysis.

For their synthesis of compound **2.25** (**Scheme 2.7**), Huang *et al*. followed a method similar to that described in **Scheme 2.5**, which took advantage of orders of reactivity between aryl fluorine and bromine. Here the requisite 2-bromo-4-hydrazinylbenzonitrile (**2.26**) was synthesised *via* selective nucleophilic aromatic substitution of 2-bromo-4-fluorobenzonitrile (**2.27**) with hydrazine in anhydrous THF (**step a**) and subsequently cyclised with 2-acetyldimedone **2.18** in the presence of acetic acid in ethanol in a microwave reactor at 150 °C to yield phenyl tetrahydroindazolone **2.28** (**step b**). Their last step was a one pot, two-step reaction where the amino cyclohexanol moiety was installed under modified Buchwald-Hartwig conditions (**step c**) followed by nitrile hydrolysis to generate the primary amide **2.25** (**step d**).

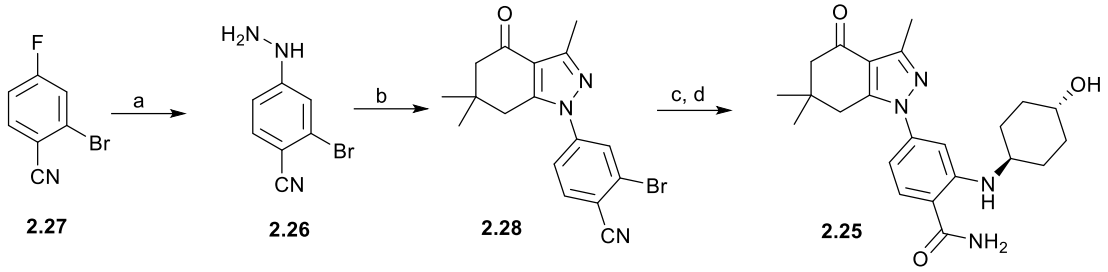

Scheme 2.7: Phenyl hydrazine mediated synthesis of **2.25**[52]

Reagents and conditions: a) NH_2NH_2, anhy. THF, r.t., 16 h; b) 2-acetyl dimedone **2.18**, EtOH, AcOH, 150 °C, microwave, 15 min.; c) *trans*-4-aminocyclohexanol, $Pd(OAc)_2$, DPPF, NaO*t*Bu, toluene, 170 °C, microwave, 3 h; d) 30% H_2O_2, 1 M NaOH, EtOH, DMSO, r.t.

Due to the reported poor stability of the trifluoromethyl analogue of **2.18** an alternative route was developed for the synthesis of **SNX-2112**, which again exploited orders of reactivity between aromatic fluorine and bromine (**Scheme 2.8**). Tetrahydroindazolone **2.23** was synthesized *via* the tosyl hydrazone mediated procedure (**Scheme 2.6**) and subsequently coupled with 2-bromo-4-fluorobenzonitrile **2.27** in a suspension of sodium hydride in dimethyl sulfoxide (DMSO) (**Scheme 2.8(a)**). The final coupling reaction of **2.29** and amino cyclohexanol, and the subsequent nitrile hydrolysis, was performed through similar reaction conditions as described above in **Scheme 2.7** (**c, d**).

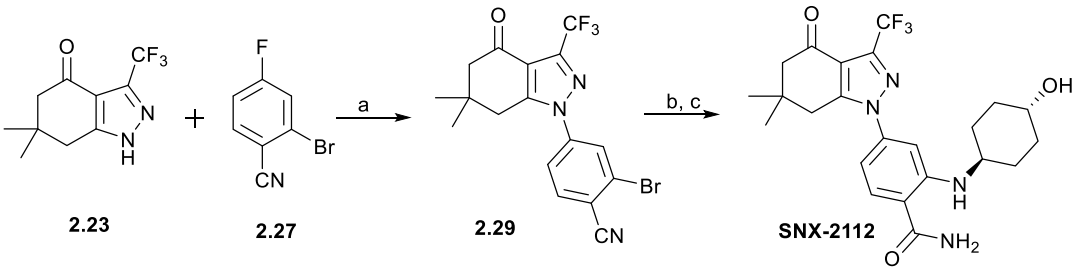

Scheme 2.8: Phenyl hydrazine mediated synthesis of **SNX-2112**[52]

Reagents and conditions: a) NaH, anhy. DMSO, 45 °C, 23 h ; b) *trans*-4-aminocyclohexanol, $Pd(OAc)_2$, DPPF, NaO*t*Bu, toluene, 170 °C, microwave, 3 h; c) 30% H_2O_2, 1 M NaOH, EtOH, DMSO, r.t.

With the goal of developing a highly selective HSP90 affinity probe, which incorporated compound **2.25** [54] Hughes *et al*. deviated from the approach employed by Huang *et al*., where in order to access a highly reactive centre for the attachment of amino cyclohexanol and various other linkers, they synthesised the fluorine analogue (**2.30**, **Scheme 2.9**). Accordingly, 2,4-difluorobenzonitrile **2.31** was reacted with hydrazine hydrate in methanol (MeOH) to give the phenylhydrazine compounds, **2.32** and **2.33**, as a mixture of regioisomers (**Scheme 2.9a**). The subsequent condensation of the regioisomeric mixture with 2-acetyldimedone **2.18** in MeOH in the presence of acetic acid expectedly afforded a mixture of compounds **2.30** and **2.34**, which were separated by column chromatography (**step b**). The amino cyclohexanol was easily introduced following a 30 minute procedure under basic conditions in DMSO at 90 °C and the subsequent nitrile hydrolysis was done using a procedure similar to the one described by Huang *et al*. (**Scheme 2.9c, d**).

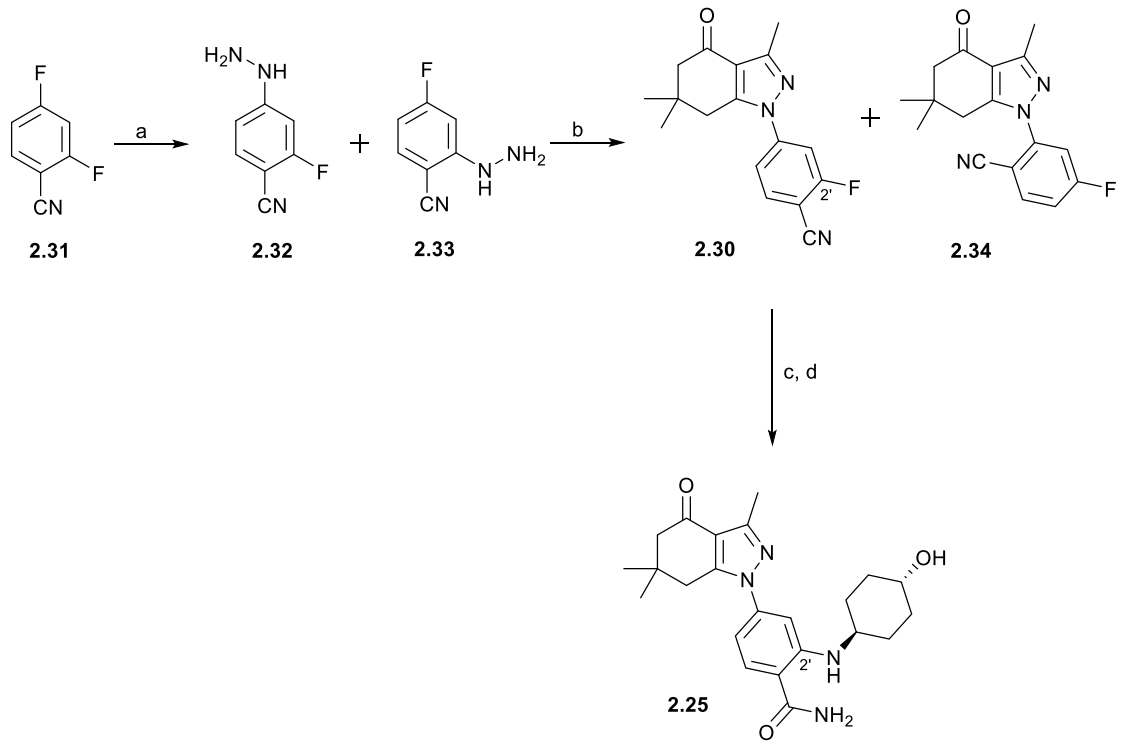

Scheme 2.9: Phenyl hydrazine mediated synthesis of **2.25** as reported by Hughes *et al*.[54]

Reagents and conditions: a) $H_2O.NH_2NH_2$, MeOH, r.t., 16 h; b) 2-acetyl dimedone **2.18**, MeOH, AcOH, r.t., 3 d.; c) *trans*-4-aminocyclohexanol, DIPEA, DMSO, 90 °C, 30 min.; d) EtOH, NaOH, 30% H_2O_2, H_2O, 90 °C - r.t., overnight

2.1.2. Critical analysis of the synthetic routes

The related syntheses of tetrahydroindazolone HSP90 inhibitors, all attempt to balance reactivity (or simplicity of a reaction), with regioselectivity and reaction efficiency. In a broad sense, the synthesis of tetrahydroindazolone HSP90 inhibitors and by extension, our desired intermediates (**2.5 and 2.6**) requires either the formation of a tetrahydroindazolone ring, followed by functionalisation with a decorated phenyl ring (**Scheme 2.10, Pathway A**), or the generation of a suitably functionalised phenyl hydrazine, which can be cyclised with dimedone analogues **2.18** and **2.35** (**Pathway B**). While similarities between these pathways exist, they each have their own potential drawbacks, which will be discussed below. Furthermore, the point at which both of these pathways converge is during the coupling of the aminocyclohexane moiety, where the presence of a fluorine (**2.30**, **2.36**), facilitates a facile substitution reaction, under basic conditions.[54, 98] While nucleophilic aromatic substitution of a bromine (**2.28** and **2.29**), requires more complex reaction conditions, including the use of expensive and comparatively sensitive palladium catalysts.[52, 96] While superficially, this would imply that synthesis of **2.30**, **2.36** is desirable, the presence of the aromatic fluorine for the coupling reaction, requires sacrifice with respect to regioselectivity, and reaction efficiency in the preparation of either phenyl hydrazine **2.32**, or the coupling of **2.31** with **2.12** and **2.23** respectively. Therefore, the key deviations in these reaction pathways, is linked to the reactivity surrounding the aromatic rings **2.27** and **2.31**.

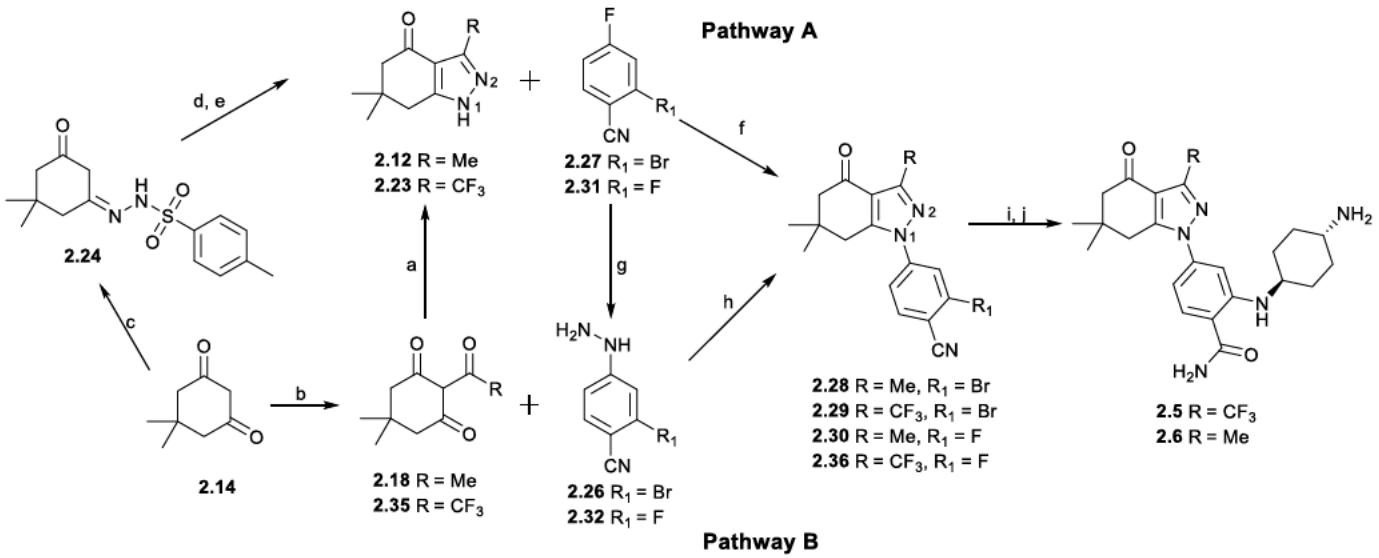

Scheme 2.10: Possible synthetic routes towards the desired scaffolds **2.5** and **2.6**:

Reagents and conditions: a) **2.12**: H_2NNH_2, THF, reflux, 2 h, 63%[99] or $H_2O.H_2NNH_2$, EtOH, r.t., overnight, 92%[98]; b) **2.18**: $(CH_3CO)_2O$, DMAP, DIPEA, DCM, r.t., 24 h[54] or CH_3COCl, TEA, MeCN, 55 °C, 3 h, 95%[98], **2.35**: Trifluoroacetic anhydride, Imidizole, $CHCl_3$, 0 °C - r.t, 45 min., 78%[106]; c) $TsNH_2NH_2$, cat. *p*-TsOH, toluene, reflux, 93%[52]; d) $(CF_3CO)_2O$, THF, TEA, 55 °C, 2 h[52]; e) NaOH, MeOH, H_2O, r.t., 3 h, 41%[52]; f) **2.29**: **2.27**, NaH, anhy. DMSO, 45 °C, 23 h, 63%[52], **2.30**: **2.31**, K_2CO_3, DMSO, r.t., overnight, 50%[98]; g) **2.26**: NH_2NH_2, anhy. THF, r.t., 16 h, 87.2%[52] or **2.32**: $H_2O.NH_2NH_2$, MeOH, r.t., 16 h[54]; h) **2.28**: EtOH, AcOH, 150 °C, microwave, 15 min., 89%[52] or **2.30**: MeOH, AcOH, r.t., 3 d., 49%[54]; (i) *trans*-4-aminocyclohexanol, $Pd(OAc)_2$, DPPF, NaO*t*Bu, toluene, 170 °C, microwave, 3 h[52]; j) 30% H_2O_2, 1 M NaOH, EtOH, DMSO, r.t.[52] or i) *trans*-4-aminocyclohexanol, DIPEA, DMSO, 90 °C, 30 min.[54]; j) EtOH, NaOH, 30% H_2O_2, H_2O, 90 °C - r.t., overnight[54]

Pathway A

It is important to note that despite the reported selectivity of arylation at the tetrahydroindazolone *N*-1 position,[96] this route introduced the possibility of the formation of the undesired *N*-2 arylated isomer as observed by Duan *et al.* (**Figure 2.2**).[107] In addition to reaction inefficiency, the likely similarities in the ^{1}H and ^{13}C NMR spectra of *N*-1 and *N*-2, arylated regioisomers, as well as a lack of suitably proximal protons and carbons for heteronuclear multiple bond correlation (HMBC) signals to be measured, the unambiguous assignment of each regioisomers would likely prove challenging.

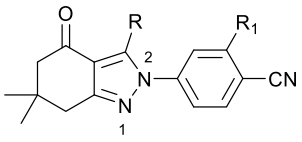

Figure 2.2: Undesired *N*-2 arylated isomer

In addition, generation of a fluorinated aryl tetrahydroindazolone analogue such as compound **2.30** and **2.36**, would require reaction with 2,4-difluorobenzonitrile **2.31.** The relative positioning of the nitrile moiety provides no significant alteration to the electronic environment of each fluorine, rendering them reactively indistinguishable. Therefore, while this approach may provide downstream advantages with respect to amine coupling, as demonstrated by Hughes *et al.*[54] it results in a mixture of regioisomers **2.30** and **2.34** (**Scheme 2.11**). In addition, the presence of two substitution susceptible groups opens the possibly of generating tetrahydroindazolone 'dimers' all of which negatively impact the efficiency of the reaction (**2.37**, **Scheme 2.11**).

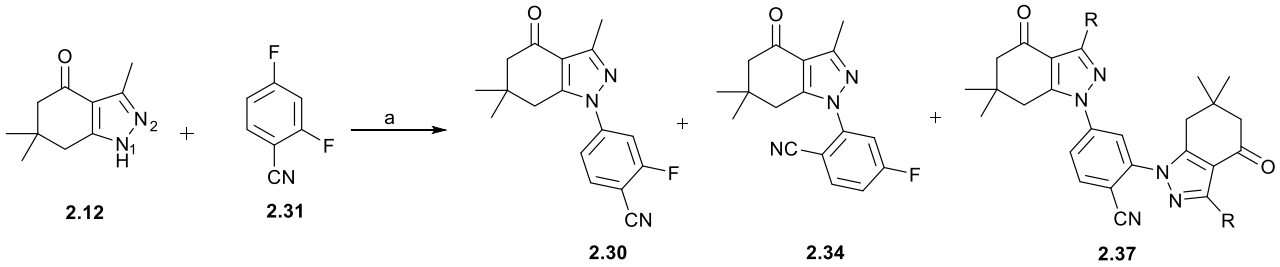

Scheme 2.11: Possible products from the *N*-arylation of **2.12** by 2,4-difluorobenzonitrile **2.31**:

Reagents and conditions: a) K_2CO_3, DMSO, r.t., overnight

Pathway B

Several of the shortcomings highlighted in **Pathway A**, could theoretically be overcome through the phenylhydrazine mediated procedure (**Pathway B**). However, the report of Huang *et al*. suggests that acyl dimedone (**2.35**, **Scheme 2.10 step a**), was not stable, which therefore precludes the formation of **2.29** and **2.36** via **Pathway B**.

Synthesis of bromine containing phenylhydrazine **2.26**, could be generated following well established reaction conditions, however, it does require the addition of excess hydrazine to prevent the formation of significant quantities of dimer **2.38** (**Figure 2.3**).

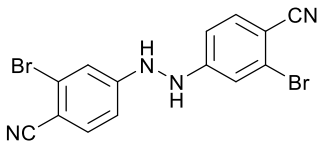

2.38

Figure 2.3: Possible dimer from **Scheme 2.10g**

Similarly to the phenomena observed for **Pathway A**, the properties of 2,4-difluorobenzonitrile **2.31**, can lead to the formation of undesired isomer **2.39**, which could be challenging to distinguish by common NMR experiments, and possibly the dimer **2.40** (**Figure 2.4**),[54] which would not be suitable for our reaction scheme.

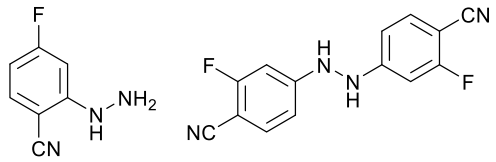

2.39 **2.40**

Figure 2.4: Possible side products from **Scheme 2.10g**

2.1.3. Summary

As highlighted in the beginning of this chapter, the synthesis of our novel target compounds **2.1 – 2.4** required the synthesis of the HSP90 inhibitory core **2.5** and **2.6**. Overall, the previously reported synthetic approaches towards the SNX class of HSP90 inhibitors revealed that our overall procedure could be distilled into two related pathways (**Scheme 2.10**). Our analysis of the reported methods, as discussed in **Section 2.1.2**, suggested that both would suffer from distinct strengths and pitfalls,

particularly regarding treatment of the halogenated benzonitrile rings. Accordingly, neither procedure offered an obvious advantage toward the synthesis of **2.1 – 2.4.** In addition, the availability of starting materials for either pathway was sporadic, making neither option preferable from that point of view. Therefore, we opted to synthesise the core scaffolds by utilising elements of both pathways, from which we could evaluate the most convenient and efficient route.

3. CHAPTER 3: RESULTS AND DISCUSSION

3.1. Synthesis of the HSP90 extracellular inhibitors

3.1.1. Synthesis of tetrahydroindazolone *via* 2-ketodimedone

The preparation of regioisomerically pure, and suitably functionalized building blocks prior to the synthesis of key precursors **2.28 – 2.30**, **2.36** was critical in ensuring the efficient synthesis of **2.5** and **2.6** (**Scheme 2.10**). As mentioned above, there was no obvious advantage following either pathway A or B, and as such we opted to investigate and analyse the steps in both pathways. Given the pivotal role of the phenylhydrazines **2.26** and **2.32**, including the potential for regioselective synthesis of **2.28 – 2.30**, **2.36** we begin here by discussing the synthesis of these phenylhydrazines, and their influence on **Pathway B**.

3.1.1.1. Synthesis of phenylhydrazine 2.26 and 2.32

Based on the availability of starting materials, our attempts with this approach began by preparing the desired phenylhydrazine as reported by Hughes *et al.* whereby a solution of **2.31** in MeOH was treated with hydrazine hydrate and stirred at room temperature for 16 hours (**Scheme 3.1**).

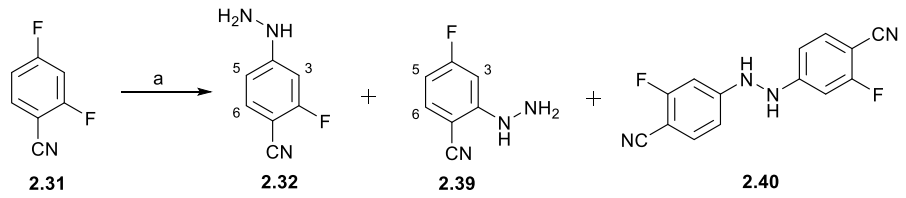

Scheme 3.1: 2,4-Difluorobenzonitrile mediated phenylhydrazine synthesis:[54]

Reagents and conditions: $H_2O.H_2NNH_2$, MeOH, r.t., 16 h

Expectedly, the reaction resulted in the formation of regioisomers **2.32**, **2.39** and the dimeric product **2.40**. Initial TLC assessment of the crude reaction mixture indicated two distinct and separable chemical species. The least polar species was isolated as an off-white solid, which ^{1}H NMR

spectroscopy revealed was a mixture of desired regioisomer **2.32**, which co-eluted with dimer **2.40**. Somewhat frustratingly, these two species were inseparable, even after repeated silica gel chromatography and recrystallization attempts. The more polar species was isolated as a suitably pure brown solid, which following NMR characterization (discussed below, **Figure 3.1**) was identified the undesired isomer **2.39**.

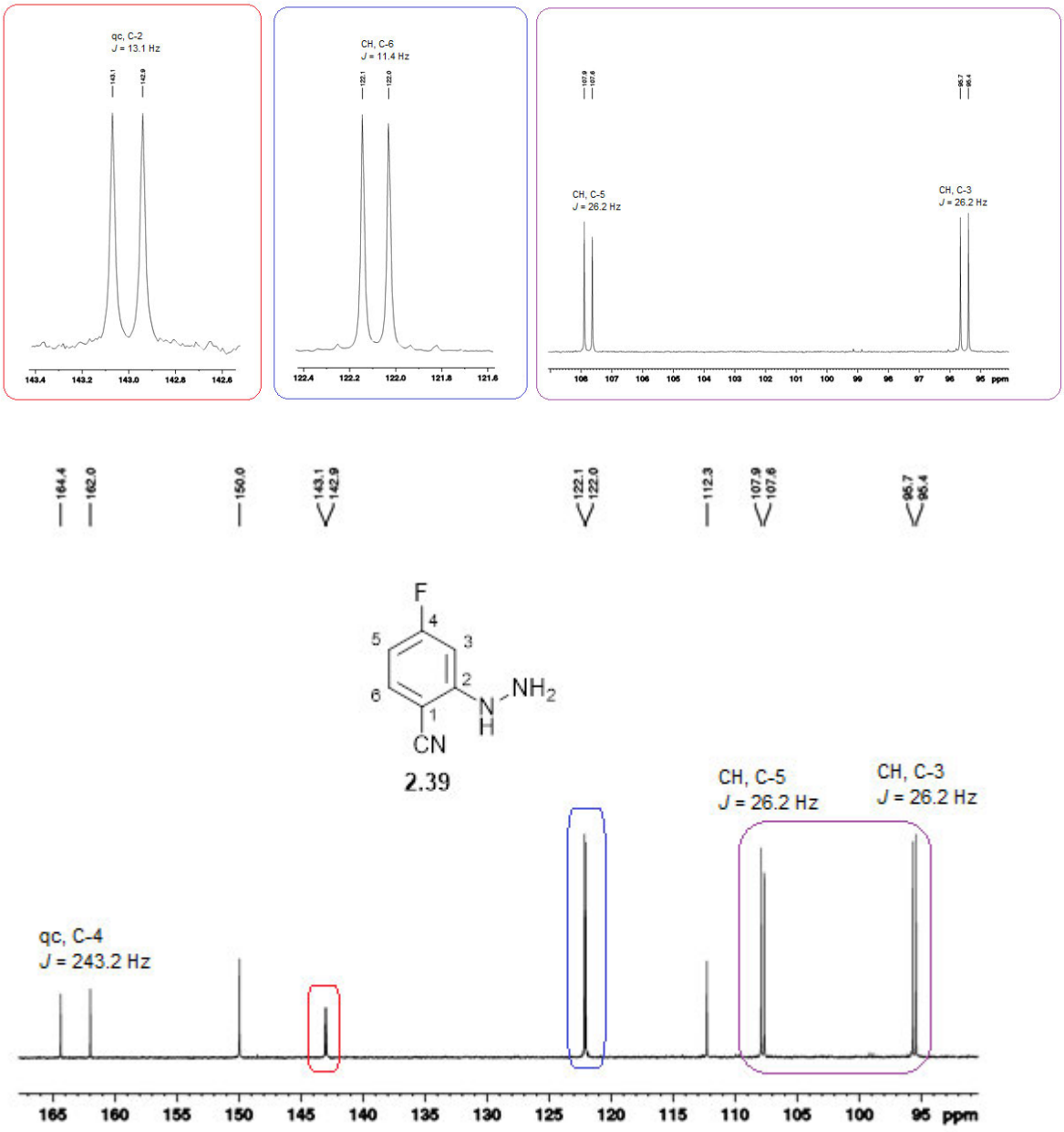

Figure 3.1: Region (δ_C 169.0 – 92.0) of the ^{13}C NMR spectrum (400 MHz, Acetone-d_6) of the undesired isomer **2.39**. This spectrum highlights the presence of two CH carbons with an *ortho* coupling to fluorine.

Both regioisomers **2.32** and **2.39**, represent a common AMX coupling system, and would be difficult to differentiate using common proton-proton coupling alone. However, in this instance, the NMR active fluorine nucleus imparts distinctive splitting patterns onto the ^{1}H and ^{13}C NMR spectra. The approximate values of carbon-fluorine ($J_{C\text{-}F}$) and proton-fluorine ($J_{H\text{-}F}$) coupling constants for aromatic compounds are documented in literature and are given in **Table 3.1** and **3.2**, respectively.[108-111] In some instances, the homonuclear (^{1}H-^{1}H) and the heteronuclear (^{1}H-^{19}F) coupling constants are similar in magnitude, and difficult to distinguish unequivocally. The coupling constants seen in a typical ^{13}C NMR spectrum are diagnostic, and when used in conjunction with two-dimensional experiments such as heteronuclear single quantum correlation (HSQC) and HMBC, facilitate unambiguous assignment.

Table 3.1: Approximate carbon-fluorine coupling constant values of fluorinated aromatic compound[108, 109]

Relative position	**Approximate *J* (Hz)**
C-F ($^{1}J_{C\text{-}F}$)	245.1
Ortho ($^{2}J_{C\text{-}F}$)	21.0
Meta ($^{3}J_{C\text{-}F}$)	7.7
Para ($^{4}J_{C\text{-}F}$)	3.3

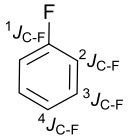

Table 3.2: Approximate proton-fluorine coupling constant values of fluorinated aromatic compound[110, 111]

Relative position	**Approximate *J* (Hz)**
Ortho ($^{3}J_{H\text{-}F}$)	9.4
Meta ($^{4}J_{H\text{-}F}$)	5.8
Para ($^{5}J_{H\text{-}F}$)	< 0.5

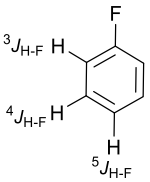

We therefore turned to the challenge of unambiguously identifying the isolated isomer, which would allow us to identify the isomer present in the mixture by inference. By way of comparison, both isomers **2.32** and **2.39** have three different proton environments designated here as H-3, H-5 and H-6. Protons H-6 and H-3 from both isomers are in very similar chemical environments, including relative positions of the neighbouring protons, and their relative proximity to the nitrile and hydrazine

functionalities. Furthermore, the proximity of protons H-6 and H-3 to the fluorine atom ($^4J_{H\text{-}F}$) is identical in both isomers. The only substantially different chemical environment between the two isomers, is that experienced by proton H-5, particularly, its proximity to the fluorine atom, and the subsequent influence on its $J_{H\text{-}F}$ coupling constant.

In addition to expected proton coupling constants and its associated splitting patterns, H-5 of isomer **2.32** is positioned *para* to the fluorine atom, and as such would experience $^5J_{H\text{-}F}$, coupling, whose corresponding coupling constant would be very small, or possibly unperceivable, under common NMR experimental set up. Conversely, isomer **2.39** proton H-5 is positioned *ortho* to the fluorine atom, whose $^3J_{H\text{-}F}$ coupling would result in a constant of substantially larger magnitude. **Table 3.3** below outlines the preliminary ^{1}H NMR analysis of the brown solid obtained from **Figure 3.1**. Based on the likely coupling constants for $^3J_{H\text{-}H}$ and $^4J_{H\text{-}F}$ coupling (8.8, 5.2 Hz) and $^4J_{H\text{-}H}$ and $^3J_{H\text{-}F}$ coupling (2.2, 9.9Hz), we tentatively assigned δ_H 7.73 – 7.69 and δ_H 7.04 – 7.01 as H-6 and H-3, respectively. Unfortunately, the splitting patterns for diagnostic H-5, were not clear and was assigned as a multiplet.

Table 3.3: ^{1}H NMR analysis of isomeric product **2.39** eluted as a brown solid (400 MHz, acetone-d_6)

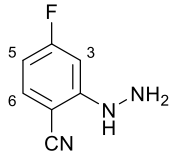

2.39

δ_H (ppm)	**integral**	**multiplicity**	***J* (Hz)**	**Preliminary Assignment**
11.00	1	s	NA[a]	NH
7.73 – 7.69	1	dd	8.8, 5.2	H-6
7.04 – 7.01	1	dd	9.9, 2.2	H-3
6.79 – 6.74	1	m	NA	H-5
5.07	2	s	NA	NH_2

a) Not Applicable.

As briefly discussed above, while indicative, the overlap between ^{1}H-^{1}H and ^{1}H-^{19}F coupling constants can be ambiguous. Consequently, ^{13}C and HSQC NMR experiments were used to conclusively distinguish between the two isomers. Isomer **2.32** contains one aromatic CH *ortho* to the fluorine atom, and its signal would therefore be split by $^{2}J_{C\text{-}F}$ coupling, with a constant of approximately 21.0 Hz. Alternatively, isomer **2.39** contains two non-equivalent aromatic CH moieties ortho to the fluorine atom, both of whose signals would be split into doublets of a similar magnitude (≈21 Hz). A detailed inspection of the ^{13}C NMR spectrum of the brown solid, revealed two carbon signals in the aromatic region were split into doublets with a *J* value of 26.2 Hz, indicating $^{2}J_{C\text{-}F}$ coupling, suggesting both were positioned *ortho* to the fluorine. Phase sensitive HSQC confirmed that both doublets correlated to individual aromatic protons. Hence, the brown solid was identified as the undesired isomer **2.39** and the desired isomer **2.32** as being part of the less polar off-white sample. The ^{1}H NMR spectrum of the off-white sample is shown in **Figure 3.2** below, analysis of the integral ratios indicated that it consisted of two compounds with a ratio of approximately 1:0.7. The overall number of protons of the main component of the mixture were seemingly in agreement with the structure of the desired product **2.32**. Specifically, the aromatic protons were accounted for by the doublet of doublets at δ_H 7.50 – 7.46 integrating for one proton and the multiplet at δ_H 6.99 – 6.94 integrating for two protons. The hydrazine NH and NH_2 were assigned to the signals at δ_H 9.00 and δ_H 4.24 – 4.15, respectively. The rest of the signals, making up the minor component, were broadly in agreement with the structure of the dimeric product **2.40**. Unfortunately, due to significant signal overlap and the similarity of the coupling constants between the two compounds, we were unable to unambiguously determine the structures of the mixture components. However, based on the outcome of subsequent reactions using the mixture, where reaction with acetylated dimedone (**2.18**), resulted in the isolation of **2.30** we were certain that the mixture contained desired product **2.32** (**Section 3.1.1.3**).

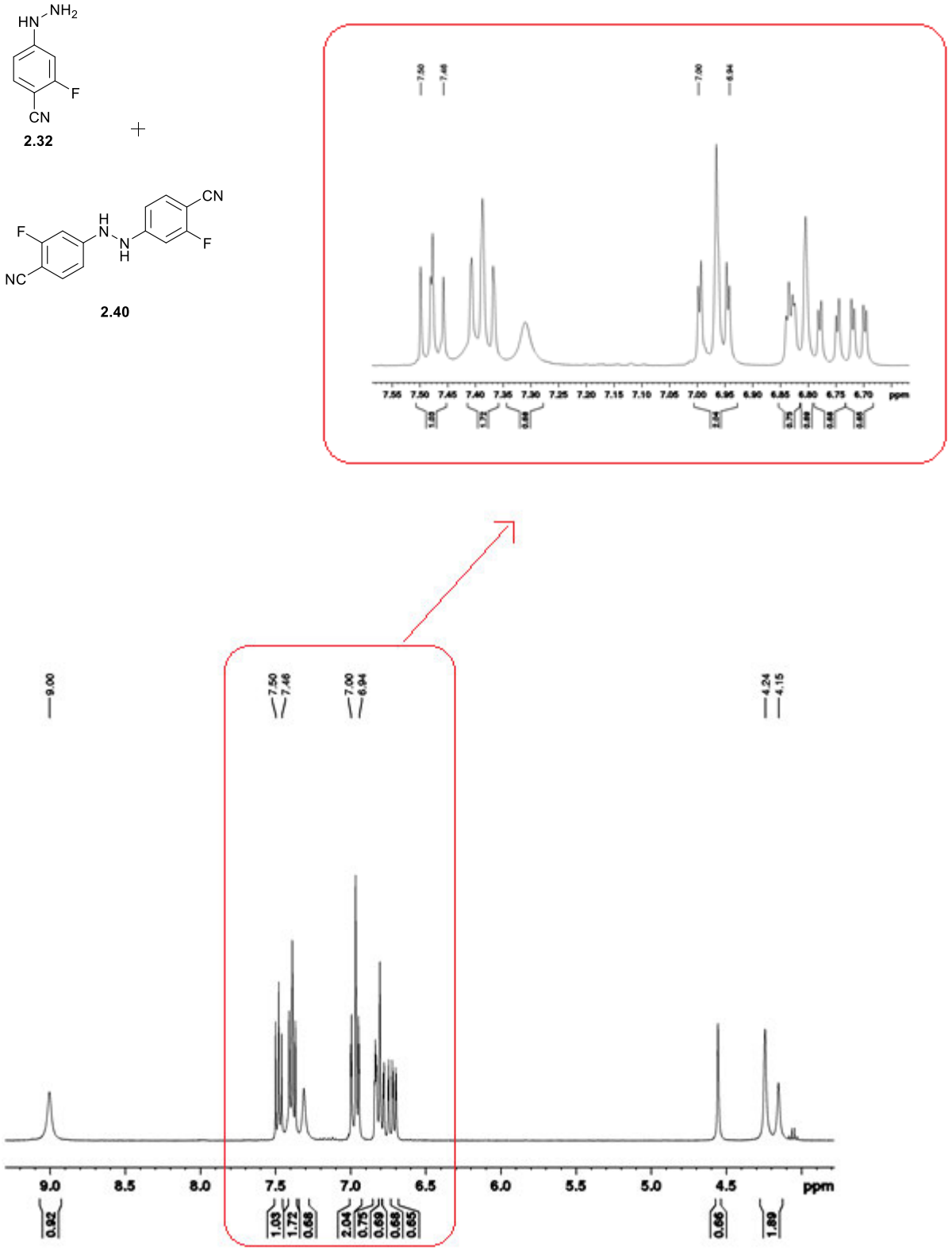

Figure 3.2: Region (δ_H 9.2 – 3.8) of the ^{1}H NMR spectrum (400 MHz, Acetone-d_6) of the sample containing a mixture of the desired isomer **2.32** and the dimeric product **2.40** (1:0.7). The region enclosed in red consists of aromatic signals from both **2.32** and **2.40**. Particularly, the doublet of doublets at δ_H 7.50 – 7.46 (1H) and the multiplet at δ_H 6.99 – 6.94 (2H) were characteristic of the aromatic signals for **2.32**, With the NH and NH_2 signals at δ_H 9.00 and 4.24 – 4.15, respectively.

Disappointingly, subsequent attempts to synthesise and purify the isomers under the exact conditions as described in **Scheme 3.1**, consistently yielded an undesired product. Although the aromatic signals observed in the ^{1}H NMR spectrum were in accordance with the expected ones, two singlets each integrating for three protons were observed at δ_H 1.98 and δ_H 1.92, respectively. Furthermore, no NH_2 signal was observed suggesting the probability of substitution on the primary amine (**Figure 3.3**). Through HSQC and HMBC experiments we determined that both methyl signals correlated to the same carbon signal at δ_C 150.8, which would be expected for a hydrazone carbon signal, thereby proposing the synthesis of the undesired compound **2.41**. HRESMS confirmed the expected mass of the undesired compound. Intuitively, our primary suspicion was acetone contamination leading to the formation of hydrazone **2.41** (**Figure 3.3**). However, the use of high purity solvents, NMR analysis of solvents and vigorous drying of glassware, did not resolve this challenge, and the reason for the unexpected side reaction remains ambiguous.

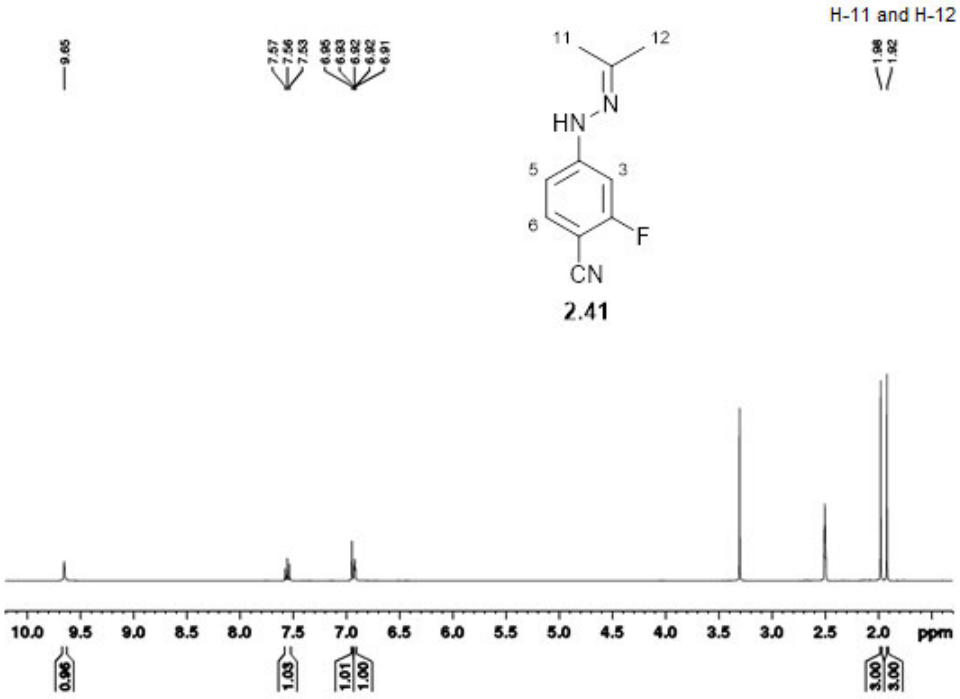

Figure 3.3: Region (δ_H 10.1 – 1.3) of the ^{1}H NMR spectrum (400 MHz, DMSO-d_6) of the undesired product **2.41**, showing the two methyl signals at 1.98 & 1.92 ppm each integrating for three protons.

In an attempt to circumvent the problem of regioisomers, we turned our attention to the alternative phenylhydrazine synthesis procedure as reported by Huang *et al.*, which incorporated 2-bromo-4-fluorobenzonitrile in an effort to take advantage of orders of reactivity between aromatic fluorine and bromine, and thus ensure regioselectivity.[52] Aside from the starting material, the method of Huang *et al.* altered slightly from that of Hughes *et al*., in that it was conducted under anhydrous conditions, in THF to successfully give the desired phenylhydrazine intermediate in 87.2% yield (**Scheme 2.10g**). Accordingly, hydrazine hydrate was distilled from NaOH pellets, under N_2(g), and immediately added dropwise, in excess to a stirring solution of 2-bromo-4-fluorobenzonitrile in anhydrous THF (**Scheme 3.2**)**.** Purification by silica gel chromatography afforded a cream white solid in good yields (71%).

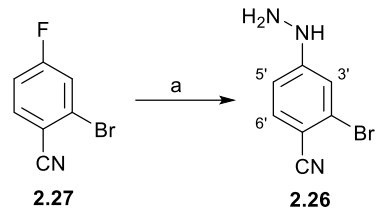

2.27 **2.26**

Scheme 3.2: 2-Bromo-4-fluorobenzonitrile mediated phenylhydrazine synthesis[52]

Reagents and conditions: a) H_2NNH_2, anhy. THF, N_2(g), r.t., 16 h, 71% yield

A diagnostic absence of fluorine coupling in the ^{1}H and ^{13}C NMR spectra confirmed that substitution occurred at the expense of the fluorine atom. The other significant change in the ^{1}H NMR spectrum was the presence of a singlet at δ_H 8.03 integrating for one proton and a broad singlet at δ_H 4.37 integrating for two protons, which were characteristic of the hydrazine NH and NH_2, respectively. Conclusive evidence of the synthesis of **2.26** was obtained from HRESMS results. In addition to **2.36**, these reactions conditions yielded dimer **2.37**, as well as dimethyl hydrazone **2.42** (**Figure 3.4**). Again, as discussed previously, **2.42** would appear to be a likely product of acetone contamination. However, this was particularly surprising, given that the reaction was conducted in freshly distilled anhydrous THF, using distilled hydrazine, in oven dried glassware. Given its low abundance, we did not look further into its formation, and continued with the synthesis**.**

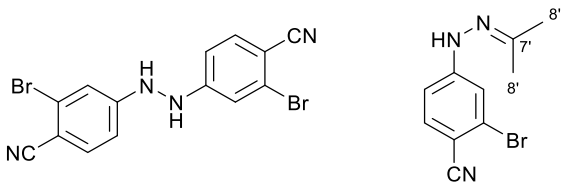

2.37 **2.42**

Figure 3.4: Side products **2.37** and **2.42** obtained from the 2-bromo-4-fluorobenzonitrile mediated phenylhydrazine synthesis.

3.1.1.2. Synthesis of functionalized β-triketones 2.18 and 2.23

The subsequent step in our synthesis was the suitable functionalization of dimedone to yield **2.18** and **2.35** (**Scheme 2.10b**). The synthesis of β-triketones has been extensively reported in literature, with the most common strategy involving the initial *O*-acylation of a 1,3-dione precursor using acyl donors such as acyl chlorides, anhydrides or carboxylic acids; and the subsequent *O*-*C* isomerisation to yield the desired compound. This rearrangement, known as the Fries rearrangement is commonly catalysed by Lewis acids such as $AlCl_3$, or bases such as imidazole and 4-dimethylamino-pyridine (DMAP).[102, 106, 112-115] Most notably, DMAP has been reported to be a particularly efficient and useful catalyst for the desired *O*-*C* isomerization.[112, 114]

Hughes *et al.* and Wu *et al.* both reported the successful preparation of 2-acetyldimedone **2.18** (**Scheme 3.3**).[54, 98] Hughes *et al.* prepared **2.18** from acetic anhydride and dimedone **2.14** in warm dichloromethane (DCM) with diisopropylethylamine (DIPEA) and catalytic DMAP.[54] Interestingly, Wu *et al.* reported a slightly different procedure only using acetyl chloride and triethylamine (TEA) in warm acetonitrile to yield the desired product in 95% yield.[98]

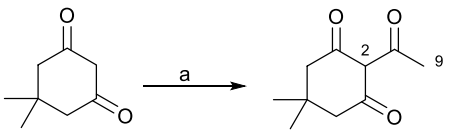

2.14 **2.18**

Scheme 3.3: Hughes *et al*.[54] and Wu *et al*.'s[98] synthesis of 2-acetyl dimedone **2.18**:

Reagents and conditions: a) $(CH_3CO)_2O$, DMAP, DIPEA, DCM, r.t., 24 h[54] or CH_3COCl, TEA, MeCN, 55 °C, 3 h, 95%[98]

Based on the availability of starting materials we followed the latter procedure where a solution of **2.14** and TEA was treated with acetyl chloride at 0 °C and subsequently heated in acetonitrile to afford an orange-yellow oil in 74-77% yields. The obtained product was fully characterized using NMR spectroscopy and the presence of a carbonyl signal at δ_C 167.4 in the ^{13}C NMR spectrum, characteristic of an ester, strongly suggested that under these conditions, we had produced **2.43** (**Figure 3.5**), which did not undergo subsequent Fries-rearrangement into the desired C-2 acylated product **2.18**.

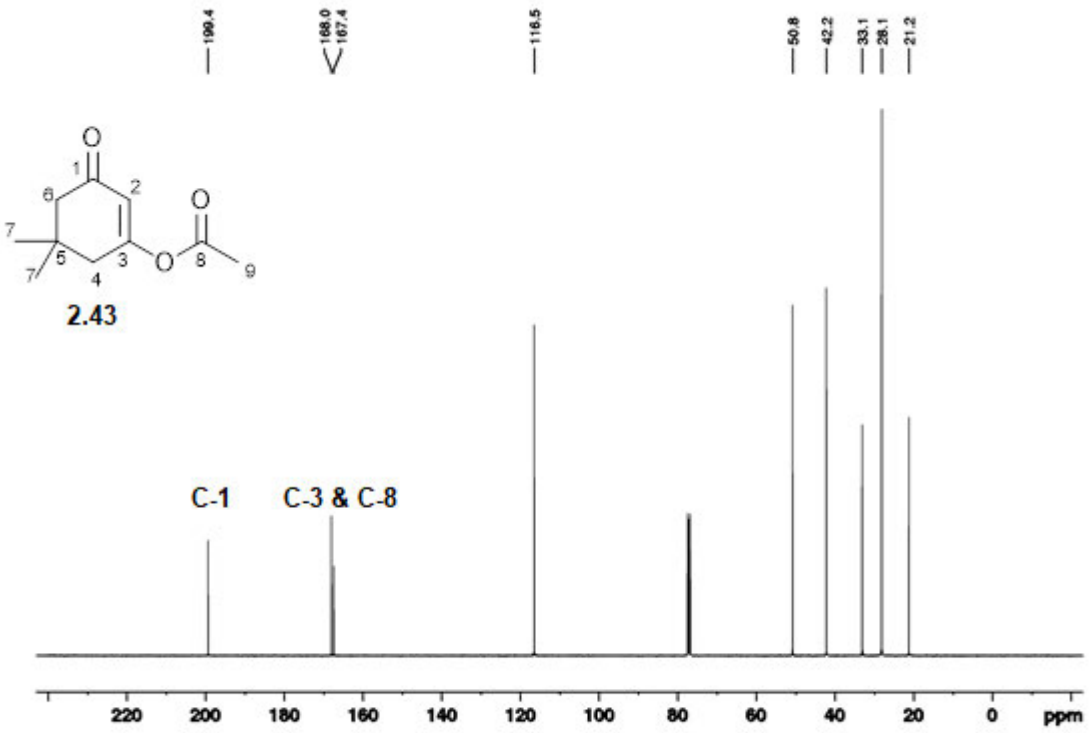

Figure 3.5: ^{13}C NMR spectrum (100 MHz, $CDCl_3$) of the *O*-acylated dimedone **2.43**, displaying the presence of the signal at 168.0 and 167.4 ppm characteristic of an ester and enol, respectively.

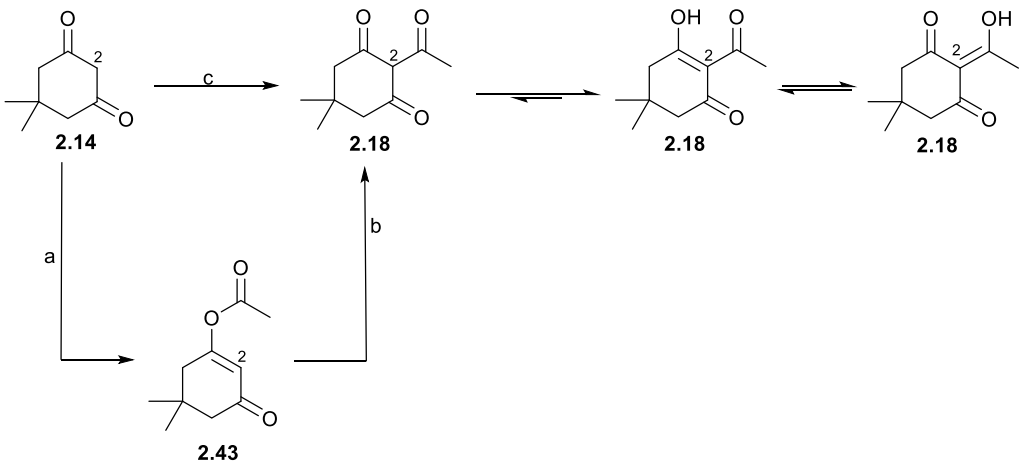

Scheme 3.4: Various conditions for dimedone acetylation:

Reagents and conditions: a) CH_3COCl, TEA, MeCN, 55 °C, 3 h; b) $AlCl_3$, 128 °C, 16 h, 47%; c) $(CH_3CO)_2O$, DMAP, DIPEA, DCM, r.t., 24 h, 57%

Thus, in continued efforts to synthesise **2.18** we then followed the same procedure described by Wu *et al.*, however, the addition of catalytic amounts of DMAP to the reaction still afforded the enol ester **2.43** in 62% yield. Deviation to a two-step procedure, where **2.43** was synthesised and purified (**Scheme 3.4a**), followed by heating at high temperatures in the presence of aluminium chloride afforded **2.18** in an overall 29% two-step yield (**step a** and **b**). The ^{1}H NMR spectroscopic data of the product corresponded excellently with literature reports, confirming that the compound tautomerized mainly towards the enol form, hence the absence of a triplet at δ_H 5.83 characteristic of H-2 (**Figure 3.6**).[116, 117] Unfortunately, the poor isolated yields were not desirable, especially for a step that was towards the beginning of our synthesis, and as result we sought to find alternative methods to afford **2.18**.

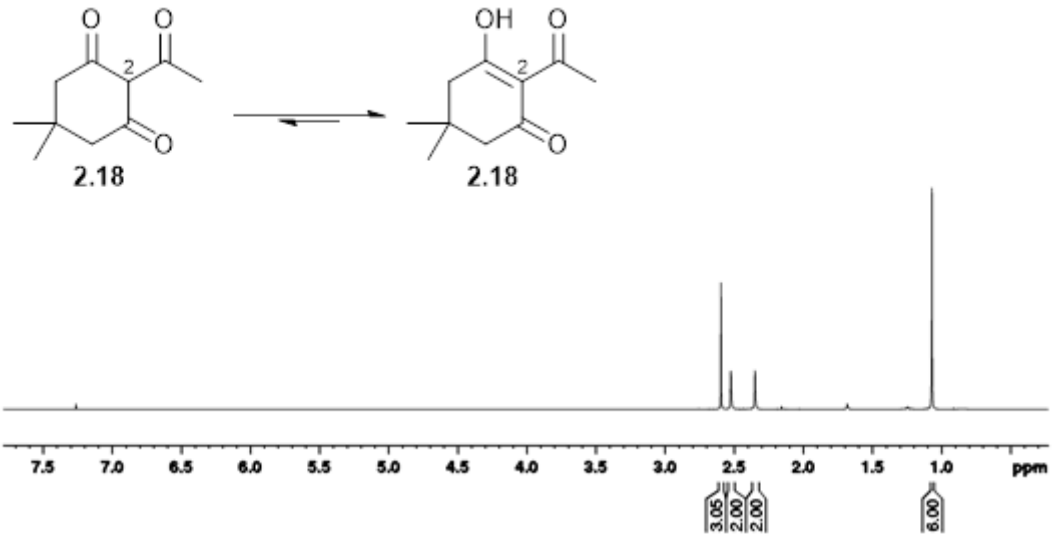

Figure 3.6: ^{1}H NMR spectrum (400 MHz, $CDCl_3$) of the desired compound **2.18** in its enolized form, the absence of a signal characteristic of H-2 is in accordance with literature reports.[117]

Alternatively, the desired C-2 acetylated isomer **2.18** could be synthesised in one pot by adapting the procedure reported by Hughes *et al.* (**Scheme 3.4c**).[54] Here **2.14** was dissolved in DCM, treated with DIPEA and DMAP, followed by the slow addition of acetic anhydride. Indeed, we were able to obtain the desired compound **2.18** in 45% yield alongside the *O*-acylated compound **2.43** in 24% yield. Compound **2.43** was subsequently isomerized to give **2.18** in 51% yield. We obtained the desired product in an overall yield of 57%, which was suitably improved from that obtained *via* the two-step approach. In the interest of avoiding multistep reactions, all our subsequent acetylation reactions were done in DCM using DIPEA as the base in the presence of catalytic DMAP.

Despite the reported instability of **2.35**, Khlenbicova *et al.* reported a procedure where **2.35** was synthesised using *N*-trifluoroacetylimidazole as the electrophilic species.[106] This could be accomplished by following one of three different synthetic routes (**Scheme 3.5**). The first route was a two-step method (**a**), whereby the *N*-trifluoroacetylimidazole was prepared from imidazole and trifluoroacetic anhydride and subsequently reacted with an equimolar solution of dimedone and imidazole in anhydrous chloroform to give **2.35** in 78% yield.

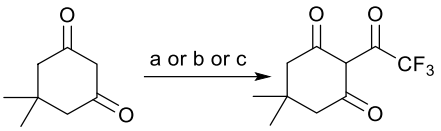

2.14 2.35

Scheme 3.5: Khlenbicova *et al*.'s synthesis of **2.35**[106]

Reagents and conditions: a) *N*-Trifluoroacetyl imidizole, Imidizole, $CHCl_3$, r.t., 1 h, 78%; b) Trifluoroacetic anhydride, Imidizole, $CHCl_3$, 0 °C - r.t, 45 min., 83%; c) TFA, 1,1-carbonyldiimidizole, Imidizole, $CHCl_3$, r.t., 45 min., 88%

Alternatively, *N*-trifluoroacetylimidazole was prepared *in situ* either from the reaction of perfluorocarboxylic acid anhydrides with an imidazole (**b**) or perfluorocarboxylic acids with 1,1-carbonyldiimidazole (**c**). Following that, inspired by this work, we then attempted the synthesis of **2.35** following **Scheme 3.5 (b)**.[106] Unfortunately, the reaction did not result in the formation of **2.35** as reported. We, however, isolated the dimedone starting material.

As reported by Huang *et al.*, it then became apparent that the β-triketone mediated procedure was not feasible for the synthesis of all our target compounds as it could not be extended to the polyfluorinated functionalities.[52] In a subsequent attempt, which will be discussed later (**Section 3.1.2**), we followed a tosyl hydrazone mediated procedure which was selectively designed for the synthesis of **2.23**. Furthermore, we were interested in investigating whether this approach could be extended to other acyl functionalities.

With the desired 2-acyldimedone **2.18** in hand, our next task was to perform the tetrahydroindazolone condensation by either following the hydrazine hydrate mediated route (**Scheme 2.10a**), or the phenylhydrazine route (**Scheme 2.10h**). Our initial attempts explored the phenylhydrazine mediated tetrahydroindazolone condensation.

3.1.1.3. Phenylhydrazine mediated tetrahydroindazolone condensation of 2.18

As previously discussed, the phenylhydrazine mediated tetrahydroindazolone condensation presents a useful synthetic approach towards our desired scaffolds with the potential of eliminating the formation of the *N*-2 arylated isomer (**Figure 2.2**).

Huang *et al.* reported a 15 minute phenylhydrazine mediated tetrahydroindazolone condensation procedure between **2.18** and **2.26** in EtOH using 4 equivalents of AcOH as a catalyst at 110 ˚C under microwave conditions (**Scheme 2.10h**).[52] Similarly, Hughes *et al.* suspended **2.18** and the regioisomeric mixture (**2.32** and **2.39**) in MeOH and stirred the reaction mixture at room temperature over 3 days, still using AcOH as a catalyst.[54] As discussed in **Chapter 2**, the use the brominated phenylhydrazine **2.26** would require the use of expensive catalysts under complex reaction conditions for the subsequent amination reaction (**Scheme 2.7**). To preclude that challenge, we were interested in using the fluorinated phenylhydrazine **2.32** instead of its brominated analogue **2.26** for the tetrahydroindazolone condensation reaction.

As described in **Section 3.1.1.1**, the isolation of **2.32** proved challenging. Accordingly, our initial cyclization reactions, which will be described below, were carried out using the mixture of **2.32** and the dimeric product **2.40**. For subsequent reactions, we deemed the attempted purification as an unnecessary step, and this condensation was carried out using the crude mixture of **2.32, 2.39** and **2.40.** Accordingly, our initial attempts with the mixture of **2.32** and **2.40** following the procedure described by Hughes *et al*. at room temperature for 22 hours afforded an off-white solid upon purification, alongside unreacted **2.40** (**Scheme 3.6**). The obtained ^{1}H NMR spectroscopic data was in excellent agreement with the data reported by Hughes *et al*. for the desired isomer **2.30**.[54] Notably, the phenylhydrazine amine protons were not observed, suggesting the substitution of both the primary and secondary amine protons. Furthermore, HRESMS data and X-ray crystallographic analysis

(**Figure 3.7**) conclusively confirmed the chemical structure of the desired product **2.30**.

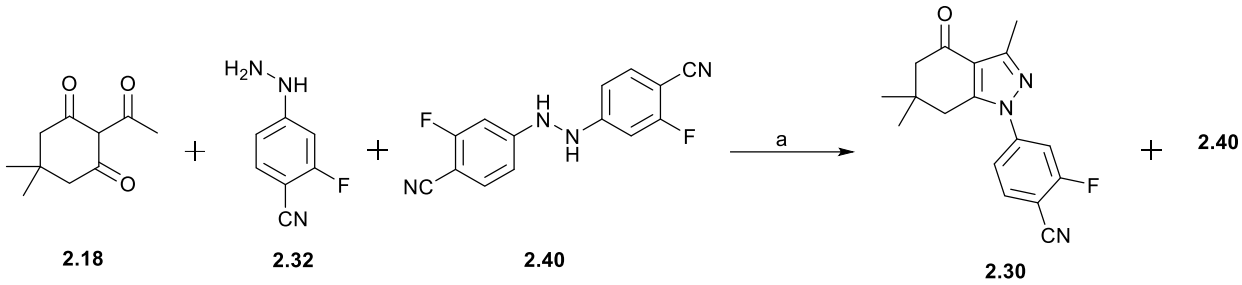

Scheme 3.6: Phenylhydrazine mediated tetrahydroindazolone condensation to yield **2.30**:

Reagents and conditions: a) MeOH, AcOH, r.t., 3 d.

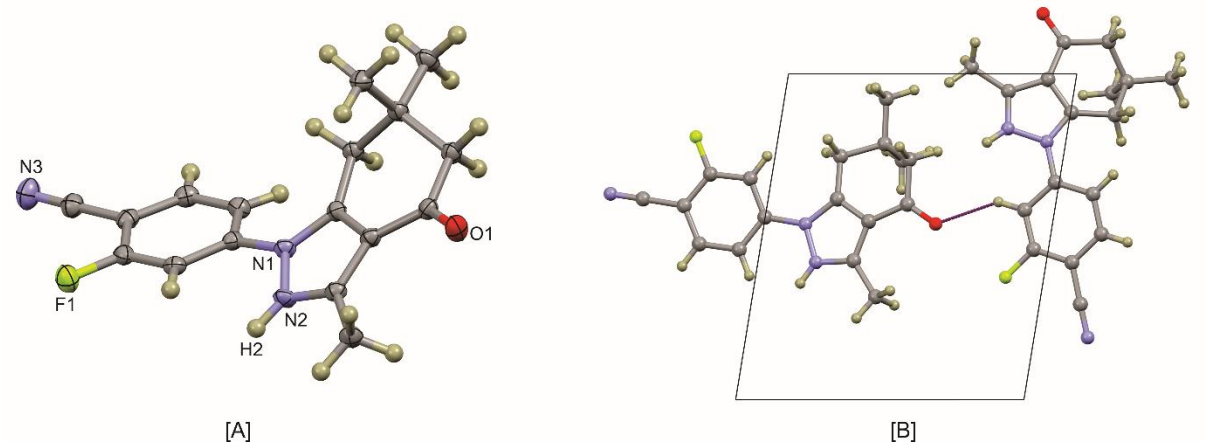

Figure 3.7: [**A**] Partially labelled structure of a single molecule of **2.30** with thermal displacement ellipsoids rendered at the 50% probability level and H-atoms shown as spheres of arbitrary radius. The asymmetric unit comprises two independent molecules and $Z = 4$. [**B**] Dimeric structure of **2.30** viewed down the *c*-axis. The dimer is stabilised by C–H···O interactions. The H···O distance is 2.404 Å. This is 0.316 Å shorter than the sum of the van der Waals radii suggesting a moderately strong interaction.

Subsequent condensation reactions using the crude material expectedly resulted in the formation of regioisomers **2.30** and **2.44** (**Scheme 3.7**), which we could separate using silica gel column chromatography.

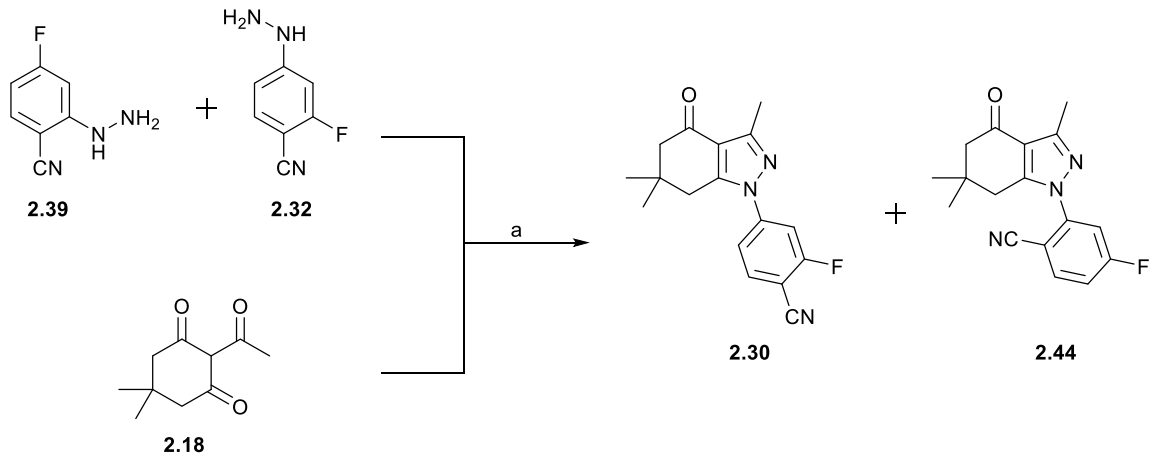

Scheme 3.7: Tetrahydroindazolone condensation to yield **2.30**:

Reagents and conditions: a) MeOH, AcOH, r.t., 3 d.

The reaction was monitored using TLC, and having previously synthesised **2.30**, we were able to instantly identify our desired product from the mixture. Upon column chromatographic purification, we, like Hughes *et al*., eluted the yellow isomeric product **2.44** prior to the desired off-white product **2.30**. Eventually, we found that under long reaction conditions the desired isomer could be obtained in higher yields. Whilst this approach was limited by regioselectivity, the presence of the reactive fluorine still deemed it superior for simple and efficient coupling of the cycloamine moiety. As previously stated in **Section 3.1.1.1**, all our successive syntheses of **2.30** followed the procedure described in **Scheme 3.7** and the pure desired isomer was obtained after silica gel column chromatography using 70% hexane: ethyl acetate mixture as the eluent.

3.1.1.4. Hydrazine hydrate mediated tetrahydroindazolone condensation of 2.18

Alternatively, the desired tetrahydroindazolone core could be accessed *via* the hydrazine hydrate mediated procedure. In the interest of optimizing the synthesis of our desired target compounds, we were interested in exploring other reported procedure for the tetrahydroindazolone condensation.

Claramunt *et al.* reported a procedure where **2.12** could be accessed from the reaction of **2.18** and hydrazine hydrate in refluxing THF.[99] Alternatively, Wu *et al*. reported a similar procedure where **2.18** was reacted with hydrazine hydrate in ethanol at room temperature.[98] Based on the ease of the reaction conditions we opted to follow Wu *et al.*'s procedure to afford the desired product as a pale yellow solid in 79% yield (**Scheme 3.8**). The obtained NMR spectroscopic data was in excellent agreement with that reported in literature.[98, 99] Particularly, the ^{13}C NMR spectrum of the starting material **2.18** had three signals characteristic of carbonyl carbons at δ_C 202.6, 198.0, 195.3, but only one carbonyl carbon signal was observed in the ^{13}C NMR spectrum of the obtained product. Finally, HRESMS analysis gave conclusive confirmation of the synthesis **2.12**.

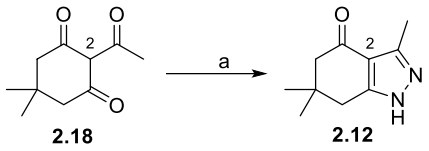

2.18 **2.12**

Scheme 3.8: Tetrahydroindazolone condensation as reported by Wu *et al*.[98]

Reagents and conditions: a) $H_2O.H_2NNH_2$, EtOH, r.t, 16 h, 79% yield

3.1.2. Tosylhydrazone mediated tetrahydroindazolone condensation

In view of the incompatibility of the β-triketone mediated tetrahydroindazolone condensation for the synthesis of **2.23**, we decided to follow the procedure selectively reported for this scaffold as described in **Scheme 2.6**. To begin our synthesis, *p*-toluenesulfonyl hydrazide (**2.45**) was readily prepared from *p*-toluenesulfonyl chloride and hydrazine hydrate at 0 ˚C using a 30 minute procedure as reported by Liu *et al.*.[118] To continue the synthesis, the tosylhydrazone (**2.24**) was prepared from **2.45** and dimedone **2.14** in warm toluene with catalytic *p*-TsOH (**Scheme 3.9**).[52] ^1H NMR spectroscopic characterization in deuterated dimethyl sulfoxide (DMSO-d_6) revealed that our product predominantly tautomerized towards the enol form instead of the reported ketone form. Overall, however, the spectroscopic data was in accordance with that reported in literature.[52]

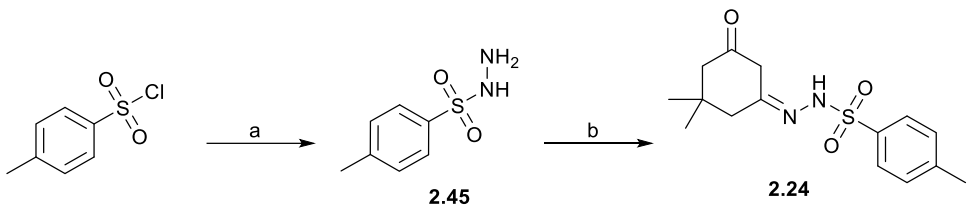

Scheme 3.9: Synthesis of tosyl hydrazone intermediate **2.24**

Reagents and conditions: a) Hydrazine hydrate, 0 °C, 30 min., 45%[118];
b) **2.14**, toluene, cat. *p*-TsOH, 95 °C, 23 h, 25%.[52]

With intermediate **2.24** in hand, we then attempted the synthesis of the tetrahydroindazolone **2.23** *via* a two-step, one pot reaction (**Scheme 3.10**). Accordingly, trifluoroacetic anhydride was added to a suspension of **2.24** and TEA in THF and stirred at 55 ˚C for 2 hours to form the presumed C-2 acylated intermediate.

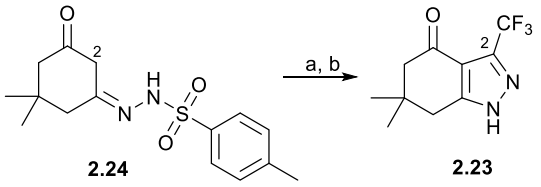

Scheme 3.10: Tosyl hydrazone mediated synthesis of **2.23**[52]

Reagents and conditions: a) $(CF_3CO)_2O$, THF, TEA, 55 °C, 2 h;

b) NaOH, MeOH, H_2O, r.t., 3 h, 15%

Then, to facilitate the cyclisation and detosylation, MeOH, and a 1:1 solution of water and 1M NaOH were added to the cooled reaction mixture and stirred for another 3 h. To our delight, after silica gel purification the desired product **2.23** was obtained in 15% yield, which was lower than the reported 30 – 35% yield.[52, 107] Spectral data was in good agreement with the data reported in literature.[52] Most notably, the singlet characteristic of H-2 was not observed indicating that the cyclisation had occurred; also, no signals were observed in the aromatic region confirming a successful detosylation.

Similarly, still in search of one general route to access both our target compounds, we attempted the synthesis of **2.12** *via* the tosyl hydrazone mediated procedure using acetic anhydride for the acylation

step (**Scheme 3.11**). Unexpectedly, the ^{1}H NMR spectrum of the obtained white solid was very similar to that of **2.24**, the aromatic proton signals were still present suggesting an unsuccessful detosylation. Moreover, a singlet integrating for one proton was observed at δ_H 4.96. This signal was characteristic of H-2, thus depicting an unsuccessful cyclisation. Interesting, however, was the presence of a singlet at δ_H 2.05 integrating for three protons which suggested that the acetylation step was successful (**Figure 3.8**).

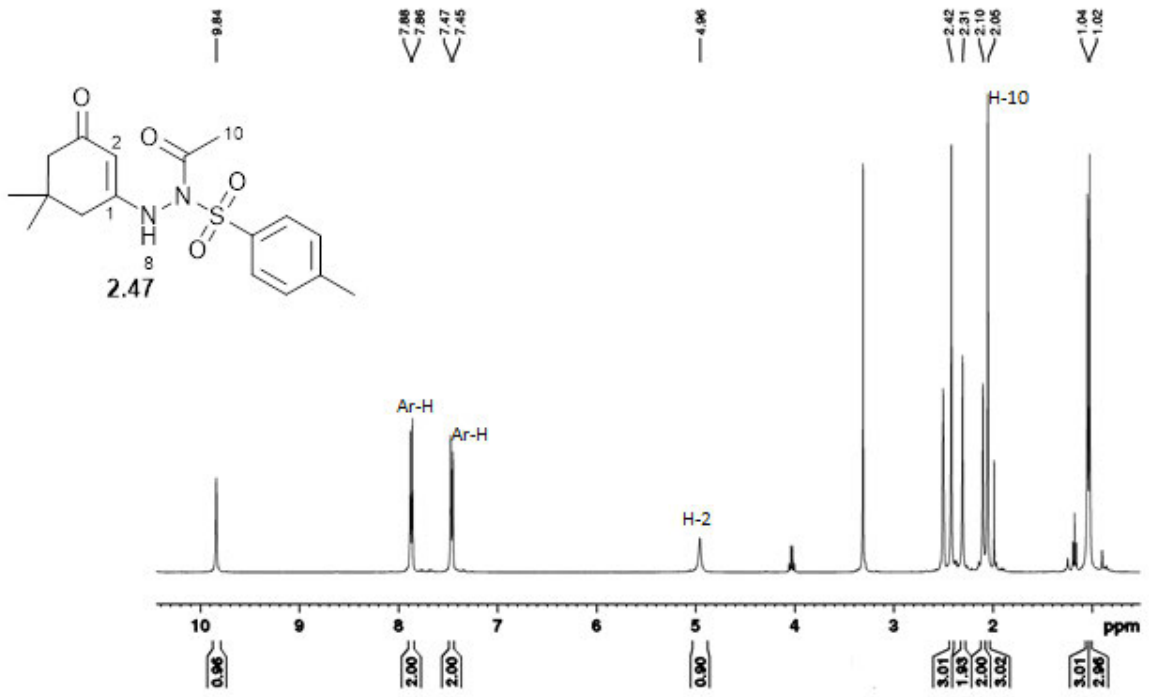

Figure 3.8: ^{1}H NMR spectrum of **2.47** obtained in DMSO-d_6. The presence of a singlet characteristic of H-10 at 2.05 ppm suggested the successful acylation, however, the presence of aromatic signals and the singlet characteristic of H-2 at 4.96 ppm, clearly implicated an unsuccessful cyclisation and detosylation.

Initially, based on NMR spectroscopic data, we envisioned that we had formed **2.46** where only the C-2 acylation reaction was successful and not the subsequent cyclization and detosylation. To our surprise, XRD data revealed that we had acylated at the hydrazone nitrogen to give intermediate **2.47** as indicated in **Scheme 3.11** and **Figure 3.9**.

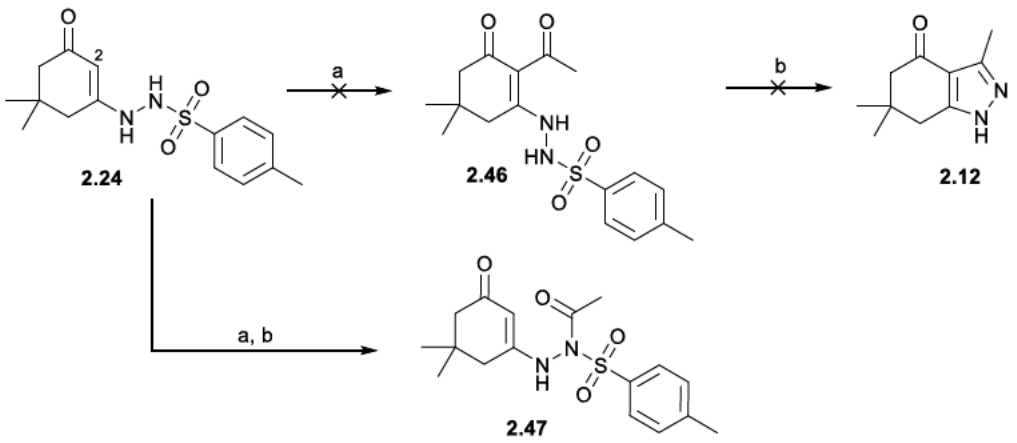

Scheme 3.11: Attempted tosyl hydrazone mediated synthesis of **2.12**

Reagents and conditions: a) $(CH_3CO)_2O$, THF, TEA, 55 °C, 2 h; b) NaOH, MeOH, H_2O, r.t., 3 h, 60%

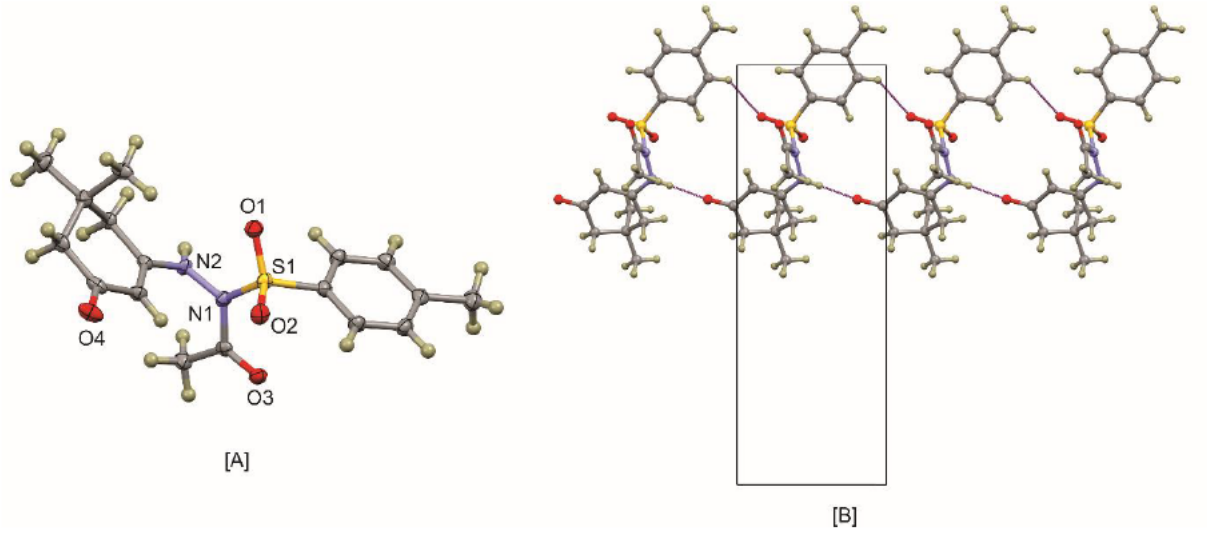

Figure 3.9: **[A]** Partially labelled structure of a single molecule of **2.47** with thermal displacement ellipsoids rendered at the 50% probability level and H-atoms shown as spheres of arbitrary radius. The asymmetric unit comprises a single molecule and $Z = 4$. **[B]** Polymeric structure of **2.47** viewed down the *c*-axis. The one-dimensional supramolecular structure is stabilised by C–H···O interactions with an H···O distance is 2.417 Å. The structure is further supported by N–H···O hydrogen bonds with an H···O distance of 2.417 Å. These distances are both substantially shorter than the sum of the van der Waals radii suggesting a moderately strong interaction.

As previously stated, Huang *et al.* reported the synthesis of **2.23** from the reaction of trifluoroacetic anhydride with *p*-toluenesulfonyl hydrazide.[52] Mechanistically, this synthesis is alleged to proceed *via* a C-2 acylated intermediate which is subsequently cyclized and detosylated under basic conditions to

give the desired **2.23**.[96, 107] In theory, however, **2.24** consists of at least two possible deprotonation sites, the sulphonamide proton and the H-2 proton. Furthermore, acylation of *N*-tosylhydrazide in the presence of TEA has previously been reported in literature.[119] Thus, the formation of **2.47** was theoretically viable. What was surprising, however, was the stability of the tosyl protecting group under basic conditions.[120]

Tosylhydrazone compounds have been extensively studied in relation to the Shapiro reaction, where ketones are converted to alkenes in the presence of a strong base *via* the tosylhydrazone intermediate.[120-122] A schematic of the reaction is outlined below (**Scheme 3.12**). For straight chain ketones, strong bases such as sodium hydride and lithium aluminium hydride, are required for successful deprotonation of the α-protons (**Scheme 3.12b**) and consequently successful synthesis of the corresponding alkene.[120, 122]

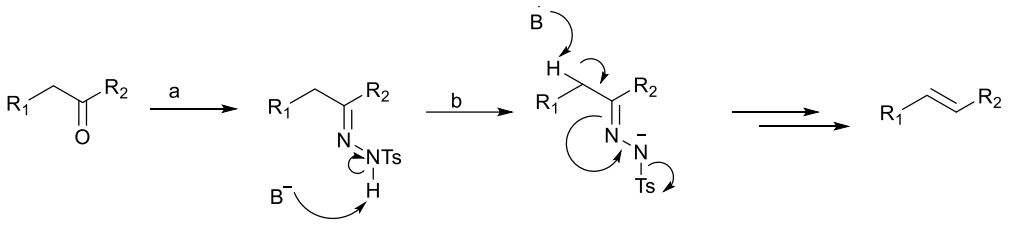

Scheme 3.12: Conversion of ketones to alkenes (Shapiro reaction)[120, 122]

Interestingly, however, Hiegel *et al*. reported that α-protons of cyclic 1,3-diketone tosylhydrazone analogues had the same relative acidity as the sulphonamide protons, hence their deprotonation could occur even under mild basic conditions.[120] In light of the above information, considering the nature of our tosylhydrazone **2.24** and the given reaction conditions, we envisioned that the reported synthesis of **2.23** (**Scheme 3.10**) could proceed through a tetrahedral intermediate either *via* **Pathway A** (**Scheme 3.13**) or **Pathway B**. For **Pathway A** the C-2 acylation of **2.24** would afford **2.48** which, upon deprotonation of the sulphonamide proton, would attack the acyl carbonyl to give the tetrahedral intermediate **2.49**. Alternatively, **2.49** could form through **Pathway B** from anion **2.50**.

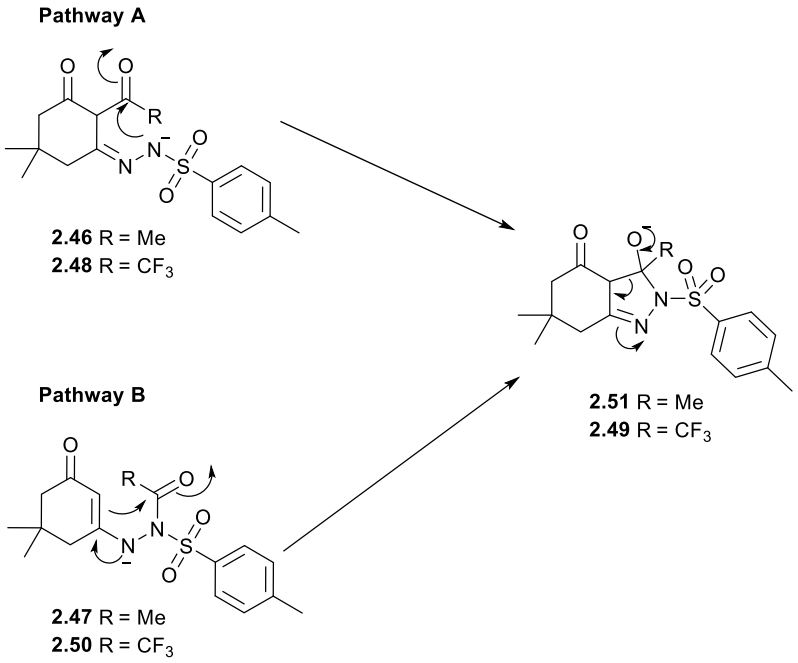

Scheme 3.13: Proposed mechanism towards the synthesis of tetrahydroindazolone **2.23** and amide **2.47**

In the same manner, we envisioned that the isolated product **2.47** could be obtained either by direct acetylation of the hydrazone nitrogen or the two-step pathway initiated by C-2 acetylation to give the tetrahedron intermediate **2.51** which subsequently collapses to give the corresponding amide product. **Figure 3.10** shows the calculated DFT relative energies of the possible structural intermediates for both pathways **A** and **B**. These results indicated that intermediates **2.47** and **2.50**, in which the hydrazine nitrogen is acylated, were lower in energy relative to their corresponding ketones **2.49** and **2.51**. Interesting, however, was the difference in predicted energy barriers between the conversion of **2.50** to the tetrahedral intermediates **2.49** (Δ 57.9 kJ.mol^{-1}) in comparison to the conversion of the methyl analogue **2.47** to **2.51** (Δ 100.6 kJ.mol^{-1}). Similarly, the conversion of the methyl ketone **2.46** to the corresponding tetrahedral intermediate **2.51** required twice as much energy (Δ 40.1 kJ.mol^{-1}), when compared to the trifluoromethyl analogue (20.9 kJ.mol^{-1}). These results clearly indicated that the formation of the tetrahedral intermediate *via* both pathways was a higher energy process for the methyl system than for the trifluoromethyl counterparts. Additionally, the significant energy difference between **2.47** and **2.51** suggests that the direct acylation of the

hydrazone nitrogen, **Pathway A** (**Scheme 3.13**), is the most plausible route for the formation of the amide intermediate **2.47**. Consequently, very harsh reactions conditions would be required for the formation of the tetrahedral intermediate **2.51** from the amide **2.47**. On the contrary, the similar energy differences for the trifluoromethyl analogue suggest that the tetrahedral intermediate **2.49** could be formed *via* either pathway, with **Pathway A** being the most energetically favoured.

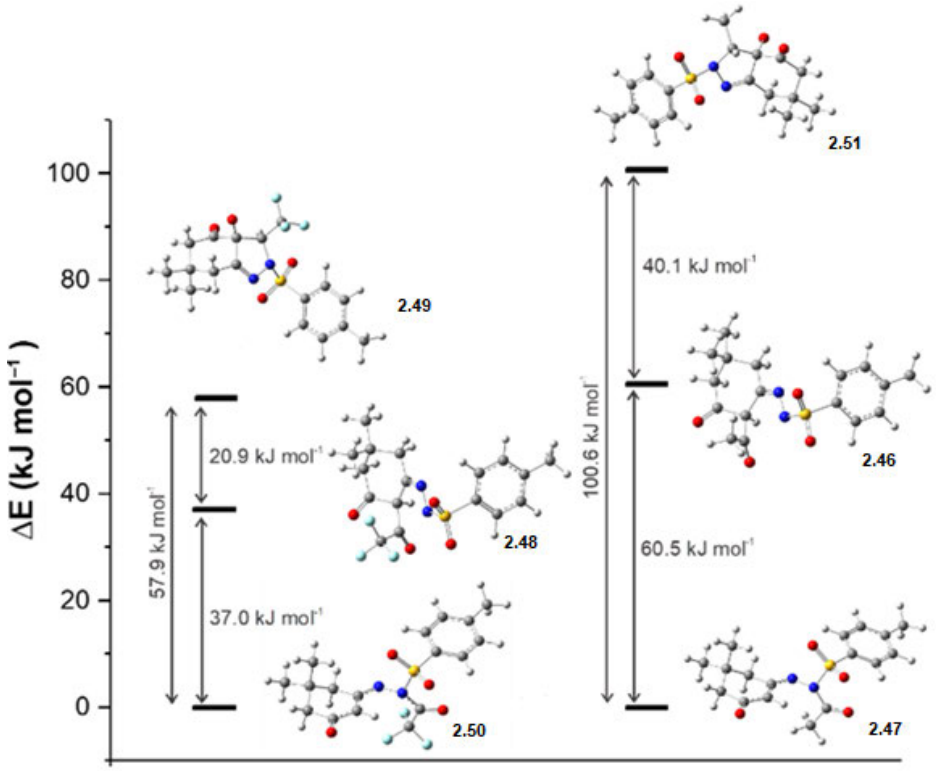

Figure 3.10: Results of the DFT simulations showing the relative potential energies of the proposed tetrahedral intermediates **2.49** and **2.51**, from either their corresponding triketones **2.48** and **2.46**, or amides **2.50** and **2.47**; respectively. The relative energies of these intermediate structures indicate that in either pathway, the reaction of the methyl system to give the intermediate **2.51** is significantly higher in energy than that of the trifluoromethyl analogue **2.49**.

Subsequently, we envisioned that various reaction conditions could be explored to facilitate the cyclisation of intermediate **2.47**. Thus, we shifted from the one pot, two-step reaction and subjected the isolated **2.47** to various reaction conditions hoping to drive the reaction forward towards cyclisation (**Scheme 3.14**). We initiated this investigation by subjecting **2.47** to the exact cyclisation conditions as reported by Huang *et al.*,[52] unfortunately, this resulted in amide hydrolysis to recover

2.24 (**Table 3.4, entry 1**). We then envisioned that the presence of water could be contributing to the hydrolysis reaction, and as a result we attempted the cyclisation in the absence of water (**entry 2**). Disappointingly, however, we still isolated the hydrolysed product. Furthermore, we investigated different bases such as TEA and sodium methoxide (**entries 3 and 4**). This attempt was also unsuccessful, resulting in the recovery of **2.24**. Although the actual mechanism of this reaction was not fully elucidated, at this point we hypothesized that MeOH, as a nucleophilic solvent, played a role in the hydrolysis reaction.

Thus, in our next modification we examined a polar aprotic solvent such as THF, still under basic conditions. No reaction was observed when we used TEA or pyridine (**entries 5 and 6**), however, an interesting product was obtained when NaOH was used (**entry 7**). NMR spectral analysis indicated that although the starting material **2.47** and the obtained product had the similar signals, the signals had shifted. Most interesting, was the observation that the signal at δ_H 4.96 in the ^{1}H NMR spectrum of **2.47** (**red spectrum, Figure 3.11**), characteristic of H-2, was no longer observed in the ^{1}H NMR spectrum of **2.52** (**blue**). Furthermore, two singlets at δ 10.45 and δ 10.42 characteristic of NH protons were observed, probably suggesting that N-9 now had an exchangeable proton, and consequently must be free of one of its substituents (**blue spectrum**).

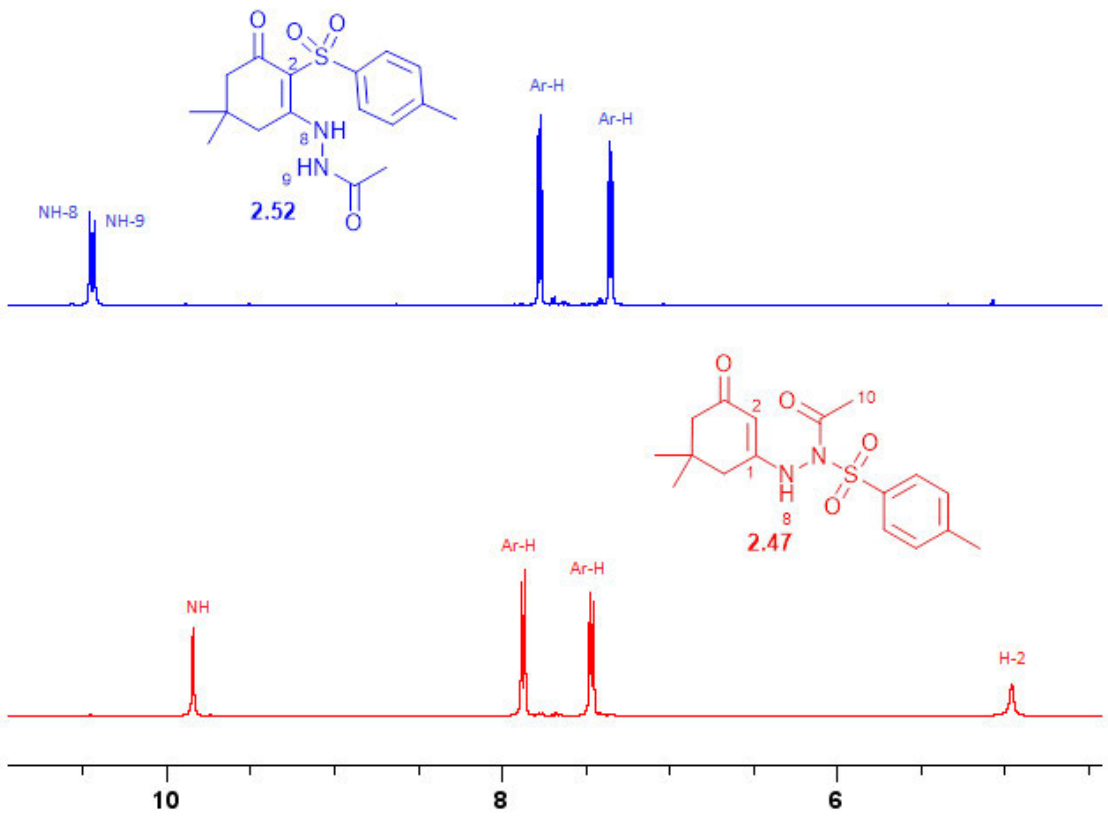

Figure 3.11: Downfield region of the ^{1}H NMR spectra of the starting material **2.47** (red) (DMSO-d_6, 400 MHz) and the unexpected product **2.52** (blue) (DMSO-d_6, 500 MHz) after an attempted cyclization using NaOH in THF. The presence of two NH signals in the blue spectrum highlighted an unsuccessful cyclisation, moreover, the detosylation attempts were also unsuccessful as evidenced by the presence of aromatic signals.

Taken together, these NMR spectroscopic data suggested that all the functional groups from the starting material were still present, but a shift had occurred resulting in the signals appearing at different chemical shifts; and that shift included a group migrating from N-9 to substitute H-2. In addition, HRESMS results revealed that the obtained product had the same mass as the starting material. Conclusive confirmation of the structure was obtained from XRD analysis, which clearly indicated that the tosyl group had migrated from the hydrazone N-9 to the C-2 position to give compound **2.52** (**Figure 3.12**). A similar effect was observed with NaH, KOH and K_2CO_3 (**entries 8 – 10**), although in lower yields. However, when tosylhydrazone **2.24** was subjected to the same reaction

conditions, it was recovered unreacted (**entry 11**). It was thus concluded that the amide group was critical for the tosyl migration reaction.

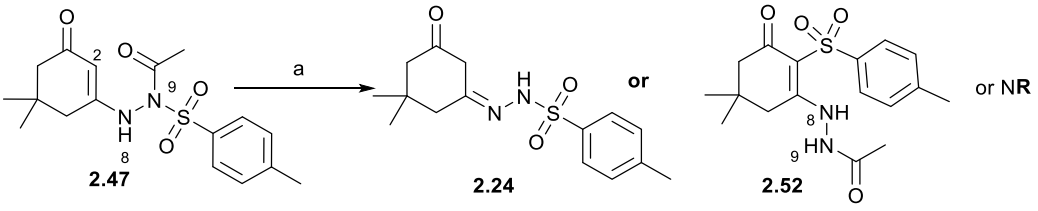

Scheme 3.14: Attempted cyclisation of **2.41** under various conditions:

Reagents and conditions: a) Starting material **2.47** or **2.24** (0.185 mmol), base in 2 mL solvent, r.t., 16 h

Table 3.4: Attempted cyclisation of **2.47** under various conditions.

Entry no.	Starting Material	Solvent	Base	Conc. (M)	Major Product	Yield (%)[a]
1	**2.47**	MeOH:H_2O 1:1	NaOH	0.25	**2.24**	90
2	**2.47**	MeOH	NaOH	0.5	**2.24**	82
3	**2.47**	MeOH	TEA	0.25	**2.24**	62
4	**2.47**	MeOH	NaOMe	0.25	**2.24**	66
5	**2.47**	THF	TEA	0.25	NR[b]	NA[c]
6	**2.47**	THF	Pyridine	0.25	NR	NA
7	**2.47**	THF	NaOH	0.25	**2.52**	76
8	**2.47**	THF	NaH	0.25	**2.52**	17
9	**2.47**	THF	KOH	0.25	**2.52**	59
10	**2.47**	THF	K_2CO_3	0.25	**2.52**	39
11	**2.24**	THF	NaOH	0.25	NR	NA

a) Isolated yields after silica gel purification. b) No reaction. c) Not applicable.

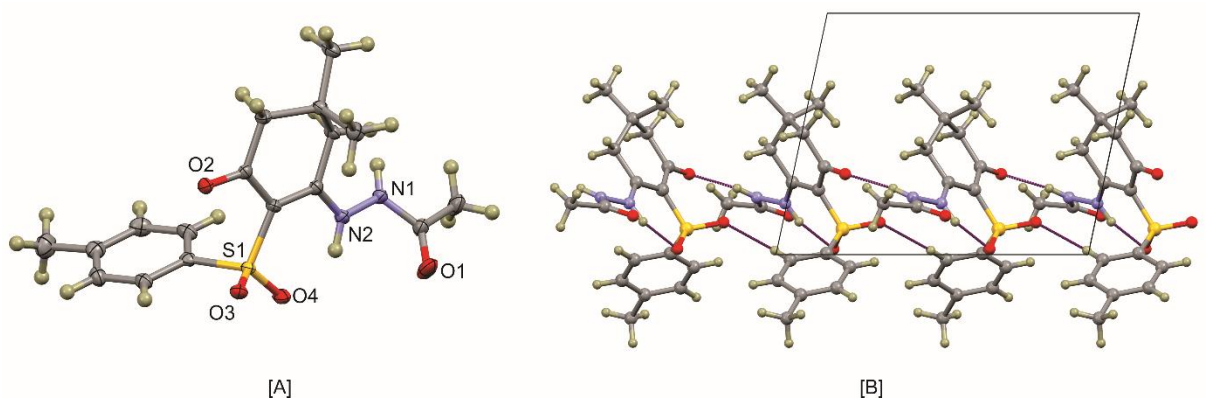

Figure 3.12: [**A**] Partially labelled structure of a single molecule of **2.52** with thermal displacement ellipsoids rendered at the 50% probability level and H-atoms shown as spheres of arbitrary radius. The asymmetric unit comprises a single molecule and *Z* = 4. [**B**] Polymeric structure of **2.52** viewed down the *b*-axis. The one-dimensional supramolecular structure is stabilised by N–H···O and C–H···O interactions with an H···O distances of 1.909 and 1.943 Å, respectively. These distances are both substantially shorter than the sum of the van der Waals radii suggesting a moderately strong interaction. The structure also shows intramolecular N–H···O interactions between the amine NH and sulfonyl O atom.

Intrigued by these results we sought to observe the effect of other acyl anhydrides on the tosyl migration, and hopefully be enlightened on the migration reaction mechanism (**Scheme 3.15**). We initiated this investigation by using butyric (**Table 3.5**, **entry 2**), isobutyric (**entry 3**) and isovaleric (**entry 4**) anhydrides and we indeed isolated the *N*-acylated compounds **2.53 – 2.55**, respectively (**Figure 3.13**). To our surprise, using acryloyl containing anhydrides (**entries 5 – 7**), resulted in the formation of the highly substituted pyrazolidinone ring-containing compounds **2.56 – 2.58**, **Figure 3.13** and **3.14**. Probably, the first step of the reaction is the nucleophilic Michael addition of N-8 followed by the amide formation at N-9 as outlined in **Scheme 3.16** below, but no further studies were done on this reaction. It should be mentioned that attempts to synthesise and isolate the trifluoracetic anhydride amide analogue under these conditions were unsuccessful, instead we obtained the cyclised and detosylated **2.23** in 15% yield.

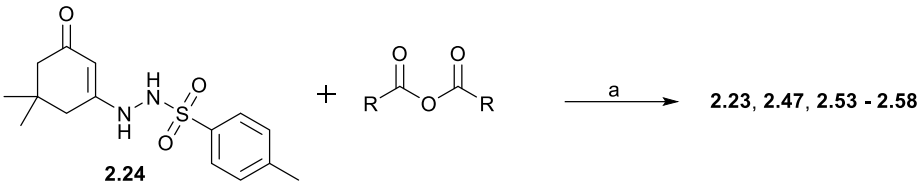

Scheme 3.15: Synthesis of amide analogues:

Reagents and conditions: a) THF, TEA, 55 °C, 2 h

Table 3.5: Synthesis of various amide analogues

Entry no.	R =	Product no.	Yield (%)[a]
1		**2.47**	60
2	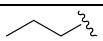	**2.53**	51
3		**2.54**	35
4	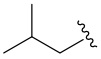	**2.55**	35
5	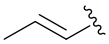	**2.56**	17
6		**2.57**	45
7		**2.58**	36
8		**2.23**	15

a) Isolated yields after silica gel purification.

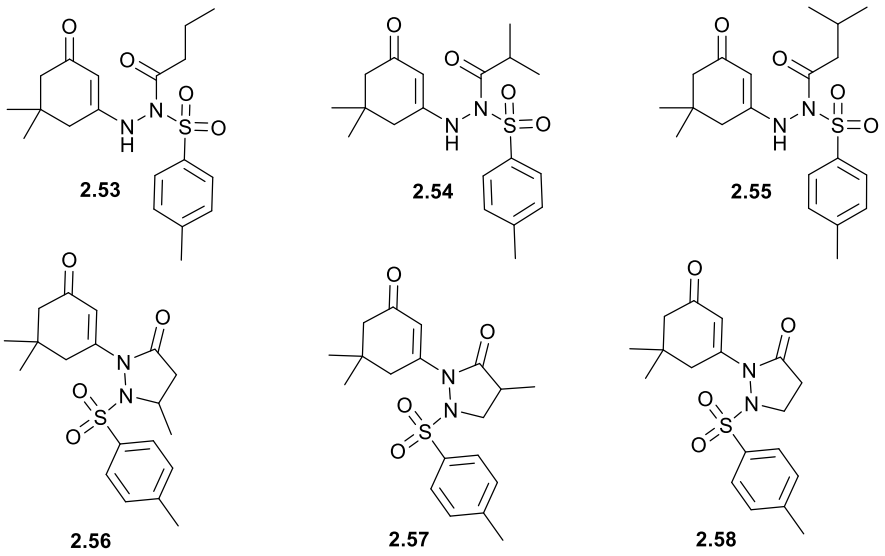

Figure 3.13: Products isolated from **Scheme 3.15** as described in **Table 3.5**

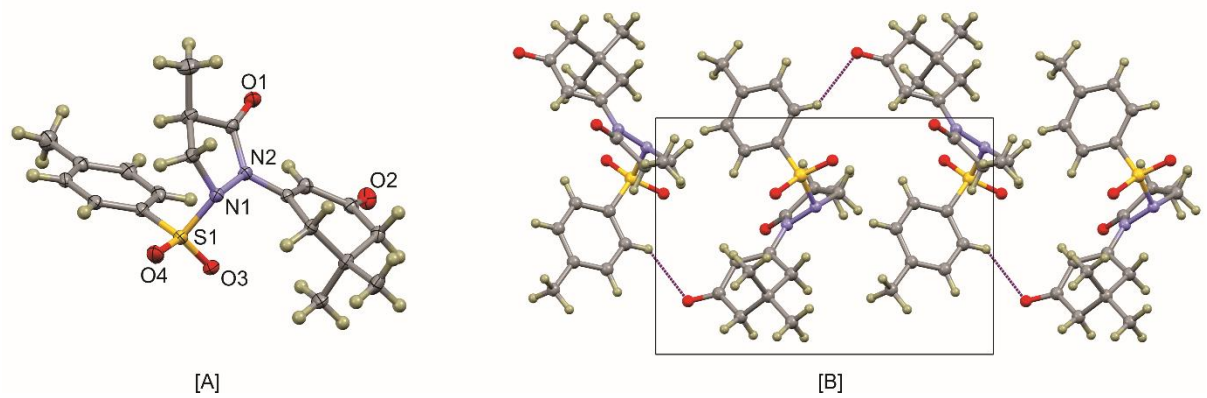

Figure 3.14: [**A**] Partially labelled structure of a single molecule of **2.56** with thermal displacement ellipsoids rendered at the 50% probability level and H-atoms shown as spheres of arbitrary radius. The asymmetric unit comprises a single molecule with Z = 4 in the $P2_1/n$ space group. [**B**] One-dimensional supramolecular structure of **2.56** viewed down the *c*-axis. The structure is stabilised by C–H···O interactions. The H···O distance is 2.469 Å. This is 0.251 Å shorter than the sum of the van der Waals radii suggesting a moderately strong interaction.

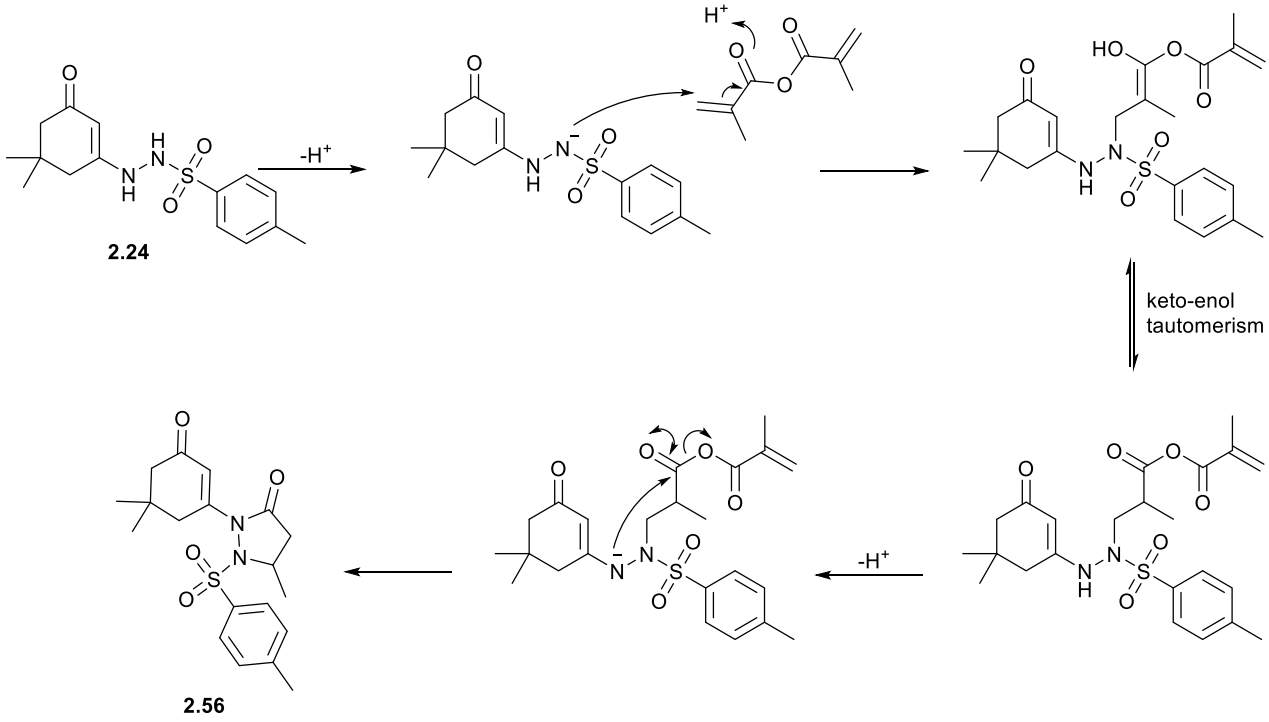

Scheme 3.16: Proposed mechanism of the synthesis of **2.56** - **2.58**

The subsequent reactions of **2.53 – 2.55** with NaOH in THF gave the corresponding rearranged products **2.59 – 2.61** in which the tosyl group migrated from the N-9 hydrazone nitrogen atom to the C-2 carbon atom (**Scheme 3.17, Table 3.6**).

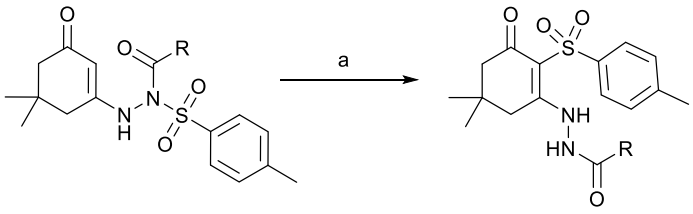

Scheme 3.17: Evaluation of the tosyl migration reaction:

Reagents and conditions: a) Starting material (0.185 mmol), NaOH (0.25 M), THF (2 mL), r.t., 16 h

Table 3.6: Evaluation of the tosyl migration reaction

Entry no.	R =	Product no.	Yield (%)[a]
1	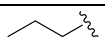	**2.59**	77
2		**2.60**	35
3	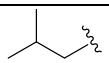	**2.61**	73

a) Isolated yields after silica gel purification.

The proposed potential mechanism is outlined in **Scheme 3.18**. We postulate that the deprotonation of the hydrazone N-8 initiates a cascade of electron movement which results in the subsequent nucleophilic attack of the sulfur atom. This could potentially occur either through a stepwise reaction *via* intermediate **2.62** (**Pathway A**) or a concerted single step reaction (**Pathway B**); both pathways would proceed through the tetrahedral transition state **2.63**. We further propose that the amide moiety acts as an electron carrier, facilitating the S-N bond cleavage to give **2.64**. Subsequently, the enamine tautomerisation and amide rearrangement results in the tosyl migrated compounds **2.52**, **2.59 – 2.61**.

Notably, the significant involvement of the amide group in the proposed mechanism corresponds with the experimental results described in **Table 3.4 Entry 11**, where no reaction was observed when the un-acylated **2.24** was subjected to the “tosyl migration” reaction conditions.

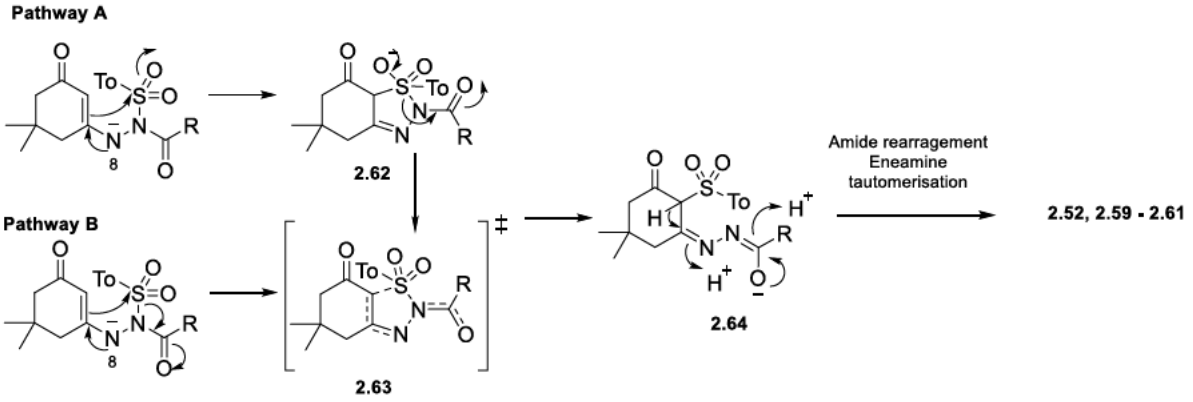

Scheme 3.18: Proposed intramolecular tosyl migration reaction mechanism either through a stepwise reaction (Pathway A) or a one-step concerted route (Pathway B) to form compounds **2.52**, **2.59** - **2.61**

To gain more insight into the tosyl migration reaction, we investigated the effect of having an alternative nucleophile, such as pyrrole, in the reaction mixture (**Scheme 3.19**). We envisioned that pyrrole would attack the tosyl group to yield **2.65**, consequently allowing for the cyclization to give **2.12**. Disappointingly, however, this reaction produced the tosyl migrated product **2.52** and not the desired compounds **2.12** and **2.65**.

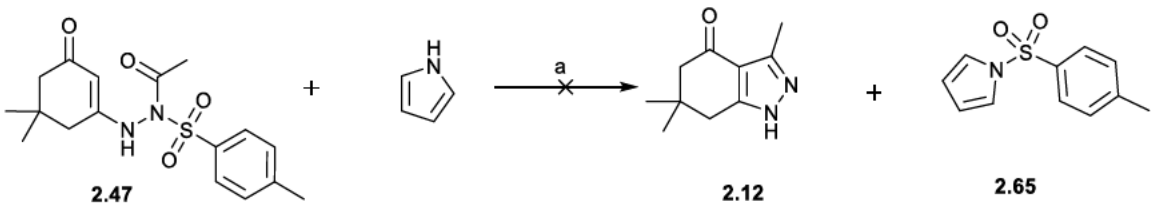

Scheme 3.19: Attempted cyclisation of **2.47** in the presence of a stronger nucleophile:

Reagents and conditions: a) NaOH (0.25 M), THF, r.t., 16 h

At this stage, it became apparent that the tosyl migration to the C-2 position was the major obstacle towards the cyclisation reaction. To overcome this obstacle, we decided to invert the order of the reaction, where we first functionalized the dimedone moiety prior to reacting it with *p*-toluenesulfonyl hydrazide **2.45** as described in **Scheme 3.20** below.

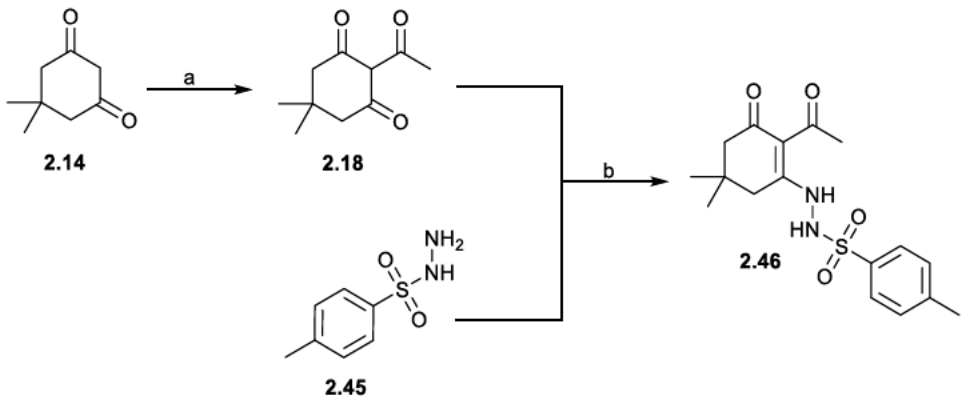

Scheme 3.20: Proposed alternative route towards the synthesis **2.46**

Reagents and conditions: a) $(CH_3CO)_2O$, DMAP, DIPEA, DCM, r.t., 24 h[54] or CH_3COCl, TEA, MeCN, 55 °C, 3 h[98]; b) toluene, cat. *p*-TsOH, 95 °C, 23 h

In principle, **2.18** and **2.45** could react to either give **2.46** or **2.66** (**Scheme 3.21**). Fortunately, either one of them could be used as a precursor for the tetrahydroindazolone condensation to give **2.12**. The obtained ^{1}H NMR spectrum was in good agreement with either one of the expected products. Most notably, two doublets integrating for two protons were observed in the aromatic region and a singlet integrating for one proton was observed at δ_H 5.75. The aromatic signals were unambiguously characteristic of the tosyl group, and the singlet was characteristic of H-2, based on these results we were confident that we had synthesised **2.46** or **2.66** which could now be subjected to the cyclisation and detosylation reaction conditions.

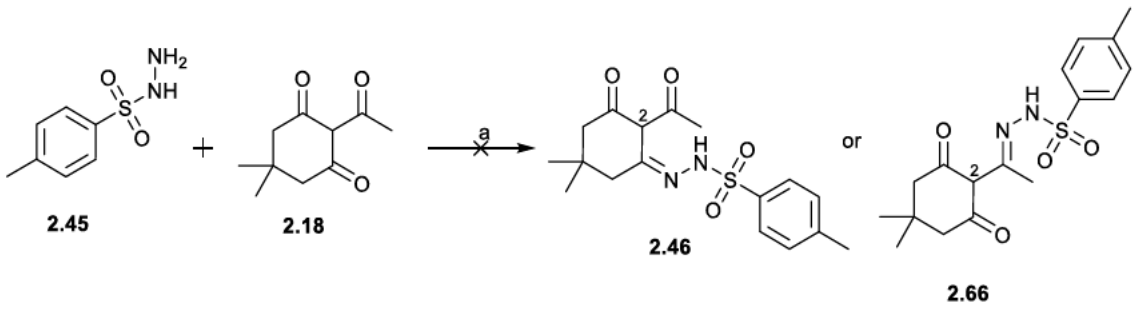

Scheme 3.21: Attempts to synthesise **2.46** or **2.66**

Reagents and conditions: a) Toluene, cat. *p*-TsOH, 95 °C, 23 h

Accordingly, the yellow solid was subjected into cyclisation and detosylation reaction conditions as described by Huang *et al.*[52] and we unexpectedly obtained the deacetylated product **2.24**. Alternatively, we attempted the cyclisation following a procedure described by Hughes *et al.* for phenylhydrazine mediated tetrahydroindazolone condensation, using acetic acid in MeOH, but unfortunately this reaction afforded an unidentified side product.

At this point, frustrated by the consistent failed attempts at the cyclisation reactions using the obtained acylated product, we needed to confirm the product structure as either **2.46** or **2.66**. Surprisingly, XRD analysis revealed that we were working with neither one of the expected products. Instead, the obtained product was an *O*-acylated hydrazone **2.67**, **Figure 3.15**.

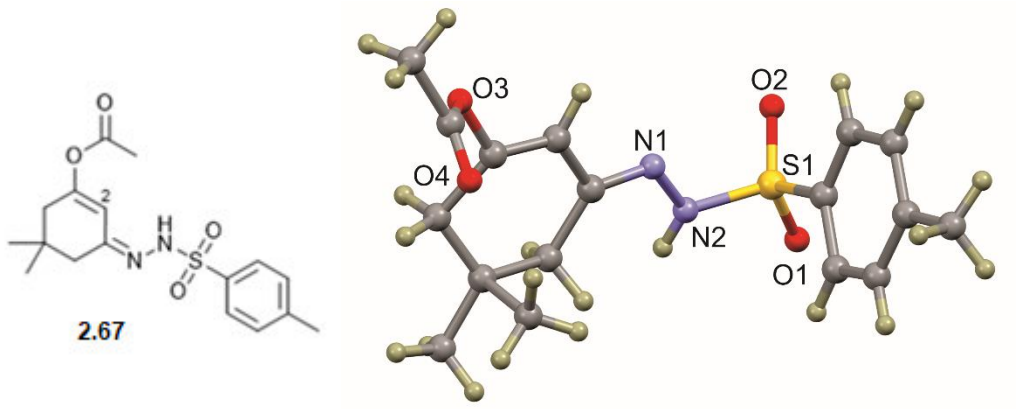

Figure 3.15: Partially labelled low-resolution structure of **2.67** showing the unexpected formation of an O-acetylated hydrazine.

Overall, based on these results, we concluded that the tosylhydrazone mediated tetrahydroindazolone condensation was not valuable for the synthesis of **2.12**. As a result, for all our subsequent reactions, **2.12** was synthesised following the procedure described in **Section 3.1.1.4**. While discouraging, the results obtained from this study represent a new opportunity in understanding the utility of sulfones in synthetic organic chemistry. In particular, the unexpected 1-5 nitrogen to carbon tosyl migration could be used for further investigations on sulfonyl migrations.

3.1.3. Coupling of 2.23 with benzonitriles

Despite the reported selectivity of the arylation of tetrahydroindazolones at the N-1 position,[96] Duan *et al*. reported the formation of the undesired N-2 arylated isomer **2.68** during the synthesis of **2.69** *via* the copper-mediated coupling of **2.23** and **2.70** (**Scheme 3.22**).[107]

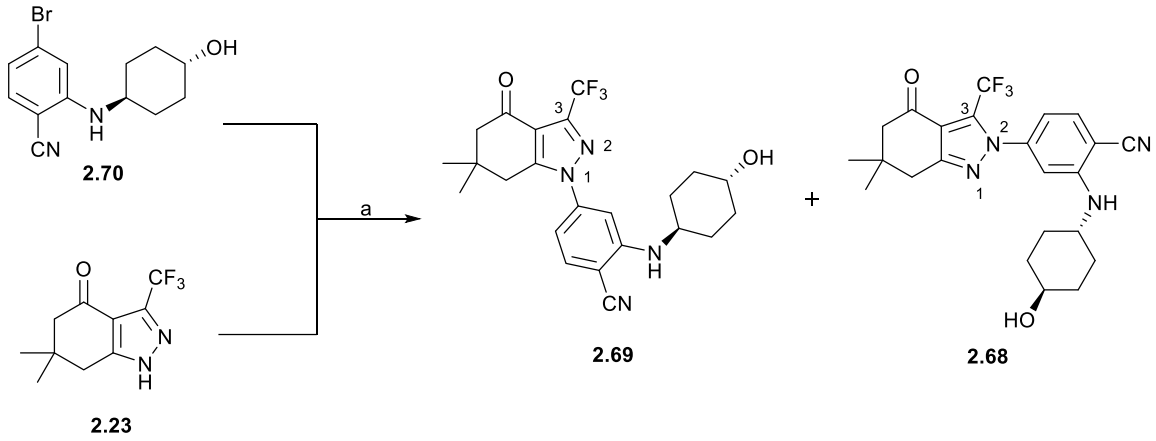

Scheme 3.22: Copper mediated Ullmann coupling of **2.23** and **2.70** as reported by Duan et al.:[107]

Reagents and conditions: a) CuI, *N*,*N*-dimethyl ethylenediamine, L-Proline, Dioxane, 98 °C

Moreover, during their study of the structure and tautomerism of tetrahydroindazolones, Claramunt *et al*. reported that **2.12** exists in two main tautomeric forms, the 1*H* tautomer and the 2*H* tautomer. Their tautomeric equilibrium studies by NMR revealed that the 2*H* tautomer was favoured compared to the 1*H* form in both DMSO-d_6 and THF-d_8, with the 1*H* tautomer being slightly more favoured in the polar solvent (**Figure 3.16**). Furthermore, only the 2*H* tautomer was observed during XRD analysis of **2.12**.[99] Based on this study, one would postulate that the N-arylation of **2.12** would result in a mixture of regioisomers, with the N-2 arylated isomer as the major product. It is worth noting that this study investigated **2.12** as an example, without varying the C-3 substituent, thus the possibility of these results varying with a CF_3 substituent cannot be ruled out. Nevertheless, considering the above information, the possibility of the synthesis of regioisomers during the N-arylation of compound **2.23** continued to be a challenge.

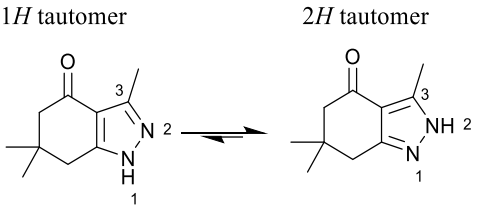

Figure 3.16: Tautomerisation of **2.12** THF-d_8[a] and DMSO-d_6[b], as reported by Claramunt *et al.*:[99]

a) Keq = [1H]/[2H] = 0.72 at 207 K

b) Keq = [1H]/[2H] = 0.79 at 300 K

To limit the number of possible undesirable reactions we opted to use 2-bromo-4-fluorobenzonitrile **2.27** instead of 2,4-difluorobenzonitrile **2.31**. The use of **2.27** allowed us to explore the orders of reactivity of the halogen substituents, hence we first selectively substituted fluorine under basic conditions. Accordingly, we followed the procedure described by Huang *et al*., where a solution of **2.23** in anhydrous DMSO was treated with NaH and stirred for 15 minutes. Thereafter, **2.27** was added and the reaction mixture was stirred at 45 °C for 23 hours. Using TLC analysis, we noted that the crude mixture consisted of three major compounds, starting materials **2.27** and **2.23**, and a prominent new spot. To our delight, after workup and silica gel purification, the desired isomer **2.29** was isolated in as an orange-yellow solid in 57% yield (**Scheme 3.23**). In accordance with the observation of Huang *et al*.[52] and Taldone *et al*.[96], the other two potential products resulting from either the N-2 arylation or bromine displacement were not isolated. The obtained NMR spectroscopic data excellently corresponded with the data reported in literature, most prominently, the absence of either fluorine-hydrogen or fluorine-carbon coupling in the aromatic region was indicative of the synthesis of the desired isomer.

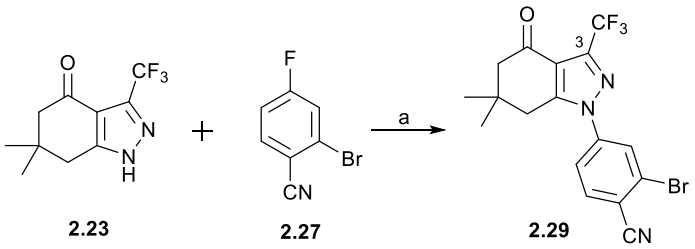

Scheme 3.23: *N*-arylation of tetrahydroindazolone **2.23**:[52]

Reagents and conditions: a) NaH, anhy. DMSO, 45 °C, 23 h, 57%

Despite the desirable selectivity afforded using **2.27**, issues observed with the subsequent *N*-arylation of **2.29** (as later discussed in **Section 3.1.4**) led us to also investigate the use of the less appealing 2,4-difluorobenzonitrile **2.31**. Wu *et al*. reported a procedure where **2.12** was coupled with **2.31** to give the desired isomer in 50% yield.[98] Unfortunately, our attempts with the procedure favoured the formation of the dimeric product **2.71** with a 13:1 ratio in relation to the mixture of regioisomers **2.36** and **2.72** (**Scheme 3.24**). Furthermore, the separation of the regioisomers by repeated silica gel chromatography was unsuccessful as the two compounds eluted very closely. Attempts to minimize the formation of the dimer by either significantly decreasing the reaction time or increasing the equivalents of **2.31** proved ineffective.

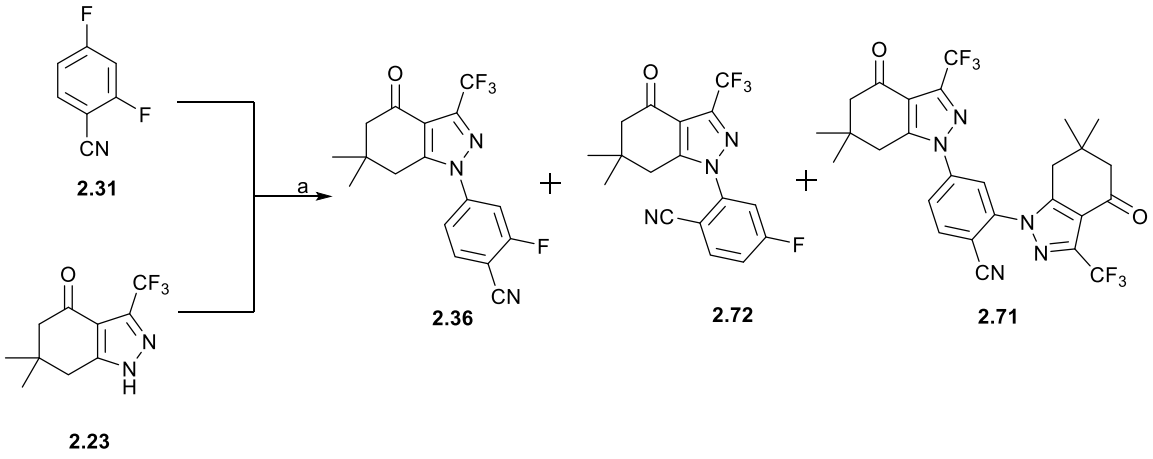

Scheme 3.24: Attempted *N*-arylation of tetrahydroindazolone **2.23**:[54]

Reagents and conditions: a) K_2CO_3, DMSO, r.t, 16 h

Subsequently, we envisioned that having **2.31** in excess to **2.23** would slow down the dimerization. Accordingly, we altered the reagent addition, a suspension of **2.23** and K_2CO_3 in anhydrous DMSO was stirred for 15 minutes; thereafter, a solution of **2.31** in anhydrous DMSO was cannulated into the reaction mixture. The reaction was stopped after 20 minutes, as soon as the dimeric product started forming, as observed by TLC analysis. Expectedly, the reaction now favoured the formation of the regioisomers compared to the dimeric compound (3:1). However, the recovery of about 50% of the unreacted starting materials implied that the reaction had to be repeated multiple times prior to getting a reasonable amount of the desired regioisomeric mixture for subsequent steps. It then became apparent that the bottleneck of this approach was the formation of the dimer even after short reaction times, and the inability to separate the two regioisomers using the available silica gel column chromatography, thus it was considered impractical and all our subsequent *N*-arylation reactions were done as described in **Scheme 3.23**.

3.1.4. Amine coupling, nitrile hydrolysis and deprotection

3.1.4.1. Synthesis of 2.5 *via* the palladium catalyzed amine coupling

The main methods reported for the formation of the aromatic carbon-nitrogen bond largely depend on the aryl substituent being displaced. Amination of aryl bromides is normally mediated by metal catalysts, such as palladium or copper, in the presence of suitable ligands.[107, 123] Palladium-mediated cross-coupling of aryl halides and amines, commonly known as the Buchwald-Hartwig reaction, encompasses a diverse range of catalysts and ligands.[124, 125] For instance, Huang *et al.* successfully demonstrated the coupling of **2.29** with aminocyclohexanol using $Pd(OAc)_2$ and DPPF as the ligand in the presence of NaO*t*Bu at 170 °C in a microwave reactor to afford the benzonitrile which was subsequently hydrated to give the corresponding benzamide in 84% yield (**Scheme 3.25**).[52]

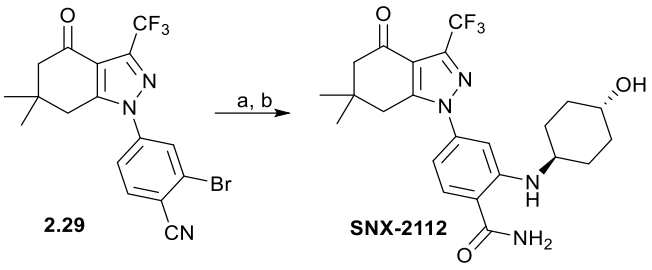

Scheme 3.25: Palladium catalysed amine coupling:[52]

Reagents and conditions: a) *trans*-4-aminocyclohexanol, $Pd(OAc)_2$, DPPF, NaO*t*Bu, toluene, 170 °C, microwave, 3 h; b) 30% H_2O_2, 1 M NaOH, EtOH, DMSO, r.t, 84%

Sadly, Taldone *et al*. reported that they were unable to reproduce the results, only detecting the desired product in trace amounts.[96] In their continued efforts to synthesise **2.69**, they screened different palladium catalysts such as $PdCl_2$, $Pd_2(dba)_3$ or $Pd(PPh_3)$, different solvents such as dimethoxyethane (DME) or DMF, and they also changed the base to K_3PO_4; however, with no success. Their best approach was using $Pd_2(dba)_3$ and DavePhos as the ligand at 50 °C overnight to afford the desired product in a low 45% yield (**Scheme 3.26**). To our great interest, was their coupling of **2.29** with *trans*-4-diaminocyclohexane to give the desired product **2.73** in 41% yield.[96] Despite the success of the coupling under the reported conditions, we were keen on investigating facile conventional reaction conditions to afford the desired product in higher yields.

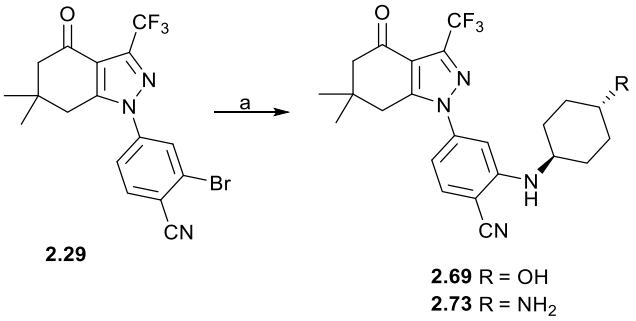

Scheme 3.26: Palladium catalysed amine coupling as reported by Taldone *et al*.:[96]

Reagents and conditions: a) *trans*-4-aminocyclohexanol/ *trans*-4-diaminocyclohexane, $Pd_2(dba)_3$, DavePhos, NaO*t*Bu, DME, 50 °C, overnight

Our initial assessment of the approach reported by Taldone *et al*. revealed one major issue, the use of an unprotected diamine, which may have dimerised, thus decreasing the yield of the desired product. To eliminate the possibility of dimerisation, we protected one amino moiety of **2.74** following a modified version of the procedure described by Masci *et al*. (**Scheme 3.27**).[126] After workup, various purification attempts were unsuccessful, thus the crude material containing **2.75** was used without further purification.

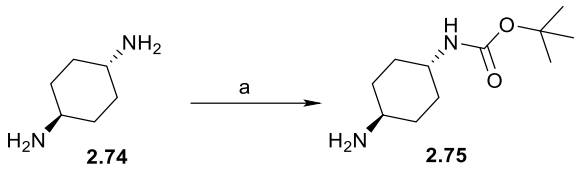

Scheme 3.27: *N*-Boc protection of trans-1,4-cyclohexanediamine:[126]

Reagents and conditions: a) Boc_2O, THF, 0 °C, 2 h

Another problem observed with the approach reported by Taldone *et al*. was the use of a catalyst and ligand that were not readily available to us, and thus we sought to investigate methods using the reagents that we already had in hand. Fortunately, there are various literature reports of palladium catalysed coupling of aryl halides with amines.[123, 125] At this point, the work done by Driver *et al*. caught our attention where they discovered the air-stable DPPF-ligated palladium complex (DPPF)$PdCl_2$, which successfully catalysed the coupling of aryl halides and primary amines in THF at 100 °C to give secondary arylamines in high yields (80-96%).[123] Accordingly, the (DPPF)$PdCl_2$ complex was prepared following a slightly modified procedure described by Davies *et al*. (**Scheme 3.28**).[127] Palladium(II) chloride ($PdCl_2$) was dissolved in refluxing acetonitrile and stirred for 4 hours under an inert atmosphere of nitrogen to yield the palladium(II)chloride diacetonitrile complex **2.76**. Thereafter, DPPF was added in a 1:1 mole ratio to the metal ion, and the reaction mixture was further stirred for 1 hour. Subsequent filtration and recrystallisation in DMF resulted in **2.77** as an orange-red solid, which was dried in vacuum and used without any further purification.

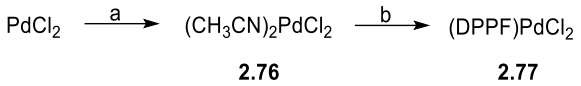

Scheme 3.28: Preparation of DPPF($PdCl_2$):[127]

Reagents and conditions: a) CH_3CN, reflux, 4 h, N_2(g); b) DPPF, reflux, 1h

Subsequently, complex **2.77** and DPPF were added to a suspension of **2.29** and NaO*t*Bu, followed by the addition of the Boc-protected amine **2.75** and reacted between 60 – 65 °C for 4 hours (**Scheme 3.29a**). Purification by silica gel chromatography afforded a yellow solid. ^{1}H NMR analysis of the obtained product indicated that the coupling was successful, however, some minor impurities were observed. Successive attempts to purify the compound using silica gel chromatography were inefficient. This was particularly challenging since only one spot was observed during TLC analysis irrespective of the solvent system used. Thus, we reasoned that the impurities were due to the amine starting material and different purification methods had to be explored. Unfortunately, attempts to recrystallise the product from several hot solvents were unsuccessful.

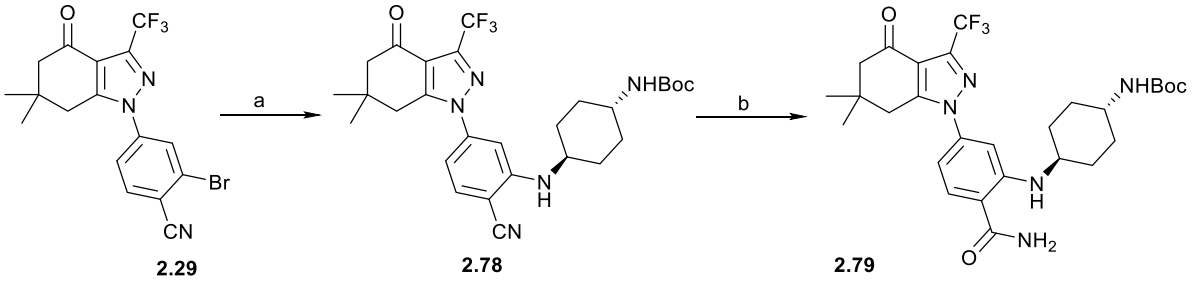

Scheme 3.29: Palladium catalysed amine coupling and subsequent nitrile hydyrolysis of **2.29**:

Reagents and conditions: a) **2.75**, **2.77**, DPPF, Na*t*OBu, THF, 60-65 °C, 4 h, 65%; b) K_2CO_3, 30% H_2O_2, DMSO, r.t., 2 - 3 h, 73%

The subsequent nitrile hydrolysis of **2.78** was catalysed by 30% H_2O_2 in DMSO following a procedure described by Wu *et al.*[98], the suspension was stirred at room temperature and the reaction was monitored by TLC (**Scheme 3.29b**). The starting material would typically be depleted after 2-3 hours, and upon purification the product **2.79** was obtained as an off-white solid. Gratifyingly, based on the

^{1}H NMR spectrum, we no longer observed the impurity observed for the synthesis **2.78**. The presence of a signal at δ_C 170.7, characteristic of an amide functional group, in the ^{13}C NMR spectrum of **2.79** was evidence of a successful hydrolysis.

Boc deprotection using TFA in DCM yielded the desired core intermediate **2.5** (**Scheme 3.30**). The product was either obtained as a free amine or TFA salt, however, in both cases full NMR spectroscopic analysis was indicative of the synthesis of the desired product.

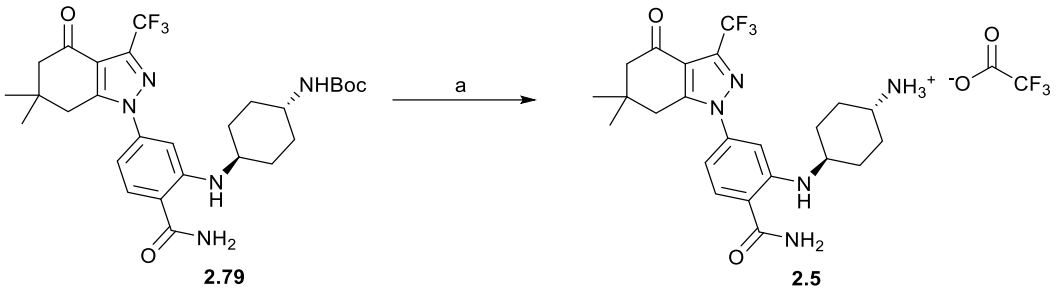

Scheme 3.30: Boc deprotection to yield the core intermediate **2.5**:

Reagents and conditions: a) TFA, DCM, r.t, 5 - 7 h, 35 - 41%

3.1.4.2. Synthesis of 2.6 *via the* base catalysed amine coupling

As previously stated, contrary to the palladium catalysed substitution of bromine described in the previous section, the displacement of the more reactive fluorine was a more simple and efficient approach, which made it an appealing route. This method enabled aryl amination using readily available and inexpensive reagents such as DIPEA. Additionally, fluorine displacement is typically caried out under conventional reaction conditions; eluding the complexity observed with metal catalysed coupling reactions. Evidently, we successfully synthesised **2.80** by subjecting **2.30** to reaction conditions reported by Hughes *et al*. (**Scheme 3.31a**), the subsequent hydrolysis was performed as described above to afford the corresponding benzamide **2.81** as a pale-yellow solid (**step b**).

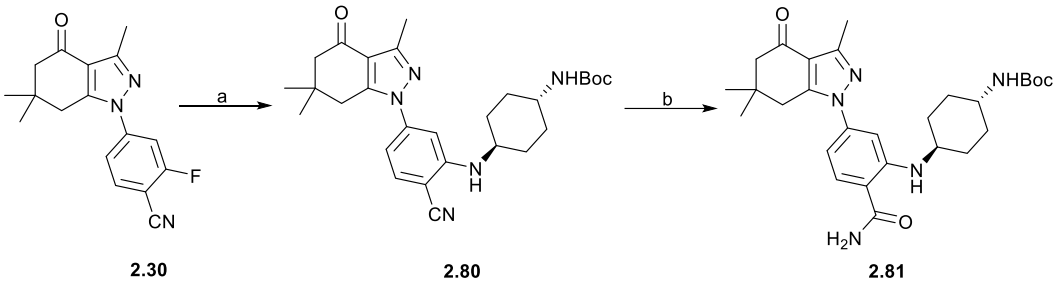

2.30 2.80 2.81

Scheme 3.31: Base catalysed amine coupling and subsequent nitrile hydrolysis of **2.30**:

Reagents and conditions: a) **2.75**, DIPEA, DMSO, 90 °C, 30 - 60 min., 74%; b) K_2CO_3, 30% H_2O_2, DMSO, r.t., 2 - 3 h, 73%

Consequent Boc deprotection following the general procedure in **Scheme 3.30** yielded the core intermediate either as a free amine or a TFA salt (**Scheme 3.32**).

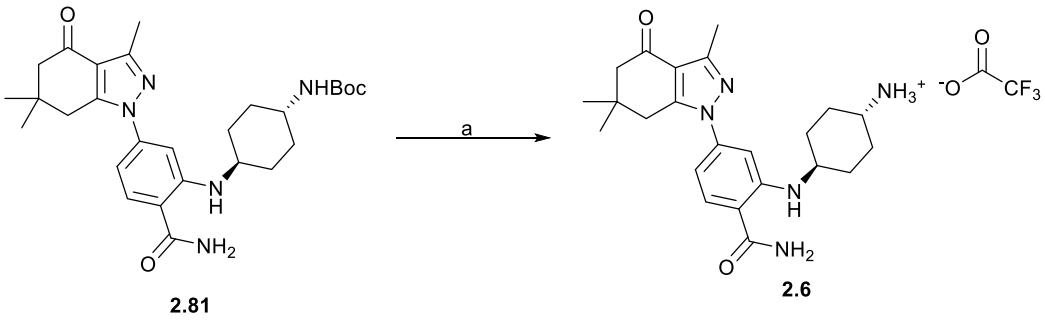

2.81 2.6

Scheme 3.32: Boc deprotection to yield the core intermediate **2.6**:

Reagents and conditions: a) TFA, DCM, r.t, 5 - 7 h, 64 - 79%

3.1.5. Completing the scaffolds

As previously discussed, the main aim of this project was to synthesize extracellular HSP90 inhibitors by tethering the already known active HSP90 inhibitor with polar *N*-alkyl chains. Upon successful synthesis we then explored the effect of these extracellular inhibitors on cancer cells and their specific mechanism of action.

We identified the sulfonic and phosphonic acid functionalities as consisting of desirable hydrophobicity required for the design of the cell-impermeable inhibitors. Compounds **2.1** and **2.2**

were designed to incorporate the sulfonic acid moiety. Compounds **2.3** and **2.4** were designed to incorporate the phosphonic acid moiety.

3.1.5.1. Synthesis of sulfonate-containing extracellular inhibitors

Nucleophilic substitution of the alkyl halide afforded the sulfonate-containing extracellular inhibitors. Direct *N*-alkylation of primary amines with alkyl halides is one of the traditional methods for the preparation of secondary amines. Theoretically, the reaction yield could be improved by using a large excess of the amine **2.5**; however, this would be a wasteful process in our case given that the amine was synthesized in our laboratory.

Our initial attempts began with the synthesis of **2.2**, where the reactants were suspended in DMF in the presence of DIPEA and heated to 50 °C (**Scheme 3.33**). After stirring for 18 hours the reaction mixture was concentrated and purified by silica gel chromatography using DCM:MeOH as the mobile phase, to yield the desired product **2.2** as a white fluffy solid.

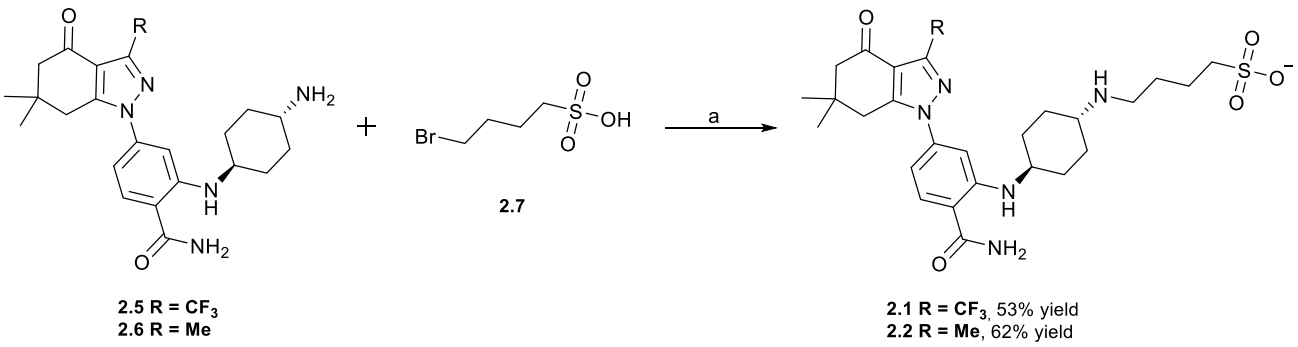

Scheme 3.33: Synthesis of the sulfonate containing extracellular HSP90 inhibitors:

Reagents and conditions: a) DIPEA, DMF, 50 °C, 18 h

The significant difference between the ^{1}H NMR spectra of the starting material **2.6** and the obtained product was the presence of signals characteristic of four additional methylene groups. Conclusive evidence of the synthesis of the desired product was obtained from HRESMS. Extracellular inhibitor **2.1** was prepared in an analogues fashion from amine **2.5**, and the synthesis of the desired product was confirmed by full NMR spectroscopic characterization and HRESMS.

3.1.5.2. Synthesis of phosphonate-containing extracellular inhibitors

The synthesis of the phosphonate-containing extracellular inhibitors **2.3** and **2.4** incorporated the formation of an amide linkage from the amines **2.5** and **2.6** with the acid **2.8**, which is a common feature in various biologically relevant molecules. One traditional method for amide synthesis is the condensation of a carboxylic acid functionality with an amine group in the presence of a carboxyl activating agent such as 1-ethyl-3-(3-dimethylaminopropyl)carbodiimide (EDCI).[128] Mechanistically, the carboxylic acid is activated by EDCI, generating an intermediate which then directs reacts with the amine to yield the desired amide. To preclude formation of side products, nucleophiles such as hydroxybenzotriazole (HOBt), *N*-hydroxysuccinimide (NHS) and DMAP can be added to the reaction mixture.[128]

To our delight, during their study of the synthesis and evaluation of HSP90 probes, Taldone *et al*. reported a similar reaction where the desired amide **2.82** was synthesised from the coupling of **2.5** and carboxylic acid **2.83** in the presence of EDCI and DMAP in DCM (**Scheme 3.34**). Unfortunately, our attempt following this procedure was unsuccessful. We reasoned that the poor solubility of the acid **2.8** in DCM was the main obstacle towards the successful synthesis of our desired compound.

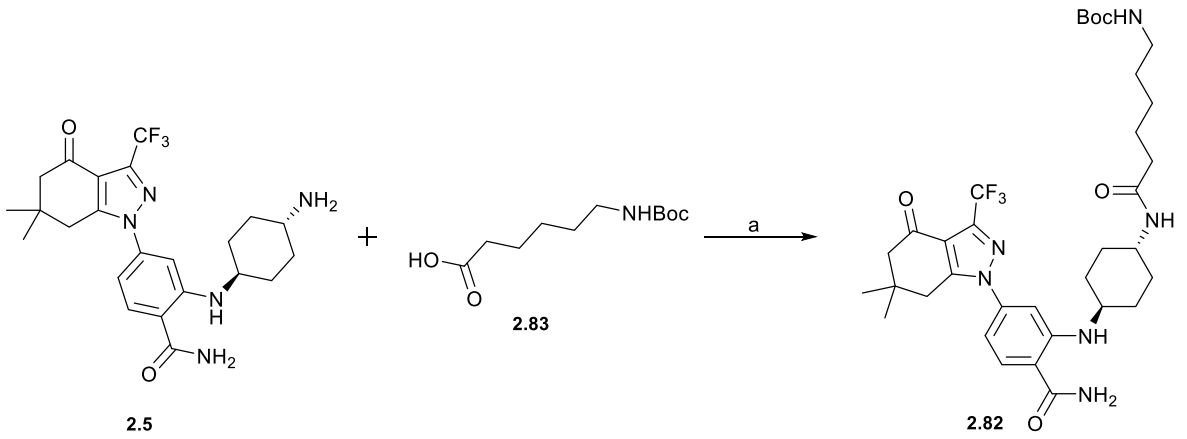

Scheme 3.34: Amide formation from **2.5** as reported by Taldone *et al*.:[96]

Reagents and conditions: a) DMAP, EDCI, DCM, r.t., 2 h, 91%

Alternatively, Dang *et al*. reported the coupling of monoprotected amine **2.74** and with 6-phenylhexanoic acid **2.84** in DMF with HOBt and EDCI in the presence of DIPEA to yield **2.85** (**Scheme 3.35**). The use of DMF was an advantage to us since it was a more polar solvent which could potentially dissolve the carboxylic acid **2.8**.

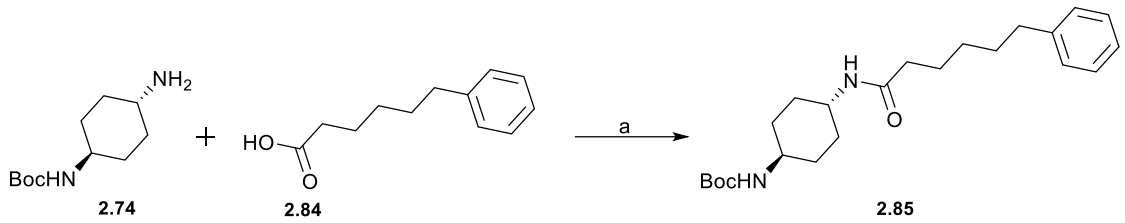

Scheme 3.35: Amide formation from **2.74** as reported by Dang *et al*.:[129]

Reagents and conditions: a) DIPEA, EDCI, HOBt, DMF, r.t., 12 - 16 h

Accordingly, following a slight modification, extracellular inhibitors **2.3** and **2.4** were prepared by coupling amine **2.5** and **2.6** with carboxylic acid **2.8** under the conditions described in **Scheme 3.36**. The reactions were monitored by TLC, no starting material could be visualized on the TLC plate. Worryingly, however, was the visualization of multiple spots on the TLC plate. The crude reaction mixture was purified by silica gel chromatography and only one spot could be isolated and characterised. Gratifyingly, this compound was characterised to be the desired product **2.4**, albeit in

poor yields. Similarly, **2.3** was synthesized following the same procedure. The structure of **2.3** was confirmed using NMR spectroscopy and HRESMS. Unfortunately, sufficient purification of these compounds proved to be challenging, with minor impurities observed in the upfield region of their ^{1}H NMR spectra. Delightfully, however, high resolution mass spectroscopic data was in agreement with the expected masses of products **2.3** and **2.4** with 98.3% and 97.3% purity, respectively.

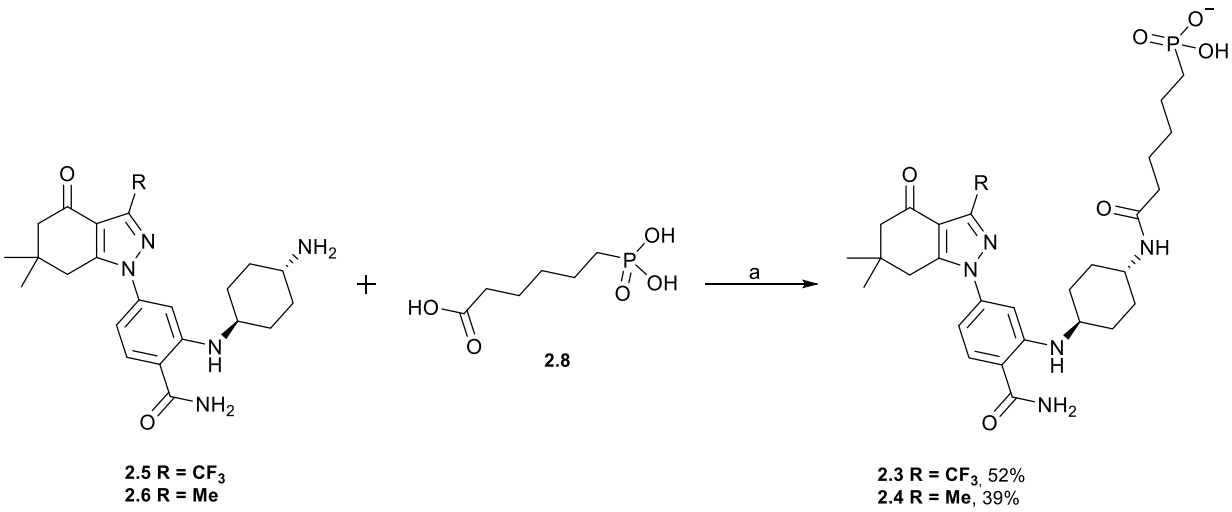

Scheme 3.36: Synthesis of the phosphonate containing extracellular HSP90 inhibitors:

Reagents and conditions: a) DIPEA, EDCI, NHS, DMF, r.t., 42 - 72 h

4. CHAPTER 4: BIOLOGICAL EVALUATION

Having synthesised our desired analogues, we submitted them for biological assessment with our collaborator Prof. Adrienne Edkins from Rhodes University**.** As stated in Chapter 1, the clinical development of intracellular HSP90 inhibitors is limited by the induction of the compensatory HSR, which triggers the overexpression of HSP70, which compensates for the depleted function of HSP90. A growing body of evidence suggests that targeting the extracellular environment would be of advantage and devoid of the drawbacks observed with intracellular HSP90 inhibition. As described previously, in order to target extracellular HSP90, we hypothesized that tethering a disordered polar substituent to a known HSP90 inhibitor, in a manner that would not disrupt the pharmacophore, we could prevent cellular penetration, and selectively inhibit extracellular HSP90 (**Figure 4.1**).

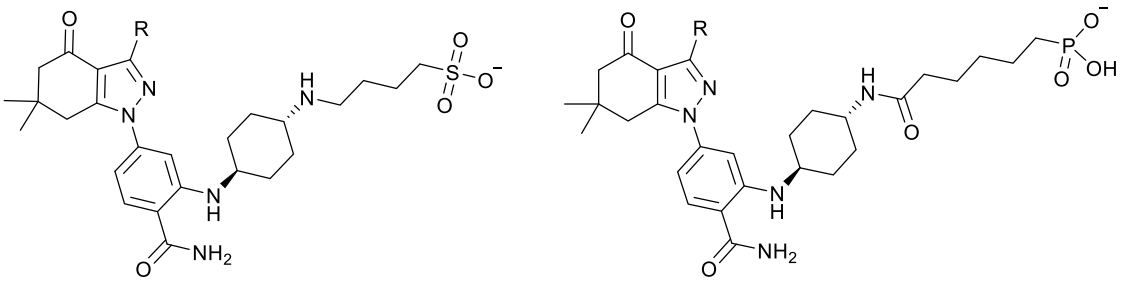

2.1 R = CF_3
2.2 R = Me

2.3 R = CF_3
2.4 R = Me

Figure 4.1: Chemical structures of target compounds synthesised in this project

As a means of assessing the success of our design hypothesis we were interested in two preliminary biological evaluations; 1. To evaluate if our modifications reduced intracellular HSP90 activity and whether they stimulated the pro-oncogenic HSR, and 2. Whether they still possessed potent cytotoxicity.

4.1. Intracellular HSP90 inhibition and HSR stimulation

CDK4 is an intercellular client of HSP90, which is degraded upon HSP90 inhibition, and is used as an indirect measure of HSP90 inhibition. Similarly, inhibition of intracellular HSP90 stimulates the HSR which results in increased expression of HSP70. Accordingly, intracellular HSP90 inhibition was determined by treatment of HeLa cells with our inhibitors, followed by quantitative Western blot analysis of cell lysates. These data were collected using a previously reported method,[130] alongside a blank (DMSO) control and a parent HSP90 inhibitor SNX2112.

From the Western blot analysis, **Figure 4.2**, we observed that in comparison to the DMSO control SNX2112 completely depleted CDK4, whilst simultaneously increasing HSP70 levels, thus indicating inhibition of intracellular HSP90 and stimulation of the HSR, at both tested concentrations (25 and 50 nM). By comparison, folded CDK4 was still detected following treatment with the modified HSP90 inhibitors at the same concentrations, while HSP70 was present at levels comparable to the DMSO control.

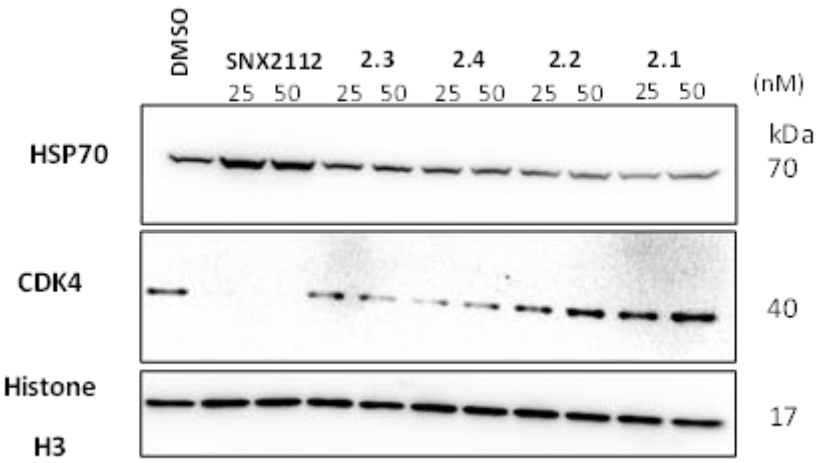

Figure 4.2: Western blot for CDK4 and HSP70 levels. HSP90 inhibition should reduce CDK4 levels and increase HSP70. This is what is observed for **SNX2112**, and the inverse effect is observed for our synthesised compounds, thus indicating reduced intracellular HSP90 inhibition. This is an example of one of five replicate blots showing the same result

Quantification of these data was achieved through densitometry readings (**Figure 4.3** and **4.4**) This analysis conformed that SNX2112 resulted in a statistically significant reduction in CDK4 abundance, whilst having the converse effect on HSP70 and CDK4 concentration. At both concentrations, compounds **2.1, 2.2** and **2.4** did not deplete CDK4 abundance below the threshold determined in the DMSO control. These data indicate a small yet significant increase in CDK4 in the presence of 2.1 and 2.2. However, this is more likely an artefact of the experiment. While compound **2.3** seemingly depleted CDK4 at 25 nM, this effect was absent at 50 nM, and was more in line with the trend observed for **2.1, 2.2** and **2.4**. HSP70 levels in the presence of all four compounds was consistent, and statistically not significantly different to those observed in the DMSO control.

Together these data suggest that our modified HSP90 inhibitors compounds were not inhibiting intracellular HSP90 nor were they stimulating the complementary HSR. While promising, this does not necessarily classify them as extracellular inhibitors.

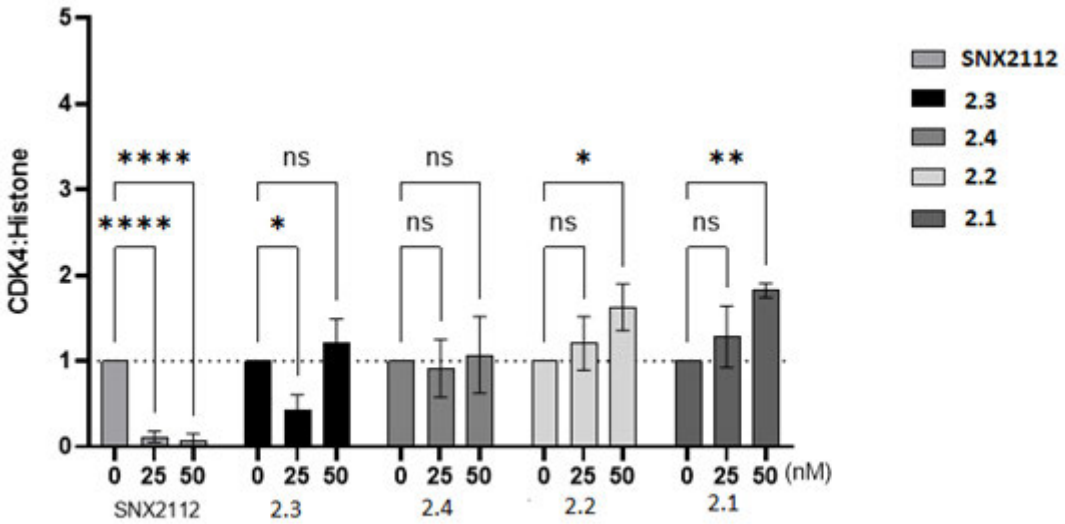

Figure 4.3: Average densitometry for the levels of CDK4 relative to Histone loading control. Data are averages of two independent replicates but show a trend consistent across five independent replicates. Statistical analysis is by two-way ANOVA comparing all to the DMSO treated control.

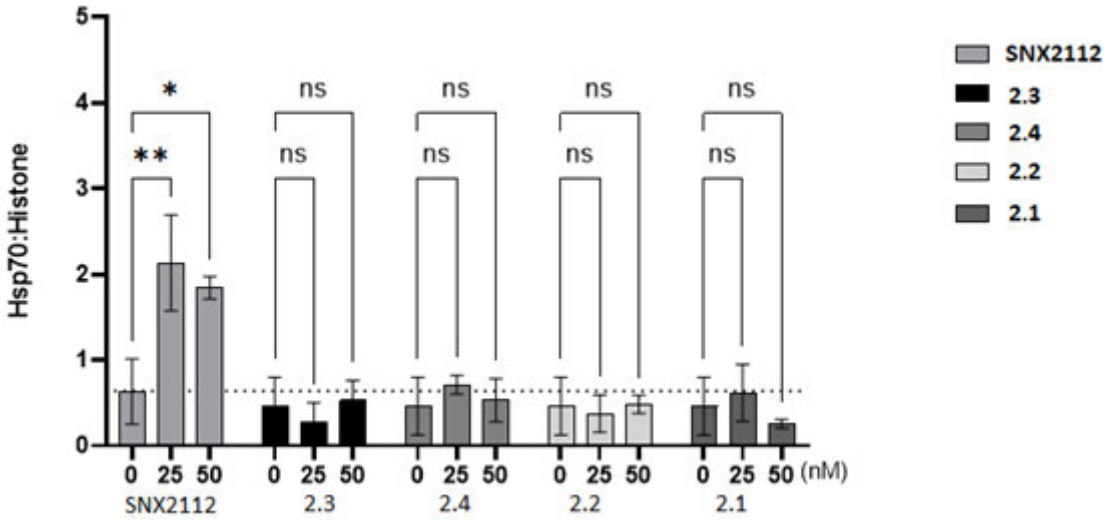

Figure 4.4: Average densitometry for the levels of HSP70 relative to Histone loading control. Data are averages of two independent replicates but show a trend consistent across five independent replicates. Statistical analysis is by two-way ANOVA comparing all to the DMSO treated control

4.2. Cytotoxicity evaluation

Finally, we evaluated the cytotoxicity activity of the synthesised compounds against a *HeLa* cell line (**Figure 4.5**). Data are reported as pIC_{50} (M), which is a negative algorithm of IC_{50} in molar concentration.[131] Higher pIC_{50} depicts greater potency; *i.e.*, pIC_{50} of six is a micromolar compound, while that of nine represents a millimolar compound.

These data show that compared to **SNX2112**, the modifications resulted in an order of magnitude reduction in cytotoxicity. The reasons for this are not clear, however the inability to disrupt intracellular HSP90, due to their cell-impermeability, is likely a factor. As mentioned in this thesis, our novel compounds were designed to target extracellular HSP90, but, the data we currently have on hand is not sufficient to confirm their mechanism of action and whether these compounds exert their activity through HSP90 binding; more assays are underway. Importantly, however, all four analogues still retained potent cytotoxic activity in the nanomolar range. Overall, there was no substantial difference in activity between the four compounds, and thus no real preferences for any of the

structural difference can be inferred. However, given the small number of compounds a structure activity relationship analysis would be premature.

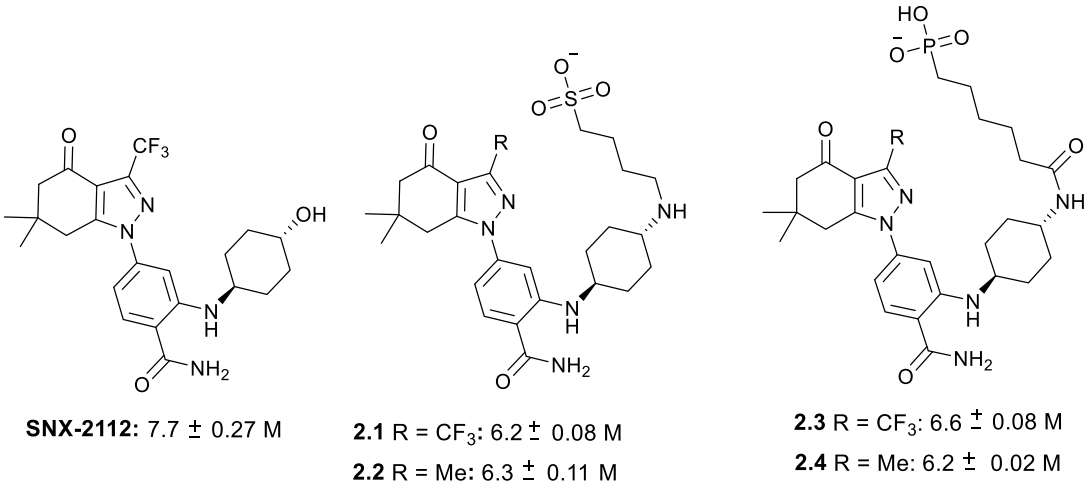

Figure 4.5: Cytotoxicity data: Average pIC_{50} values of the synthesised compounds against a *HeLa* cell line

4.3. Conclusion

Biological results reported in this chapter displayed the potential therapeutic value of cell-impermeable compounds as extracellular HSP90 inhibitors; furthermore, a structure-activity investigation of these compounds presents a valuable research probe for future studies.

Our modification impeded intracellular HSP90 activity and did not induce the compensatory HSR. We further confirmed that our novel synthesised compounds, **2.1** – **2.4**, displayed potent cytotoxicity in the nanomolar range against a *HeLa* cell line; however, with an order of magnitude less potent than the parent compound, **SNX2112**. Presumably, to some extent, the reduced cytotoxicity was due to the reduced HSP90 inhibition. Furthermore, the inhibition of extracellular activity, will have additional features beyond cytotoxicity such as inhibition of metastasis. If these compounds are not found to disrupt extracellular or intracellular HSP90, then they represent an exciting new class of inhibitors, which act *via* a currently unknown cytotoxicity pathway. Ongoing biological assessments include

confirmation of ATPase activity in an HSP90 enzyme-based assay, as well as longer terms evidence of metastasis inhibition through wound healing assays

In addition to cytotoxicity, such extracellular targeted inhibitors, could further be useful in treatment of cancers with an extracellular HSP90 dependant metastasis. These data support the feasibility of targeting extracellular HSP90 as a novel anticancer strategy. Conclusively, compounds synthesised during this project present a good starting point for the development of extracellular HSP90 inhibitors.

5. CHAPTER 5: CONCLUSION AND FUTURE WORK

With the intention of introducing hydrophobicity for the development of extracellular HSP90 inhibitors, we envisioned that the desired compounds could be afforded through the introduction of polar alkyl chains containing sulfonic acid and phosphonic acid moieties, onto a well-characterized and potent intracellular HSP90 inhibitor. Based on the results reported by Hughes *et al*., this was to be achieved by linking the polar alkyl functionalities on the C-2' position of the HSP90 inhibitors.[54]

The HSP90 inhibitor was synthesized using developed methodology, as well as modified methodology, there was no obviously superior method, rather the synthetic approach was mainly determined by the C-3 substituent. As previously mentioned, given the key role of the benzonitrile **2.27** and **2.31**, and the interest in synthesising regioisomerically pure precursors prior to the condensation to yield **2.28 - 2.30** and **2.36**, we were initially interested in investigating **Pathway B**, which eliminated the potential of forming the *N*-2 arylated intermediates (**Scheme 2.10**).

Key intermediate **2.30** was efficiently afforded from the condensation of **2.18** and phenylhydrazine **2.32** (**Scheme 5.1**). The major challenge with this method was the purification of the phenylhydrazine **2.32**. This challenge could be overcome by using the brominated phenylhydrazine. However, with our great interest in a simple and efficient subsequent amination, we opted to proceed with the procedure originating from 2,4-difluorobenzonitrile. The subsequent amination of **2.30** was performed using cost-effective and simple procedures under basic conditions (**step d**) to yield the desired intermediate in 74% yield. Subsequent nitrile hydrolysis (**step e**) and Boc deprotection afforded the amine intermediate **2.6** in good yields (79%).

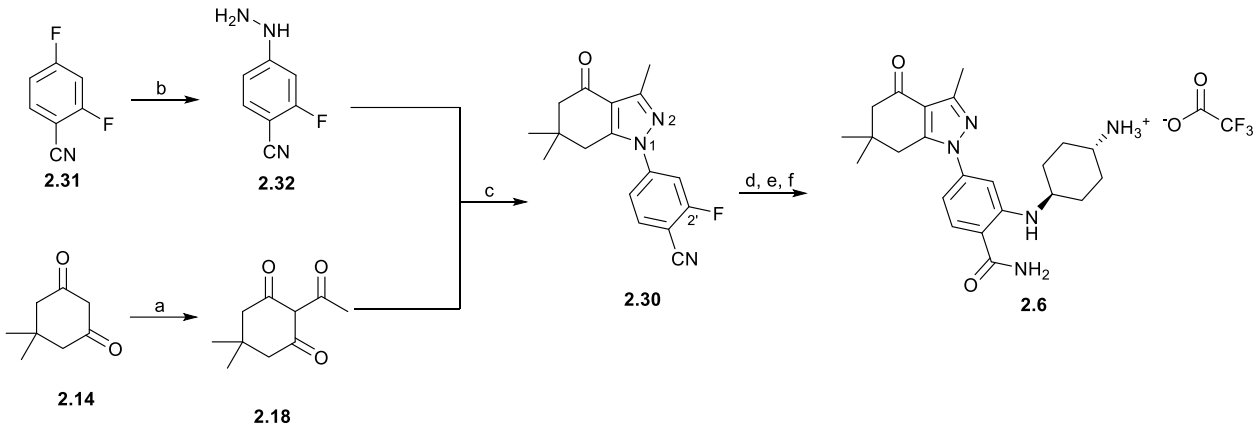

Scheme 5.1: Synthesis of intermediate **2.30** *via* Pathway B:

Reagents and conditions: a) $(CH_3CO)_2O$, DMAP, DIPEA, DCM, r.t., 24 h, 57% yield; b) $H_2O.NH_2NH_2$, MeOH, r.t., 16 h; c) MeOH, AcOH, r.t., 3 d., 30% yield over step b and c; d) DIPEA, DMSO, 90 °C, 30 - 60 min., 74% yield; e) K_2CO_3, 30% H_2O_2, DMSO, r.t., 2 – 3 h, 60% yield.; f) TFA, DCM, r.t., 5 -7 h, 79% yield.

The instability of the trifluoromethyl β-triketone analogue of **2.18** precluded the synthesis of the key intermediates **2.29** *via* **Pathway B**. Alternatively, tetrahydroindazolone **2.23** was obtained following the tosylhydrazone mediated procedure (**Scheme 5.2a**, **b**). Unfortunately, attempts to expand the tosylhydrazone mediated procedure for the synthesis of the methyl-containing tetrahydroindazolone were unsuccessful (**Section 3.1.2**). The subsequent *N*-arylation of **2.23** could be done using 2-bromo-4-fluorobenzonitrile or 2,4-difluorobenzonitrile. Interested in an efficient late-stage amination, we initially attempted the *N*-arylation using 2,4-difluorobenzonitrile. However, we formed the dimeric compound as the major product; furthermore, the two regioisomers could not be separated using conventional separation techniques such as silica gel chromatography and recrystallization (**Section 3.1.3**). Alternatively, the reaction of **2.23** and 2-bromo-4-fluorobenzonitrile **2.27** gave the desired product **2.29** which was subsequently aminated under complex and expensive Buchwald conditions (**step d**) to yield the desired compound in 65% yield. Similarly, the subsequent nitrile hydrolysis (**step e**) and Boc deprotection afforded the amine intermediate **2.5** in 41% yields. Given that the key intermediates **2.29** and **2.30** were synthesised using different pathways, the obtained overall yields of the two precursors could not be directly compared.

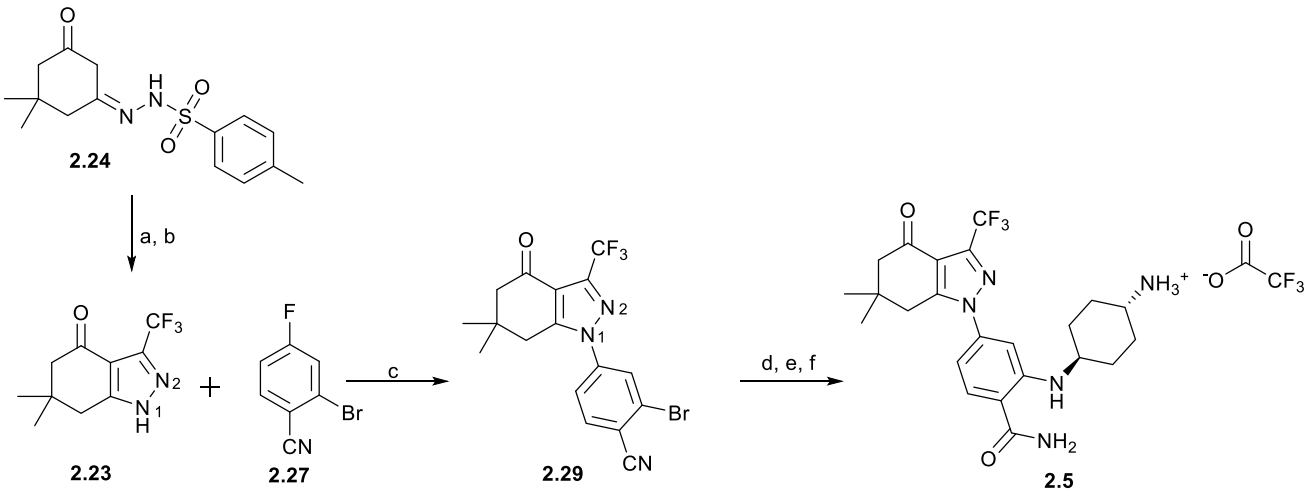

Scheme 5.2: Synthesis of intermediate **2.29** *via* Pathway A:

Reagents and conditions: a) $(CF_3CO)_2O$, THF, TEA, 55 °C, 2 h; b) NaOH, MeOH, H_2O, r.t., 3 h, 15% yield; c) NaH, anhy. DMSO, 45 °C, 23 h, 57% yield; d) DPPF[$PdCl_2$], DPPF, Na*t*OBu, THF, 60-65 °C, 4 h, 65% yield; e) K_2CO_3, 30% H_2O_2, DMSO, r.t., 2 – 3 h, 73% yield.; f) TFA, DCM, r.t., 5 -7 h, 41% yield.

The use of base-catalysed reactions for the nucleophilic displacement of the bromine in **2.7**, successfully afforded us with our desired sulfonic acid containing target compounds in moderate yields (**Scheme 5.3a**). The extracellular inhibitors containing the phosphonic acid moiety were afforded in moderate yields through the coupling of the amine intermediates with the carboxylic acid moiety of **2.8** (**Scheme 5.3b**). In conclusion, we were successful in developing and synthesizing potential extracellular HSP90 inhibitors.

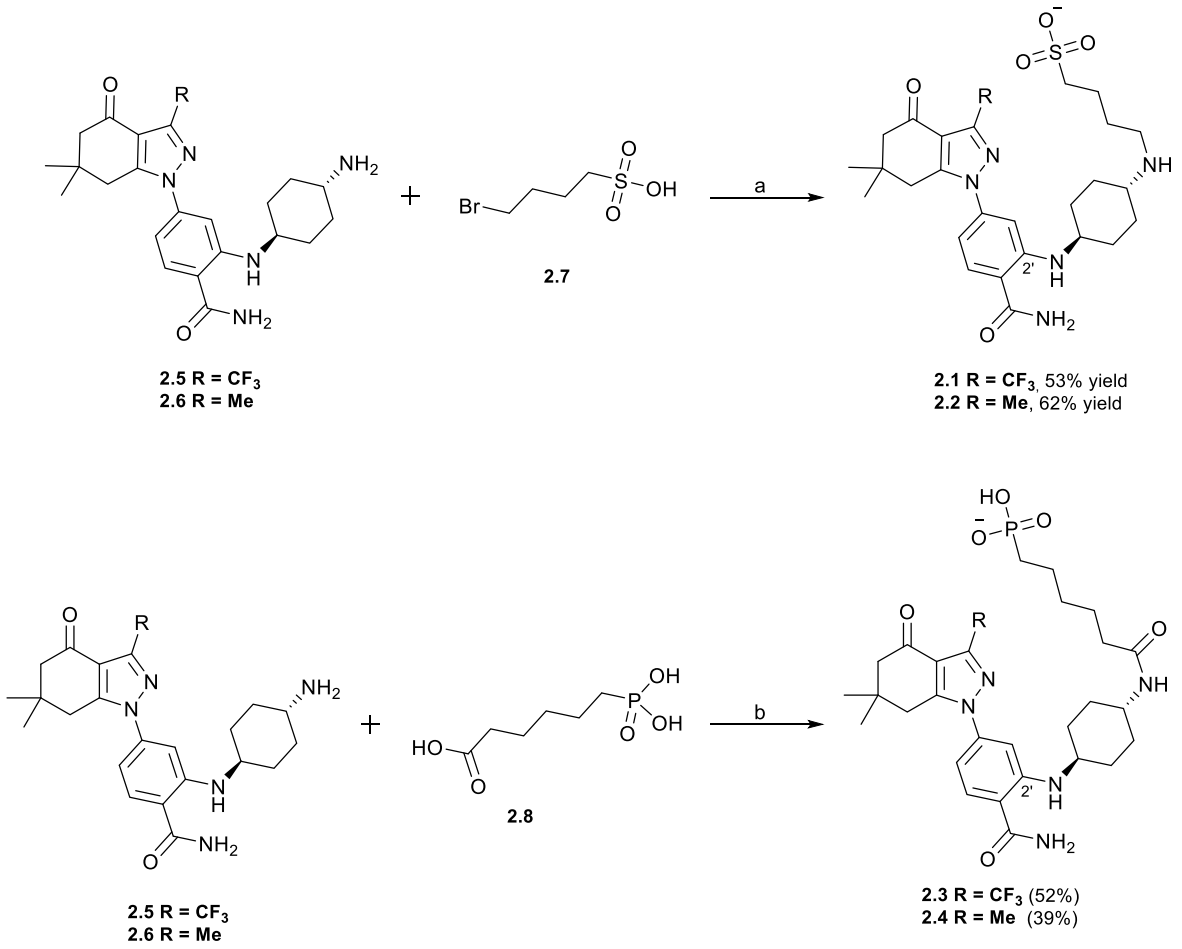

Scheme 5.3: Synthesis of the desired extracellular HSP90 inhibitors:

Reagents and conditions: a) DIPEA, DMF, 50 °C, 18 h; b) DIPEA, EDCI, NHS, DMF, r.t., 42 - 72 h

Upon successful synthesis, the analogues were sent for biological evaluation. Consistent with our hypothesis, we demonstrated that our compounds did not disrupt intracellular HSP90 activity. An important observation from this study is that our novel compounds displayed potent cytotoxicity in the nanomolar range, without induction of the HSR. While encouraging, these data do not confirm extracellular activity. These compounds are still undergoing a suite of additional biological assessments including, screening for HSP90 ATPase activity, wound healing assays and refolding assays using extracellular HSP90 clients, which will be reported in due course. Membrane permeability assays and stability studies would also be necessary for future work.

Given the potential of these analogues, an extensive SAR investigation is required. The ongoing biological assessments and SAR are needed to drive future design. An advancement towards the synthesis and biological evaluation of a library of these analogues, with varying polar alkyl chain lengths and polar moieties, would offer valuable insights on how successful these cell impermeable SNX analogues would be as potential extracellular HSP90 inhibitors.

Having done an extensive investigation on the synthetic procedures, the methodology followed in this project will be used for future target synthesis. We propose that the methyl containing analogues be synthesised following the procedure described in **Scheme 5.1**, where the key intermediate results from the condensation of a β-triketone and 2,4-difluorobenzonitrile. Two alternatives would be available for this synthesis: the condensation of a β-triketone with 2-bromo-4-fluorobenzonitrile, or the *N*-arylation of a methyl containing tetrahydroindazolone. However, drawbacks such as the synthesis of inseparable *N*-arylated isomers and the use expensive palladium catalysts under complex reaction conditions for the amination reaction would greatly limit their use. However, limited by the instability of the corresponding β-triketone, the synthesis of the trifluoromethyl analogues would follow the tosylhydrazone mediated procedure as described in **Scheme 5.2**.

6. CHAPTER 6: EXPERIMENTAL DATA

6.1. General Experimental Procedures

6.1.1. Solvents and reagents

Solvents and commercially available reagents used for this project were purchased from Honeywell or Sigma-Aldrich and used without further purification. All reactions that included the use of air and/or moisture sensitive reagents were carried out under an inert atmosphere of nitrogen using oven-dried glassware and anhydrous solvents.

6.1.2. Chromatographic Separations

Thin layer chromatography (TLC) analysis was performed on aluminium supported silica gel 60 TLC plates, coated with fluorescent indicator F_{254} and visualized by an ultraviolet (UV) light.

6.1.3. Spectroscopic Techniques

All nuclear magnetic resonance (NMR) spectra were recorded either on a Bruker 400 MHz or 500 MHz UltraShield NMR spectrometer. Proton chemical shifts are listed in ppm referenced against the NMR solvent as the internal standard ($CDCl_3$: δ 7.26; CD_3OD: δ 3.31; $(CD_3)_2SO$: δ 2.50; $(CD_3)_2CO$: δ 2.05). Carbon chemical shifts are listed in ppm relative to the NMR solvent peak ($CDCl_3$: δ 77.16; CD_3OD: δ 49.00; $(CD_3)_2SO$: δ 39.52; $(CD_3)_2CO$: δ 29.84). NMR spectral data is reported as: chemical shift, integration, multiplicity (b = broad, s = singlet, d = doublet, t = triplet, q = quartet, m = multiplet) and coupling constants (*J*) in Hertz (Hz).

High resolution mass spectrometric (HRMS) data was obtained using a Waters Synapt G2 TOF instrument with an ESI source. All data were reported in m/z values.

Infrared (IR) spectral data was obtained using an Alpha II FTIR spectrometer and the IR data is reported as absorption frequency (cm^{-1}).

Important to note that full spectral assignment of the synthesised compounds depended on the complexity of the obtained NMR spectra, interchangeable signals and signals under the solvent/water signal were denoted using * and # symbols, respectively. MS and IR spectra were obtained only when necessary and for final compounds.

6.1.4. X-ray crystallography

The X-ray data were recorded on a Bruker Apex Duo equipped with an Oxford Instruments Cryojet operating at 100(2) K and an Incoatec microsource operating at 30 W power. Crystal and structure refinement data are given in **Table 6.1**. The data were collected with CuKα (λ = 1.54178 Å) radiation at a crystal-to-detector distance of 50 mm. The following conditions were used for the data collection: omega and phi scans with exposures taken at 30 W X-ray power and 0.50° frame widths using APEX2.[132] The data were reduced with the programme SAINT[132] using outlier rejection, scan speed scaling, as well as standard Lorentz and polarisation correction factors. A SADABS semi-empirical multi-scan absorption correction[132] was applied to the data. Direct methods, SHELX-2014[133] and WinGX[134] were used to solve all three structures. All non-hydrogen atoms were located in the difference density map and refined anisotropically with SHELX-2014[133]. All hydrogen atoms were included as idealised contributors in the least squares process. Their positions were calculated using a standard riding model with C-$H_{aromatic}$ distances of 0.93 Å and U_{iso} = 1.2 Ueq, C-$H_{methylene}$ distances of 0.99 Å and U_{iso} = 1.2 Ueq and C–H_{methyl} distances of 0.98 Å and U_{iso} = 1.5 Ueq.

Table 6.1: Summary of crystal data and structure refinement details for compounds **02.30**, **02.47**, **02.52**, **02.56**.

Crystal Data	**02.30**	**02.47**	**02.52**	**02.56**
Chemical Formula	$C_{17}H_{17}F_6N_3O$	$C_{17}H_{22}N_2O_4S$	$C_{17}H_{22}N_2O_4S$	$C_{19}H_{24}N_2O_4S$
Molar Mass g mol^{-1}	298.33	350.42	350.42	376.46
Crystal system, space group	Triclinic, *P*-1	Monoclinic, $P2_1/n$	Monoclinic, $P2_1/c$	Monoclinic, $P2_1/n$
a, b, c/Å	10.4797(2), 12.0558(3), 13.6439(4)	7.2227(3), 19.7174(7), 12.6186(4)	9.3227(2), 17.0119(3), 11.8285(2)	9.0527(2), 12.6999(3), 16.9128(4)
α, β, γ °	α = 67.062(1) β = 67.791(1) γ = 89.387 (1)	β = 103.355(1)	β = 102.039(1)	β = 101.277(2)
Temperature/K	100(2)	100(2)	100(2)	100(2)
Z	4	4	4	4
V/Å^3	1450.72(6)	1748.45(11)	1834.70(6)	1906.90(8)
T_{min}, T_{max}				
S	1.04	1.07	1.08	1.05
μ/mm^{-1}	0.79	1.85	1.76	1.73
Crystal Dim./mm	0.31 × 0.21 × 0.10	0.56 × 0.23 × 0.19	0.27 × 0.07 × 0.04	0.49 × 0.20 × 0.13
Data Collection				
Total, unique data	31771, 5106	22828, 3135	24304, 3276	33963, 3633
R_{int}	0.021	0.025	0.023	0.036
Refinement				
Final R indices, [I>2σ(I)]	R_1 = 0.045, wR_2 = 0.119	R_1 = 0.035, wR_2 = 0.091	R_1 = 0.032, wR_2 = 0.088	R_1 = 0.034, wR_2 = 0.091

6.1.5. DFT Simulations

The simulations were performed using Gaussian 09W[135] at the CAMB3LYP/6-311G(d,p) level of theory. Single first polarization functions (d,p) were added to increase the accuracy of the simulations. The X-ray coordinates were used for input structures where possible. No symmetry constraints were imposed and normal geometry convergence criteria were applied. The input files were prepared using GaussView 5.0[136]; the same program was used to analyse the output files. Geometry optimizations and frequency calculations were performed using the level of theory described above. The absence of negative frequency eigenvalues suggests that the geometry optimized structures were true minima on the global potential energy surface.

6.1.6. Cytotoxicity

The *HeLa* cervical carcinoma cell line was cultured in Dulbecco's Modified Eagle's Medium (DMEM) supplemented with 10% (v/v) fetal bovine serum (FBS), 1% (v/v) pencillin-streptomycin-amphotericin (PSA) and 1% (v/v) GlutaMAX. Cytotoxicity of the compounds was tested using the previously described resazurin viability assay.[137] SNX2112 was used as the positive control to compare the cytotoxicity of analogues.

6.1.7. Western Blot Analysis

HeLa cells were treated overnight with compounds and lysates prepared in RIPA buffer. Proteins in the lysates were resolved by sodium dodecyl sulphate-polyacrylamide gel electrophoresis (SDS-PAGE) followed by transfer to nitrocellulose membranes for western blot analysis using the accepted modifications of the original protocols.[138, 139] SNX2112 was used as the positive control for loss of CDK4 and upregulation of HSP70 in response to HSP90 inhibition. Detection of the levels of HSP70 (stress-inducible isoform), CDK4 (obligate HSP90 client protein) and histone H3 (loading control) in untreated and treated *HeLa* cell lysates were determined using specific antibodies against the target proteins coupled to chemiluminescent detection via a species-specific secondary antibody, as per our previously published protocol.[140]

6.1.8. Other general procedures

The numbering on compounds does not follow the official IUPAC rules. The atoms were numbered to allow for simpler characterisation assignments.

6.2. Experimental data: Synthesis of the HSP90 extracellular inhibitors

6.2.1. Dimedone acetylation

6.2.1.1. Triethylamine mediated dimedone acetylation

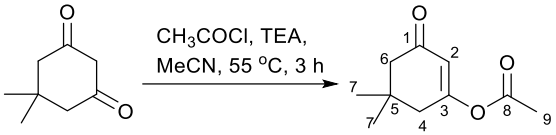

2.43

Dimedone (150 mg, 1.07 mmol, 1.00 eq.) and triethylamine (0.160 mL, 1.12 mmol, 1.10 eq.) were dissolved in acetonitrile (1.30 mL) and cooled to 0 °C in an ice bath. Acetyl chloride (800 µL, 1.12 mmol, 1.10 eq.) was added dropwise and the reaction mixture was heated to 55 ˚C. Following 3 hours of stirring, the observed white solid was filtered off and the resultant filtrate was concentrated *in vacuo* to yield a dark brown oil which was purified using silica gel column chromatography (hexane: EtOAc, 8:2) yielding enol-ester **2.43** as a yellow oil (146 mg, 0.801 mmol, 75% yield).

3-Acetoxy-5,5-dimethyl-2-cyclohexenone (**2.43**): yellow oil (75% yield); IR (ν_{max} cm^{-1}) 2959, 1769, 1666, 1359; ^{1}H NMR ($CDCl_3$, 400 MHz): δ_H 5.83 (1H, t, *J* = 1.2 Hz, H-2), 2.35 (2H, d, *J* = 1.2 Hz, H-4), 2.19 (2H, s, H-6), 2.14 (3H, s, H-9), 1.04 (6H, s, H-7); ^{13}C NMR ($CDCl_3$, 100 MHz): δ_C 199.4 (CO, C-1), 168.0 (q_C, C-3), 167.4 (CO, C-8), 116.5 (CH, C-2), 50.8 (CH_2, C-6), 42.2 (CH_2, C-4), 33.1 (q_C, C-5), 28.1 (2 x CH_3, C-7), 21.2 (CH_3, C-9) ppm.

6.2.1.2. Fries rearrangement of 3-acetoxy-5,5-dimethyl-2-cyclohexenone 2.43

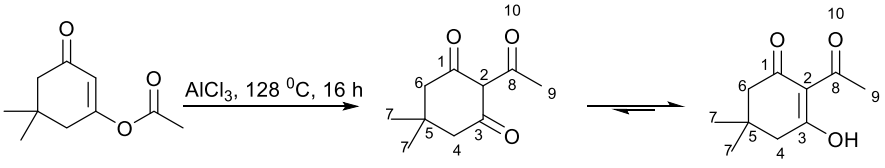

2.43 **2.18**

Enol-ester **2.43** (146 mg, 0.801 mmol, 1.00 eq.) was treated with anhydrous $AlCl_3$ (214 mg, 1.60 mmol, 2.00 eq.) and heated to 120 °C for 16 hours to yield a black sticky crude material. The crude material was quenched with ice, extracted twice with EtOAc, the combined organic layers were washed with brine, dried over $MgSO_4$ and concentrated *in vacuo* to yield a dark brown oil which was purified using silica gel column chromatography to yield the product as an orange-yellow oil (69.0 mg, 0.379 mmol, 47% yield).

2-Acetyldimedone (**2.18, isolated in enol form**): Orange-yellow oil (47% yield); IR (ν_{max} cm^{-1}) 2953, 2498, 1575, 1513, 1463; ^1H NMR ($CDCl_3$, 400 MHz): δ_H 2.59 (3H, s, H-9), 2.52 (2H, s, H-4), 2.35 (2H, s, H-6), 1.07 (6H, s, H-7); ^{13}C NMR ($CDCl_3$, 100 MHz): δ_C 202.6 (CO, C-8), 198.0 (CO, C-1), 195.3 (CO, C-3), 112.5 (q_C, C-2), 52.6 (CH_2, C-6), 47.1 (CH_2, C-4), 30.8 (q_C, C-5), 28.6 (2 x CH_3, C-7), 28.3 (CH_3, C-9) ppm. ESI-MS *m/z* 179.1182 (calculated for $[M+H]^+$ $C_{10}H_{15}N_2O$ 179.1184). Spectral data was in accordance with that previously reported.[116, 117]

6.2.1.3. DIPEA mediated dimedone acetylation

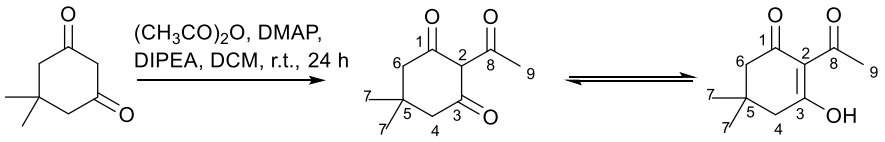

2.18

Acetic anhydride (710 µL, 7.49 mmol, 1.05 eq.) was added dropwise to a solution of dimedone (1.00 g, 7.13 mmol, 1.00 eq.), DIPEA (1.30 mL, 7.49 mmol, 1.05 eq.) and DMAP (440 mg, 0.357 mmol, 0.05 eq.) in DCM (20 mL), and the pale-yellow reaction mixture was stirred at room temperature. After 24 hours the mixture was concentrated *in vacuo* and partitioned between 1 M HCl and EtOAc. The organic layer was collected and washed with brine, dried over $MgSO_4$, filtered, and concentrated *in vacuo* to yield a crude yellow oil which was purified by silica gel chromatography (hexane: EtOAc, 7:3) to yield **2.18** as an orange-yellow oil (586 mg, 45% yield) alongside the *O*-acylated compound **2.43** in 24% yield.

Subsequent Fries rearrangement of **2.43** gave **2.18** in 57% overall yield (741 mg, 0.407 mmol, 57% yield). Spectral data was in accordance with the one reported for **2.18** in **Section 6.2.1.2**.

6.2.2. Phenylhydrazine synthesis

6.2.2.1. 2,4-Difluorobenzonitrile mediated phenyl hydrazine synthesis

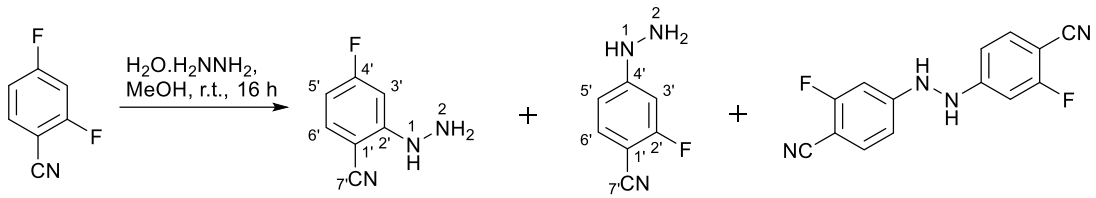

Hydrazine hydrate (180 mg, 3.59 mmol, 5.00 eq.) was added dropwise to a solution of 2,4-difluorobenzonitrile (100 mg, 0.719 mmol, 1.00 eq.) in MeOH (1.00 mL). The clear reaction mixture was stirred at room temperature for 16 hours. MeOH was then removed *in vacuo* and the crude material was partitioned between EtOAc (1 mL), water (0.7 mL) and 1M NaOH (0.3 mL). The organic layer was washed with sat. brine (0.5 mL), dried over anhydrous $MgSO_4$ and concentrated *in vacuo* to yield a cream white solid. The crude solid was purified by silica gel chromatography (hexane: EtOAc, 7:3) to first elute a mixture of the desired isomer **2.32** and the dimeric product **2.40** (61.0 mg) as an off-white solid and the polar isomeric product **2.39** as a brown solid (28.0 mg, 0.185 mmol, 26% yield).

4'-Fluoro-2'-hydrazinylbenzonitrile (**2.39**): brown solid (26% yield); ^{1}H NMR ($(CD_3)_2CO$, 400 MHz): δ_H 11.00 (1H, s, NH-1), 7.73 – 7.69 (1H, dd, *J* = 8.8, 5.2 Hz, H-6'), 7.04 – 7.01 (1H, dd, *J* = 9.9, 2.2 Hz, H-3'), 6.79 – 6.74 (1H, ddd, *J* = 9.4, 8.9, 2.3 Hz, H-5'), 5.07 (2H, s, NH_2-2); ^{13}C NMR ($(CD_3)_2CO$, 100 MHz): δ_C 163.2 (CF, d, *J* = 243.2 Hz, C-4'), 150.0 (CN, C-7'), 143.0 (q_C, d, *J* = 13.1 Hz, C-2'), 122.1 (CH, d, *J* = 11.4 Hz, C-6'), 112.3 (q_C, C-1'), 107.8 (CH, d, *J* = 26.7 Hz, C-5'), 95.5 (CH, d, *J* = 26.2 Hz, C-3') ppm.

6.2.2.2. 2-Bromo-4-fluorobenzonitrile mediated phenylhydrazine synthesis

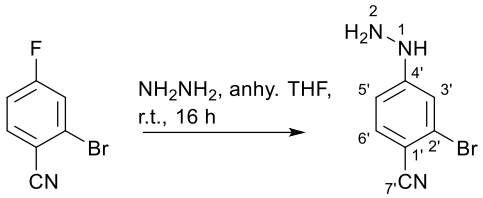

2.26

Anhydrous hydrazine (1.92 g, 59.9 mmol, 12.0 eq.) was added dropwise to a clear solution of 2-bromo-4-fluorobenzonitrile (1.00 g, 4.99 mmol, 1.00 eq.) in anhydrous THF (25.0 mL). The pale-yellow reaction mixture was stirred at room temperature under an inert atmosphere of nitrogen for 16 hours. A white precipitate formed. More THF was added to dissolve the observed solids and washed with sat. $NaHCO_3$ until the pH of the solution was approximately 8.5. The organic layer was dried over anhydrous $MgSO_4$ and concentrated *in vacuo* to yield **2.26** as an off-white solid (752 mg, 3.55 mmol, 71% yield).

2'-Bromo-4'-hydrazinylbenzonitrile (**2.26**): off-white solid (71% yield); ^{1}H NMR (DMSO, 400 MHz): δ_H 8.03 (1H, s, NH-1), 7.47 (1H, d, *J* = 8.8 Hz, H-6'), 7.07 (1H, d, *J* = 2.0 Hz, H-3'), 6.75 – 6.72 (1H, dd, *J* = 8.8, 2.0 Hz, H-5'), 4.37 (2H, s, NH_2-2); ^{13}C NMR (DMSO, 100 MHz): δ_C 156.2 (q_C, C-4'), 134.9 (CH, C-6'), 125.5 (q_C, C-2'), 119.0 (CN, C-7'), 113.1 (CH, C-3'), 109.9 (CH, C-5'), 98.1 (q_C, C-1') ppm. ESI-MS *m/z* 211.9820 (calculated for $[M+H]^+$ $C_7H_7{}^{79}BrN_3$ 211.9823).

6.2.3. Tetrahydroindazolone condensation

6.2.3.1. Hydrazine hydrate mediated tetrahydroindazolone condensation

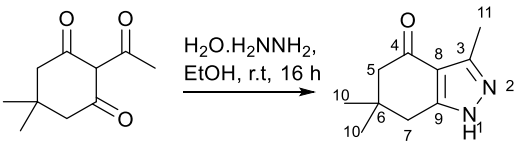

2.18 **2.12**

Hydrazine hydrate (10.0 mg, 0.206 mmol, 1.50 eq.) was added dropwise to a solution of **2.18** (25.0 mg, 0.137mmol, 1.00 eq.) in EtOH (1 mL). The reaction mixture was stirred at room temperature for 16 hours, thereafter, concentrated *in vacuo* to give a brownish-black crude reaction mixture which was subjected to silica gel column chromatography (hexane: EtOAc, 1:1) yielding **2.12** as a pale-yellow solid (19.0 mg, 0.107 mmol, 79% yield).

3,6,6-Trimethyl-1,5,6,7-tetrahydro-4*H*-indazol-4-one (**2.12**): pale yellow powdery solid (79% yield); IR (ν_{max} cm^{-1}) 3410, 3194, 2956, 2925, 1642, 1593; ^{1}H NMR ($CDCl_3$, 400 MHz): δ_H 2.68 (2H, s, H-7), 2.53 (3H, s, H-11), 2.34 (2H, s, H-4), 1.08 (6H, s, H-10); ^{13}C NMR ($CDCl_3$, 100 MHz): δ_C 194.8 (CO, C-4), 154.3 (q_C, C-9), 145.1 (q_C, C-3), 114.7 (q_C, C-8), 53.1 (CH_2, C-5), 36.5 (q_C, C-6), 35.7 (CH_2, C-7), 28.5 (2 x CH_3, C-10), 12.1 (CH_3, C-11) ppm. ESI-MS *m/z* 179.1182 (calculated for $[M+H]^+$ $C_{10}H_{15}N_2O$ 179.1184). Spectral data was in accordance with that previously reported.[98, 99]

6.2.3.2. Tosyl hydrazine mediated tetrahydroindazolone condensation

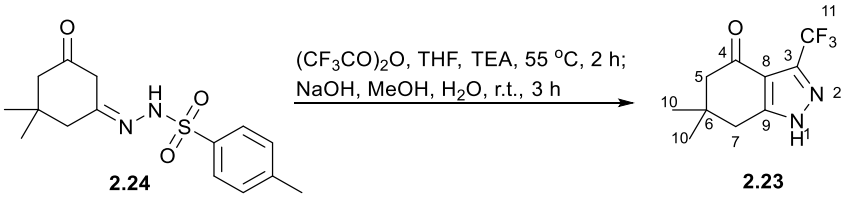

Trifluoroacetic anhydride (0.220 mL, 1.59 mmol, 1.00 eq.) was added to a suspension of **2.24** (500 mg, 1.59 mmol, 1 eq.), TEA (2.88 mL, 20.7 mmol, 13 eq.) and THF (9 mL). The reaction mixture was heated to 55 ˚C to give an orange solution which was stirred for 2 hours. After cooling to room temperature, the mixture was quenched with sat. NH_4Cl (20 mL) and extracted with EtOAc (3 x 20 mL). The combined organic fractions were washed with sat. brine (20 mL), dried over anhydrous $MgSO_4$, concentrated in *vacuo* to yield an orange-brown oil which was purified with silica gel chromatography to yield **2.23** as an orange-yellow solid (55.0 mg, 0.237 mmol, 15% yield).

6,6-Dimethyl-3-(trifluoromethyl)-1,5,6,7-tetrahydro-*4H*-indazol-4-one (**2.23**): orange-yellow solid (15% yield); IR (ν_{max} cm^{-1}) 3230, 3124, 2961, 1665, 1511, 1482; ^{1}H NMR (DMSO, 500 MHz): δ_H 13.86 (1H, s, NH-8), 2.80 (2H, s, H-6), 2.37 (2H, s, H-4), 1.04 (6H, s, H-7); ^{13}C NMR (DMSO, 125 MHz): δ_C 190.0 (CO, C-3), 152.0 (q_c, C-1), 138.9 (q_c, q, J = 38.7 Hz, C-10), 120.9 (CF_3, q, J = 269.5 Hz, C-11), 113.5 (q_c, C-2), 52.1 (CH_2, C-4), 35.3 (q_c, C-5), 33.7 (CH_2, C-6), 27.6 (CH_3, C-7) ppm. HRESMS *m/z* 233.0901 (calculated for $C_{10}H_{12}F_3N_2O$ $[M+H]^+$ 233.0902).

6.2.3.3. Phenyl hydrazine mediated tetrahydroindazolone condensation

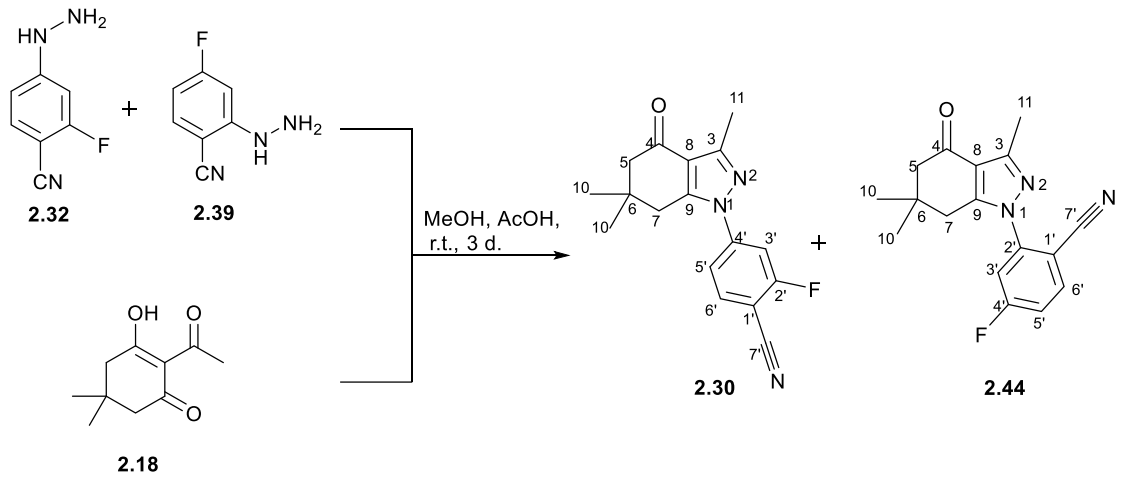

An orange solution of **2.18** (503 mg, 2.76 mmol, 1.00 eq.) and the crude material from an upscale (x 10) of **Section 6.2.2.1** (417 mg, 2.76 mmol, 1.00 eq.) in MeOH (1.70 mL) was treated with acetic acid (40.0 µL, 0.690 mmol, 0.25 eq.) and stirred at room temperature for 5 days. Thereafter, the reaction mixture was concentrated *in vacuo* and purified using silica gel chromatography to first elute the undesired isomeric product **2.44** (449 mg, 1.51 mmol, 21% yield over two-steps) as a yellow powder and the desired product **2.30** as an off-white solid (647 mg, 2.18 mmol, 30% yield over two-steps).

2'-Fluoro-4'-(3,6,6-trimethyl-4-oxo-4,5,6,7-tetrahydro-1*H*-indazol-1-yl)-benzonitrile (**2.30**): off-white solid (30% yield over two-steps); IR (ν_{max} cm^{-1}) 2962, 2937, 2873, 2229, 1669, 1617; ^{1}H NMR ($CDCl_3$, 400 MHz): δ_H 7.76 – 7.73 (1H, dd, J = 8.5, 7.0 Hz, H-6'), 7.52 – 7.45 (2H, m, H-3' and H-5'), 2.87 (2H, s, H-7), 2.53 (3H, s, H-11), 2.42 (2H, s, H-5), 1.13 (6H, s, H-10); ^{13}C NMR ($CDCl_3$, 100 MHz): δ_C 193.2

(CO, C-4), 163.6 (CF, d, *J* = 260.7 Hz, C-2'), 151.5 (CH, C-3), 149.4 (q_C, C-9), 144.1 (q_C, d, *J* = 10.6 Hz, C-4'), 134.4 (CH, d, *J* = 1.6 Hz, C-6'), 118.6 (q_C, C-8), 118.5 (CH, C-5'), 113.3 (CN, C-7'), 111.1 (CH, d, *J* = 23.7 Hz, C-3'), 100.1 (q_C, d, *J* = 15.7 Hz, C-1'), 52.3 (CH_2, C-5), 38.0 (CH_2, C-7), 36.1 (q_C, C-6), 28.5 (2 x CH_3, C-10), 13.5 (CH_3, C-11) ppm.

4'-Fluoro-2'-(3,6,6-trimethyl-4-oxo-4,5,6,7-tetrahydro-1*H*-indazol-1-yl)-benzonitrile (**2.44**): yellow powder (21% yield over two-steps); ^{1}H NMR ($CDCl_3$, 400 MHz): δ_H 8.25 – 8.22 (1H, dd, *J* = 9.0, 5.4 Hz, H-6'), 7.38 – 7.35 (1H, dd, *J* = 9.9, 2.1 Hz, H-3'), 7.06 – 7.03 (1H, td, *J* = 9.1, 2.2 Hz, H-5'), 3.55 (2H, s, H-7), 3.02 (3H, s, H-11), 2.67 (2H, s, H-5), 1.25 (6H, s, H-10); ^{13}C NMR ($CDCl_3$, 100 MHz): δ_C 196.2 (CO, C-4), 164.8 (CF, d, *J* = 249.1 Hz, C-4'), 156.9 (q_C, C-3), 153.6 (q_C, d, *J* = 14.2 Hz, C-2'), 151.2 (q_C, C-9), 143.1 (CN, C-7'), 123.5 (CH, d, *J* = 11.2 Hz, C-6'), 115.7 (q_C, C-8), 112.8 (CH, d, *J* = 28.2 Hz, C-5'), 110.6 (q_C, C-1'), 100.1 (CH, d, *J* = 23.8 Hz, C-3'), 53.1 (CH_2, C-5), 39.0 (CH_2, C-7), 32.4 (q_C, C-6), 28.6 (2 x CH_3, C-10), 26.4 (CH_3, C-11) ppm.

6.2.4. *N*-arylation of tetrahydroindazolone 2.23

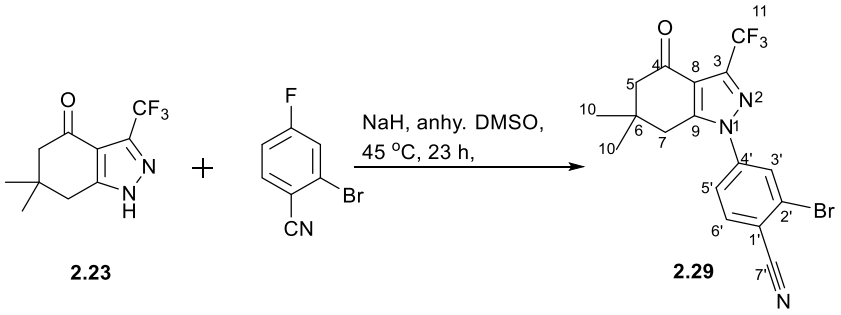

2.23 **2.29**

A solution of **2.23** (349 mg, 1.50 mmol, 1.00 eq.) in anhydrous DMSO (7 mL) was treated with NaH (60.0 mg, 1.50 mmol, 1.00 eq.) and stirred for 15 minutes. Thereafter, 2-bromo-4-fluorobenzonitrile (480 mg, 2.40 mmol, 1.60 eq.) was added and the reaction mixture was stirred at 45 °C for 23 hours. Thereafter, the reaction mixture was cooled to room temperature, quenched with sat. NH_4Cl, diluted with water and washed with EtOAc (x 3). The combined organic layers were washed with sat. brine, dried over anhydrous $MgSO_4$, filtered and concentrated *in vacuo* to give a brown crude material which

was purified using silica gel chromatography to give **2.29** as an orange-yellow solid (353 mg, 0.856 mmol, 57% yield).

2'-Bromo-4'-(6,6-dimethyl-4-oxo-3-(trifluoromethyl)-4,5,6,7-tetrahydro-1*H*-indazol-1-yl) benzonitrile (**2.29**): orange-yellow solid (57% yield); IR (ν_{max} cm^{-1}) 2963, 2951, 2925, 2870, 2854, 2233, 1682, 1593; ^{1}H NMR (DMSO, 400 MHz): δ_H 8.21 – 8.18 (2H, m, H-6', H-3'), 7.92 – 7.89 (1H, dd, *J* = 8.5, 2.1 Hz, H-5'), 3.05 (2H, s, H-7), 2.45 (2H, s, H-5), 1.05 (6H, s, 2 x CH_3); ^{13}C NMR (DMSO, 100 MHz): δ_C 190.1 (q_C, C-4) , 152.9 (q_C, C-9), 141.4 (q_C, C-4'), 139.4 (q_C, q, *J* = 39.1 Hz, C-3) , 136.0 (CH, C-6'), 128.3 (CH, C-3'), 125.5 (q_C, C-2'), 123.8 (CH, C-5'), 120.4 (q_C, q, *J* = 270.7 Hz, C-11) , 116.6 (q_C, C-8), 115.9 (CN, C-7'), 114.8 (q_C, C-1'), 51.6 (CH_2, C-5), 35.5 (q_C, C-6), 35.3 (CH_2, C-7), 27.5 (2 x CH_3, C-10).

6.2.5. Amination of benzonitriles 2.29 and 2.30

6.2.5.1. Palladium catalysed amination of 2.29

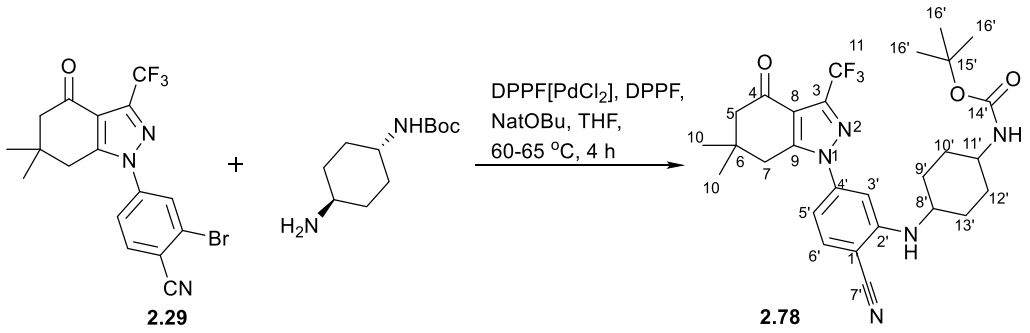

$DPPF[PdCl_2]$ (5 mol%) and DPPF (10 mol%) were consecutively added to a solution of **2.29** (333 mg, 0.809 mmol, 1.00 eq.) and Na^tOBu (155 mg, 1.62 mmol, 2.00 eq.) in anhydrous THF (4.5 mL) to give a reddish-brown suspension. Thereafter, *tert*-butyl-(4-aminocyclohexyl)carbamate (520 mg, 2.43 mmol, 3.00 eq.) was added and the reaction mixture was stirred between 60 – 65 °C. After 30 min TLC analysis indicated only the presence of a spot with an R_f value similar to the starting material, however, it was fluorescent purple spot under UV. The reaction was stopped, filtered through a flash silica plug,

concentrated *in vacuo*. The resulting suspension was purified using silica gel chromatography to obtain **2.78** as an off-white solid (287 mg, 0.526 mmol, 65% yield).

***tert*-butyl(4-((2-cyano-5-(6,6-dimethyl-4-oxo-3-(trifluoromethyl)-4,5,6,7-tetrahydro-1*H*-indazol-1-yl)phenyl)amino)cyclohexyl)carbamate** (**2.78**): off-white solid (65% yield); ^{1}H NMR ($CDCl_3$, 400 MHz): δ_H 7.51 (1H, d, *J* = 8.3 Hz, H-6'), 6.81 (1H, d, *J* = 1.8 Hz, H-3'), 6.70-6.67 (1H, dd, *J* = 8.3, 1.9 Hz, H-5'), 4.66 (1H, d, *J* = 7.7 Hz, NH), 4.43 – 4.39 (2H, m, NH), 3.54 – 3.46 (1H, 3, H-11'), 3.40 – 3.32 (2H, m, H-8'), 2.83 (2H, s, H-7), 2.47 (2H, s, H-5), 2.17 – 2.10 (4H, m), 2.00 – 1.99 (2H, m), 1.43 (18H, 2 x s, H-16'), 1.38 – 1.15 (6H, m), 1.13 (6H, s, H-10); ^{13}C NMR ($CDCl_3$, 100 MHz): δ_C 189.8 (CO, C-4), 155.4 (CO, C-14'), 150.7 (q_C, C-8), 150.3 (q_C, C-2'), 142.6 (q_C, C-4'), 141.1 (q_c, q, *J* = 39.3 Hz, C-3), 134.3 (CH, C-6'), 120.4 (CF_3, q, *J* = 270.1 Hz, C-11), 116.8 (q_C, C-9), 116.7 (CN, C-7'), 111.1 (CH, C-5'), 106.6 (CH, C-3'), 96.5 (q_C, C-1'), 79.3 (q_C, C-15'), 52.4 (CH_2, C-5), 51.4 (CH, C-8'), 49.1 (CH, C-11'), 37.5 (CH_2, C-7), 35.8 (q_C, C-6), 32.2 (2 x CH_2), 31.6 (2 x CH_2), 28.5 (3 x CH_3, C-16'), 28.4 (2 x CH_3, C-10) ppm.

6.2.5.2. Base catalysed amination of 2.30

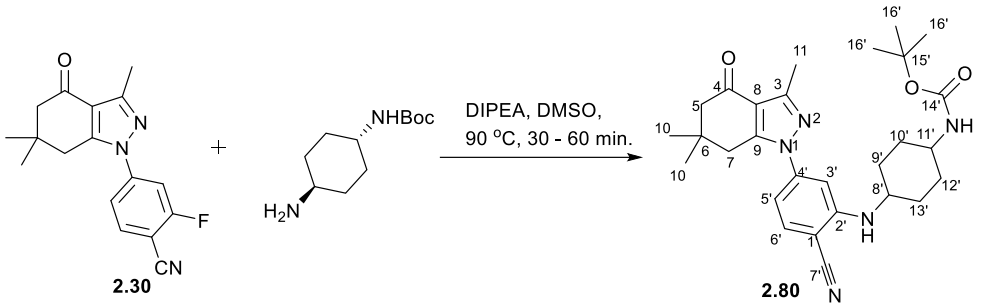

2.30 (79.0 mg, 0.225 mmol, 1.00 eq.) and *tert*-butyl-(4-aminocyclohexyl)carbamate (193 mg, 0.900 mmol, 4.00 eq.) were dissolved in DMSO (1 mL) and treated with DIPEA (120 µL, 0.675 mmol, 3.00 eq.). The reaction mixture was heated to 90 °C and stirred for 1 hour to give a black reaction mixture. The crude reaction mixture was purified using silica gel chromatography to obtain **2.80** as an off-white solid (82.0 mg, 0.167 mmol, 74% yield).

***tert*-butyl(4-((2-cyano-5-(3,6,6-trimethyl-4-oxo-4,5,6,7-tetrahydro-1*H*-indazol-1-yl)phenyl)amino)cyclohexyl)carbamate** (**2.80**): Off-white solid (74% yield); IR (ν_{max} cm^{-1}) 3399, 3296, 2933, 2861, 2206, 1707, 1661; ^{1}H NMR ($CDCl_3$, 400 MHz): δ_H 7.47 (1H, d, *J* = 8.4 Hz, H-6'), 6.84 (1H, d, *J* = 1.8 Hz, H-3'), 6.69-6.69 – 6.66 (1H, dd, *J* = 8.3, 1.8 Hz, H-5'), 4.57 (1H, d, *J* = 7.7 Hz, NH), 4.40 (1H, bs, NH), 3.48 (1H, bs, H-8'), 3.43 – 3.34 (1H, m, H-11'), 2.80 (2H, s, H-7), 2.54 (3H, s, H-11), 2.40 (2H, s, H-5), 2.18 – 2.11 (4H, m, H-10', H-12'), 1.45 (9H, s, H-16'), 1.40-1.23 (4H, m, H-9', H-13'), 1.11 (6H, s, H-10); ^{13}C NMR ($CDCl_3$, 100 MHz): δ_C 193.4 (CO, C-4), 155.3 (CO, C-14'), 150.6 (q_C, C-3), 150.3 (q_C, C-4'), 149.2 (q_C, C-9), 143.7 (q_C, C-2'), 134.1 (CH, C-6'), 117.8 (q_C, C-8), 117.3 (CN, C-7'), 110.7 (CH, C-5'), 105.8 (CH, C-3'), 95.1 (q_C, C-1'), 79.7 (q_C, C-15'), 52.5 (CH_2, C-5), 51.3 (CH, C-11'), 49.2 (CH, C-8'), 37.9 (CH_2, C-7), 36.0 (q_C, C-6), 32.0 (2 x CH_2, C-9', C-13'), 31.7 (2 x CH_2, C-10', C-12'), 28.6 (5 x CH_3, C-10, C-16'), 13.5 (CH_3, C-11) ppm.

6.2.6. Nitrile hydrolysis of benzonitriles 2.78 and 2.80

General procedure for the nitrile hydrolysis of 2.78 and 2.80: The nitrile (1.0 eq.) and K_2CO_3 (2.2 eq.) were suspended in DMSO. The reaction mixture was then treated with 30% H_2O_2 and stirred at room temperature. After 2 – 3 hours the crude reaction mixture was poured into ice-water and filtered; the precipitate was recrystallized from ethyl acetate to obtain the desired products.

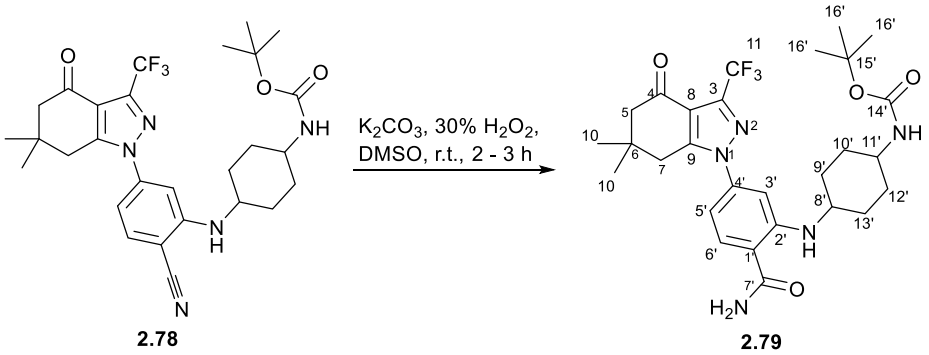

2.78 **2.79**

2.79 was synthesised following the general procedure using **2.78** (506 mg, 0.927 mmol, 1.00 eq.), K_2CO_3 (282 mg, 2.04 mmol, 2.20 eq.) and 30% H_2O_2 (150 µL) in DMSO (3 mL) to obtain **2.79** as a white solid (381 mg, 0.677 mmol, 73% yield).

***tert*-butyl(4-((2-carbamoyl-5-(6,6-dimethyl-4-oxo-3-(trifluoromethyl)-4,5,6,7-tetrahydro-1*H*-indazol-1-yl)phenyl)amino)cyclohexyl)carbamate** (**2.79**): White solid (73% yield); IR (ν_{max} cm^{-1}) 3336, 2933, 1677, 1586, 1511, 1451; ^{13}C NMR (DMSO, 125 MHz): δ_C 190.1 (CO, C-4), 170.7 (CO, C-7'), 154.8 (q_C, C-14'), 151.9 (q_c, C-9), 149.5 (q_c, C-4'), 140.6 (q_c, C-2'), 130.6 (CH, C-6'), 120.6 (CF_3, q, *J* = 274.8 Hz, C-11), 115.3 (q_c, C-8), 114.0 (q_c, C-1'), 108.9 (CH, C-5'), 106.9 (CH, C-3'), 51.7 (CH_2, C-5), 49.6 (CH, C-8'), 40.4 (CH, C-11'), 36.0 (CH_2, C-7), 35.1 (q_c, C-6), 31.3 (2 x CH_2, C-10', C-12'), 31.1 (2 x CH_2, C-9', C-13'), 28.2 (3 x CH_3, C-16'), 27.5 (2 x CH_3, C-10) ppm.

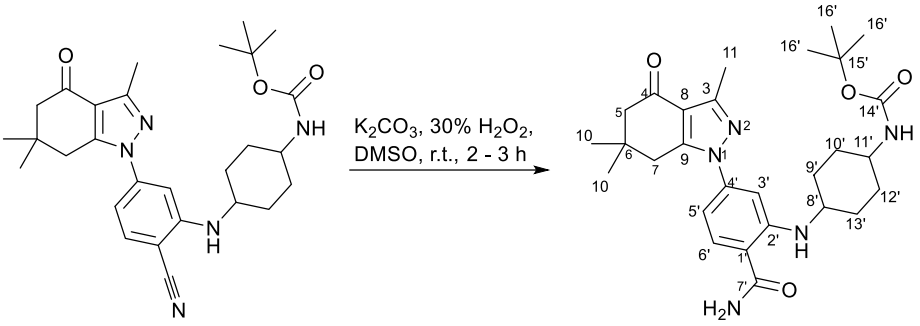

2.80 **2.81**

2.81 was synthesised following the general procedure using **2.80** (80.0 mg, 0.163 mmol, 1.00 eq.), K_2CO_3 (49.0 mg, 0.358 mmol, 2.20 eq.) and 30% H_2O_2 (25.0 µL) in DMSO (0.5 mL) to obtain the product as a white fluffy solid (50.0 mg, 0.098 mmol, 60% yield).

***tert*-butyl(4-((2-carbamoyl-5-(3,6,6-trimethyl-4-oxo-4,5,6,7-tetrahydro-1*H*-indazol-1-yl)phenyl)amino)cyclohexyl)carbamate** (**2.81**): White fluffy solid (60% yield); IR (ν_{max} cm^{-1}) 3358, 3174, 2922, 1698, 1675, 1649, 1626; ^1H NMR ($CDCl_3$, 500 MHz): δ_H 8.05 (1H, d, *J* = 7.5 Hz, NH), 7.46 (1H, d, *J* = 8.4 Hz, H-6'), 6.76 (1H, d, *J* = 1.9 Hz, H-3'), 6.60-6.58 (1H, dd, *J* = 8.4, 2.0 Hz, H-5'), 5.77 (2H, bs, NH_2), 4.42 (1H, s, NH), 3.48 (1H, s, H-8'), 3.34-3.26 (1H, m, H-11'), 2.80 (2H, s, H-7), 2.54 (3H, s, H-11), 2.39 (2H, s, H-5), 2.15-2.03 (4H, m, H-10', H-12'), 1.44 (9H, s, H-16'), 1.41-1.21 (4H, m, H-9', H-13'), 1.10

(6H, s, H-10); ^{13}C NMR ($CDCl_3$, 125 MHz): δ_C 193.5 (CO, C-4), 171.1 (CO, C-7'), 155.4 (CO, C-14'), 151.2 (q_C, C-3), 150.3 (q_C, C-4'), 149.3 (q_C, C-9), 142.9 (q_C, C-2'), 129.9 (CH, C-6'), 117.5 (q_C, C-8), 113.8 (q_C, C-1'), 110.5 (CH, C-5'), 108.2 (CH, C-3'), 79.5 (q_C, C-15'), 52.5 (CH_2, C-5), 52.0 (CH, C-11'), 49.2 (CH, C-8'), 37.9 (CH_2, C-7), 36.0 (q_C, C-6), 31.9 (2 x CH_2, C-9', C-13'), 31.1 (2 x CH_2, C-10', C-12'), 28.6 (5 x CH_3, C-10, C-16'), 13.6 (CH_3, C-11) ppm.

6.2.7. Removal of the Boc protecting group to yield 2.5 and 2.6

General procedure for the removal of the Boc protecting group: The Boc protected compounds were dissolved in a 4:1 DCM: TFA solution and stirred at room temperature. After 5 – 7 hours, the reaction mixture was concentrated in *vacuo* and the crude material was purified by silica gel chromatography (DCM: MeOH: NH_3, 20:1:0.1-5:1:0.1) to afford the desired product either as a TFA salt or free amine.

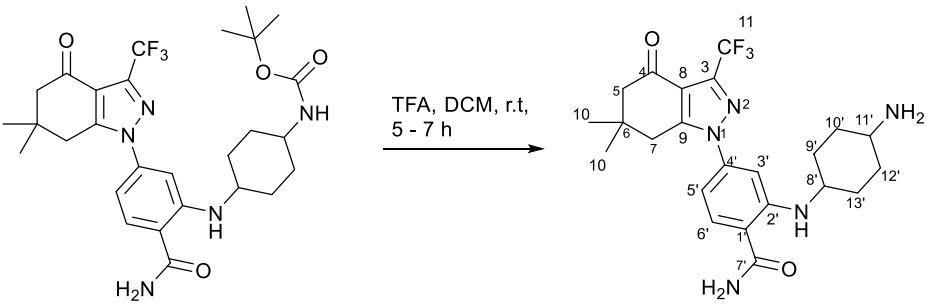

2.79 **2.5**

2.5 was synthesised following the general procedure using **2.79** (500 mg, 0.887 mmol, 1.00 eq.) in a 15.0 mL solution of DCM: TFA (4:1) to afford **2.5** as an off-white solid (170 mg, 41% yield);

2-((4-aminocyclohexyl)amino)-4-(6,6-dimethyl-4-oxo-3-(trifluoromethyl)-4,5,6,7-tetrahydro-1*H*-indazol-1-yl)benzamide (**2.5**, **isolated as a free amine**): Off-white solid (41% yield); IR (ν_{max} cm^{-1}) 3421, 2931, 2865, 1654, 1620, 1579, 1507; ^1H NMR (DMSO, 400 MHz): δ_H 8.35 (1H, d, *J* = 7.6 Hz, NH), 7.96 (1H, bs, NH_2), 7.78 (1H, d, *J* = 8.4 Hz, H-6'), 7.30 (1H, bs, NH_2), 6.87 (1H, d, *J* = 2.0 Hz, H-3'), 6.72-6.70 (1H, dd, *J* = 8.4, 2.1 Hz, H-5'), 3.31 (1H, bs, H-8'), 2.97 (2H, s, H-7), 2.66 (1H, bs, H-11'), 2.45 (2H, s, H-5), *2.05-1.97 (2H, m, H-9'), *1.84-1.75 (2H, m, H-10'), *1.21 (4H, quin., *J* = 11.5, 9.7 Hz, H-12', H-13'),

1.04 (6H, s, H-10); ^{13}C NMR (DMSO, 100 MHz): δ_C 190.1 (CO, C-4), 170.7 (CO, C-7'), 151.9 (q_c, C-9), 149.5 (q_c, C-4'), 140.6 (q_c, C-2'), 138.3 (q_c, q, *J* = 39.1 Hz, C-3), 130.6 (CH, C-6'), 120.6 (CF_3, q, *J* = 270.1 Hz, C-11), 115.3 (q_c, C-8), 113.9 (q_c, C-1'), 108.8 (CH, C-5'), 106.8 (CH, C-3'), 51.7 (CH_2, C-5), 49.8 (CH, C-8'), 49.5 (CH, C-11'), 36.0 (CH_2, C-7), 35.1 (q_c, C-6), 33.9 (2 x CH_2, C-10', C-12'), 31.0 (2 x CH_2, C-9', C-13'), 27.5 (2 x CH_3, C-10) ppm.

*Signals interchangeable.

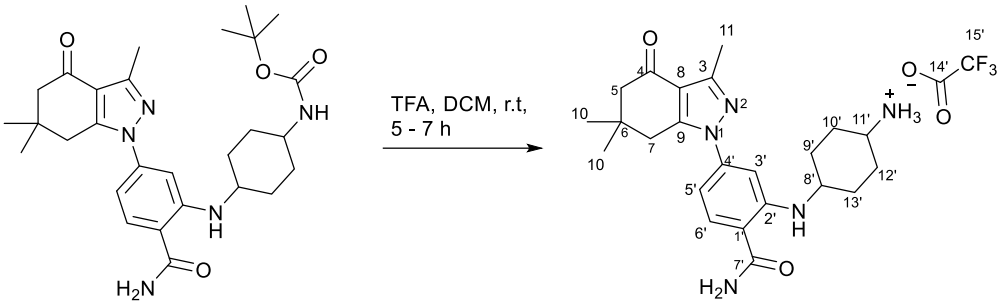

2.81 **2.6**

2.6 was synthesised following the general procedure using **2.81** (218 mg, 0.428 mmol, 1.00 eq.) in a 7.5 mL solution of DCM: TFA (4:1) to afford **2.6** as an off-white solid (139 mg, 79% yield).

2-((4-aminocyclohexyl)amino)-4-(3,6,6-trimethyl-4-oxo-4,5,6,7-tetrahydro-1*H*-indazol-1-yl)benzamide (**2.6**, **isolated as a TFA salt**): off-white solid (79% yield); ^{1}H NMR (DMSO, 400 MHz): δ_H 8.36 (1H, s, NH), 8.02 – 7.93 (4H, 2 x s, 2 x NH_2), 7.75 (1H, d, *J* = 8.5 Hz, H-6'), 6.82 (1H, d, *J* = 2.0 Hz, H-3'), 6.69 – 6.67 (1H, dd, *J* = 8.5, 2.0 Hz, H-5'), 3.35 (1H, bs, H-8'), 3.07 (1H, bs, H-11'), 2.93 (2H, s, H-7), 2.40 (3H, s, H-11), 2.33 (2H, s, H-5), 2.09 – 2.07 (2H, m, H-9', H-13'), 2.00 – 1.96 (2H, m, H-10', H-12'), 1.55 – 1.45 (2H, m, H-10', H-12'), 1.33 – 1.23 (2H, m, H-9', H-13'), 1.02 (6H, s, H-10); ^{13}C NMR (DMSO, 100 MHz): δ_C 192.8 (CO, C-4), 170.9 (CO, C-7'), 158.1 (CO, q, *J* = 31.3 Hz, C-14'), 149.5 (q_c, C-9), 149.4 (q_c, C-4'), 148.2 (q_c, C-3), 141.6 (q_c, C-2'), 130.5 (CH, C-6'), 117.2 (CF_3, q, *J* = 301.1 Hz, C-15'), 116.4 (q_c, C-8), 112.8 (q_c, C-1'), 108.4 (CH, C-5'), 105.7 (CH, C-3'), 51.8 (CH_2, C-5), 49.1 (CH, C-8'), 48.7 (CH, C-11'), 36.6 (CH_2, C-7), 35.3 (q_c, C-6), 30.2 (2 x CH_2, C-9', C-13'), 29.0 (2 x CH_2, C-10', C-12'), 27.7 (2 x CH_3, C-10), 13.1 (CH_3, C-11) ppm.

2-((4-aminocyclohexyl)amino)-4-(3,6,6-trimethyl-4-oxo-4,5,6,7-tetrahydro-1*H*-indazol-1-yl)benzamide (**2.6**,**isolated as a free amine**): off-white solid (64% yield); IR (ν_{max} cm^{-1}) 3300, 2926, 2864, 1653, 1617; ^{1}H NMR (DMSO, 400 MHz): δ_H 8.34 (1H, d, *J* = 7.7 Hz, NH), 7.88 (1H, bs, NH_2), 7.73 (1H, d, *J* = 8.5 Hz, H-6'), 7.20 (1H, bs, NH_2), 6.77 (1H, d, *J* = 1.8 Hz, H-3'), 6.68 – 6.66 (1H, dd, *J* = 8.4, 1.8 Hz, H-5'), 3.29 (1H, bs, H-8'), 2.93 (2H, s, H-7), 2.69 – 2.60 (1H, m, H-11'), 2.40 (3H, s, H-11), 2.33 (2H, s, H-5), 2.05 – 1.97 (2H, m, H-9', H-13'), 1.84 – 1.74 (2H, m, H-10'), 1.26 – 1.15 (4H, m,H-12', H-13'),1.02 (6H, s, H-10); ^{13}C NMR (DMSO, 100 MHz): δ_C 192.8 (CO, C-4), 170.9 (CO, C-7'), 149.5 (q_c, C-9), 149.4 (q_c, C-4'), 148.2 (q_c, C-3), 141.6 (q_c, C-2'), 130.5 (CH, C-6'), 116.3 (q_c, C-8), 112.6 (q_c, C-1'), 108.0 (CH, C-5'), 105.5 (CH, C-3'), 51.7 (CH_2, C-5), 49.8 (CH, C-8'), 49.6 (CH, C-11'), 36.6 (CH_2, C-7), 35.2 (q_c, C-6), 34.1 (2 x CH_2, C-9', C-13'), 31.1 (2 x CH_2, C-10', C-12'), 27.7 (2 x CH_3, C-10), 13.1 (CH_3, C-11) ppm.

6.2.8. Synthesis of sulfonic acid containing extracellular inhibitors 2.1 and 2.2

General procedure for bromine displacement to yield 2.1 and 2.2: The reactants were suspended in DMF and stirred 50 °C. After 18 hours the reaction mixture was concentrated *in vacuo* and purified using silica gel chromatography with an appropriate eluent. The structures were confirmed by full NMR spectroscopy, IR and HRESMS.

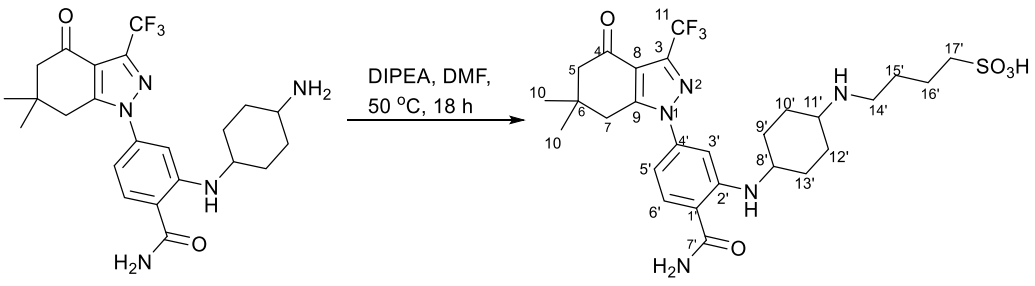

2.5 **2.1**

2.1 was synthesised following the general procedure using **2.5** (100 mg, 0.216 mmol, 1.00 eq.), 4-bromo-1-butanesulfonic acid (52.0 mg, 0.216 mmol, 1.00 eq.), DIPEA (120 µL, 0.647 mmol, 3.00 eq.) in DMF (1.00 mL) to afford the desired product as a white powder (71.0 mg, 0.114 mmol, 53% yield).

4-((4-((2-carbamoyl-5-(6,6-dimethyl-4-oxo-3-(trifluoromethyl)-4,5,6,7-tetrahydro-1*H*-indazol-1-yl)phenyl)amino)cyclohexyl)amino)butane-1-sulfonic acid (**2.1**): White powder (53% yield); IR (ν_{max} cm^{-1}) 3410, 3349, 3215, 2950, 2857, 1660, 1627, 1579, 1509; ^{1}H NMR (DMSO, 400 MHz): δ_H 8.37 (1H, d, *J* = 7.7 Hz, NH), 7.99 (1H, bs, NH), 7.79 (1H, d, *J* = 8.5 Hz, H-6'), 7.76 – 7.41 (3H, m), 7.33 (1H, bs, NH), 6.93 (1H, d, *J* = 1.9 Hz, H-3'), 6.74 – 6.71 (1H, dd, *J* = 8.4, 1.9 Hz, H-5'), #3.37 – 3.29 (H-8'), 3.10 – 2.98 (1H, m, H-11'), 2.97 (2H, s, H-7), 2.93 (2H, t, *J* = 7.0 Hz, H-17'), #2.50 – 2.38 (4H, m, H-5, H-14'), 2.18 – 2.03 (4H, m, H-9', H-10'), 1.76 – 1.62 (4H, m, H-15', H-16'), 1.56 – 1.41 (2H, m, H-12'), 1.32 – 1.18 (2H, m, H-13'), 1.04 (6H, s, H-10); ^{13}C NMR (DMSO, 100 MHz): δ_C 190.2 (CO, C-4), 170.7 (CO, C-7'), 152.0 (q_C, C-9), 149.4 (q_C, C-4'), 140.6 (q_C, C-2'), 138.4 (q_C, q, *J* = 39.0 Hz, C-3), 130.7 (CH, C-6'), 120.6 (q_C, q, *J* = 270.5 Hz, C-11), 115.3 (q_C, C-8), 114.1 (q_C, C-1'), 109.2 (CH, C-5'), 107.0 (CH, C-3'), 55.3 (CH, C-11'), 51.7 (CH_2, C-5), 50.5 (CH_2, C-14'), 49.2 (CH, C-8'), 44.1 (CH_2, C-17'), 36.0 (CH_2, C-7), 35.1 (q_C, C-6), 30.2 (2 x CH_2), 27.5 (2 x CH_3, C-10), 27.2 (2 x CH_2), 25.0 (CH_2), 22.3 (CH_2) ppm. ESI-MS *m/z* 600.2469 (calculated for $[M+H]^+$ $C_{27}H_{37}N_5O_5SF_3$ 600.2467).

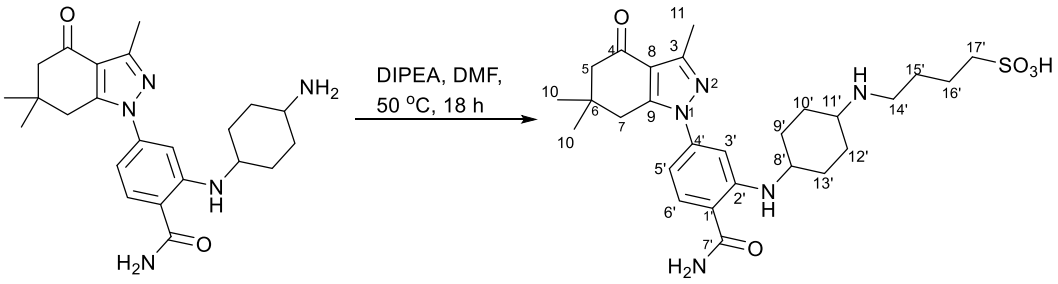

2.6 **2.2**

2.2 was synthesised following the general procedure using **2.6** (110 mg, 0.269 mmol, 1.00 eq.), 4-bromobutane-1-sulfonic acid (64.0 mg, 0.269 mmol, 1.00 eq.) and DIPEA (140 µL, 0.806 mmol, 3.00 eq.) in DMF (1.00 mL) to afford the desired product as a white fluffy solid (94.0 mg, 0.166 mmol, 62% yield).

4-((4-((2-carbamoyl-5-(3,6,6-trimethyl-4-oxo-4,5,6,7-tetrahydro-1*H*-indazol-1-yl)phenyl)amino)cyclohexyl)amino)butane-1-sulfonic acid (**2.2**): White fluffy solid (62% yield); IR

(ν_{max} cm^{-1}) 3358, 2938, 1651, 1621, 1581, 1551; ^{1}H NMR (DMSO, 500 MHz): δ_H 8.36 (1H, d, *J* = 7.7 Hz, NH), 7.93 (1H, bs, NH), 7.75 (1H, d, *J* = 8.6 Hz, H-6'), 7.71 – 7.44 (6H, m), 7.23 (1H, bs, NH), 6.83 (1H, d, *J* = 1.91 Hz, H-3'), 6.69 – 6.67 (1H, dd, *J* = 8.4, 1.9 Hz, H-5'), #3.36 (bs, H-8'), 3.06 – 3.02 (1H, m, H-11'), 2.92 – 2.89 (4H, m, H-7), #2.50 – 2.46 (2H, m), 2.40 (3H, s, H-11), 2.33 (2H, s, H-5), 2.11 (4H, d, *J* = 10.6 Hz), 1.76 – 1.62 (4H, m), 1.59 – 1.45 (2H, m), 1.28 – 1.21 (2H, m), 1.02 (6H, s, H-10); ^{13}C NMR (DMSO, 125 MHz): δ_C 192.8 (CO, C-4), 170.9 (CO, C-7'), *149.5 (q_C, C-9), *149.4 (q_C, C-4'), 148.2 (q_C, C-3), 141.6 (q_C, C-2'), 130.5 (CH, C-6'), 116.3 (q_C, C-8), 112.8 (q_C, C-1'), 108.4 (CH, C-5'), 105.7 (CH, C-3'), 55.2 (CH, C-11'), 51.8 (CH_2, C-5), 50.6 (CH_2), 49.2 (CH, C-8'), 44.0 (CH_2), 36.6 (CH_2, C-7), 35.3 (q_C, C-6), 30.3 (2 x CH_2), 27.8 (2 x CH_3, C-10), 27.1 (2 x CH_2), 25.0 (CH_2), 22.4 (CH_2), 13.1 (CH_3, C-11) ppm. ESI-MS *m/z* 546.2756 (calculated for $[M+H]^+$ $C_{27}H_{40}N_5O_5S$ 546.2750).

6.2.9. Synthesis of phosphonic acid containing extracellular inhibitors 2.3 and 2.4

General procedure for the amide formation to yield 2.3 and 2.4: The amine was added to a round bottomed flask containing a solution of DIPEA in DMF, the resulting mixture was stirred at room temperature for 1 hour. Thereafter, a solution of carboxylic acid, EDCI and NHS in DMF was added to the reaction mixture and continued stirring at room temperature for 3 days. Multiple new spots were observed in the TLC of the crude material. Only one spot was successfully isolated during silica gel chromatography and fully characterised using NMR spectroscopy, HRESMS and IR.

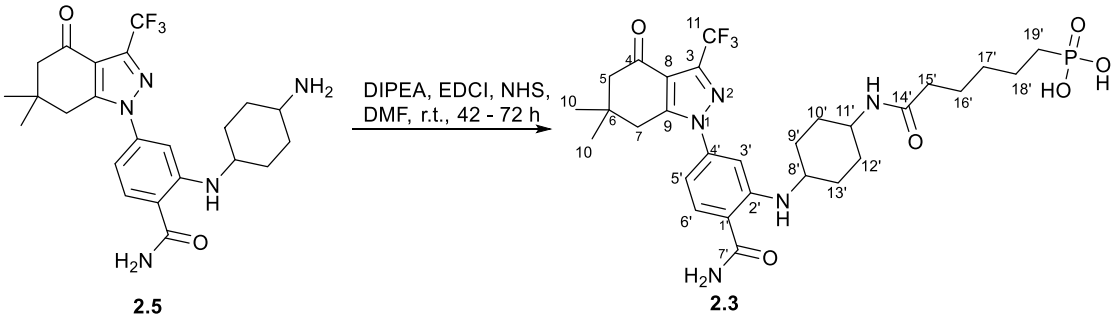

2.5 **2.3**

2.3: The general procedure was followed using **2.5** (55 mg, 1.0 eq., 0.12 mmol), DIPEA (0.28 mL, 13 eq., 1.5 mmol) in DMF (0.50 mL); and carboxylic acid (35 mg, 1.5 eq., 0.18 mmol), EDCI (34 mg, 1.5 eq.,

0.18 mmol), NHS (16 mg, 1.2 eq., 0.14 mmol) in DMF (0.50 mL) to yield **2.3** as an off-white solid (40 mg, 0.062 mmol, 52% yield).

(6-((4-((2-carbamoyl-5-(6,6-dimethyl-4-oxo-3-(trifluoromethyl)-4,5,6,7-tetrahydro-1*H*-indazol-1-yl)phenyl)amino)cyclohexyl)amino)-6-oxohexyl)phosphonic acid (**2.3**): Off-white solid (52% yield); IR (ν_{max} cm^{-1}) 3232, 3125, 2936, 2873, 1665, 1576, 1509, 1482; ^{1}H NMR (DMSO, 400 MHz): δ_H 8.36 (1H, d, *J* = 7.6 Hz, NH), 7.96 (1H, s, NH), 7.78 (1H, d, *J* = 8.5 Hz, H-6'), 7.72 (1H, d, *J* = 7.6 Hz, NH), 7.30 (1H, bs, NH), 6.89 (1H, d, *J* = 1.7 Hz, H-3'), 6.72-6.70 (1H, dd, *J* = 8.4, 1.7 Hz, H-5'), 3.60 – 3.51 (m, H-11'), 3.38 – 3.28 (m, H-8'), 2.97 (2H, s, H-5), 2.44 (2H, s, H-7), 2.29 – 2.16 (1H, m), *2.05-1.97 (4H, m), *1.82 – 1.79 (2H, m), *1.52 – 1.19 (17H, m), 1.04 (6H, s, H-10); ^{13}C NMR (DMSO, 100 MHz): δ_C 190.2 (CO, C-4), 171.4 (CO, C-14'), 170.7 (CO, C-7'), 151.9 (q_C, C-9), 149.5 (q_C, C-4'), 140.6 (q_C, C-2'), 138.3 (q_C, q, *J* = 39.0 Hz, C-3), 130.7 (CH, C-6'), 120.6 (q_C, q, *J* = 270.5 Hz, C-11), 115.3 (q_C, C-8), 113.9 (q_C, C-1'), 108.9 (CH, C-5'), 106.8 (CH, C-3'), 51.7 (CH_2, C-5), 49.6 (CH, C-8'), 47.0 (CH, C-11'), 36.0 (CH_2, C-7), 35.4 (CH_2, C-15'), 35.1 (q_C, C-6), 31.1 (2 x CH_2), 30.7 (2 x CH_2), 29.5 (? X CH_2), 28.1 (CH_2), 27.5 (2 x CH_3, C-10), 25.2 (CH_2), 23.3 (2 x CH_2) ppm. ESI-MS *m/z* 642.2668 (calculated for $[M+H]^+$ $C_{29}H_{40}N_5O_6PF_3$ 642.2668).

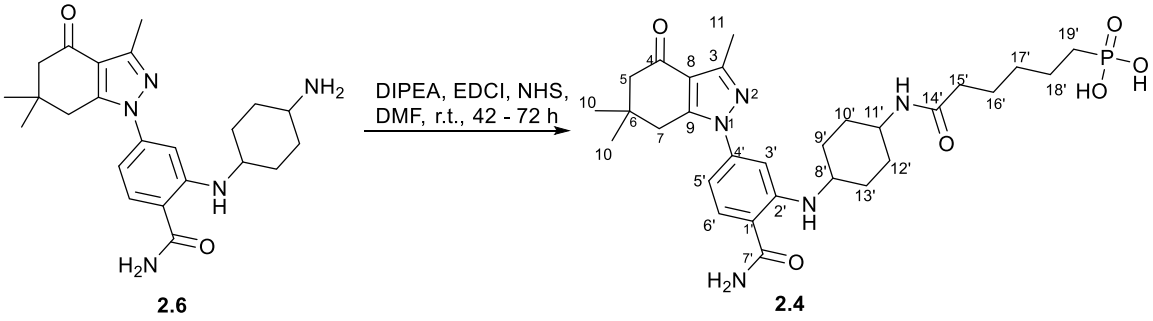

2.6 **2.4**

2.4: The general procedure was followed using **2.6** (68 mg, 1.0 eq., 0.17 mmol), DIPEA (0.38 mL, 13 eq., 2.2 mmol) in DMF (0.60 mL); and carboxylic acid (49 mg, 1.5 eq., 0.25 mmol), EDCI (48 mg, 1.5 eq., 0.25 mmol), NHS (23 mg, 1.2 eq., 0.20 mmol) in DMF (0.60 mL) to yield **2.4** as an off-white solid (38 mg, 0.065 mmol, 39% yield).

(6-((4-((2-carbamoyl-5-(3,6,6-trimethyl-4-oxo-4,5,6,7-tetrahydro-1*H*-indazol-1-yl)phenyl)amino)cyclohexyl)amino)-6-oxohexyl)phosphonic acid (**2.4**): Off-white solid (39% yield); ^{1}H NMR (DMSO, 500 MHz): δ_H 8.34 (1H, d, *J* = 7.9 Hz, NH), 7.89 (1H, bs, NH), 7.75 – 7.71 (2H, m, H-6'), 7.21 (1H, bs), 6.79 (1H, d, *J* = 1.9 Hz, H-3'), 6.68 – 6.66 (1H, dd, *J* = 8.5, 1.9 Hz, H-5'), 6.63 (1H, bs), 3.60 – 3.50 (2 x CH, m, H-11'), #3.37 – 3.28 (1H, m, H-8'), 2.93 (2H, m, H-7), 2.40 (3H, s, H-11), 2.33 (2H, s, H-5), 2.06 – 1.99 (6H, m), 1.85 – 1.78 (2H, m), 1.53 – 1.18 (24H, m), 1.01 (6H, s, H-10); ^{13}C NMR (DMSO, 125 MHz): δ_C 192.8 (CO, C-4), 171.4 (CO, C-14'), 170.9 (CO, C-7'), *149.49 (q_C, C-9), *149.47 (q_C, C-4'), 148.2 (q_C, C-3), 141.6 (q_C, C-2'), 130.5 (CH, C-6'), 116.4 (q_C, C-8), 112.7 (q_C, C-1'), 108.1 (CH, C-5'), 105.6 (CH, C-3'), 51.7 (CH_2, C-5), 49.6 (CH, C-8'), 47.1 (CH, C-11'), 36.7 (CH_2, C-7), 35.4 (q_C, C-6), 35.2 (2 x CH_2), 34.2 (2 x CH_2), 31.1 (2 x CH_2), 30.7 (2 x CH_2), 27.7 (2 x CH_3, C-10), 25.3 (CH_2), 23.4 (CH_2), 13.1 (CH_3, C-11) ppm. ESI-MS *m/z* 588.2947 (calculated for $[M+H]^+$ $C_{29}H_{43}N_5O_6P$ 588.2951).

6.3. Experimental data: Investigation of an unexpected 1-5 nitrogen to carbon tosyl migration (compounds described in Section 3.1.2.)[141]

6.3.1. *N*-acylation of 2.24

General procedure for the preparation of compounds 2.47, 2.53 – 2.58: Acid anhydride 1 eq. was added to a suspension of **2.24** (500 mg, 1.62 mmol, 1.00 eq.), in TEA (13.0 eq.) and THF (9.00 mL). The reaction mixture was heated to 55 ˚C, forming an orange solution, which was stirred for 2 hours. After cooling to room temperature, the mixture was quenched with sat. NH_4Cl (20 mL) and extracted with EtOAc (3 x 20 mL). The combined organic fractions were washed with sat. brine (20 mL), dried over anhydrous $MgSO_4$, concentrated *in vacuo* to yield an orange-brown oil and purified with silica gel chromatography to yield compounds **2.47, 2.53 – 2.58.**[141]

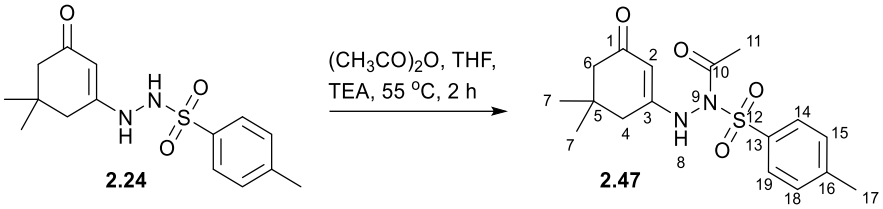

2.47 was synthesised following the general procedure using acetic anhydride (150 µL, 1.62 mmol, 1.00 eq.) and TEA (2.94 mL, 21.1 mmol, 13.0 eq.) to obtain **2.47** as a white solid (341 mg, 0.974 mmol, 60% yield).

***N*-acetyl-*N*'-(5,5-dimethyl-3-oxocyclohex-1-en-1-yl)-4-methylbenzenesulfonohydrazide** (**2.47**): White solid (60% yield); ^{1}H NMR (DMSO, 400 MHz): δ_H 9.84 (1H, s, NH-8), 7.87 (2H, d, *J* = 8.5 Hz, H-14, H-19), 7.46 (2H, d, *J* = 8.5 Hz, H-15, H-18), 4.96 (1H, s, H-2), 2.42 (3H, s, H-17), 2.30 (2H, s, H-4), 2.10 (2H, s, H-6), 2.05 (3H, s, H-11), 1.04 (3H, s, H-7), 1.02 (3H, s, H-7); ^{13}C NMR (DMSO, 100 MHz): δ_C 195.6 (CO, C-1), 170.5 (CO, C-10), 162.0 (q_c, C-3), 145.3 (q_c, C-16), 135.0 (q_c, C-13), 129.5 (CH, C-15, C-18), 128.7 (CH, C-14, C-19), 97.4 (CH, C-2), 50.3 (CH_2, C-6), 38.7 (CH_2, C-4), 32.7 (q_c, C-5), 27.6 (CH_3, C-7), 27.6 (CH_3, C-7), 21.9 (CH_3, C-11), 21.1 (CH_3, C-17) ppm. ESI-MS *m/z* 351.1377 (calculated for $C_{17}H_{23}N_2O_4S$ $[M+H]^+$ 351.1379).

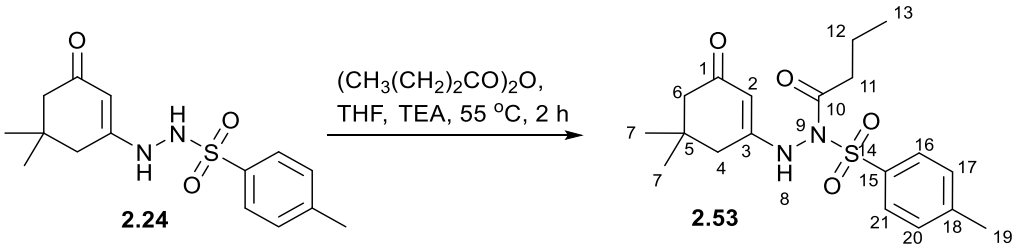

2.53 was synthesised following the general procedure using butyric anhydride (270 µL, 1.62 mmol, 1.00 eq.) and TEA (2.94 mL, 21.1 mmol, 13.0 eq.) to obtain **2.53** as a yellow solid (313 mg, 0.826 mmol, 51% yield).

***N*-butyryl-*N*'-(5,5-dimethyl-3-oxocyclohex-1-en-1-yl)-4-methylbenzenesulfonohydrazide** (**2.53**): Yellow solid (51% yield); ^{1}H NMR (DMSO, 400 MHz): δ_H 9.83 (1H, s, NH-8), 7.87 (2H, d, *J* = 8.3 Hz, H-

16, H-21), 7.46 (2H, d, *J* = 8.3 Hz, H-17, H-20), 4.94 (1H, s, H-2), 2.48-2.14 (1H, m, H-11), 2.42 (3H, H-19), 2.31 (2H, s, H-4), 2.26-2.14 (1H, m, H-11), 2.10 (2H, s, H-6), 1.42 (2H, sex, *J* = 7.4 Hz, H-12), 1.05 (3H, s, H-7), 1.02 (3H, s, H-7), 0.76 (3H, t, *J* = 7.4 Hz, H-13); ^{13}C NMR (DMSO, 100 MHz): δ_C 195.6 (CO, C-1), 172.8 (CO, C-10), 162.2 (q_C, C-3), 145.3 (q_C, C-18), 135.2 (q_C, C-15), 129.5 (CH, C-17, C-20), 128.7 (CH, C-16, C-21), 97.4 (CH, C-2), 50.3 (CH_2, C-6), 38.8 (CH_2, C-4), 35.0 (CH_2, C-11), 32.8 (q_C, C-5), 27.6 (2 x CH_3, C-7), 21.1 (CH_3, C-19), 16.8 (CH_2, C-12), 13.2 (CH_3, C-13) ppm. ESI-MS *m/z* 379.1689 (calculated for $C_{19}H_{27}N_2O_4S$ $[M+H]^+$ 379.1692).

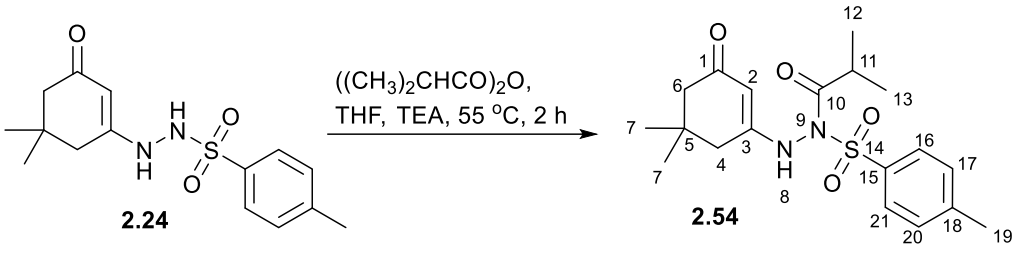

2.54 was synthesised following the general procedure using isobutyric anhydride (270 µL, 1.62 mmol, 1.00 eq.) and TEA (2.94 mL, 21.1 mmol, 13.0 eq.) to obtain **2.54** as a yellow solid (214 mg, 0.567 mmol, 35% yield).

***N*'-(5,5-dimethyl-3-oxocyclohex-1-en-1-yl)-*N*-isobutyryl-4-methylbenzenesulfonohydrazide** (**2.54**): Yellow solid (35% yield); ^{1}H NMR (DMSO, 400 MHz): δ_H 9.91 (1H, s, NH-8), 7.87 (2H, d, *J* = 8.4 Hz, H-16, H-21), 7.46 (2H, d, *J* = 8.4 Hz, H-17, H-20), 4.93 (1H, s, H-2), 2.73-2.66 (1H, m, H-11), 2.42 (3H, s, H-19), 2.33 (2H, s, H-4), 2.10 (2H, d, *J* = 1.4 Hz, H-6), 1.05 (3H, s, H-7), 1.02 (3H, s, H-7), 0.97 (3H, d, *J* = 6.9 Hz, H-12), 0.91 (3H, d, *J* = 6.9 Hz, H-13); ^{13}C NMR (DMSO, 100 MHz): δ_C 195.7 (CO, C-1), 176.9 (CO, C-10), 162.6 (q_C, C-3), 145.3 (q_C, C-18), 135.3 (q_C, C-15), 129.5 (CH, C-17, C-20), 128.6 (CH, C-16, C-21), 97.6 (CH, C-2), 50.3 (CH_2, C-6), 38.9 (CH_2, C-4), 32.8 (q_C, C-5), 31.7 (CH, C-11), 27.7 (CH_3, C-7), 27.6 (CH_3, C-7), 21.1 (CH_3, C-19), 18.8 (CH_3, C-12), 18.1 (CH_3, C-13) ppm. ESI-MS *m/z* 379.1693 (calculated for $C_{19}H_{27}N_2O_4S$ $[M+H]^+$ 379.1692).

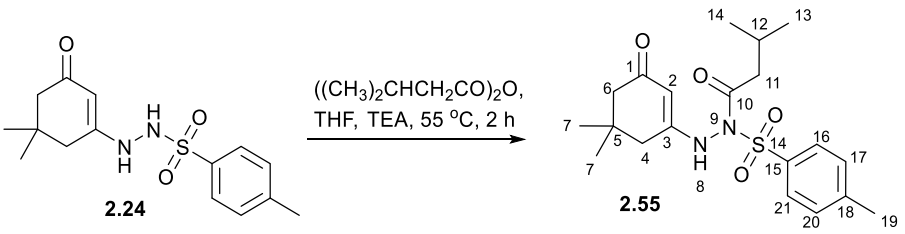

2.55 was synthesised following the general procedure using isovaleric anhydride (320 µL, 1.62 mmol, 1.00 eq.) and TEA (2.94 mL, 21.1 mmol, 13.0 eq.) to obtain **2.55** as a yellow solid (223 mg, 0.567 mmol, 35% yield).

***N*'-(5,5-dimethyl-3-oxocyclohex-1-en-1-yl)-4-methyl-*N*-(3-methylbutanoyl)benzenesulfonohydrazide** (**2.55**): Yellow solid (35% yield); ^{1}H NMR (DMSO, 400 MHz): δ_H 9.84 (1H, s, NH), 7.88 (2H, d, *J* = 8.4 Hz, H-17, H-22), 7.46 (2H, d, *J* = 8.3 Hz, H-18, H-21), 4.94 (1H, s, H-2), 2.42 (3H, s, H-20), 2.37-2.32 (3H, m, H-4, H-11), 2.15-2.04 (3H, m, H-6, H-11), 1.96-1.86 (1H, m, H-12), 1.05 (3H, s, H-7), 1.02 (3H, s, H-7b, 0.79 (3H, d, *J* = 6.6 Hz, H-13), 0.76 (3H, d, *J* = 6.6 Hz, H-14); ^{13}C NMR (DMSO, 100 MHz): δ_C 195.6 (CO, C-1), 172.3 (CO, C-10), 162.2 (q_C, C-3), 145.2 (q_C, C-19), 135.3 (q_C, C-16), 129.4 (CH, C-18, C-21), 128.6 (CH, C-17, C-22), 97.5 (CH, C-2), 50.3 (CH_2, C-6), 41.9 (CH_2, C-11), 38.8 (CH_2, C-4), 32.8 (q_C, C-5), 27.7 (CH_3, C-7), 24.1 (CH, C-12), 22.1 (CH_3, C-14), 21.8 (CH_3, C-13), 21.1 (CH_3, C-20) ppm. ESI-MS *m/z* 393.1842 (calculated for $C_{20}H_{29}N_2O_4S$ $[M+H]^+$ 393.1848).

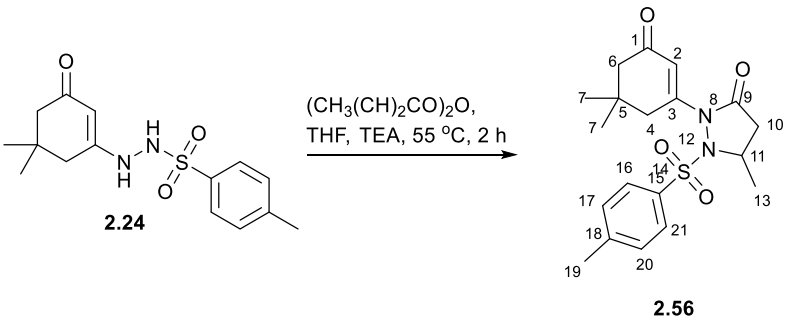

2.56 was synthesised following the general procedure using crotonic anhydride (240 µL, 1.62 mmol, 1.00 eq.) and TEA (2.94 mL, 21.1 mmol, 13.0 eq.) to obtain **2.56** as a yellow solid (104 mg, 0.275 mmol, 17% yield).

2-(5,5-dimethyl-3-oxocyclohex-1-en-1-yl)-5-methyl-1-tosylpyrazolidin-3-one (**2.56**): Yellow solid (17% yield); ^{1}H NMR (DMSO, 500 MHz): δ_H 7.75 (2H, d, *J* = 8.3 Hz, H-16, H-21), 7.55 (2H, d, *J* = 8.3 Hz, H-17, H-20), 6.23 (1H, s, H-2), 4.47 (1H, quin, *J* = 7.5 Hz, H-11), 2.87 (1H, d, *J* = 17.7 Hz, H-4), 2.45 (3H, s, H-19), 2.36 (1H, d, *J* = 17.7 Hz, H-4), 2.21 (2H, s, H-6), 1.98 (1H, d, *J* = 17.9 Hz, H-10), 1.53 (1H, dd, *J* = 17.9, 7.5 Hz, H-10), 1.23 (3H, d, *J* = 7.5 Hz, H-13), 1.06 (3H, s, H-7), 1.04 (3H, s, H-7); ^{13}C NMR (DMSO, 100 MHz): δ_C 198.3 (CO, C-1), 171.6 (CO, C-9), 153.9 (q_C, C-3), 146.5 (q_C, C-18), 130.8 (CH, C-17, C-20), 129.9 (q_C, C-15), 128.9 (CH, C-16, C-21), 114.1 (CH, C-2), 54.0 (CH, C-11), 50.2 (CH_2, C-6), 39.0 (CH_2, C-4), 36.1 (CH_2, C-10), 32.8 (q_C, C-5), 27.9 (CH_3, C-7), 27.6 (CH_3, C-7), 21.2 (CH_3, C-19), 20.5 (CH_3, C-13) ppm. ESI-MS *m/z* 377.1534 (calculated for $C_{19}H_{25}N_2O_4S$ $[M+H]^+$ 377.1535).

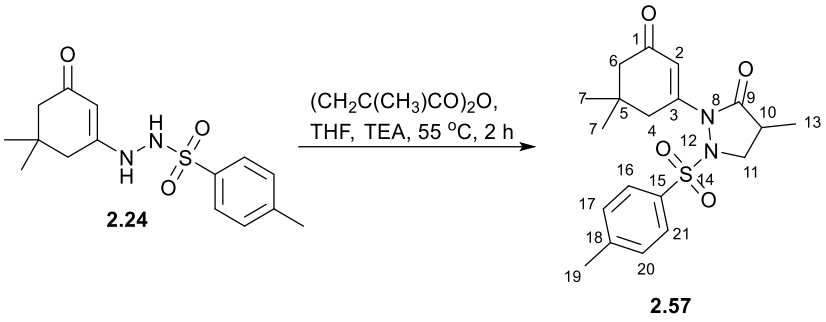

2.24 **2.57**

2.57 was synthesised following the general procedure using methacrylic anhydride (240 µL, 1.62 mmol, 1.00 eq.) and TEA (2.94 mL, 21.1 mmol, 13.0 eq.) to obtain **2.57** as a yellow solid (274 mg, 0.729 mmol, 45% yield).

2-(5,5-dimethyl-3-oxocyclohex-1-en-1-yl)-4-methyl-1-tosylpyrazolidin-3-one (**2.57**): Yellow solid (45% yield); ^{1}H NMR (DMSO, 400 MHz): δ_H 7.76 (2H, d, *J* = 8.2 Hz, H-16, H-21), 7.54 (2H, d, *J* = 8.3 Hz, H-17, H-20), 6.21 (1H, s, H-2), 4.36 (1H, dd, *J* = 13.5, 8.4 Hz, H-11), 3.56 (1H,t, *J* = 13.5 Hz, H-11), 2.88 (1H, d, *J* = 17.8 Hz, H-4), 2.45 (3H, s, H-19), 2.42-2.35 (1H, m, H-4), 2.20 (2H, s, H-6), 1.54 (1H, bs, H-10), 1.05 (6H, 2 x s, H-7), 0.83 (3H, d, *J* = 6.7 Hz, H-13)); ^{13}C NMR (DMSO, 100 MHz): δ_C 198.2 (CO, C-1), 174.4 (CO, C-9), 153.8 (q_C, C-3), 146.4 (q_C, C-18), 130.7 (CH, C-17, C-20), 130.2 (q_C, C-15), 128.8 (CH, C-16, C-21), 114.2 (CH, C-2), 53.4 (CH_2, C-11), 50.3 (CH_2, C-6), 39.0 (CH_2, C-4), 34.3 (CH, C-10), 32.6 (q_C,

C-5), 28.0 (CH_3, C-7a), 27.6 (CH_3, C-7b), 21.2 (CH_3, C-19), 13.2 (CH_3, C-13) ppm. ESI-MS *m/z* 377.1534 (calculated for $C_{19}H_{25}N_2O_4S$ $[M+H]^+$ 377.1535).

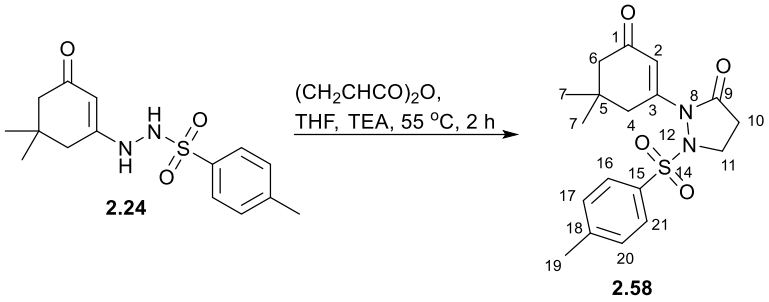

2.24 **2.58**

2.58 was synthesised following the general procedure using acrylic anhydride (190 µL, 1.62 mmol, 1.00 eq.) and TEA (2.94 mL, 21.1 mmol, 13.0 eq.) to obtain **2.58** as a yellow solid (211 mg, 0.583 mmol, 36% yield).

2-(5,5-dimethyl-3-oxocyclohex-1-en-1-yl)-1-tosylpyrazolidin-3-one (**2.58**) Yellow solid (36% yield); ^{1}H NMR (DMSO, 400 MHz): δ_H 7.76 (2H, d, *J* = 8.3 Hz, H-15, H-20), 7.56 (2H, d, *J* = 8.2 Hz, H-16, H-19), 6.24 (1H, s, H-2), 4.04 (2H, br d, *J* = 0.12 Hz, H-11), 2.86 (1H, s, H-4), 2.46 (3H, s, H-18), 2.39 (1H, s, H-4), 2.19 (2H, s, H-6), 1.49-1.16 (2H, m, H-10), 1.05 (6H, s, H-7); ^{13}C NMR (DMSO, 100 MHz): δ_C 198.2 (CO, C-1), 172.0 (CO, C-9), 153.8 (q_C, C-3), 146.4 (q_C, C-18), 130.8 (CH, C-17, C-20), 130.0 (q_C, C-14), 128.5 (CH, C-15, C-20), 113.7 (CH, C-2), 50.2 (CH_2, C-6), 46.4 (CH_2, C-11), 39.4 (CH_2, C-4), 32.7 (q_C, C-5), 29.6 (CH_2, C-10), 27.8 (CH_3, C-7), 21.2 (CH_3, C-18) ppm. ESI-MS *m/z* 363.1375 (calculated for $C_{18}H_{23}N_2O_4S$ $[M+H]^+$ 363.1379).

6.3.2. 1-5 Nitrogen to carbon tosyl migration

General procedure for the preparation of compounds 2.52, **2.59 – 2.61:** NaOH (5.3 eq.) was added to a suspension of the *N*-acylated starting material (1.0 eq.) in THF (6.0 mL), and stirred at room temperature for 16 hours. Thereafter, the mixture was quenched with sat. NH_4Cl (15 mL) and extracted with EtOAc (3 x 15 mL). The combined organic fractions were washed with sat. brine (15

mL), dried over anhydrous $MgSO_4$, concentrated in *vacuo* and purified with silica gel chromatography to yield compounds **2.52**, **2.59 – 2.61**.[141]

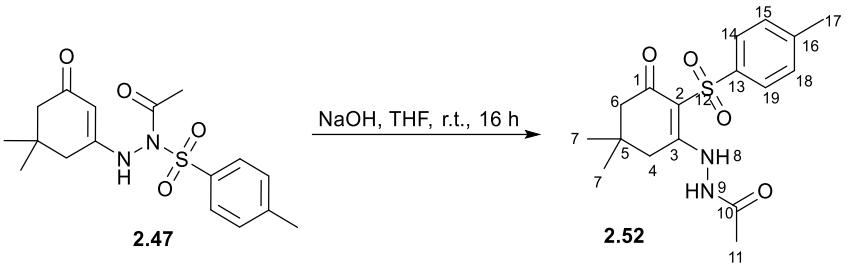

2.52 was synthesised following the general procedure using **2.47** (64.8 mg, 0.185 mmol, 1.00 eq.) to obtain **2.52** as a pale yellow solid (49.3 mg, 0.141 mmol, 76% yield).

***N*'-(5,5-dimethyl-3-oxo-2-tosylcyclohex-1-en-1-yl)acetohydrazide** (**2.52**): Pale yellow solid (76% yield); ^{1}H NMR (DMSO, 500 MHz): δ_H 10.45 (1H, s, NH-8), 10.42 (1H, s, NH-9), 7.76 (2H, d, *J* = 8.2 Hz, H-14, H-19), 7.34 (2H, d, *J* = 8.2 Hz, H-15, H-18), 2.53 (2H, s, H-4), 2.37 (3H, s, H-17), 2.05 (2H, s, H-6), 1.96 (3H, s, H-11), 0.90 (6H, s, H-7); ^{13}C NMR (DMSO, 125 MHz): δ_C 189.2 (CO, C-1), 169.0 (CO, C-10), 167.7 (q_c, C-3), 142.8 (q_c, C-16), 140.6 (q_c, C-13), 128.8 (CH, C-15, C-18), 126.8 (CH, C-14, C-19), 105.1 (q_C, C-2), 50.0 (CH_2, C-6), 38.3 (CH_2, C-4), 30.5 (q_C, C-5), 27.3 (CH_3, C-7), 20.9 (CH_3, C-17), 20.4 (CH_3, C-11) ppm. ESI-MS *m/z* 351.1378 (calculated for $C_{17}H_{23}N_2O_4S$ $[M+H]^+$ 351.1379).

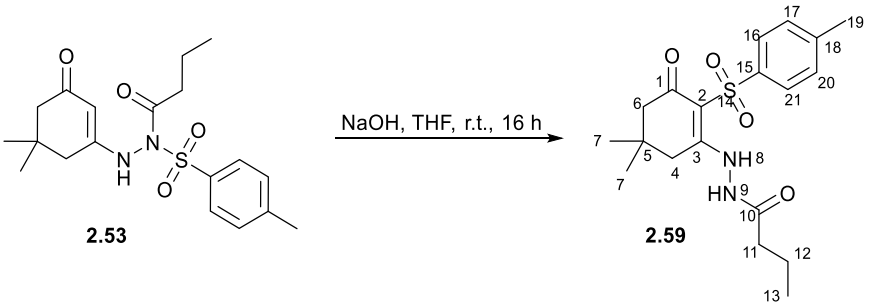

2.59 was synthesised following the general procedure using **2.53** (70.0 mg, 0.185 mmol, 1.00 eq.) to obtain **2.59** as an orange solid (53.9 mg, 0.142 mmol, 77% yield).

***N*'-(5,5-dimethyl-3-oxo-2-tosylcyclohex-1-en-1-yl)butyrohydrazide** (**2.59**): Orange solid (77% yield); ^{1}H NMR (DMSO, 400 MHz): δ_H 10.45 (2H, bs, NH-8, NH-9), 7.76 (2H, d, *J* = 8.2 Hz, H-16, H-21), 7.34 (2H, d, *J* = 8.2 Hz, H-17, H-20), 2.51 (2H, s, H-4), 2.37 (3H, s, H-19), 2.20 (2H, t, *J* = 7.3 Hz, H-11), 2.05 (2H, s, H-6), 1.61 (2H, sex, *J* = 7.3 Hz, H-12), 0.92 (3H, t, *J* = 7.3 Hz, H-13), 0.89 (6H, s, H-7); ^{13}C NMR (DMSO, 100 MHz): δ_C 189.3 (CO, C-1), 171.8 (CO, C-10), 167.8 (q_c, C-3), 142.9 (q_c, C-18), 140.6 (q_c, C-15), 128.9 (CH, C-17, C-20), 126.9 (CH, C-16, C-21), 105.2 (q_C, C-2), 50.0 (CH_2, C-6), 38.4 (CH_2, C-4), 35.0 (CH_2, C-11), 30.5 (q_C, C-5), 27.4 (CH_3, C-7), 21.0 (CH_3, C-20), 18.2 (CH_2, C-12), 13.6 (CH_3, C-13) ppm. ESI-MS *m/z* 379.1689 (calculated for $C_{19}H_{27}N_2O_4S$ $[M+H]^+$ 379.1692).

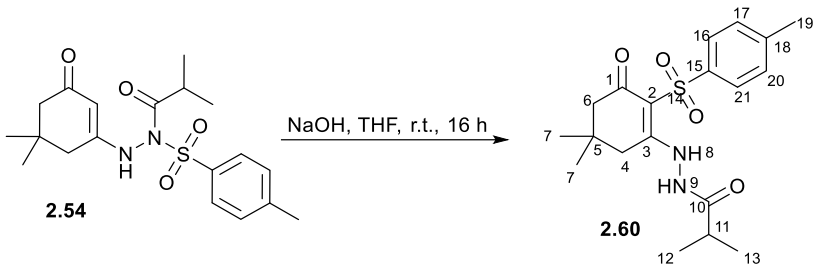

2.60 was synthesised following the general procedure using **2.54** (70.0 mg, 0.185 mmol, 1.00 eq.) to obtain **2.60** as an orange solid (24.5 mg, 0.065 mmol, 35% yield).

***N*'-(5,5-dimethyl-3-oxo-2-tosylcyclohex-1-en-1-yl)isobutyrohydrazide** (**2.60**): Orange solid (35% yield); ^{1}H NMR (DMSO, 500 MHz): δ_H 10.43 (2H, bs, NH-8, NH-9), 7.77 (2H, d, *J* = 8.3 Hz, H-16, H-21), 7.35 (2H, d, *J* = 8.3 Hz, H-17, H-20), 2.52-2.47 (4H, m, H-4, H-11), 2.37 (3H, s, H-19), 2.05 (2H, s, H-6), 1.12 (3H, s, H-12), 1.10 (3H, s, H-13), 0.89 (6H, s, H-7); ^{13}C NMR (DMSO, 125 MHz): δ_C 189.3 (CO, C-1), 175.7 (CO, C-10), 168.0 (q_c, C-3), 142.9 (q_c, C-18), 140.6 (q_c, C-15), 128.9 (CH, C-17, C-20), 126.9 (CH, C-16, C-21), 105.2 (q_C, C-2), 50.0 (CH_2, C-6), 38.2 (CH_2, C-4), 32.3 (CH, C-11), 30.5 (q_C, C-5), 27.4 (CH_3, C-7), 21.0 (CH_3, C-19), 19.1 (2 x CH_3, C-12, C-13) ppm. ESI-MS *m/z* 379.1693 (calculated for $C_{19}H_{27}N_2O_4S$ $[M+H]^+$ 379.1692).

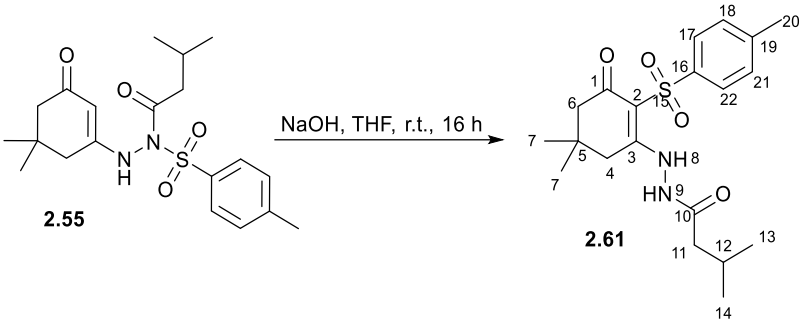

2.61 was synthesised following the general procedure using **2.55** (72.6 mg, 0.185 mmol, 1.00 eq.) to obtain **2.61** as an orange solid (53.0 mg, 0.135 mmol, 73% yield).

***N*'-(5,5-dimethyl-3-oxo-2-tosylcyclohex-1-en-1-yl)-3-methylbutanehydrazide** (**2.61**): Orange solid (73% yield); ^{1}H NMR (DMSO, 400 MHz): δ_H 10.44 (2H, bs, NH-8, NH-9), 7.77 (2H, d, *J* = 8.3 Hz, H-17, H-22), 7.34 (2H, d, *J* = 8.3 Hz, H-18, H-21), 2.51 – 2.50 (2H, m, H-4), 2.36(3H, s, H-20), 2.12-2.02 (5H, m, H-6, H-11, H-12), 0.95 (3H, s, H-13), 0.93 (3H, s, H-14), 0.88 (6H, s, H-7); ^{13}C NMR (DMSO, 100 MHz): δ_C 189.3 (CO, C-1), 171.3 (CO, C-10), 167.8 (q_c, C-3), 142.9 (q_c, C-19), 140.6 (q_c, C-16), 128.9 (CH, C-18, C-21), 126.9 (CH, C-17, C-22), 105.2 (q_C, C-2), 50.0 (CH_2, C-6), 42.2 (CH_2, C-11), 38.5 (CH_2, C-4), 30.5 (q_C, C-5), 27.4 (CH_3, C-7), 25.3 (CH, C-12), 22.3 (2 x CH_3, C-13, C-14), 21.0 (CH_3, C-20) ppm. ESI-MS *m/z* 393.1844 (calculated for $C_{20}H_{29}N_2O_4S$ $[M+H]^+$ 393.1848).

REFERENCES

1. Hoter, A.; El-Sabban, M. E.; Naim, H. Y., *Int. J. Mol. Sci.* **2018,** *19*, 2560.
2. Verghese, J.; Abrams, J.; Wang, Y.; Morano, K. A., *Microbiol. Mol. Biol. Rev.* **2012,** *76*, 115-158.
3. Zarouchlioti, C.; Parfitt, D. A.; Li, W.; Gittings, L. M.; Cheetham, M. E., *Philos. Trans. R. Soc. Lond. B Biol. Sci.* **2018,** *373*, 20160534.
4. Liu, Y.; Chang, A., *EMBO J.* **2008,** *27*, 1049-1059.
5. Hou, J.; Tang, H.; Liu, Z.; Österlund, T.; Nielsen, J.; Petranovic, D., *FEMS Yeast Res.* **2014,** *14*, 481-494.
6. Santiago, A. M.; Gonçalves, D. L.; Morano, K. A., *Exp. Cell Res.* **2020,** *395*, 112240.
7. Solaini, G.; Baracca, A.; Lenaz, G.; Sgarbi, G., *Biochim. Biophys. Acta* **2010,** *1797*, 1171-1177.
8. Melber, A.; Haynes, C. M., *Cell Res.* **2018,** *28*, 281-295.
9. Bartoszewska, S.; Collawn, J. F., *Cell. Mol. Biol. Lett.* **2020,** *25*, 1-20.
10. Pieczenik, S. R.; Neustadt, J., *Exp. Mol. Pathol.* **2007,** *83*, 84-92.
11. Dai, C., *Philos. Trans. R. Soc. Lond. B Biol. Sci.* **2018,** *373*, 20160525.
12. Powers, M. V.; Workman, P., *FEBS Lett.* **2007,** *581*, 3758-3769.
13. Edkins, A. L.; Price, J. T.; Pockley, A. G.; Blatch, G. L., *Philos. Trans. R. Soc. Lond. B Biol. Sci.* **2018,** *373*, 20160521.
14. Whitesell, L.; Lindquist, S. L., *Nat. Rev. Cancer* **2005,** *5*, 761-772.
15. Calderwood, S. K., *Philos. Trans. R. Soc. Lond. B Biol. Sci.* **2018,** *373*, 20160524.
16. Pockley, A. G.; Henderson, B., *Philos. Trans. R. Soc. Lond. B Biol. Sci.* **2018,** *373*, 20160522.
17. Malyshev, I., A General Description of HSPs, The Molecular Structure of HSP70 and The HSP70 Cycle. In *Immunity, Tumors and Aging: The Role of HSP70*, Springer: Dordrecht, 2013; pp 1-13.
18. Pirkkala, L.; Sistonen, L., *Encycl. Life Sci.* **2001**, 1-7.
19. Lindquist, S., *Annu. Rev. Biochem.* **1986,** *55*, 1151-1191.

20. Albakova, Z.; Mangasarova, Y.; Sapozhnikov, A., *Front. Immunol.* **2021,** *12*, 660085.

21. Miyata, Y.; Nakamoto, H.; Neckers, L., *Curr. Pharm. Des.* **2013,** *19*, 347-365.

22. Albakova, Z.; Armeev, G. A.; Kanevskiy, L. M.; Kovalenko, E. I.; Sapozhnikov, A. M., *Cells* **2020,** *9*, 587.

23. Koay, Y. C.; McConnell, J. R.; Wang, Y.; Kim, S. J.; Buckton, L. K.; Mansour, F.; McAlpine, S. R., *ACS Med. Chem. Lett.* **2014,** *5*, 771-776.

24. Garcia-Carbonero, R.; Carnero, A.; Paz-Ares, L., *Lancet Oncol.* **2013,** *14*, e358-e369.

25. Castelli, C.; Rivoltini, L.; Rini, F.; Belli, F.; Testori, A.; Maio, M.; Mazzaferro, V.; Coppa, J.; Srivastava, P. K.; Parmiani, G., *Cancer Immunol. Immunother.* **2004,** *53*, 227-233.

26. Li, L.; Wang, L.; You, Q.-D.; Xu, X.-L., *J. Med. Chem.* **2019,** *63*, 1798-1822.

27. Seo, Y. H., *Arch. Pharm. Res.* **2015,** *38*, 1582-1590.

28. Jackson, S. E., Hsp90: structure and function. In *Molecular chaperones*, Springer: Berlin, 2012; pp 155-240.

29. Sreedhar, A. S.; Kalmár, É.; Csermely, P.; Shen, Y.-F., *FEBS Lett.* **2004,** *562*, 11-15.

30. Li, W.; Tsen, F.; Sahu, D.; Bhatia, A.; Chen, M.; Multhoff, G.; Woodley, D. T., *Int. Rev. Cell Mol. Biol.* **2013,** *303*, 203-235.

31. Zou, M.; Bhatia, A.; Dong, H.; Jayaprakash, P.; Guo, J.; Sahu, D.; Hou, Y.; Tsen, F.; Tong, C.; O'Brien, K., *Oncogene* **2017,** *36*, 2160-2171.

32. Pearl, L. H.; Prodromou, C., *Annu. Rev. Biochem.* **2006,** *75*, 271-294.

33. Prodromou, C.; Pearl, L. H., *Curr. Cancer Drug Targets* **2003,** *3*, 301-323.

34. Meyer, P.; Prodromou, C.; Hu, B.; Vaughan, C.; Roe, S. M.; Panaretou, B.; Piper, P. W.; Pearl, L. H., *Mol. Cell* **2003,** *11*, 647-658.

35. Huai, Q.; Wang, H.; Liu, Y.; Kim, H.-Y.; Toft, D.; Ke, H., *Structure* **2005,** *13*, 579-590.

36. So˝ ti, C.; Vermes, A.; Haystead, T. A.; Csermely, P., *Eur. J. Biochem.* **2003,** *270*, 2421-2428.

37. Wegele, H.; Wandinger, S. K.; Schmid, A. B.; Reinstein, J.; Buchner, J., *J. Mol. Biol.* **2006,** *356*, 802-811.

38. Sahu, D.; Zhao, Z.; Tsen, F.; Cheng, C.-F.; Park, R.; Situ, A. J.; Dai, J.; Eginli, A.; Shams, S.; Chen, M., *Mol. Biol. Cell* **2012,** *23*, 602-613.

39. Cheng, C.-F.; Sahu, D.; Tsen, F.; Zhao, Z.; Fan, J.; Kim, R.; Wang, X.; O'Brien, K.; Li, Y.; Kuang, Y., *J. Clin. Investig.* **2011,** *121*.

40. Sgobba, M.; Forestiero, R.; Degliesposti, G.; Rastelli, G., *J. Chem. Inf. Model.* **2010,** *50*, 1522-1528.

41. Allan, R. K.; Mok, D.; Ward, B. K.; Ratajczak, T., *J. Biol. Chem.* **2006,** *281*, 7161-7171.

42. Marcu, M. G.; Schulte, T. W.; Neckers, L., *J. Natl. Cancer Inst.* **2000,** *92*, 242-248.

43. Jhaveri, K.; Modi, S., *Adv. Pharmacol.* **2012,** *65*, 471-517.

44. Jhaveri, K.; Taldone, T.; Modi, S.; Chiosis, G., *Biochim. Biophys. Acta* **2012,** *1823*, 742-755.

45. Li, Y.; Zhang, T.; Schwartz, S. J.; Sun, D., *Drug Resist. Updat.* **2009,** *12*, 17-27.

46. Prodromou, C.; Roe, S. M.; O'Brien, R.; Ladbury, J. E.; Piper, P. W.; Pearl, L. H., *Cell* **1997,** *90*, 65-75.

47. Solit, D. B.; Chiosis, G., *Drug Discov. Today* **2008,** *13*, 38-43.

48. Ge, J.; Normant, E.; Porter, J. R.; Ali, J. A.; Dembski, M. S.; Gao, Y.; Georges, A. T.; Grenier, L.; Pak, R. H.; Patterson, J., *J. Med. Chem.* **2006,** *49*, 4606-4615.

49. Sydor, J. R.; Normant, E.; Pien, C. S.; Porter, J. R.; Ge, J.; Grenier, L.; Pak, R. H.; Ali, J. A.; Dembski, M. S.; Hudak, J., *Proc. Natl. Acad. Sci. U. S. A.* **2006,** *103*, 17408-17413.

50. Drysdale, M. J.; Brough, P. A., *Curr. Top. Med. Chem.* **2008,** *8*, 859-868.

51. Soga, S.; Shiotsu, Y.; Akinaga, S.; Sharma, S. V., *Curr. Cancer Drug Targets* **2003,** *3*, 359-369.

52. Huang, K. H.; Veal, J. M.; Fadden, R. P.; Rice, J. W.; Eaves, J.; Strachan, J.-P.; Barabasz, A. F.; Foley, B. E.; Barta, T. E.; Ma, W., *J. Med. Chem.* **2009,** *52*, 4288-4305.

53. Sidera, K.; Patsavoudi, E., *Recent Pat. Anticancer Drug Discov.* **2014,** *9*, 1-20.

54. Hughes, P. F.; Barrott, J. J.; Carlson, D. A.; Loiselle, D. R.; Speer, B. L.; Bodoor, K.; Rund, L. A.; Haystead, T. A., *Biorg. Med. Chem.* **2012,** *20*, 3298-3305.

55. Kim, J. Y.; Cho, T.-M.; Park, J. M.; Park, S.; Park, M.; Nam, K. D.; Ko, D.; Seo, J.; Kim, S.; Jung, E., *Oncogene* **2022**, 1-9.

56. Donnelly, A. C.; Mays, J. R.; Burlison, J. A.; Nelson, J. T.; Vielhauer, G.; Holzbeierlein, J.; Blagg, B. S., *J. Org. Chem.* **2008,** *73*, 8901-8920.

57. Byrd, K. M.; Subramanian, C.; Sanchez, J.; Motiwala, H. F.; Liu, W.; Cohen, M. S.; Holzbeierlein, J.; Blagg, B. S., *Chem. Eur. J.* **2016,** *22*, 6921-6931.

58. Marcu, M. G.; Chadli, A.; Bouhouche, I.; Catelli, M.; Neckers, L. M., *J. Biol. Chem.* **2000,** *275*, 37181-37186.

59. Zhao, H.; Garg, G.; Zhao, J.; Moroni, E.; Girgis, A.; Franco, L. S.; Singh, S.; Colombo, G.; Blagg, B. S., *Eur. J. Med. Chem.* **2015,** *89*, 442-466.

60. Chang, D.-J.; An, H.; Kim, K.-s.; Kim, H. H.; Jung, J.; Lee, J. M.; Kim, N.-J.; Han, Y. T.; Yun, H.; Lee, S., *J. Med. Chem.* **2012,** *55*, 10863-10884.

61. Gupta, S. D.; Bommaka, M. K.; Banerjee, A., *Eur. J. Med. Chem.* **2019,** *178*, 48-63.

62. Seo, Y. H., *J. Cancer Prev.* **2015,** *20*, 5-11.

63. Cortajarena, A. L.; Yi, F.; Regan, L., *ACS Chem. Biol.* **2008,** *3*, 161-166.

64. Wang, W.; Liu, Y.; Zhao, Z.; Xie, C.; Xu, Y.; Hu, Y.; Quan, H.; Lou, L., *Cancer Sci.* **2016,** *107*, 782-790.

65. McConnell, J. R.; Alexander, L. A.; McAlpine, S. R., *Bioorg. Med. Chem. Lett.* **2014,** *24*, 661-666.

66. Hance, M. W.; Nolan, K. D.; Isaacs, J. S., *Cancers (Basel)* **2014,** *6*, 1065-1097.

67. Li, W.; Sahu, D.; Tsen, F., *Biochim. Biophys. Acta* **2012,** *1823*, 730-741.

68. Sidera, K.; Patsavoudi, E., *Cell cycle* **2008,** *7*, 1564-1568.

69. Cho, T.-M.; Kim, J. Y.; Kim, Y.-J.; Sung, D.; Oh, E.; Jang, S.; Farrand, L.; Hoang, V.-H.; Nguyen, C.-T.; Ann, J., *Cancer Lett.* **2019,** *447*, 141-153.

70. Schaefer, L.; Reinhardt, D. P., *Adv. Drug Deliv. Rev.* **2016,** *97*, 1-3.

71. Theocharis, A. D.; Skandalis, S. S.; Gialeli, C.; Karamanos, N. K., *Adv. Drug Deliv. Rev.* **2016,** *97*, 4-27.

72. Insua-Rodríguez, J.; Oskarsson, T., *Adv. Drug Deliv. Rev.* **2016,** *97*, 41-55.

73. Huxley-Jones, J.; Foord, S. M.; Barnes, M. R., *Drug Discov. Today* **2008,** *13*, 685-694.

74. Multhaupt, H. A.; Leitinger, B.; Gullberg, D.; Couchman, J. R., *Adv. Drug Deliv. Rev.* **2016,** *97*, 28-40.

75. Järveläinen, H.; Sainio, A.; Koulu, M.; Wight, T. N.; Penttinen, R., *Pharmacol. Rev.* **2009,** *61*, 198-223.

76. Huang, J.; Olivenstein, R.; Taha, R.; Hamid, Q.; Ludwig, M., *Am. J. Respir. Crit. Care Med.* **1999,** *160*, 725-729.

77. Postma, D. S.; Timens, W., *Proc. Am. Thorac. Soc.* **2006,** *3*, 434-439.

78. Al-Muhsen, S.; Johnson, J. R.; Hamid, Q., *J. Allergy Clin. Immunol.* **2011,** *128*, 451-462.

79. Hogg, J. C.; Timens, W., *Annu. Rev. Pathol.* **2009,** *4*, 435-459.

80. Wight, T. N.; Merrilees, M. J., *Circ. Res.* **2004,** *94*, 1158-1167.

81. Herrera, J.; Henke, C. A.; Bitterman, P. B., *J. Clin. Investig.* **2018,** *128*, 45-53.

82. Flood-Page, P.; Menzies-Gow, A.; Phipps, S.; Ying, S.; Wangoo, A.; Ludwig, M. S.; Barnes, N.; Robinson, D.; Kay, A. B., *J. Clin. Investig.* **2003,** *112*, 1029-1036.

83. Cuzzocrea, S.; McDonald, M. C.; Mota-Filipe, H.; Mazzon, E.; Costantino, G.; Britti, D.; Mazzullo, G.; Caputi, A. P.; Thiemermann, C., *Arthritis Rheum.* **2000,** *43*, 320-328.

84. Calvier, L.; Miana, M.; Reboul, P.; Cachofeiro, V.; Martinez-Martinez, E.; De Boer, R. A.; Poirier, F.; Lacolley, P.; Zannad, F.; Rossignol, P., *Arterioscler. Thromb. Vasc. Biol.* **2013,** *33*, 67-75.

85. Eustace, B. K.; Sakurai, T.; Stewart, J. K.; Yimlamai, D.; Unger, C.; Zehetmeier, C.; Lain, B.; Torella, C.; Henning, S. W.; Beste, G., *Nat. Cell Biol.* **2004,** *6*, 507-514.

86. Wong, D. S.; Jay, D. G., *Adv. Cancer Res.* **2016,** *129*, 141-163.

87. Picard, D., *Biochim. Biophys. Acta* **2012,** *1823*, 605-606.

88. Sierra, J. R.; Cepero, V.; Giordano, S., *Mol. Cancer* **2010,** *9*, 1-13.

89. Stellas, D.; El Hamidieh, A.; Patsavoudi, E., *BMC Cell Biol.* **2010,** *11*, 1-9.

90. Dong, H.; Zou, M.; Bhatia, A.; Jayaprakash, P.; Hofman, F.; Ying, Q.; Chen, M.; Woodley, D. T.; Li, W., *Sci. Rep.* **2016,** *6*, 1-9.

91. Dong, H.; Luo, L.; Zou, M.; Huang, C.; Wan, X.; Hu, Y.; Le, Y.; Zhao, H.; Li, W.; Zou, F., *Am. J. Physiol. Lung Cell. Mol. Physiol.* **2017,** *313*, L1006-L1015.

92. Tsutsumi, S.; Scroggins, B.; Koga, F.; Lee, M. J.; Trepel, J.; Felts, S.; Carreras, C.; Neckers, L., *Oncogene* **2008,** *27*, 2478-2487.

93. López-Otín, C.; Overall, C. M., *Nat. Rev. Mol. Cell Biol.* **2002,** *3*, 509-519.

94. Bernstein, A. S.; Jay, D. G., Signaling Functions of Extracellular Hsp90 (eHsp90) in Cancer Metastasis. In *Heat Shock Proteins in Signaling Pathways*, Springer: 2019; pp 329-344.

95. Barrott, J. J.; Hughes, P. F.; Osada, T.; Yang, X.-Y.; Hartman, Z. C.; Loiselle, D. R.; Spector, N. L.; Neckers, L.; Rajaram, N.; Hu, F., *Chem. Biol.* **2013,** *20*, 1187-1197.

96. Taldone, T.; Zatorska, D.; Patel, P. D.; Zong, H.; Rodina, A.; Ahn, J. H.; Moulick, K.; Guzman, M. L.; Chiosis, G., *Biorg. Med. Chem.* **2011,** *19*, 2603-2614.

97. Barta, T. E.; Veal, J. M.; Rice, J. W.; Partridge, J. M.; Fadden, R. P.; Ma, W.; Jenks, M.; Geng, L.; Hanson, G. J.; Huang, K. H., *Bioorg. Med. Chem. Lett.* **2008,** *18*, 3517-3521.

98. Wu, Z.-W.; Song, S.-Y.; Li, L.; Lu, H.-L.; Lieberman, B.; Huang, Y.-S.; Mach, R. H., *Biorg. Med. Chem.* **2015,** *23*, 1463-1471.

99. Claramunt, R. M.; López, C.; Pérez-Medina, C.; Pinilla, E.; Torres, M. R.; Elguero, J., *Tetrahedron* **2006,** *62*, 11704-11713.

100. Schenone, P.; Mosti, L.; Menozzi, G., *J. Heterocycl. Chem.* **1982,** *19*, 1355-1361.

101. Cheng, M.-F.; Ou, L.-C.; Chen, S.-C.; Chang, W.-T.; Law, P.-Y.; Loh, H. H.; Chao, Y.-S.; Shih, C.; Yeh, S.-H.; Ueng, S.-H., *Biorg. Med. Chem.* **2014,** *22*, 4694-4703.

102. Lee, J. C.; Hong, K. H.; Becker, A.; Tash, J. S.; Schönbrunn, E.; Georg, G. I., *Eur. J. Med. Chem.* **2021,** *214*, 113232.

103. Dalla Croce, P.; La Rosa, C., *Synthesis* **1984**, 982-983.

104. Bycroft, B. W.; Chan, W. C.; Chhabra, S. R.; Hone, N. D., *J. Chem. Soc., Chem. Commun.* **1993**, 778-779.

105. Andersonmckay, J.; Savage, G. P.; Simpson, G. W., *Aust. J. Chem.* **1996,** *49*, 163-166.

106. Khlebnicova, T.; Isakova, V.; Baranovsky, A.; Borisov, E.; Lakhvich, F., *J. Fluor. Chem.* **2006,** *127*, 1564-1569.

107. Duan, S.; Venkatraman, S.; Hong, X.; Huang, K.; Ulysse, L.; Mobele, B. I.; Smith, A.; Lawless, L.; Locke, A.; Garigipati, R., *Org. Process Res. Dev.* **2012,** *16*, 1787-1793.

108. Hansen, P.; Berg, A.; Jakobsen, H.; Manzara, A.; Michl, J., *Org. Magn. Reson.* **1977,** *10*, 179-187.

109. Roberts, J. D.; Weigert, F. J., *J. Am. Chem. Soc.* **1971,** *93*, 2361-2369.

110. Bak, B.; Shoolery, J.; Williams III, G. A., *J. Mol. Spectrosc.* **1958,** *2*, 525-538.

111. Mohanty, S.; Venkateswarlu, P., *Mol. Phys.* **1966,** *11*, 329-336.

112. Goncalves, S.; Nicolas, M.; Wagner, A.; Baati, R., *Tetrahedron Lett.* **2010,** *51*, 2348-2350.

113. Khlebnikova, T.; Piven, Y. A.; Isakova, V.; Lakhvich, F., *Russ. J. Org. Chem.* **2012,** *48*, 1277-1282.

114. Rubinov, D. B.; Rubinova, I. L.; Akhrem, A. A., *Chem. Rev.* **1999,** *99*, 1047-1066.

115. Liu, H.-G.; Wu, C.-S.; Wang, J.-F.; Yang, D.-Y., *Tetrahedron Lett.* **2003,** *44*, 3137-3141.

116. Armaly, A. M.; Bar, S.; Schindler, C. S., *Org. Lett.* **2017,** *19*, 3962-3965.

117. Kanwar, A.; Eduful, B. J.; Barbeto, L.; Carletti Bonomo, P.; Lemus, A.; Vesely, B. A.; Mutka, T. S.; Azhari, A.; Kyle, D. E.; Leahy, J. W., *ACS Med. Chem. Lett.* **2017,** *8*, 797-801.

118. Liu, C.; Ding, L.; Guo, G.; Liu, W.; Yang, F.-L., *Org. Biomol. Chem.* **2016,** *14*, 2824-2827.

119. Namba, K.; Shoji, I.; Nishizawa, M.; Tanino, K., *Org. Lett.* **2009,** *11*, 4970-4973.

120. Hiegel, G. A.; Burk, P., *J. Org. Chem.* **1973,** *38*, 3637-3639.

121. Shapiro, R. H., *Tetrahedron Lett.* **1968,** *9*, 345-347.

122. Adlington, R. M.; Barrett, A. G., *Acc. Chem. Res.* **1983,** *16*, 55-59.

123. Driver, M. S.; Hartwig, J. F., *J. Am. Chem. Soc.* **1996,** *118*, 7217-7218.

124. Heravi, M. M.; Kheilkordi, Z.; Zadsirjan, V.; Heydari, M.; Malmir, M., *J. Organomet. Chem.* **2018,** *861*, 17-104.

125. Yang, B. H.; Buchwald, S. L., *J. Organomet. Chem.* **1999,** *576*, 125-146.

126. Masci, D.; Hind, C.; Islam, M. K.; Toscani, A.; Clifford, M.; Coluccia, A.; Conforti, I.; Touitou, M.; Memdouh, S.; Wei, X., *Eur. J. Med. Chem.* **2019,** *178*, 500-514.

127. Davies, J. A.; Hartley, F. R.; Murray, S. G., *J. Chem. Soc., Dalton Trans.* **1979**, 1705-1708.

128. Montalbetti, C. A.; Falque, V., *Tetrahedron* **2005,** *61*, 10827-10852.

129. Dang, X.; Zhang, L.; Franco, A.; Li, J.; Rocha, A. G.; Devanathan, S.; Dolle, R. E.; Bernstein, P. R.; Dorn, G. W., *J. Med. Chem.* **2020,** *63*, 7033-7051.

130. Mbaba, M.; de la Mare, J.-A.; Sterrenberg, J. N.; Kajewole, D.; Maharaj, S.; Edkins, A. L.; Isaacs, M.; Hoppe, H. C.; Khanye, S. D., *J. Biol. Inorg. Chem.* **2019,** *24*, 139-149.

131. Thakur, A.; Kumar, A.; Sharma, V. k.; Mehta, V., *bioRxiv* **2022**. DOI: 10.1101/2022.10.15.512366

132. A., B., *APEX2, SAINT and SADABS*. Bruker AXS Inc.: Madison, Wisconsin, USA, 2012.

133. Sheldrick, G. M., *Acta Cryst.* **2015,** *71*, 3-8.

134. Farrugia, L. J., *J. Appl. Crystallogr.* **2012,** *45*, 849-854.

135. Frisch, M.J.; Trucks, G.W.; Schlegel, H.B.; Scuseria, G.E.; Robb, M.A.; Cheeseman, J.R.; Scalmani, G.; Barone, V.; Mennucci, B.; Petersson, G.A.; Nakatsuji, H.; Caricato, M.; Li, X.; Hratchian, H.P.; Izmaylov, A.F.; Bloino, J.; Zheng, G.; Sonnenberg, J.L.; Hada, M.; Ehara, M.; Toyota, K.; Fukuda, R.; Hasegawa, J.; Ishida, M.; Nakajima, T.; Honda, Y.; Kitao, O.; Nakai, H.; Vreven, T.; Montgomery Jr., J.A.; Peralta, J.E.; Ogliaro, F.; Bearpark, M.; Heyd, J.J.; Brothers, E.; Kudin, K.N.; Staroverov, V.N.; Kobayashi, R.; Normand, J.; Raghavachari, K.; Rendell, A.; Burant, J.C.; Iyengar, S.S.; Tomasi, J.; Cossi, M.; Rega, N.; Millam, J.M.; Klene, M.; Knox, J.E.; Cross, J.B.; Bakken, V.; Adamo, C.; Jaramillo, J.; Gomperts, R.; Stratmann, R.E.; Yazyev, O.; Austin, A.J.; Cammi, R.; Pomelli, C.; Ochterski, J.W.; Martin, R.L.; Morokuma, K.; Zakrzewski,

V.G.; Voth, G.A.; Salvador, P.; Dannenberg; J.J., Dapprich; S., Daniels, A.D.; Farkas, O.; Foresman, J.B.; Ortiz, J.V.; Cioslowski, J.; Fox, D.J. Gaussian 09, Revision B.01. Gaussian Inc., Wallingford CT. 2009136. Dennington, R., Keith, T. and Millam, J., *GaussView, Version 5*. Semichem Inc.: Shawnee Mission KS, 2009.

137. Mbaba, M.; Dingle, L. M.; Cash, D.; de la Mare, J.-A.; Laming, D.; Taylor, D.; Hoppe, H. C.; Edkins, A. L.; Khanye, S. D., *Eur. J. Med. Chem.* **2020,** *187*, 111924.

138. Laemmli, U. K., *Nature* **1970,** *227*, 680-685.

139. Towbin, H.; Staehelin, T.; Gordon, J., *Proc. Natl. Acad. Sci. U. S. A.* **1979,** *76*, 4350-4354.

140. Hunter, M. C.; O'Hagan, K. L.; Kenyon, A.; Dhanani, K. C.; Prinsloo, E.; Edkins, A. L., *PLoS One* **2014,** *9*, e86842.

141. Mathenjwa, G. S.; Akerman, M. P.; Bode, M.; Veale, C., *Synlett* **2022,** *33*, 1907-1912.

APPENDIX A: SELECTED ^{1}H and ^{13}C NMR SPECTRA

APPENDIX A1: ^{1}H and ^{13}C NMR SPECTRA FOR COMPOUNDS DESCRIBED IN SECTION 6.2

Appendix A1.1: ^{1}H NMR (400 MHz) and ^{13}C NMR (100 MHz) spectra of 4-((4-((2-carbamoyl-5-(6,6-dimethyl-4-oxo-3-(trifluoromethyl)-4,5,6,7-tetrahydro-1*H*-indazol-1-yl)phenyl)amino)cyclohexyl)amino)butane-1-sulfonic acid (**2.1**) in DMSO

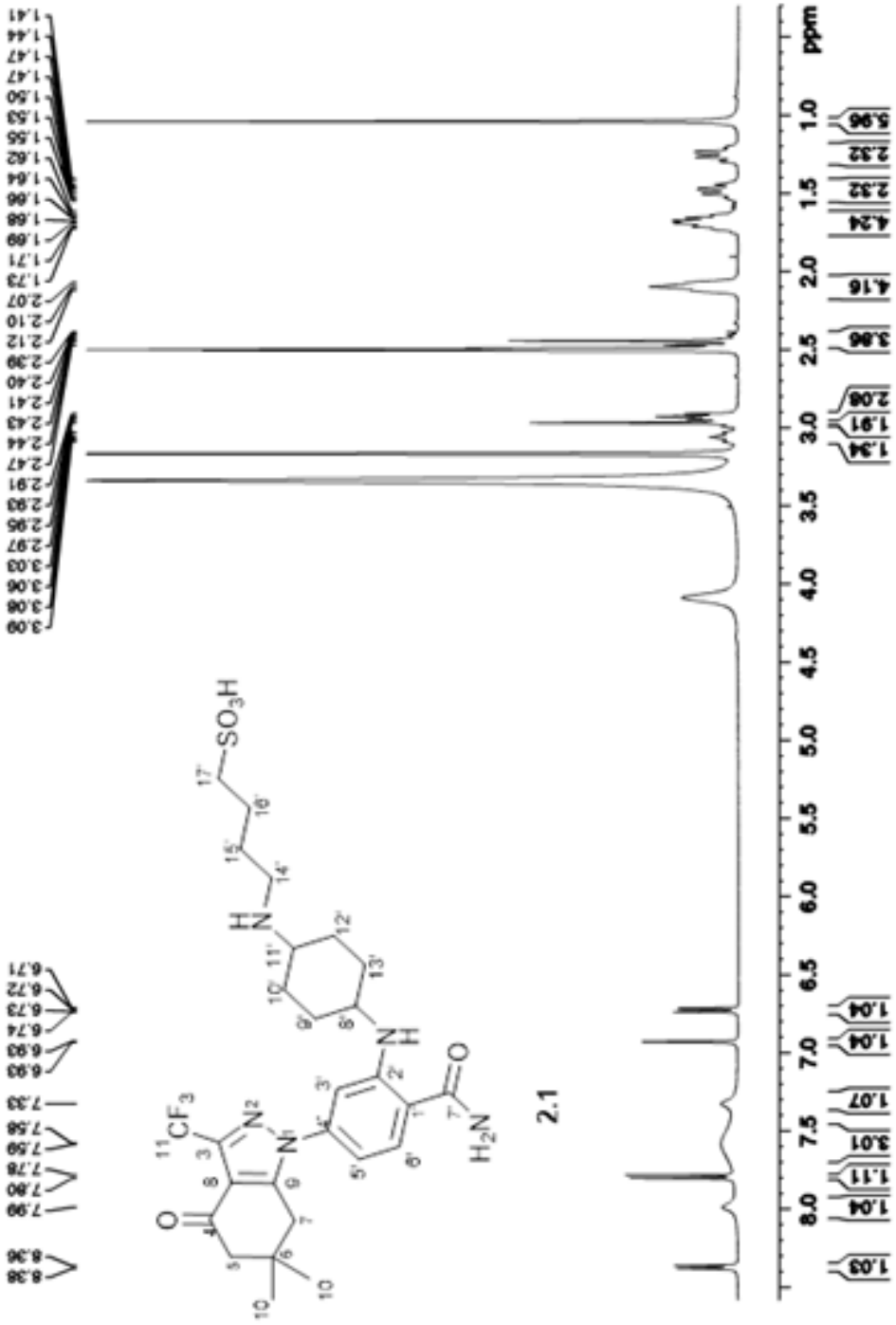

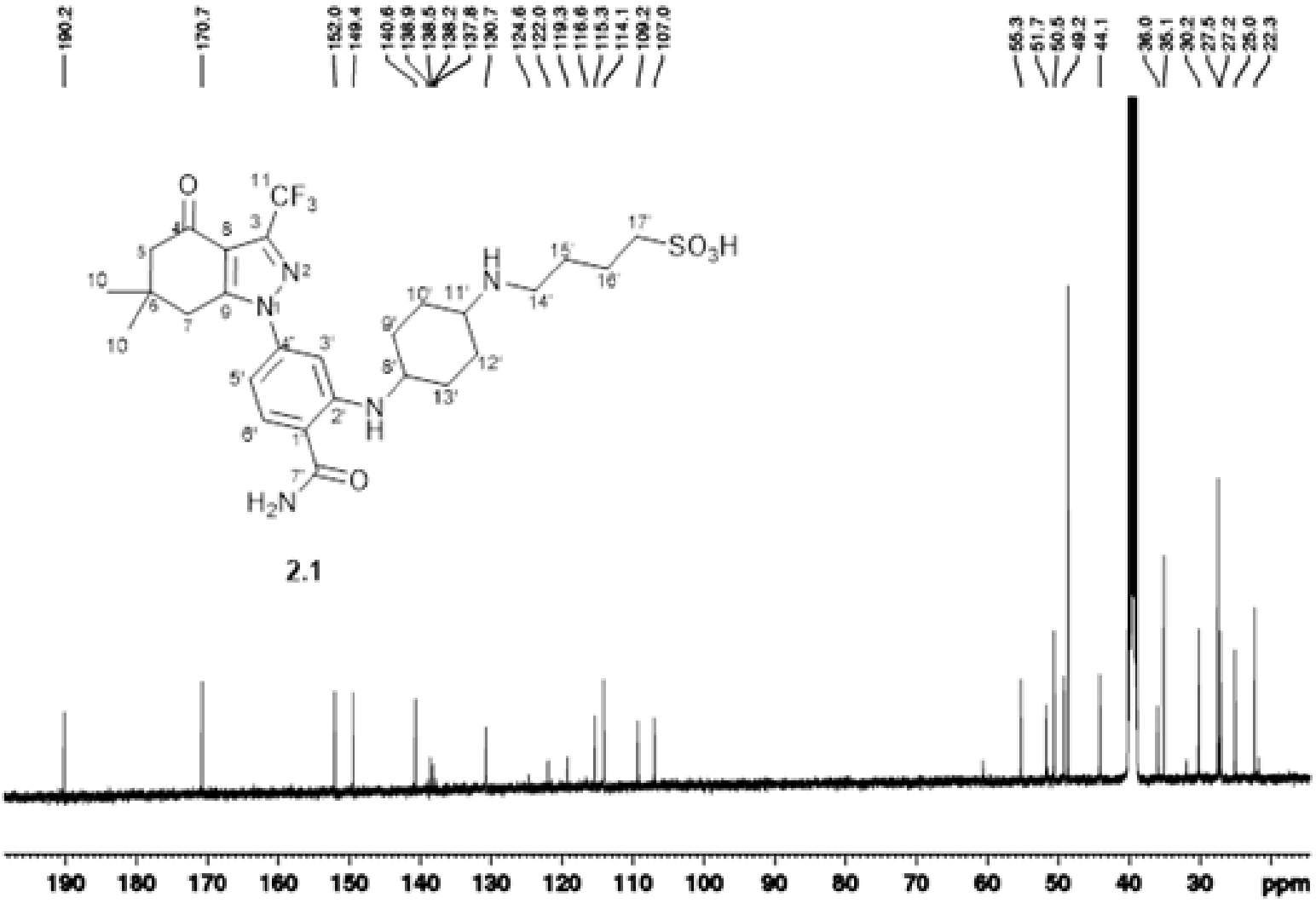
190.2
170.7
152.0
149.4
140.6
138.9
138.5
138.2
137.8
130.7
124.6
122.0
119.3
116.6
115.3
114.1
109.2
107.0
55.3
51.7
50.5
49.2
44.1
36.0
35.1
30.2
27.5
27.2
25.0
22.3
O
11
CF3
3
8
5
N2
10
6
N1
9
7
10
4'
3'
5'
2'
6'
1'
7'
O
H2N
N
H
10'
11'
9'
8'
12'
13'
14'
15'
16'
17'
SO3H
190
180
170
160
150
140
130
120
110
100
90
80
70
60
50
40
30
ppm

2.1

Appendix A1.2: ^{1}H NMR (500 MHz) and ^{13}C NMR (125 MHz) spectra of 4-((4-((2-carbamoyl-5-(3,6,6-trimethyl-4-oxo-4,5,6,7-tetrahydro-1*H*-indazol-1-yl)phenyl)amino)cyclohexyl)amino)butane-1-sulfonic acid (**2.2**) in DMSO

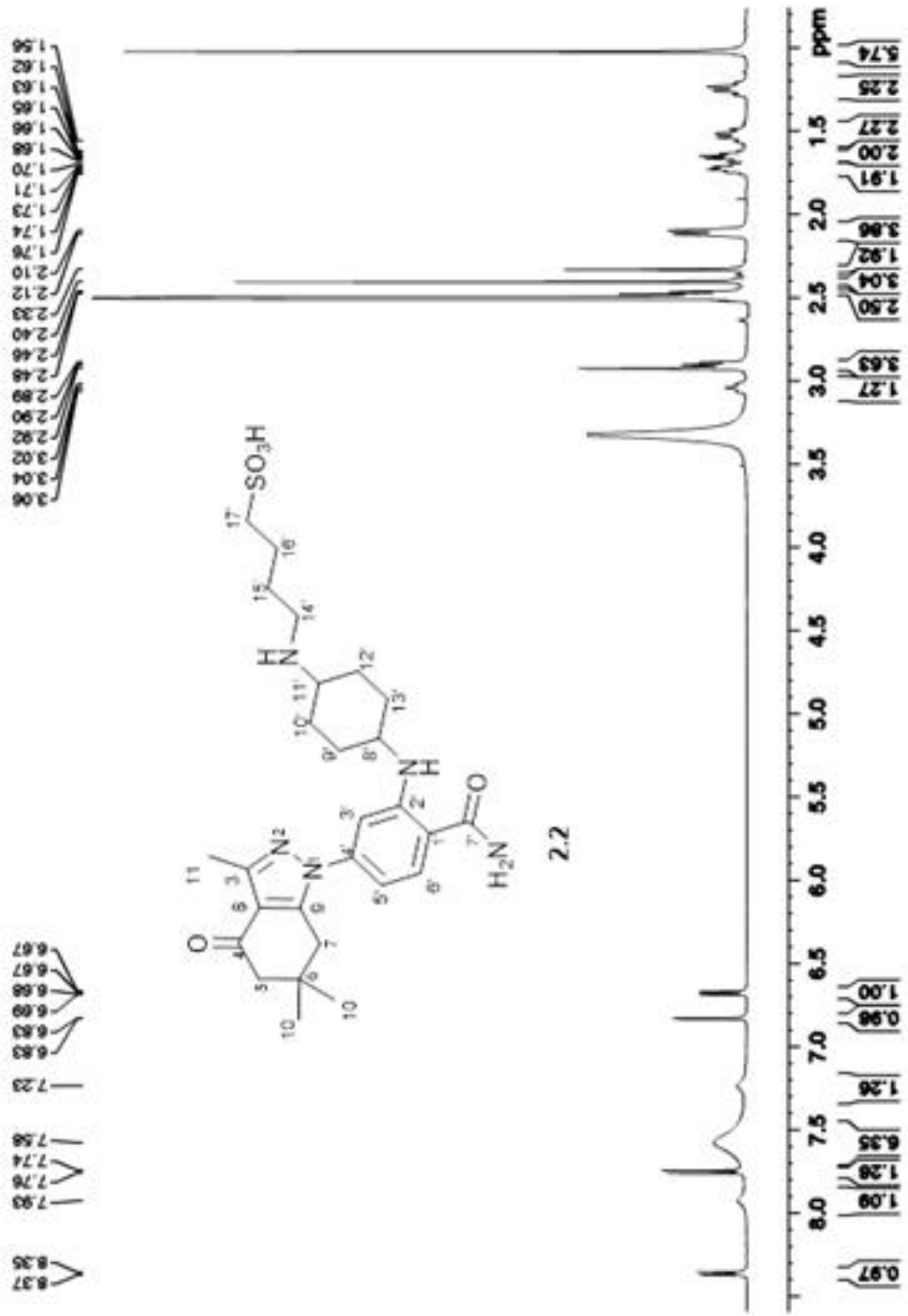

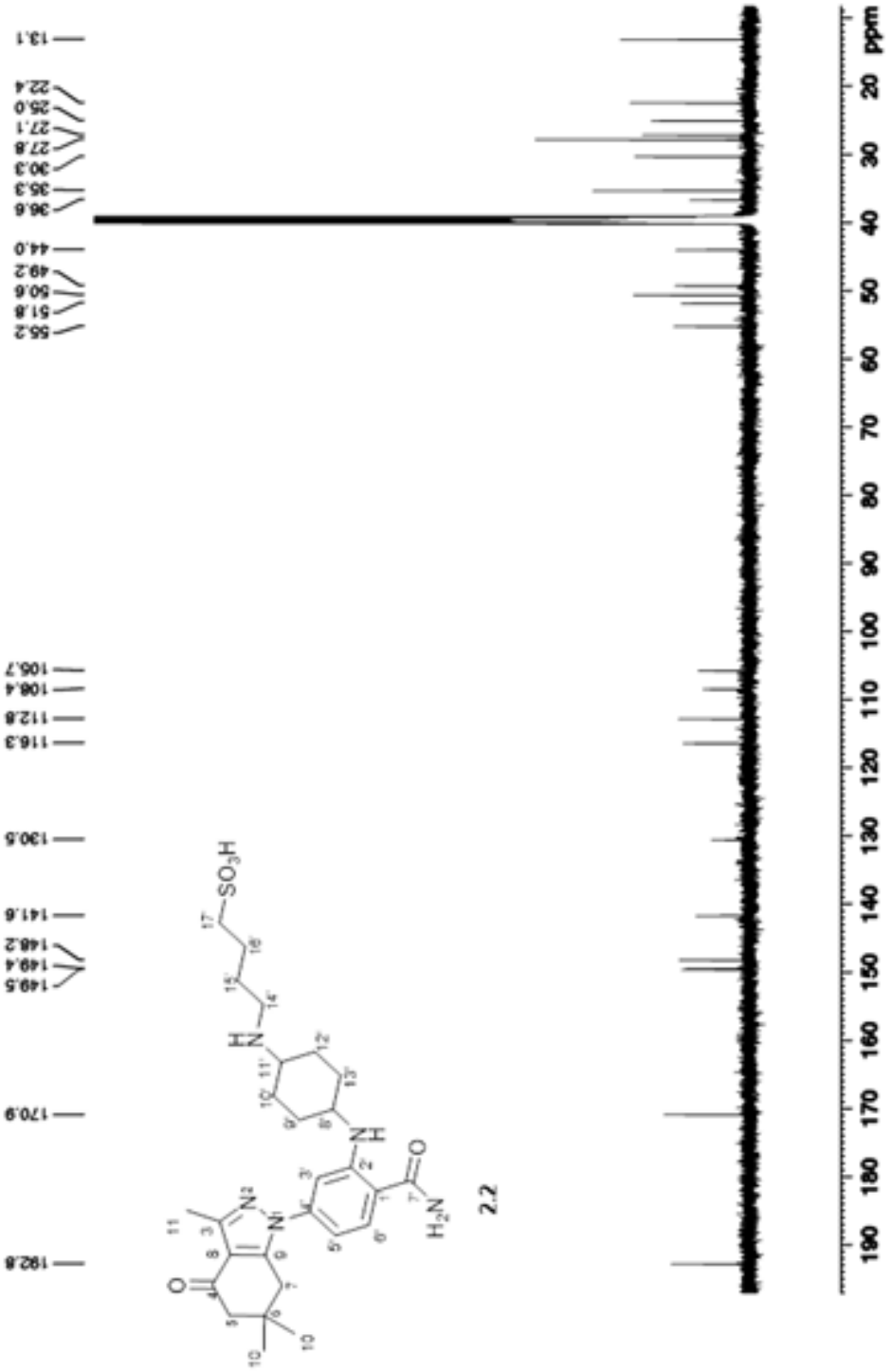
13.1
22.4
25.0
27.1
27.8
30.3
35.3
36.6
44.0
49.2
50.6
51.8
55.2
105.7
106.4
112.6
116.3
130.5
141.6
148.2
148.4
149.5
170.9
192.8
2.2
ppm

Appendix A1.3: ^{1}H NMR (400 MHz) and ^{13}C NMR (100 MHz) spectra of (6-((4-((2-carbamoyl-5-(6,6-dimethyl-4-oxo-3-(trifluoromethyl)-4,5,6,7-tetrahydro-1*H*-indazol-1-yl)phenyl)amino)cyclohexyl)amino)-6-oxohexyl)phosphonic acid (**2.3**) in DMSO

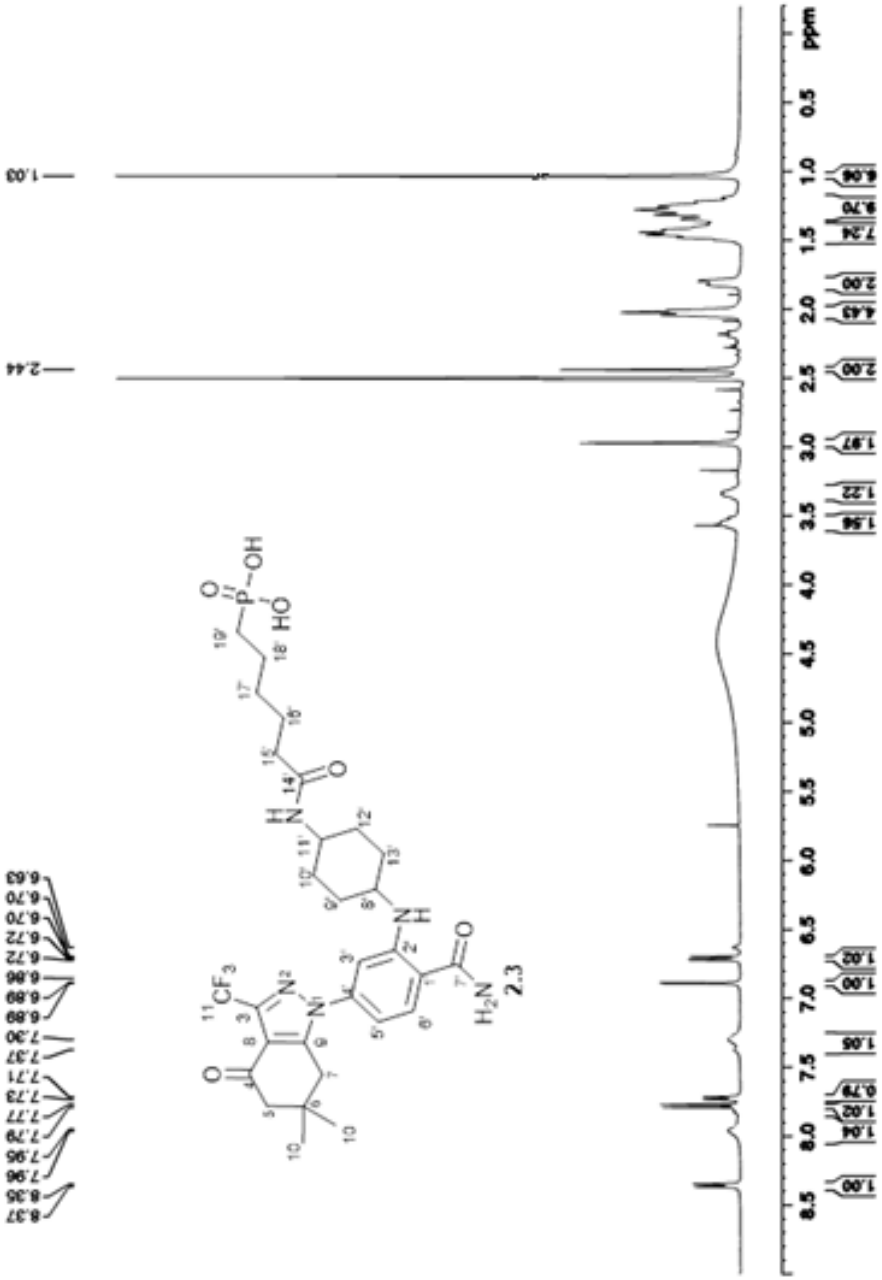

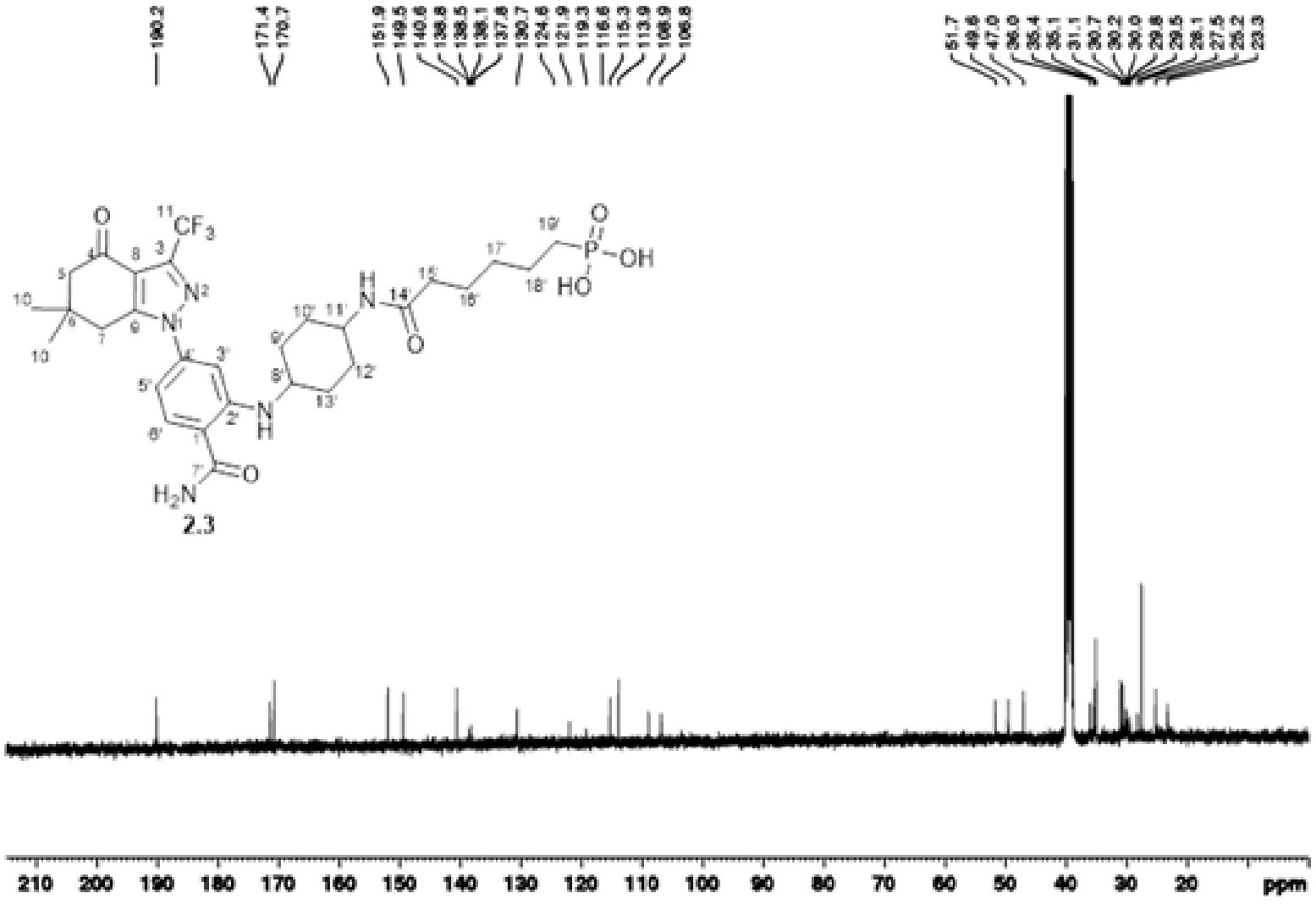
190.2
171.4
170.7
151.9
149.5
140.6
138.8
138.5
136.1
137.8
130.7
124.6
121.9
119.3
116.6
115.3
113.9
108.9
106.8
51.7
49.6
47.0
36.0
35.4
35.1
31.1
30.7
30.2
30.0
29.8
29.5
26.1
27.5
25.2
23.3
O
11 CF3
3
8
4
5
10
6
7
9
N2
N1
10'
4'
3'
5'
6'
1'
2'
7'
O
H2N
N
H
8'
9'
10'
11'
12'
13'
14'
O
15'
17'
18'
19'
P
O
OH
HO
2.3
210
200
190
180
170
160
150
140
130
120
110
100
90
80
70
60
50
40
30
20
ppm

Appendix A1.4: ^{1}H NMR (500 MHz) and ^{13}C NMR (125 MHz) spectra of (6-((4-((2-carbamoyl-5-(3,6,6-trimethyl-4-oxo-4,5,6,7-tetrahydro-1*H*-indazol-1-yl)phenyl)amino)cyclohexyl)amino)-6-oxohexyl)phosphonic acid (**2.4**) in DMSO

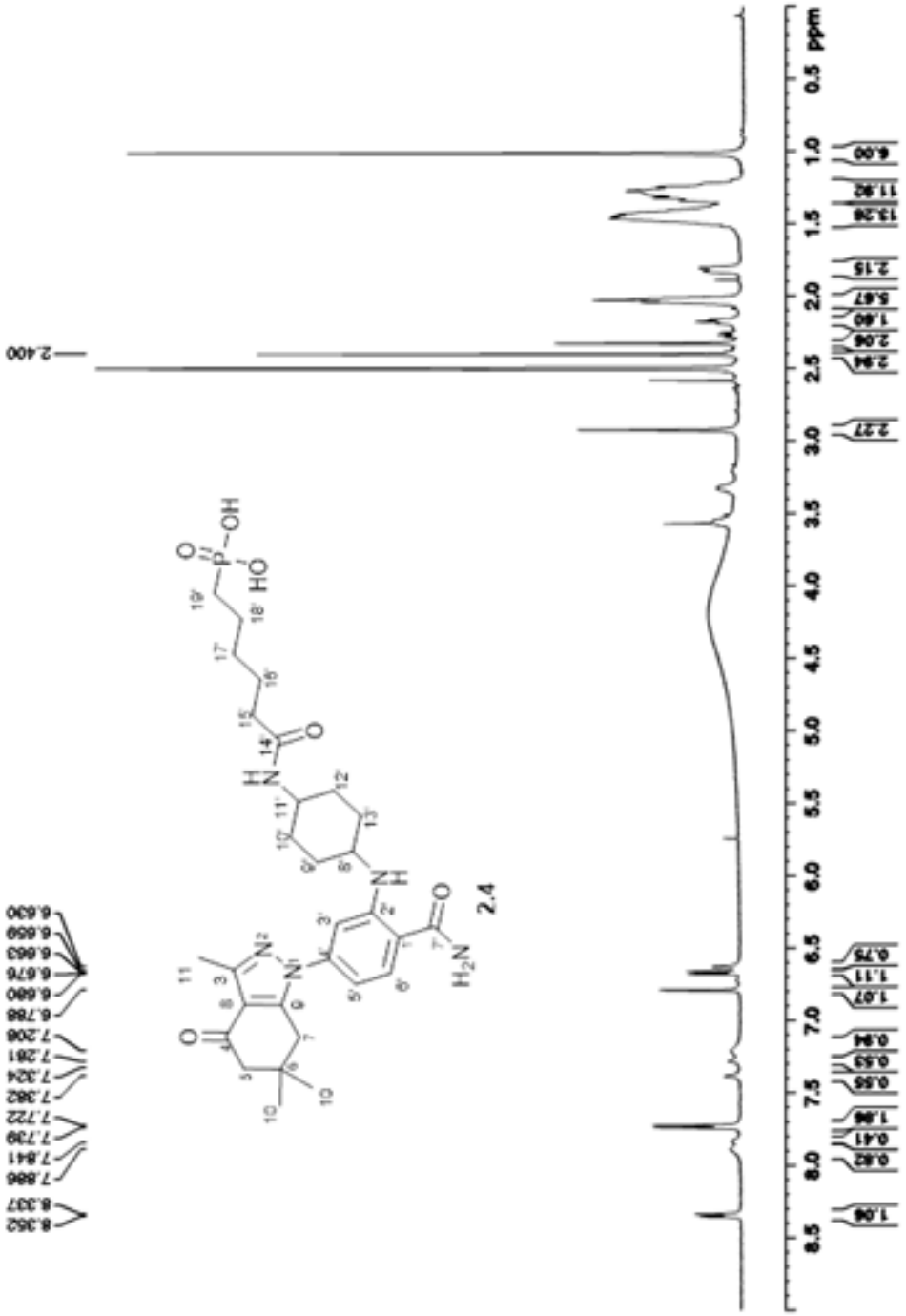

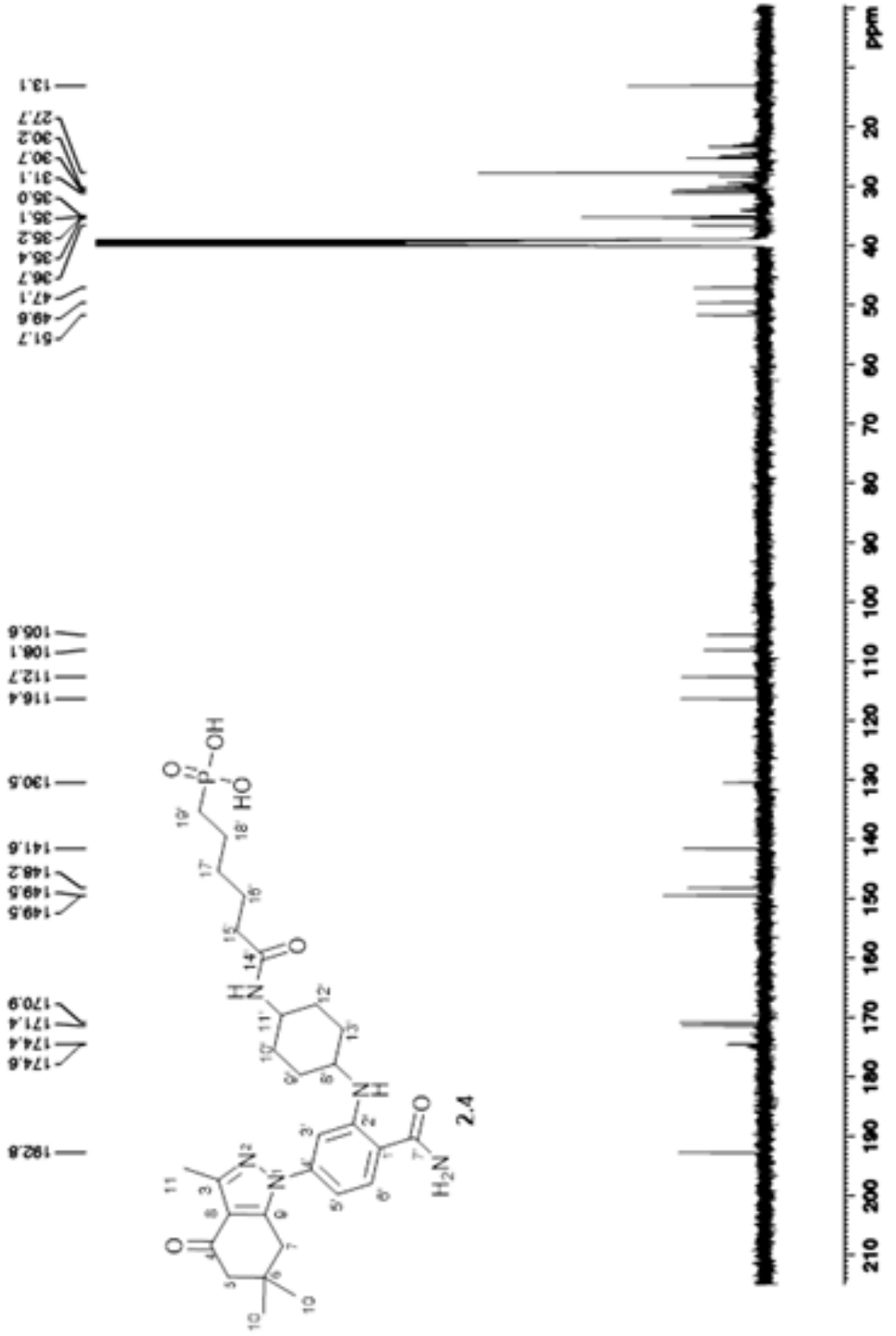
13.1
27.7
30.2
30.7
31.1
35.0
35.1
35.2
35.4
36.7
47.1
49.6
51.7
105.6
106.1
112.7
116.4
130.5
141.6
148.2
149.5
149.5
170.9
171.4
174.4
174.6
182.8
ppm
2.4

Appendix A1.5: ^{1}H NMR (400 MHz) and ^{13}C NMR (100 MHz) spectra of 2-((4-aminocyclohexyl)amino)-4-(6,6-dimethyl-4-oxo-3-(trifluoromethyl)-4,5,6,7-tetrahydro-1*H*-indazol-1-yl)benzamide (**2.5, isolated as a free amine**) in DMSO

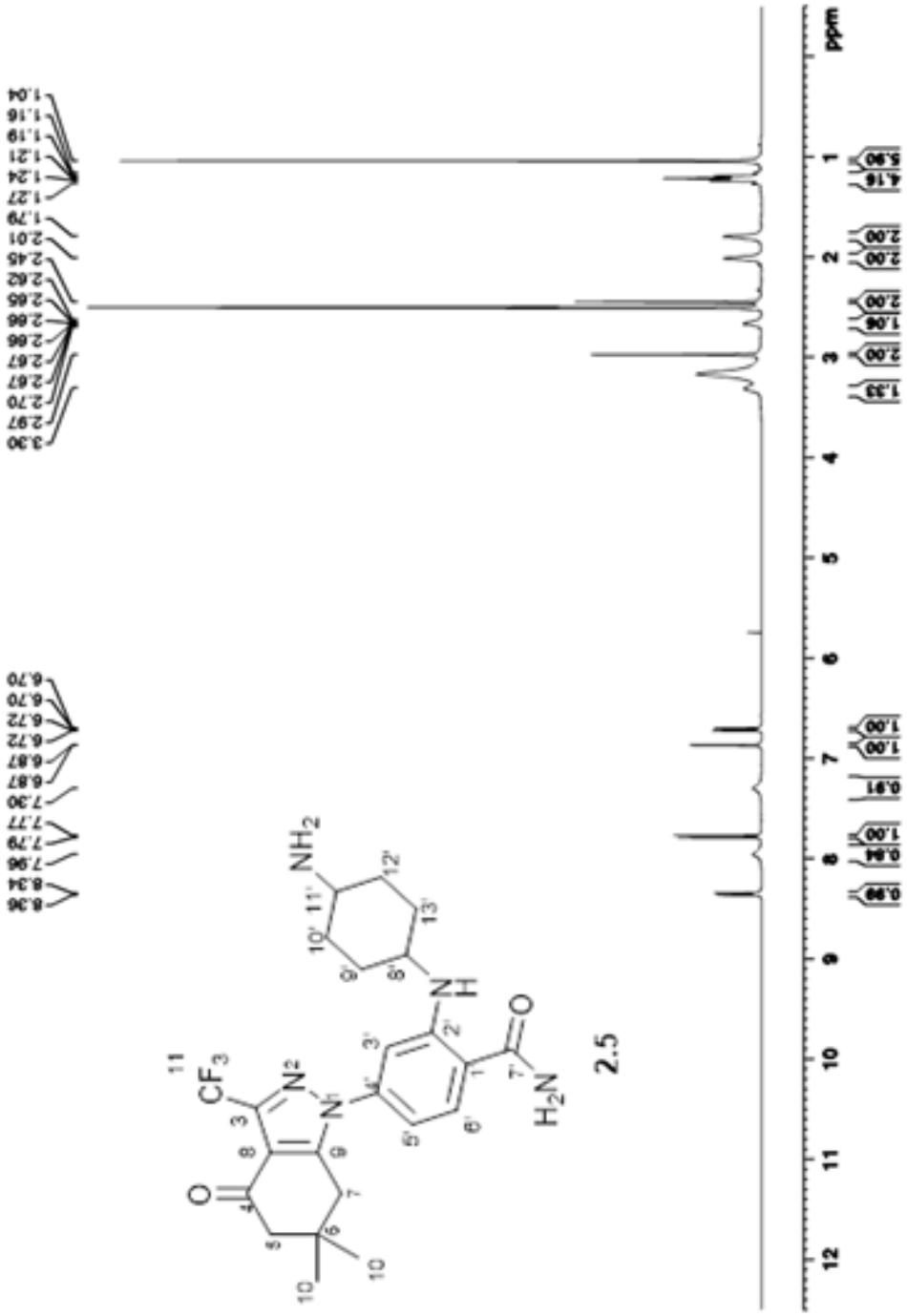

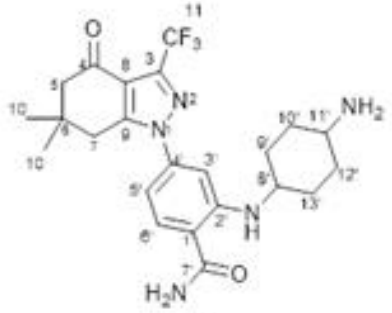
O
11
CF3
3
8
4
5
N2
10
6
N1
9
7
10'
3'
4'
5'
6'
1'
2'
N
H
7'
O
H2N
9'
10'
11'
NH2
12'
13'

2.5

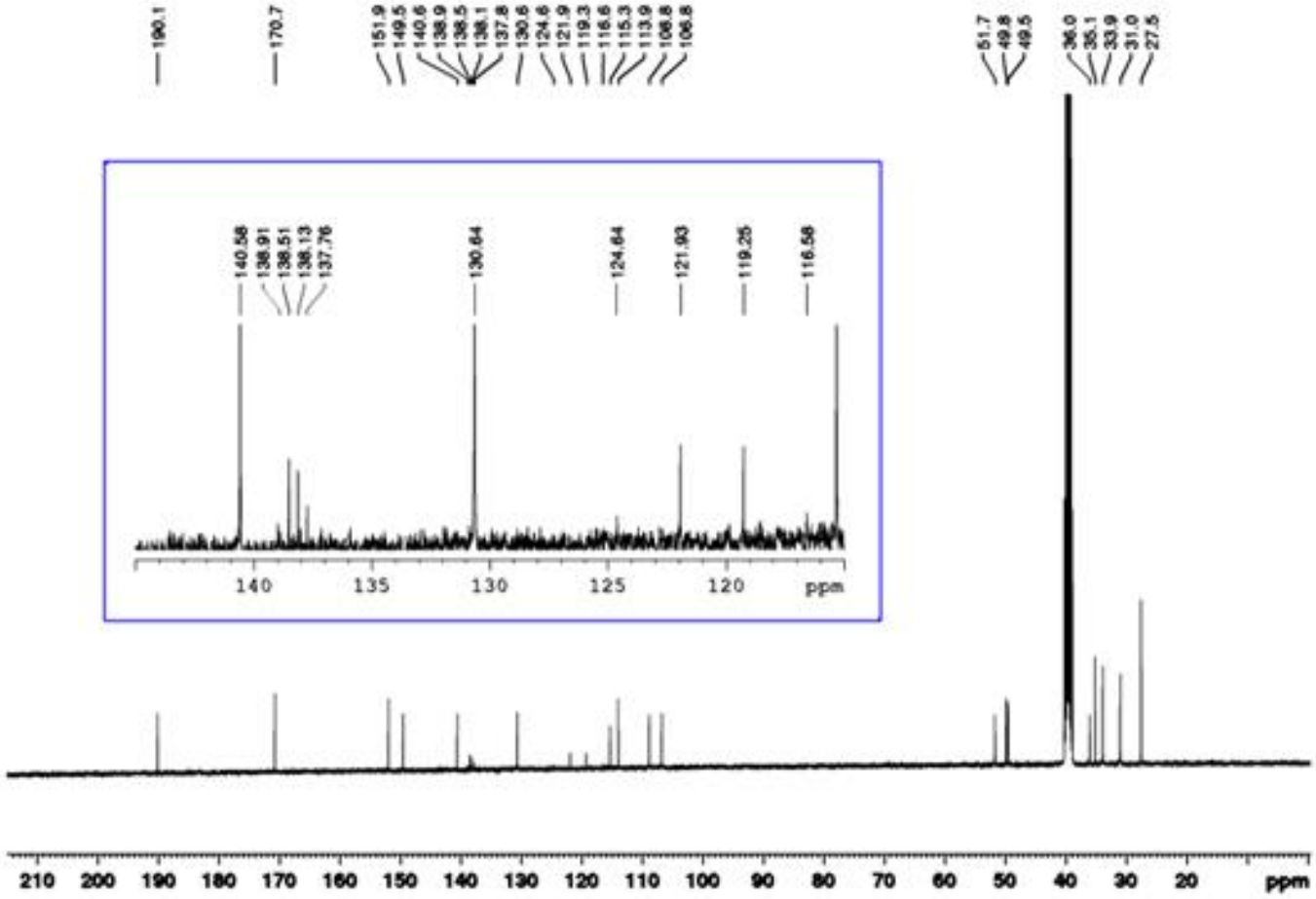
190.1
170.7
151.9
149.5
140.6
138.9
138.5
138.1
137.8
130.6
124.6
121.9
119.3
116.6
115.3
113.9
108.8
106.8
51.7
49.8
49.5
36.0
35.1
33.9
31.0
27.5
140.58
138.91
138.51
138.13
137.76
130.64
124.64
121.93
119.25
116.58
140
135
130
125
120
ppm
210
200
190
180
170
160
150
140
130
120
110
100
90
80
70
60
50
40
30
20
ppm

Appendix A1.6: ^{1}H NMR (400 MHz) and ^{13}C NMR (100 MHz) spectra of 2-((4-aminocyclohexyl)amino)-4-(3,6,6-trimethyl-4-oxo-4,5,6,7-tetrahydro-1*H*-indazol-1-yl)benzamide (**2.6**, **isolated as a TFA salt**) in DMSO

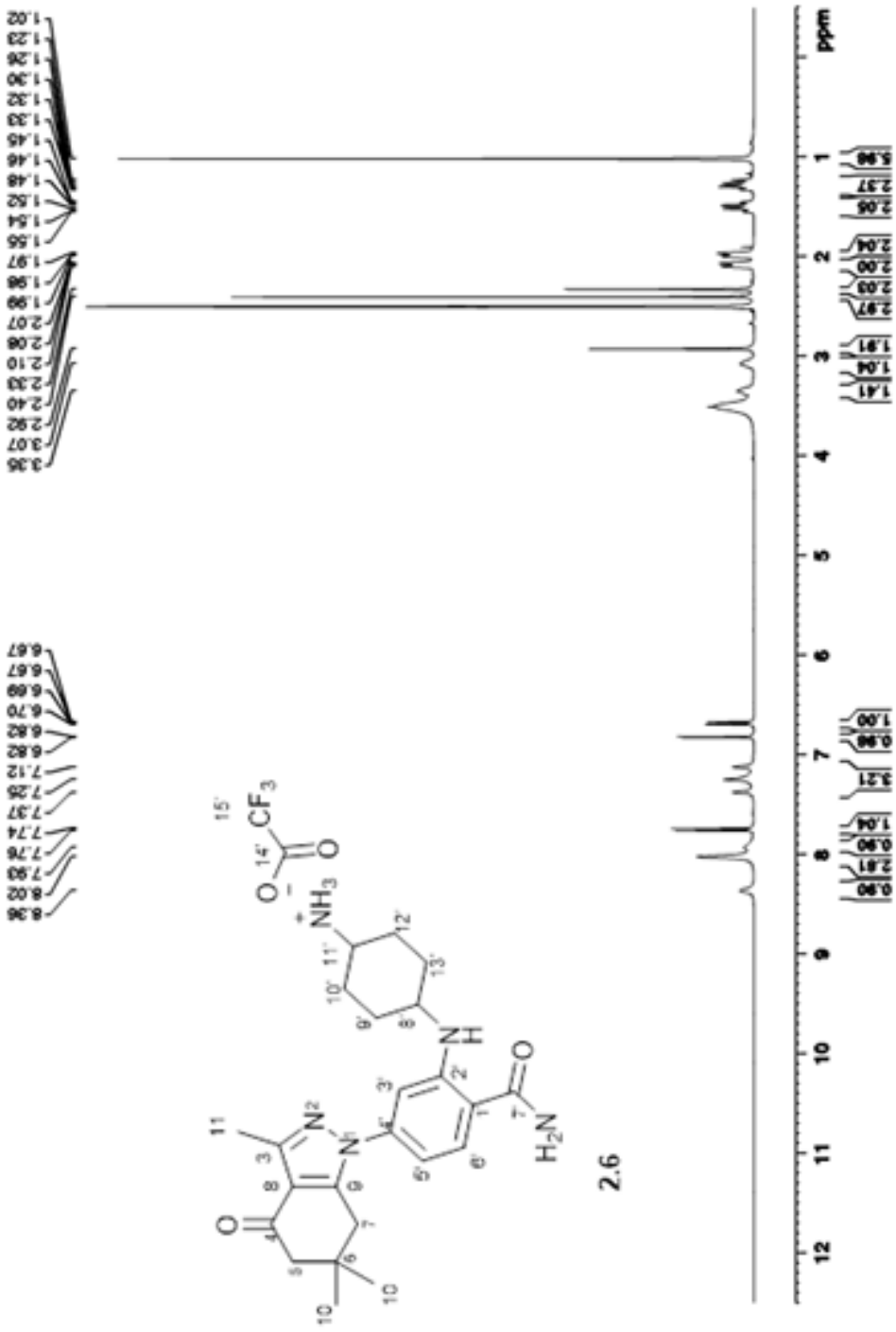

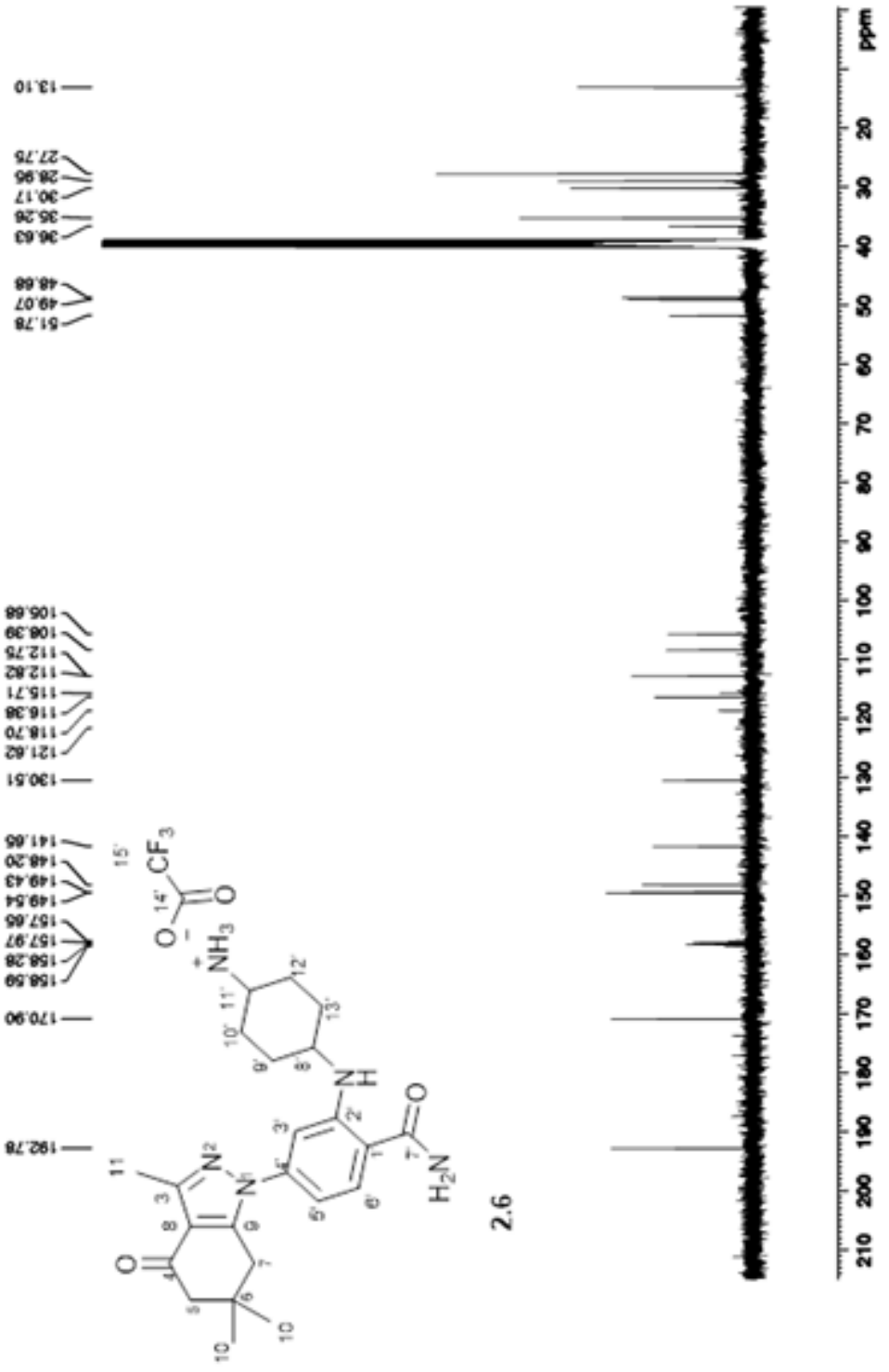
13.10
27.75
28.96
30.17
36.26
36.63
48.68
49.07
51.78
105.68
106.39
112.75
112.82
115.71
116.38
118.70
121.62
130.51
141.65
148.20
149.43
149.54
157.65
157.97
158.28
158.59
170.90
182.78
ppm
2.6

Appendix A1.7: ^{1}H NMR (400 MHz) and ^{13}C NMR (100 MHz) spectra of 3,6,6-trimethyl-1,5,6,7-tetrahydro-4*H*-indazol-4-one (**2.12**) in $CDCl_3$

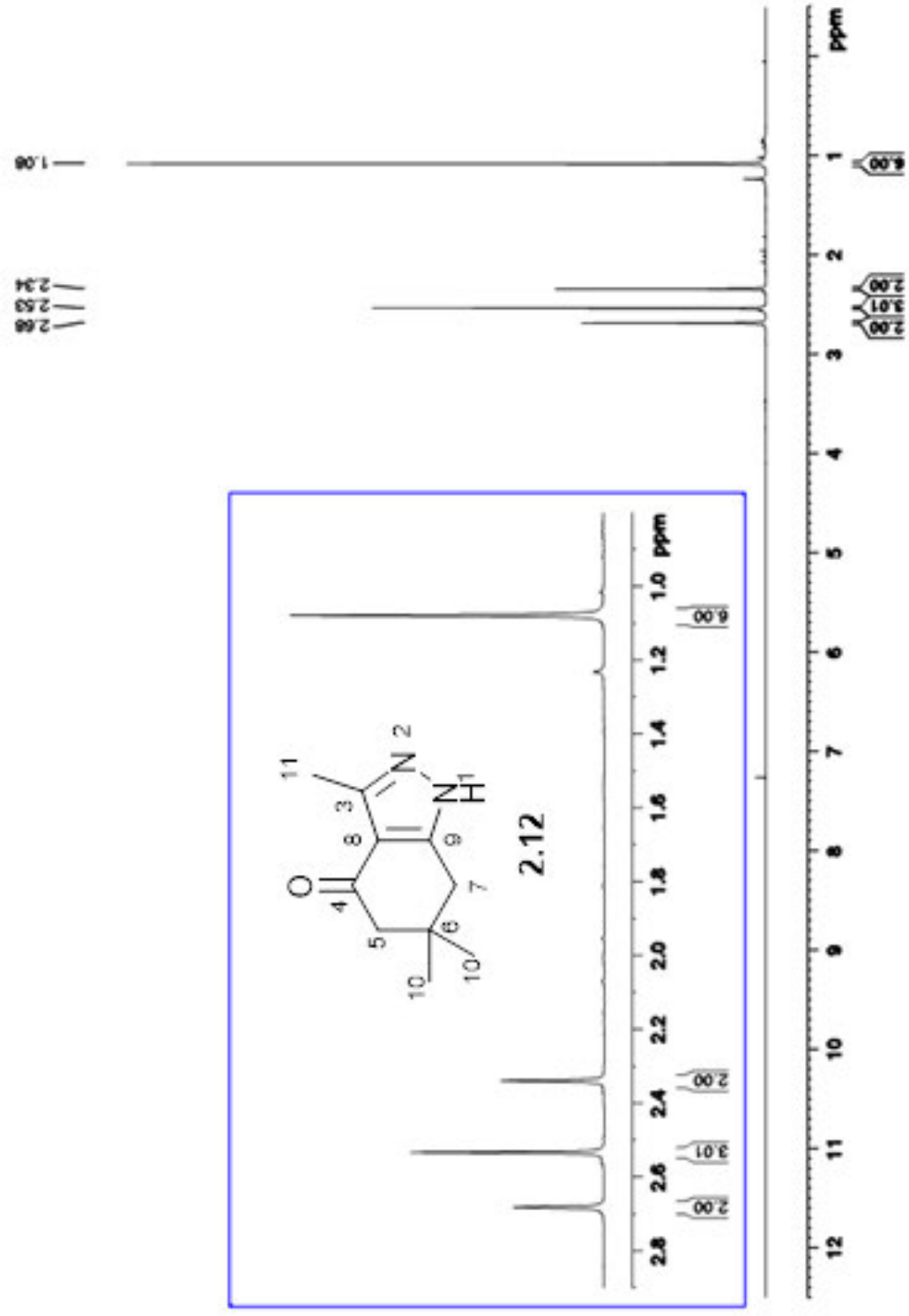

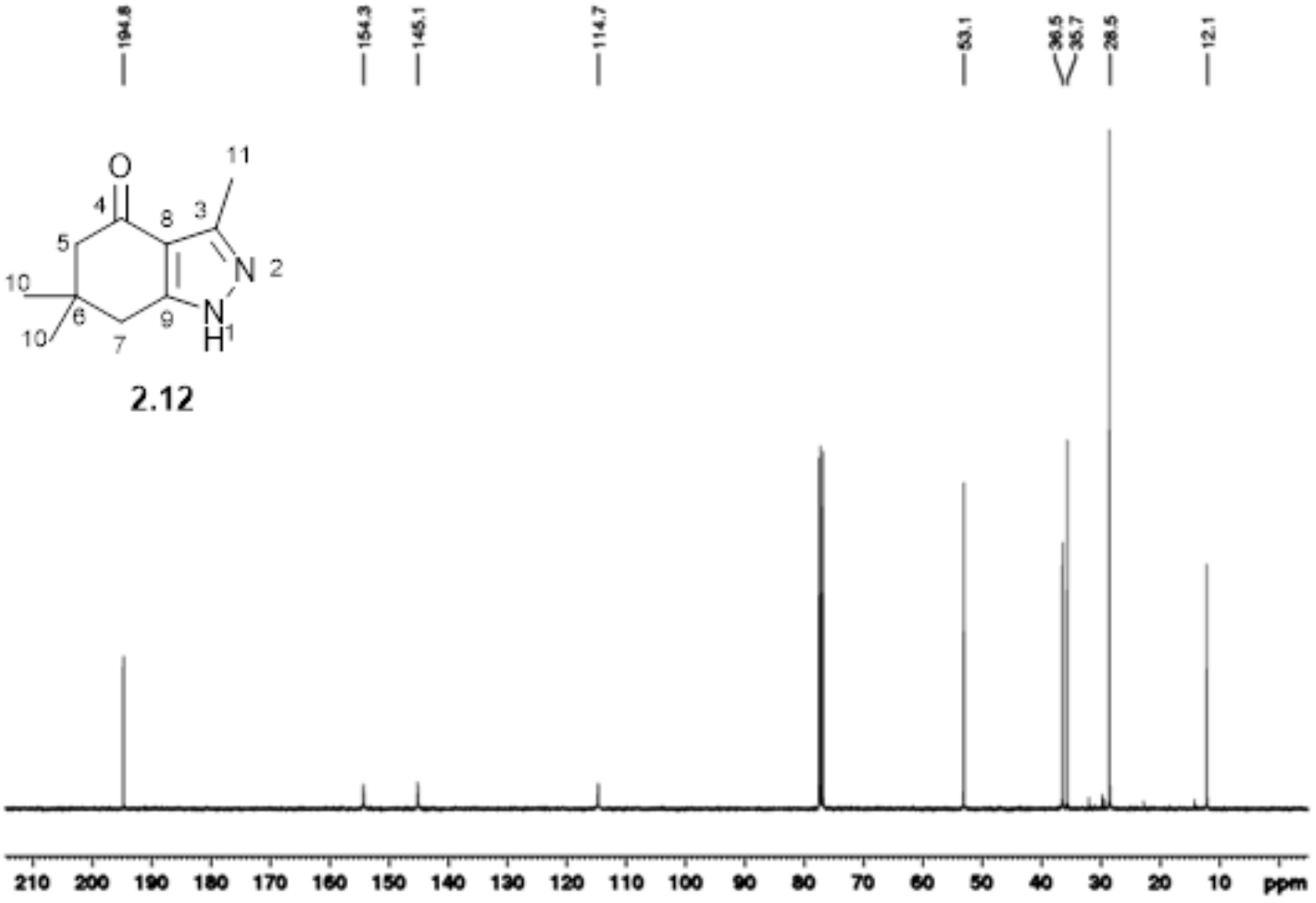
194.8
154.3
145.1
114.7
53.1
36.5
35.7
28.5
12.1
O
11
4
3
8
5
N
2
10
6
9
N
H
1
10
7
210 200 190 180 170 160 150 140 130 120 110 100 90 80 70 60 50 40 30 20 10 ppm

2.12

Appendix A1.8: ^{1}H NMR (400 MHz) and ^{13}C NMR (100 MHz) spectra of 2-acetyldimedone (**2.18**) in $CDCl_3$

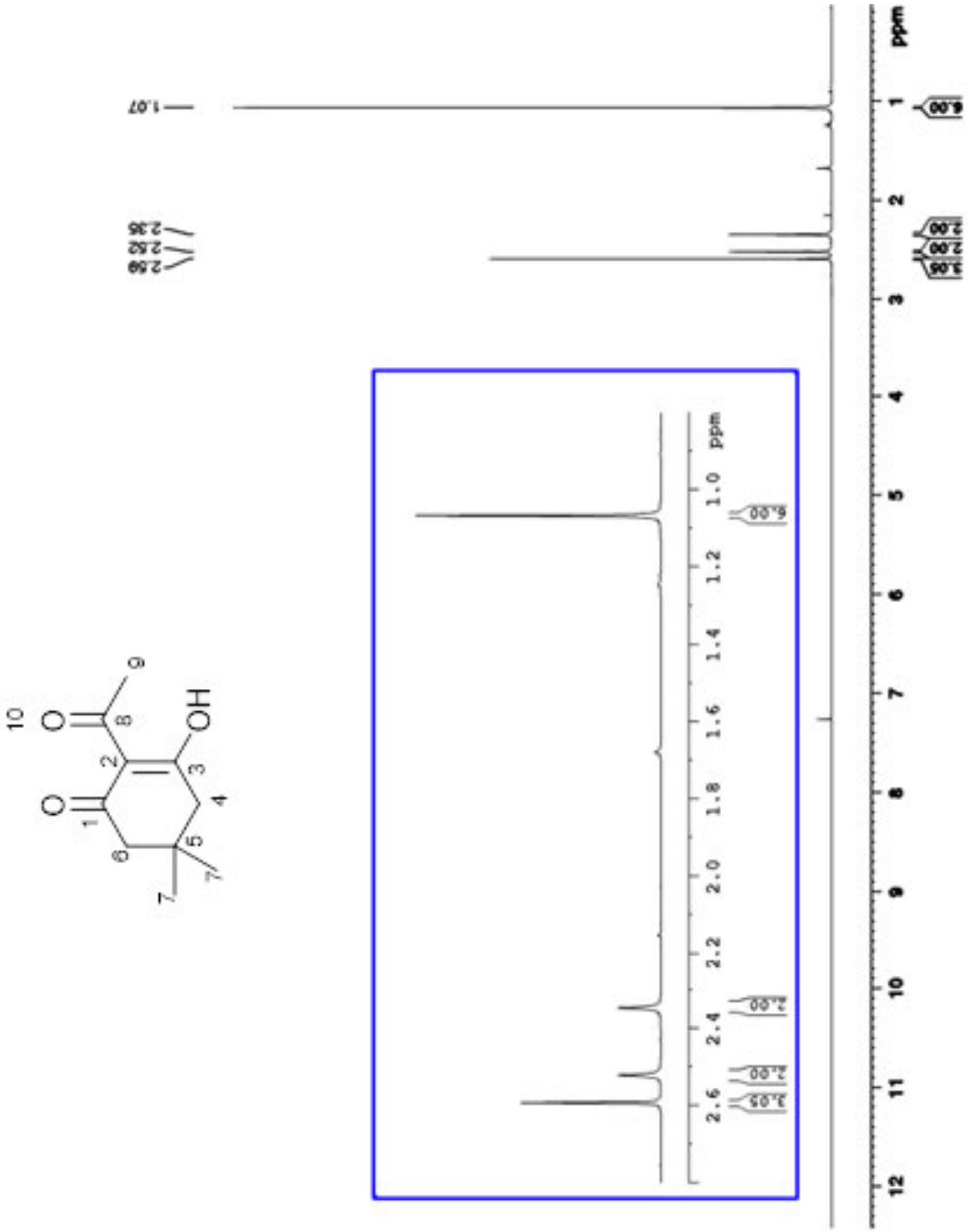

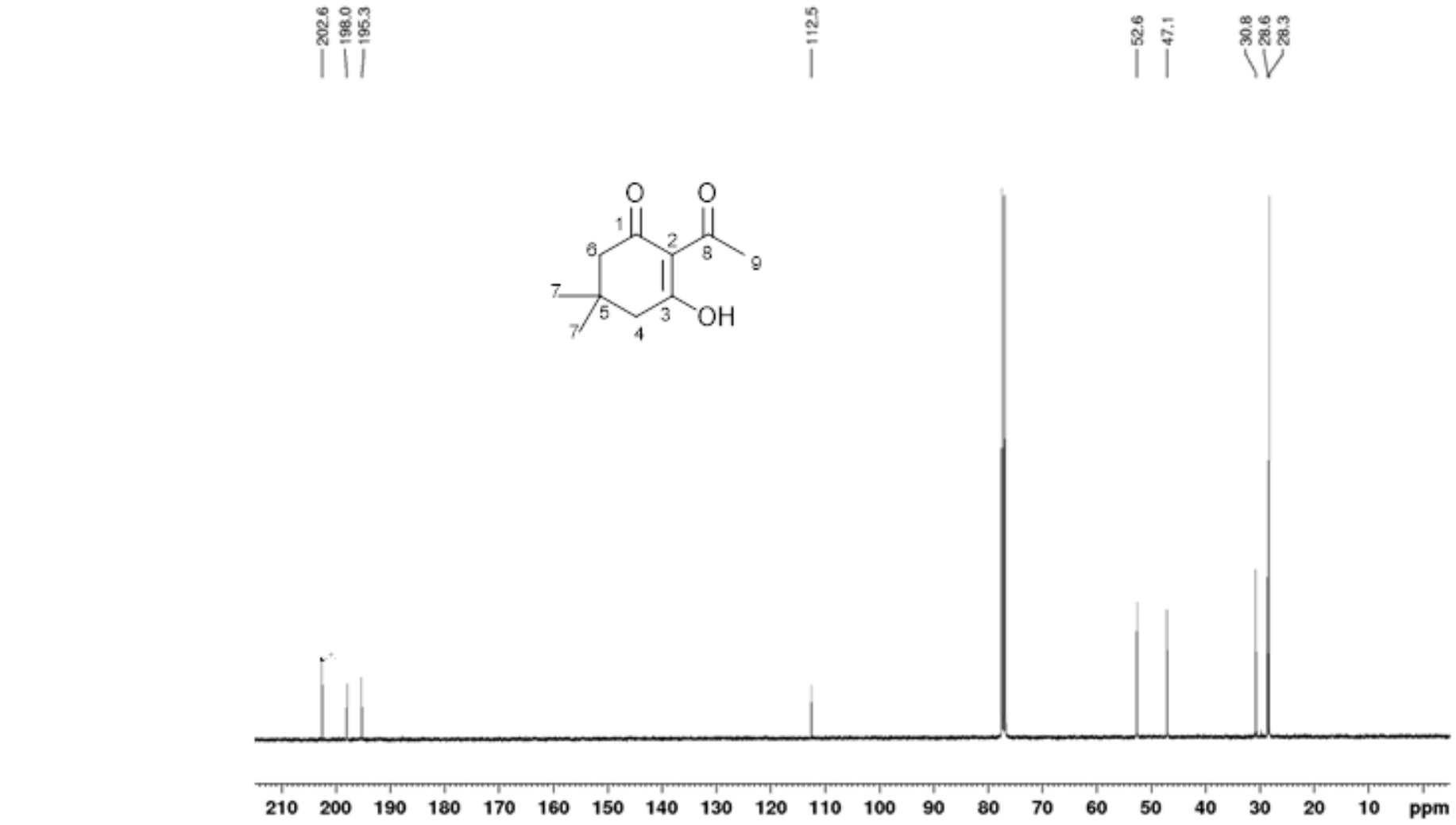
202.6
198.0
195.3
112.5
52.6
47.1
30.8
28.6
28.3
O
O
1
2
6
8
9
7
5
3
OH
7
4
210 200 190 180 170 160 150 140 130 120 110 100 90 80 70 60 50 40 30 20 10 ppm

Appendix A1.9: ^{1}H NMR (500 MHz) and ^{13}C NMR (125 MHz) spectra of 6,6-dimethyl-3-(trifluoromethyl)-1,5,6,7-tetrahydro-*4H*-indazol-4-one (**2.23**) in DMSO

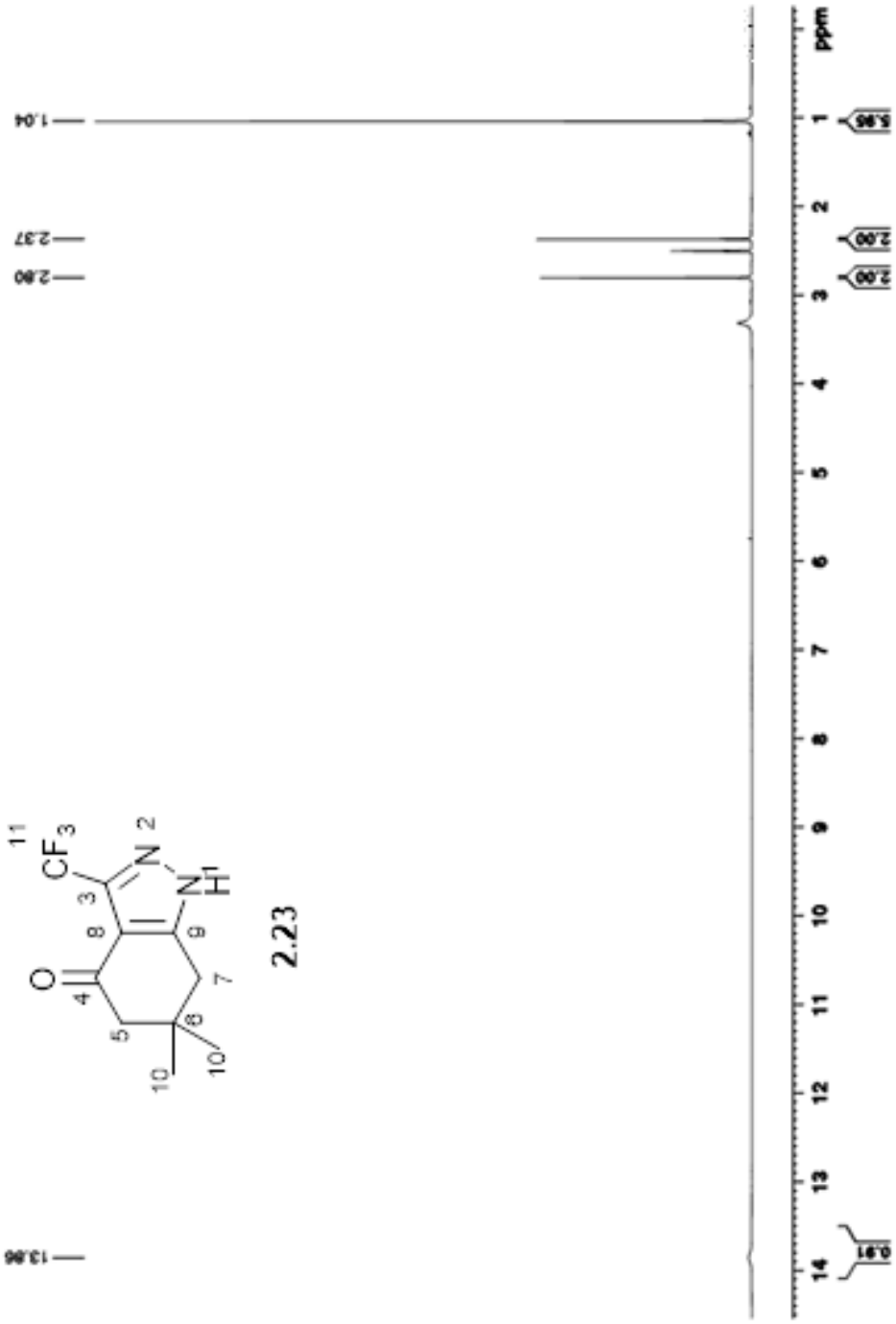

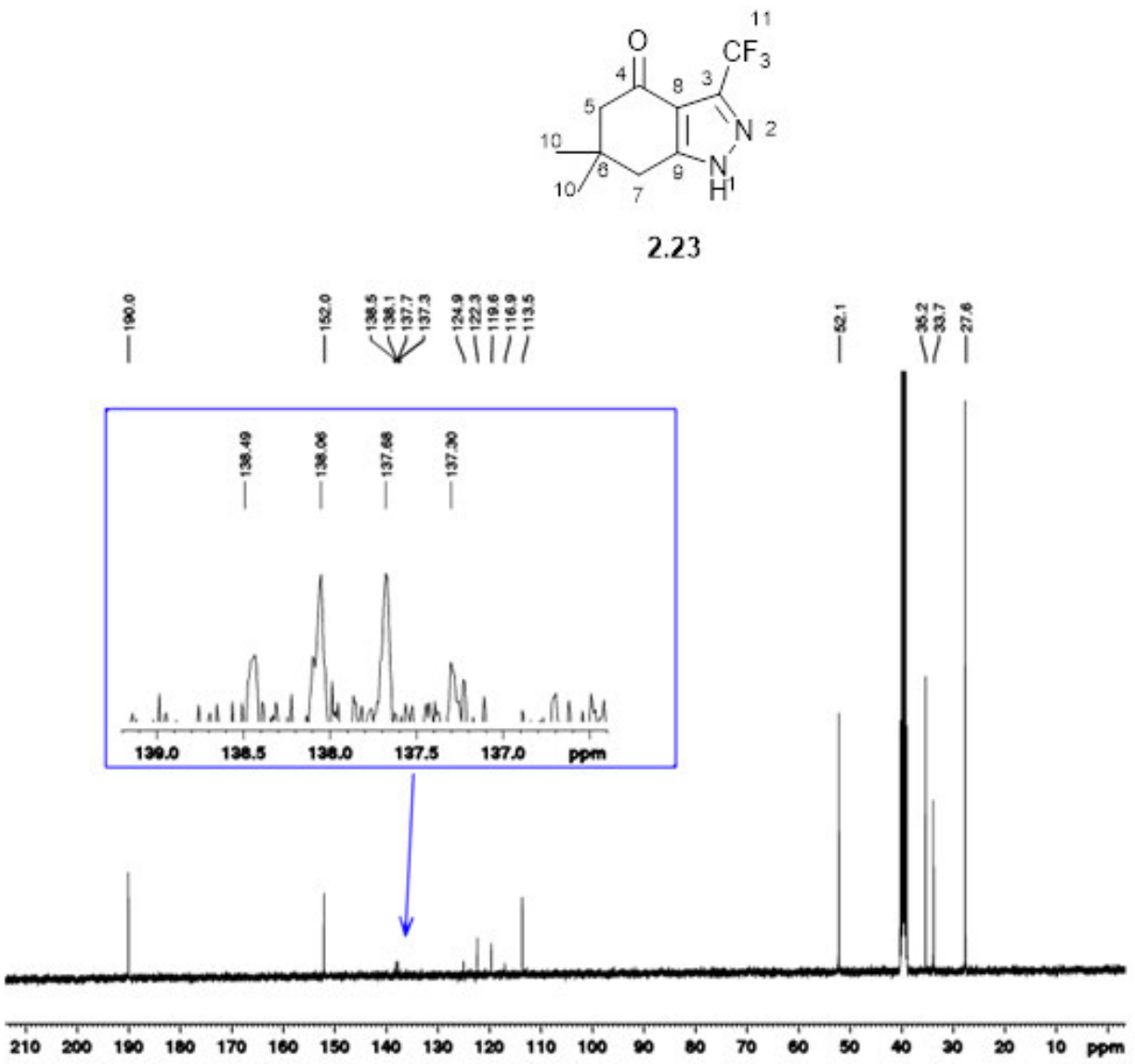
O
CF3
11
4
8
3
5
N
2
10
8
9
N
H
1
10
7
2.23
190.0
152.0
138.5
138.1
137.7
137.3
124.9
122.3
119.6
116.9
113.5
52.1
35.2
33.7
27.6
138.49
138.06
137.68
137.30
139.0
138.5
138.0
137.5
137.0
ppm
210 200 190 180 170 160 150 140 130 120 110 100 90 80 70 60 50 40 30 20 10 ppm

Appendix A1.10: ^{1}H NMR (400 MHz) and ^{13}C NMR (100 MHz) spectra of 2'-bromo-4'-hydrazinylbenzonitrile (**2.26**) in DMSO

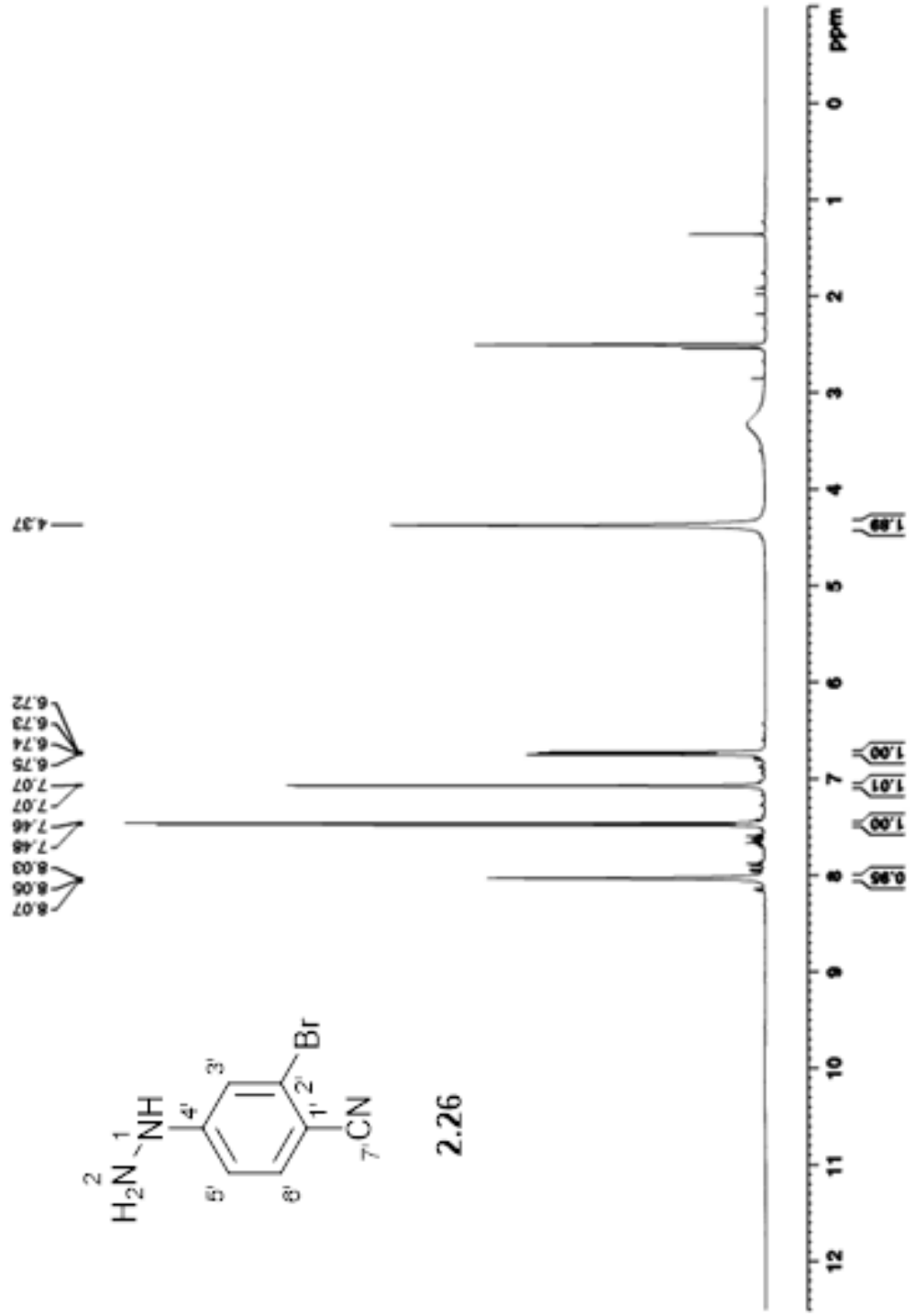

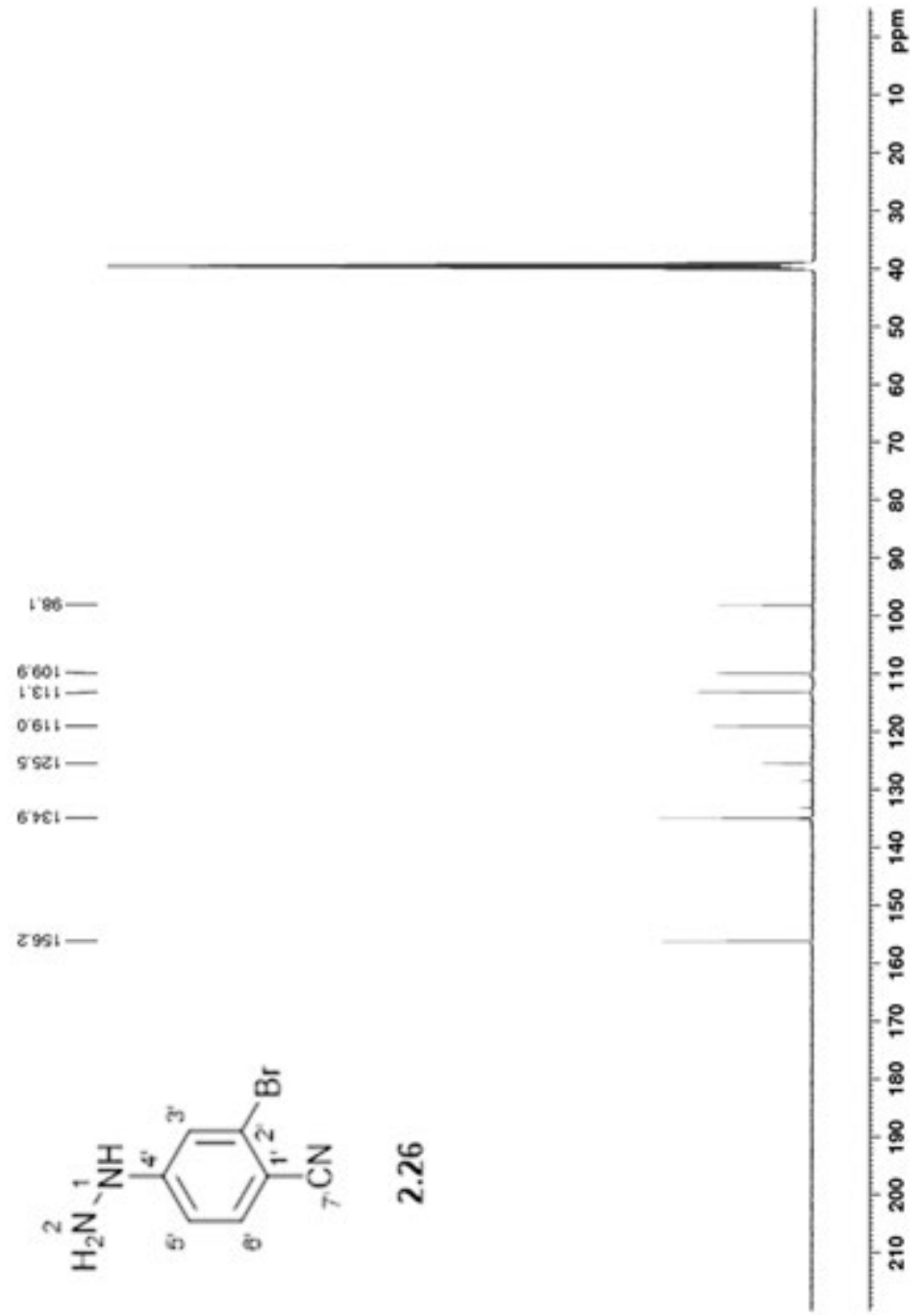
156.2
134.9
125.5
119.0
113.1
109.9
98.1
ppm
10
20
30
40
50
60
70
80
90
100
110
120
130
140
150
160
170
180
190
200
210
Br
CN
NH
H2N
1
2
1'
2'
3'
4'
5'
6'
7'

2.26

Appendix A1.11: ^{1}H NMR (400 MHz) and ^{13}C NMR (100 MHz) spectra of 2'-bromo-4'-(6,6-dimethyl-4-oxo-3-(trifluoromethyl)-4,5,6,7-tetrahydro-1*H*-indazol-1-yl) benzonitrile (**2.29**) in DMSO

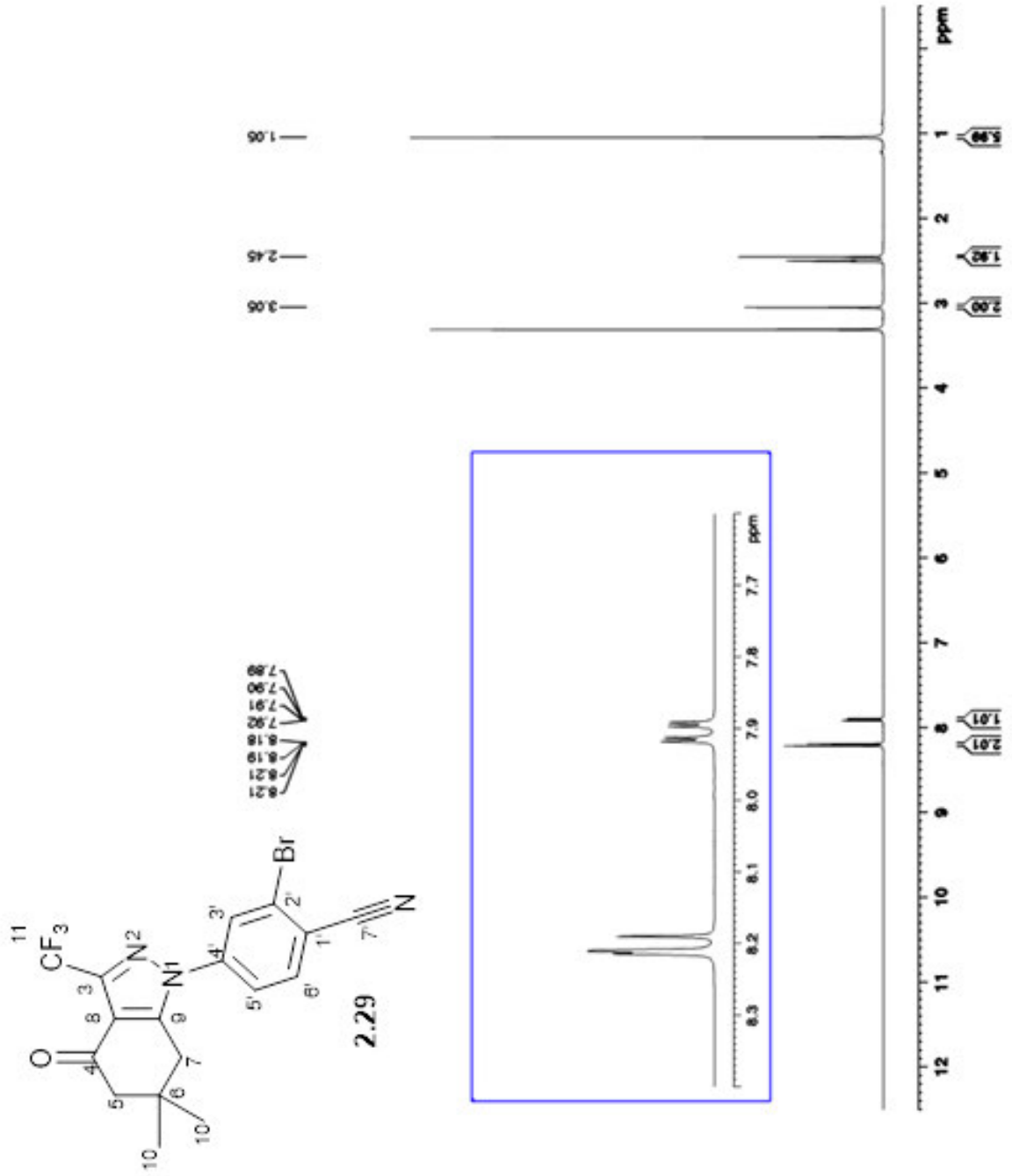

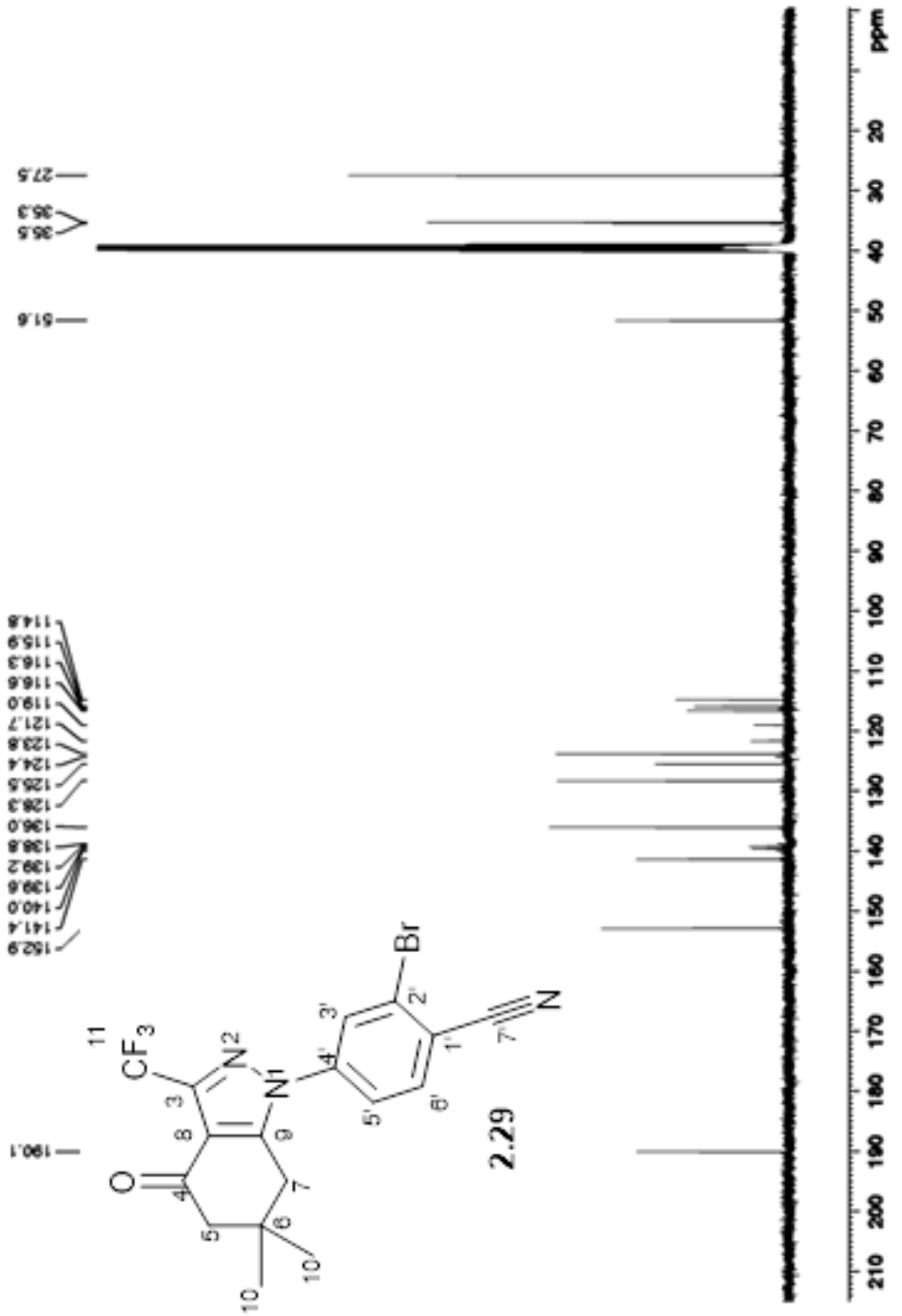
27.5
35.3
35.5
51.6
114.8
115.9
116.3
116.6
119.0
121.7
123.8
124.4
125.5
128.3
136.0
138.8
139.2
139.6
140.0
141.4
152.9
180.1
Br
N
O
CF3
N1
N2
2.29
ppm

Appendix A1.12: ^{1}H NMR (400 MHz) and ^{13}C NMR (100 MHz) spectra of 2'-fluoro-4'-(3,6,6-trimethyl-4-oxo-4,5,6,7-tetrahydro-1*H*-indazol-1-yl)-benzonitrile (**2.30**) in $CDCl_3$

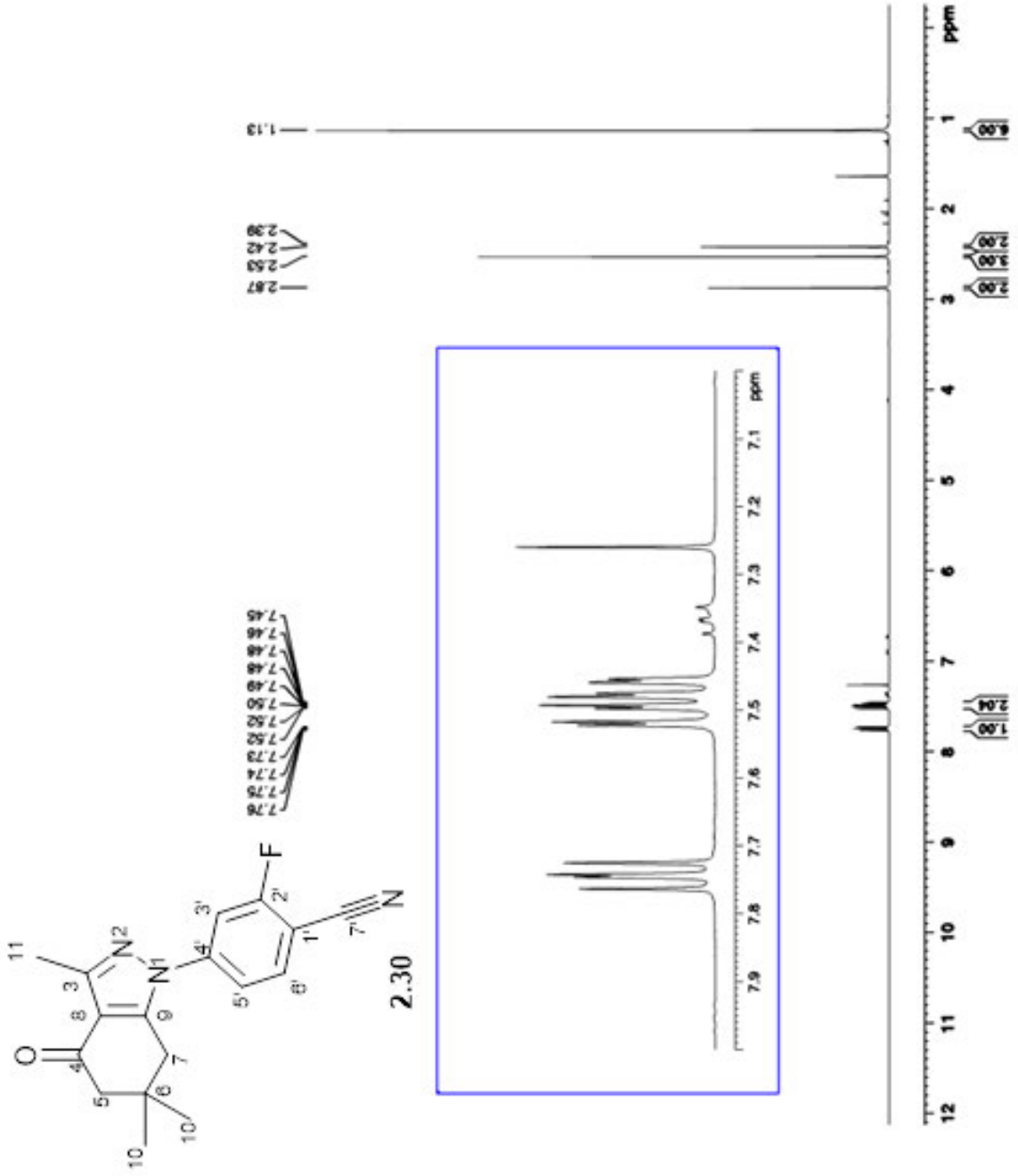

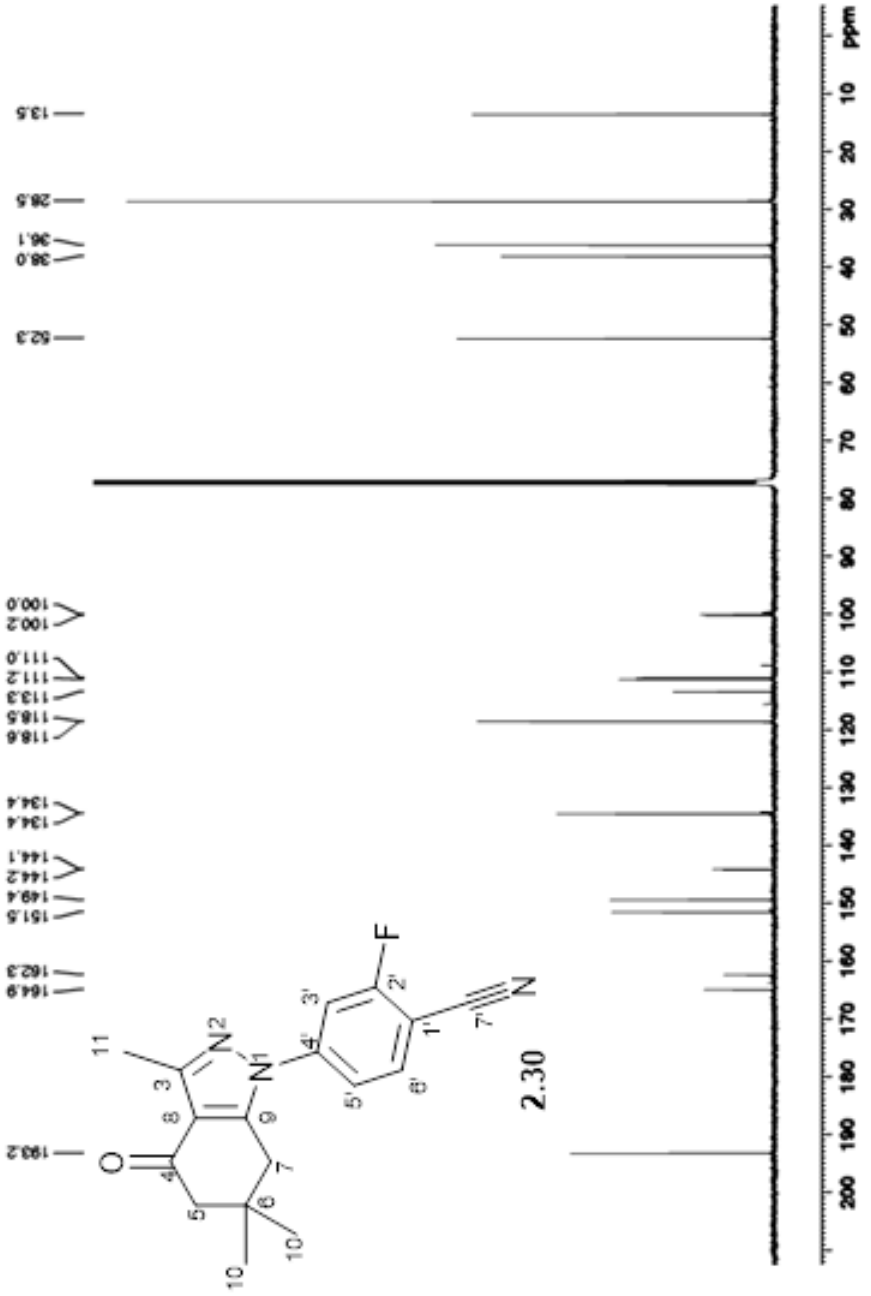
13.5
28.5
36.1
36.0
52.3
100.0
100.2
111.0
111.2
113.3
118.5
118.6
134.4
134.4
144.1
144.2
149.4
151.5
162.3
164.9
193.2
ppm
10
20
30
40
50
60
70
80
90
100
110
120
130
140
150
160
170
180
190
200
O
N1
N2
F
N
2.30

Appendix A1.13: ^{1}H NMR (400 MHz) and ^{13}C NMR (100 MHz) spectra of 4'-fluoro-2'-hydrazinylbenzonitrile (**2.39**) in $((CD_3)_2CO$

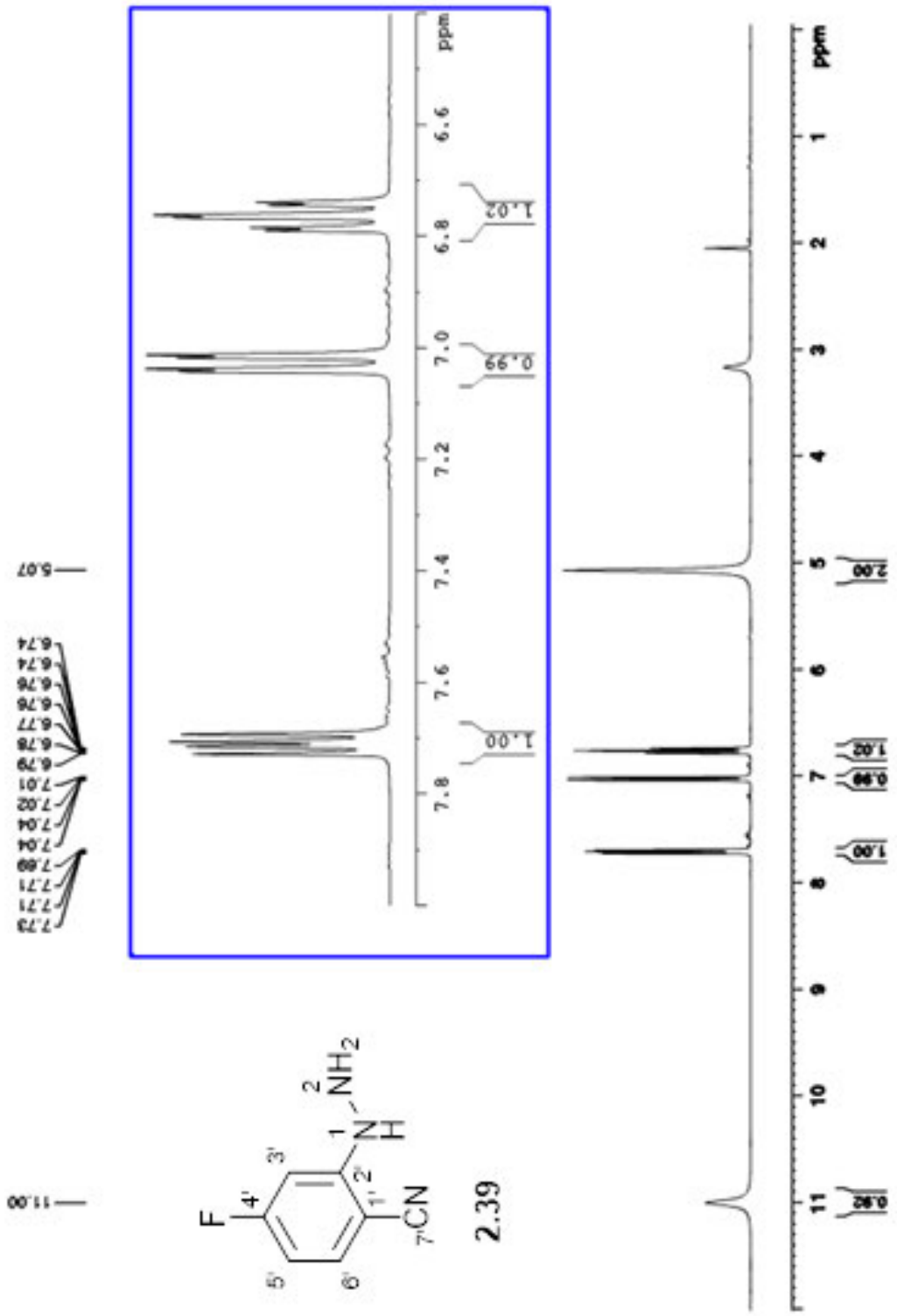

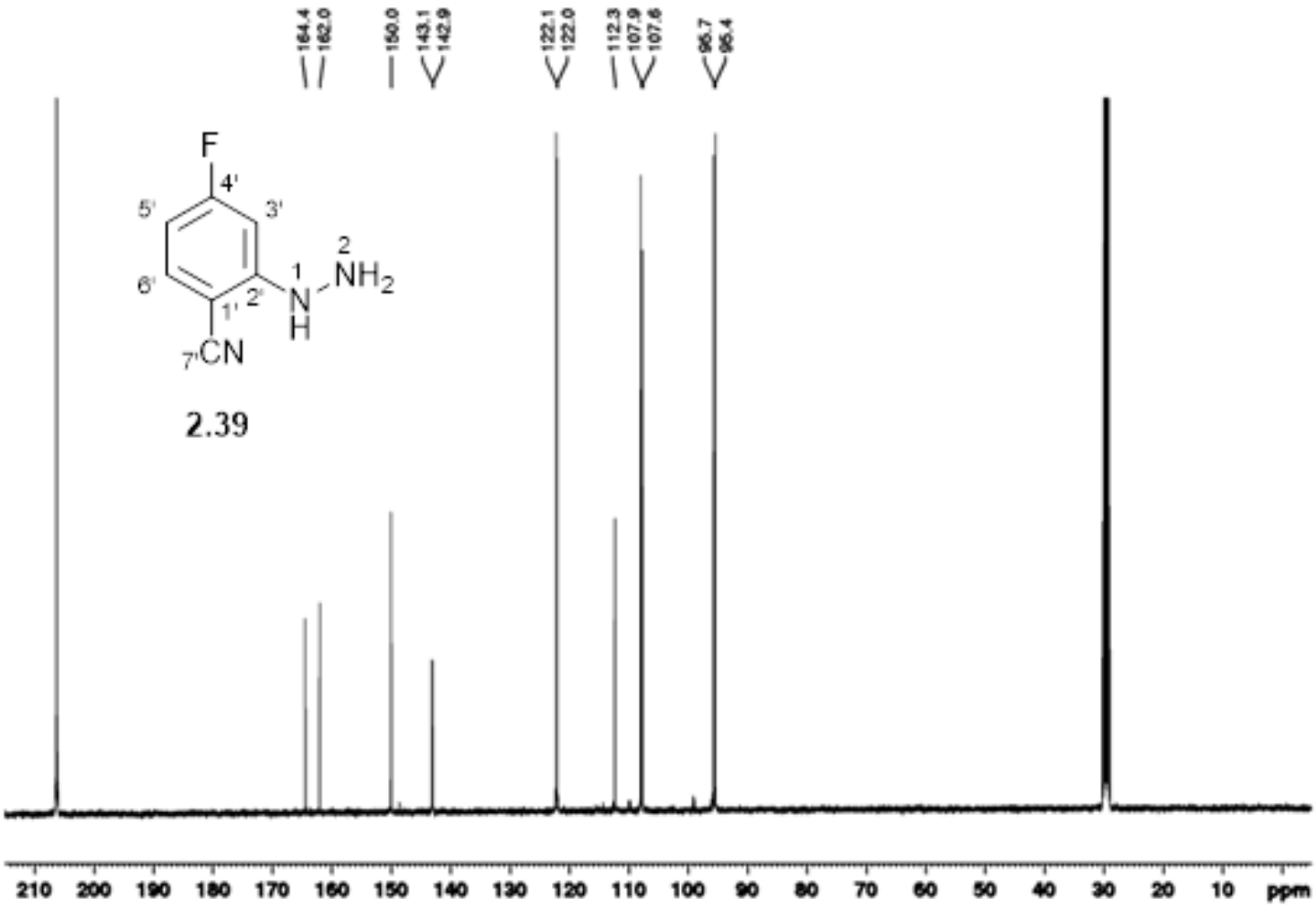
164.4
162.0
150.0
143.1
142.9
122.1
122.0
112.3
107.9
107.6
96.7
96.4
F
4'
5'
3'
6'
1'
2'
1
N
H
2
NH2
7'CN
2.39
210 200 190 180 170 160 150 140 130 120 110 100 90 80 70 60 50 40 30 20 10 ppm

Appendix A1.14: ^{1}H NMR (400 MHz) and ^{13}C NMR (100 MHz) spectra of 3-acetoxy-5,5-dimethyl-2-cyclohexenone (**2.43**) in $CDCl_3$

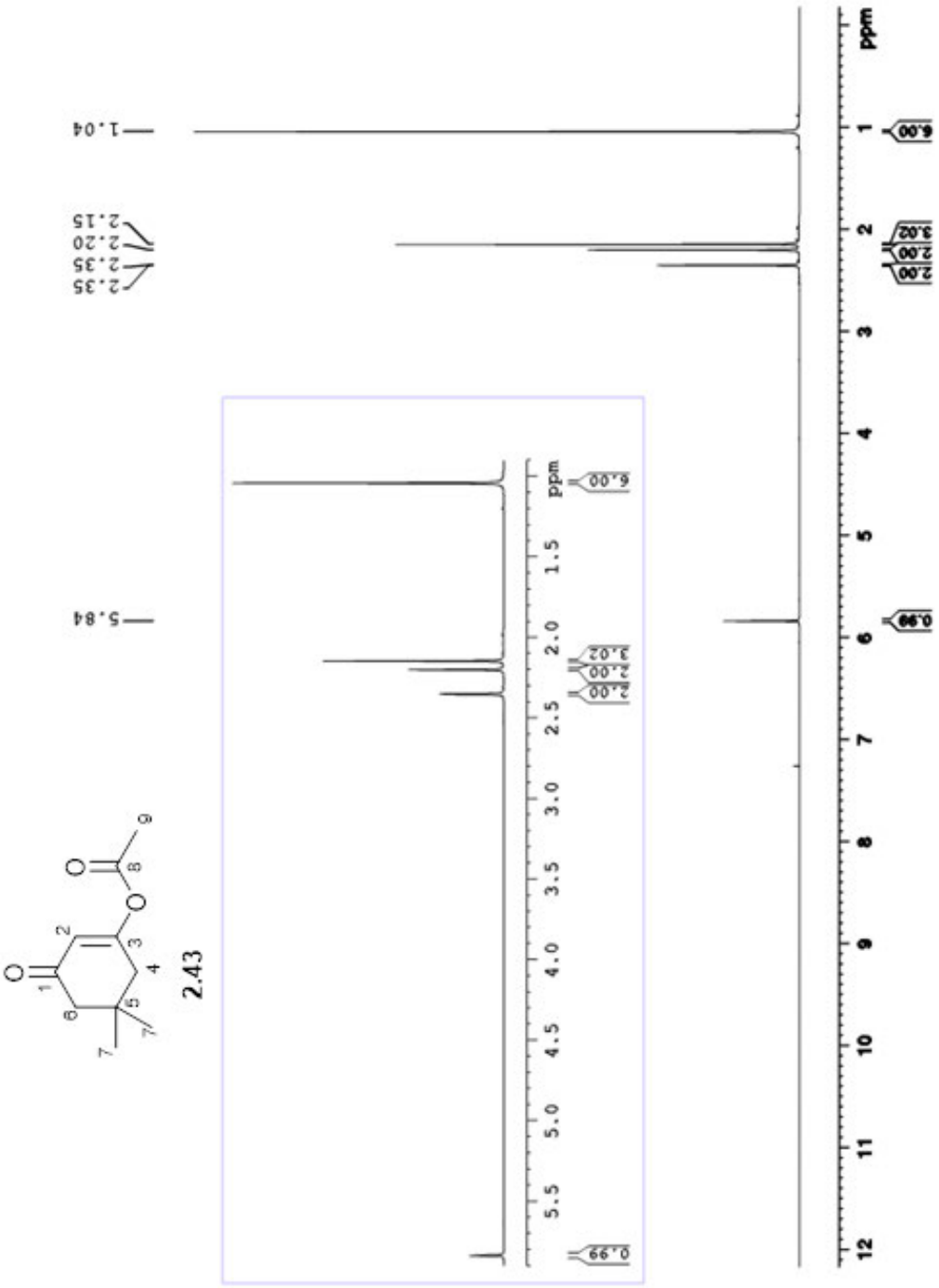

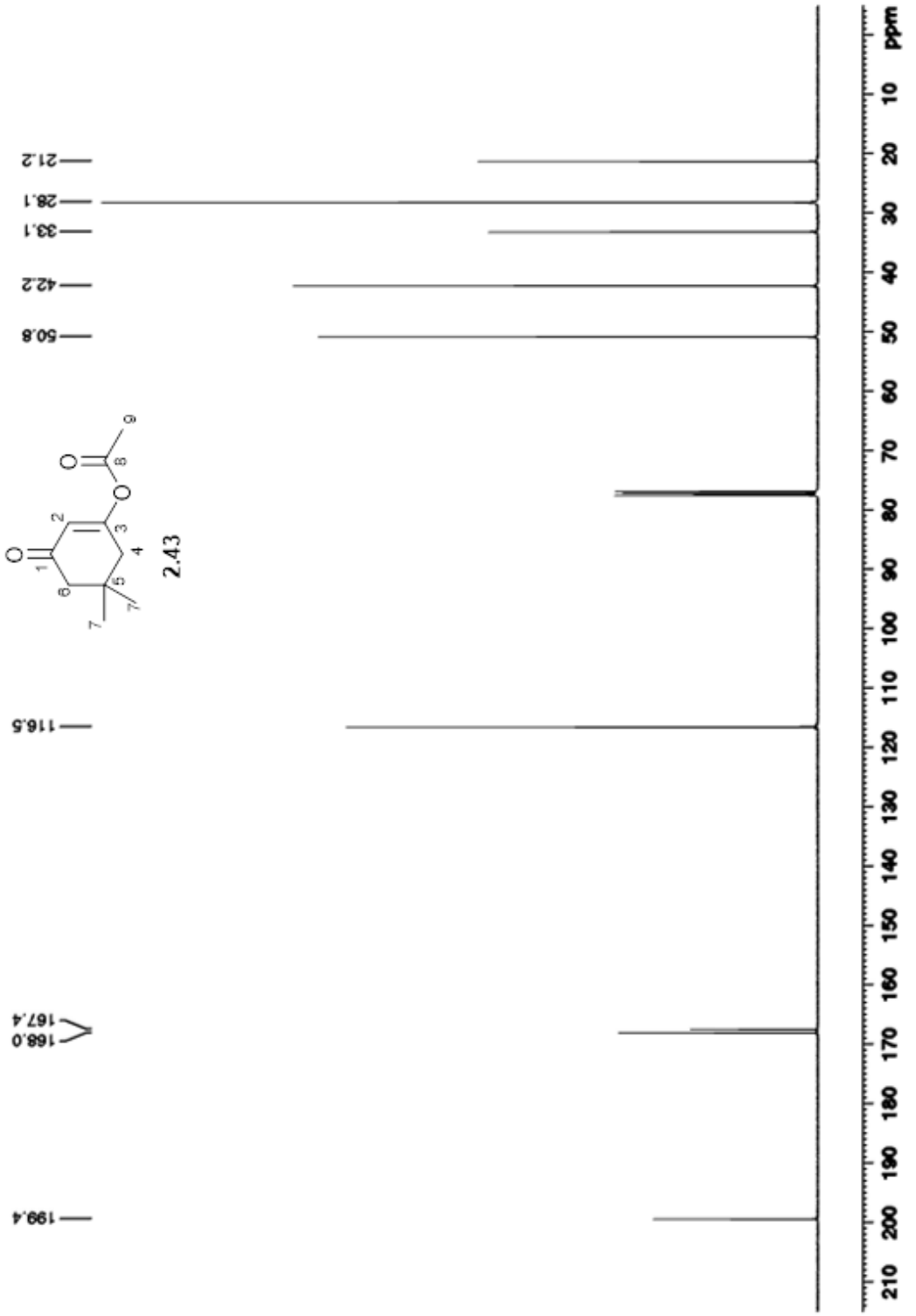
199.4
168.0
167.4
116.5
50.8
42.2
33.1
28.1
21.2
ppm
10
20
30
40
50
60
70
80
90
100
110
120
130
140
150
160
170
180
190
200
210
2.43

Appendix A1.15: ^{1}H NMR (400 MHz) and ^{13}C NMR (100 MHz) spectra of 4'-fluoro-2'-(3,6,6-trimethyl-4-oxo-4,5,6,7-tetrahydro-1*H*-indazol-1-yl)-benzonitrile (**2.44**) in $CDCl_3$

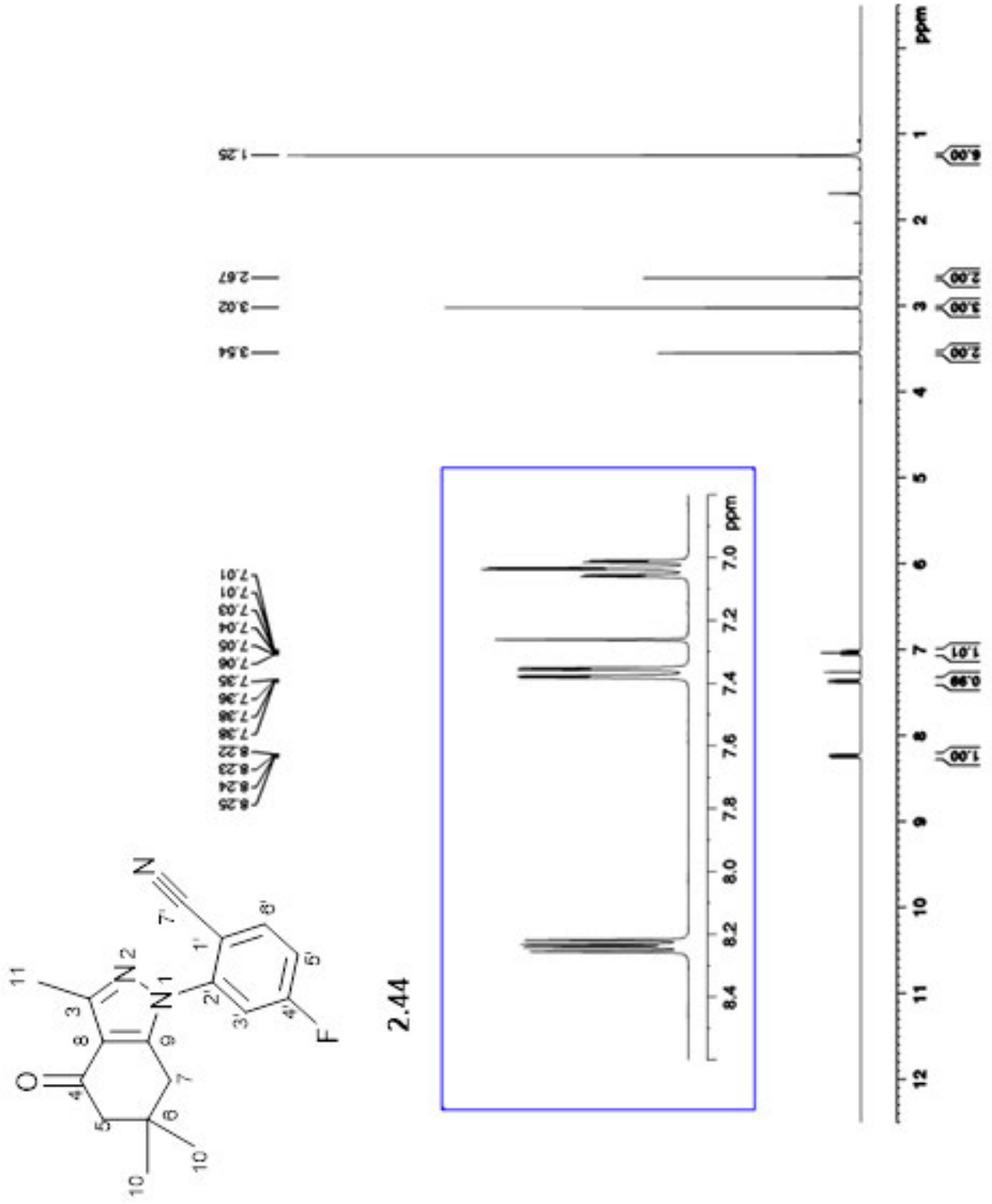

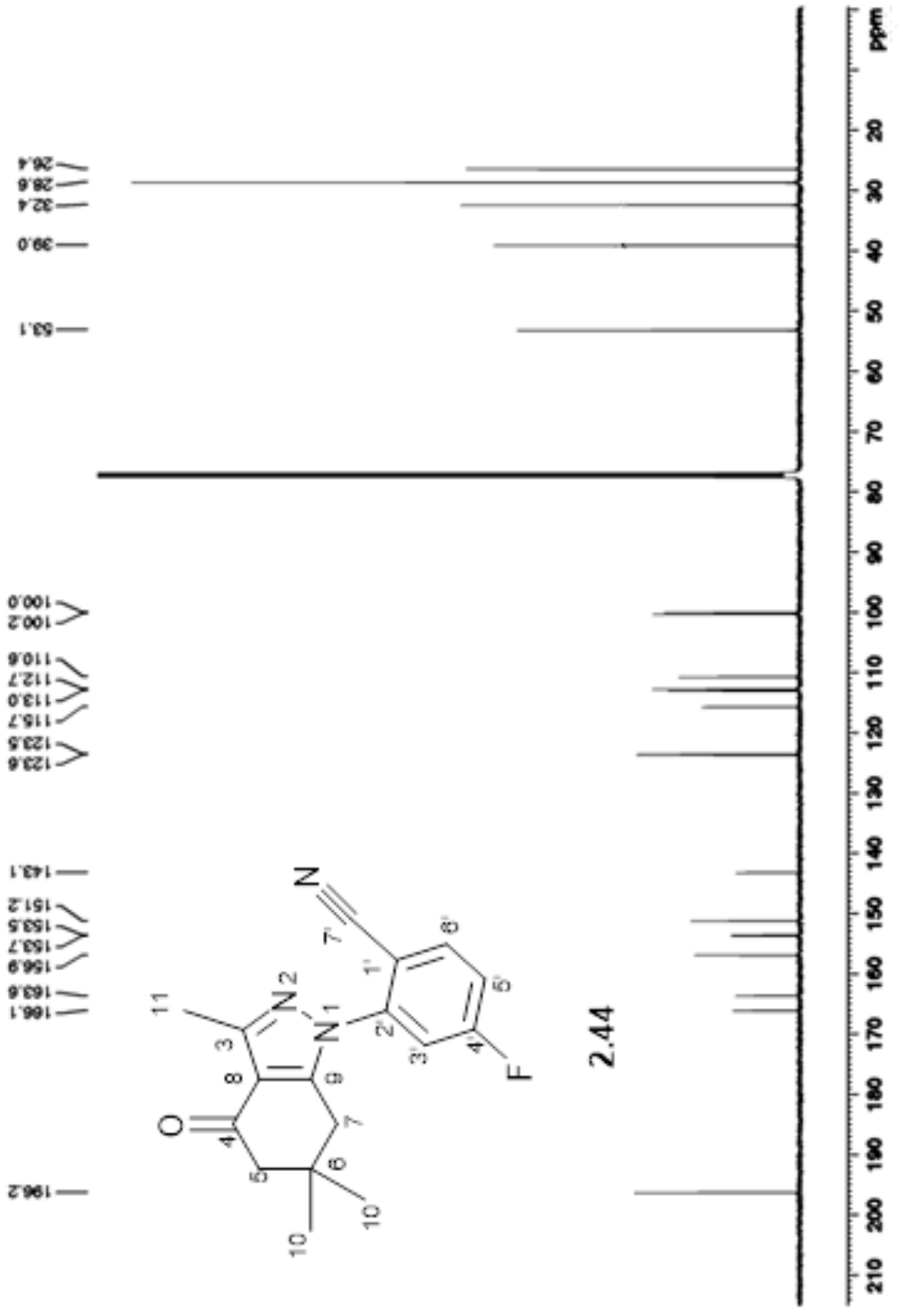
26.4
28.6
32.4
39.0
53.1
100.0
100.2
110.6
112.7
113.0
115.7
123.5
123.6
143.1
151.2
153.5
153.7
156.9
163.6
166.1
196.2
ppm
2.44

Appendix A1.16: ^{1}H NMR (400 MHz) and ^{13}C NMR (100 MHz) spectra of *tert*-butyl-(4-((2-cyano-5-(6,6-dimethyl-4-oxo-3-(trifluoromethyl)-4,5,6,7-tetrahydro-1*H*-indazol-1-yl)phenyl)amino)cyclohexyl)carbamate (**2.78**) in $CDCl_3$

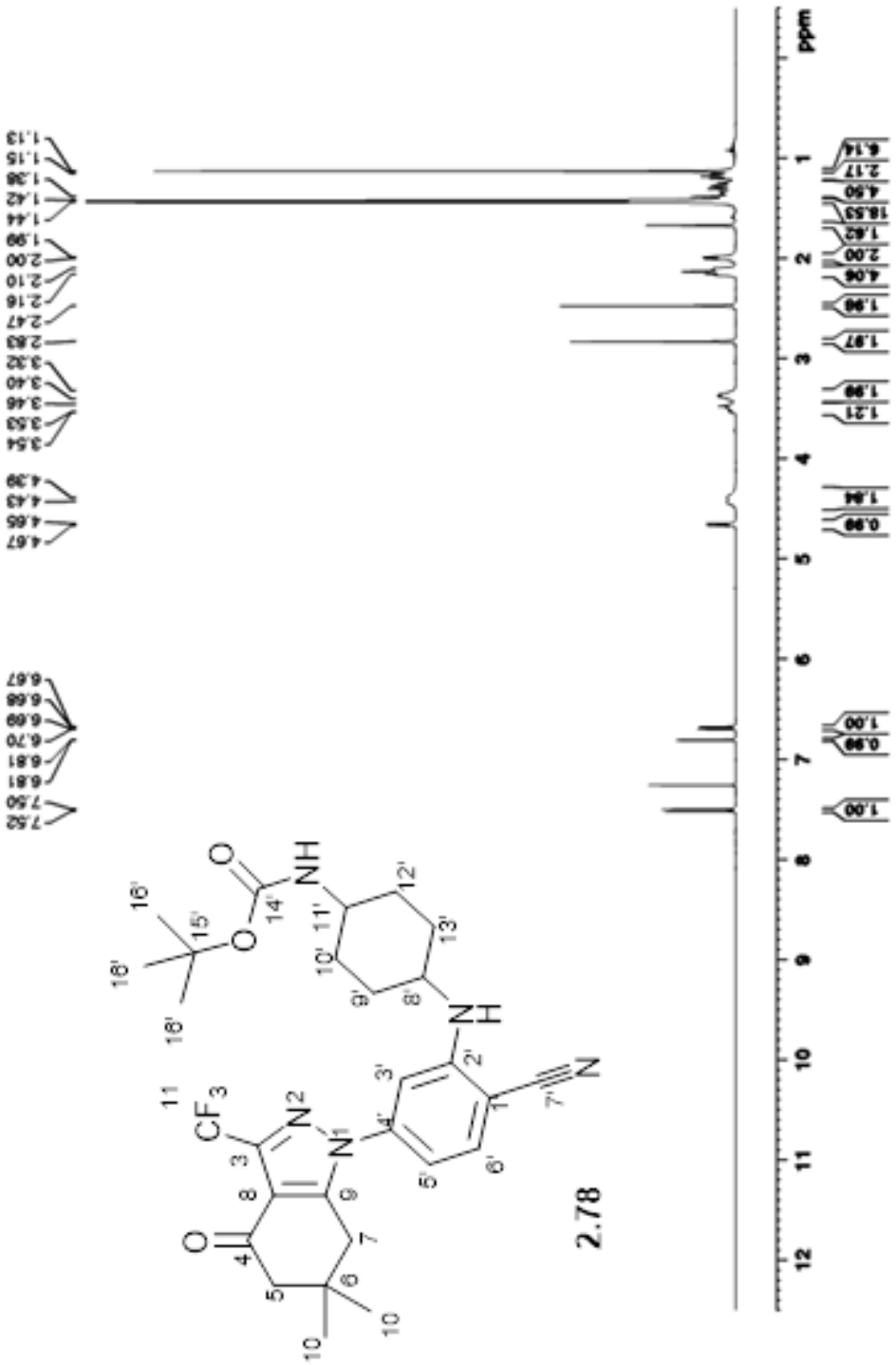

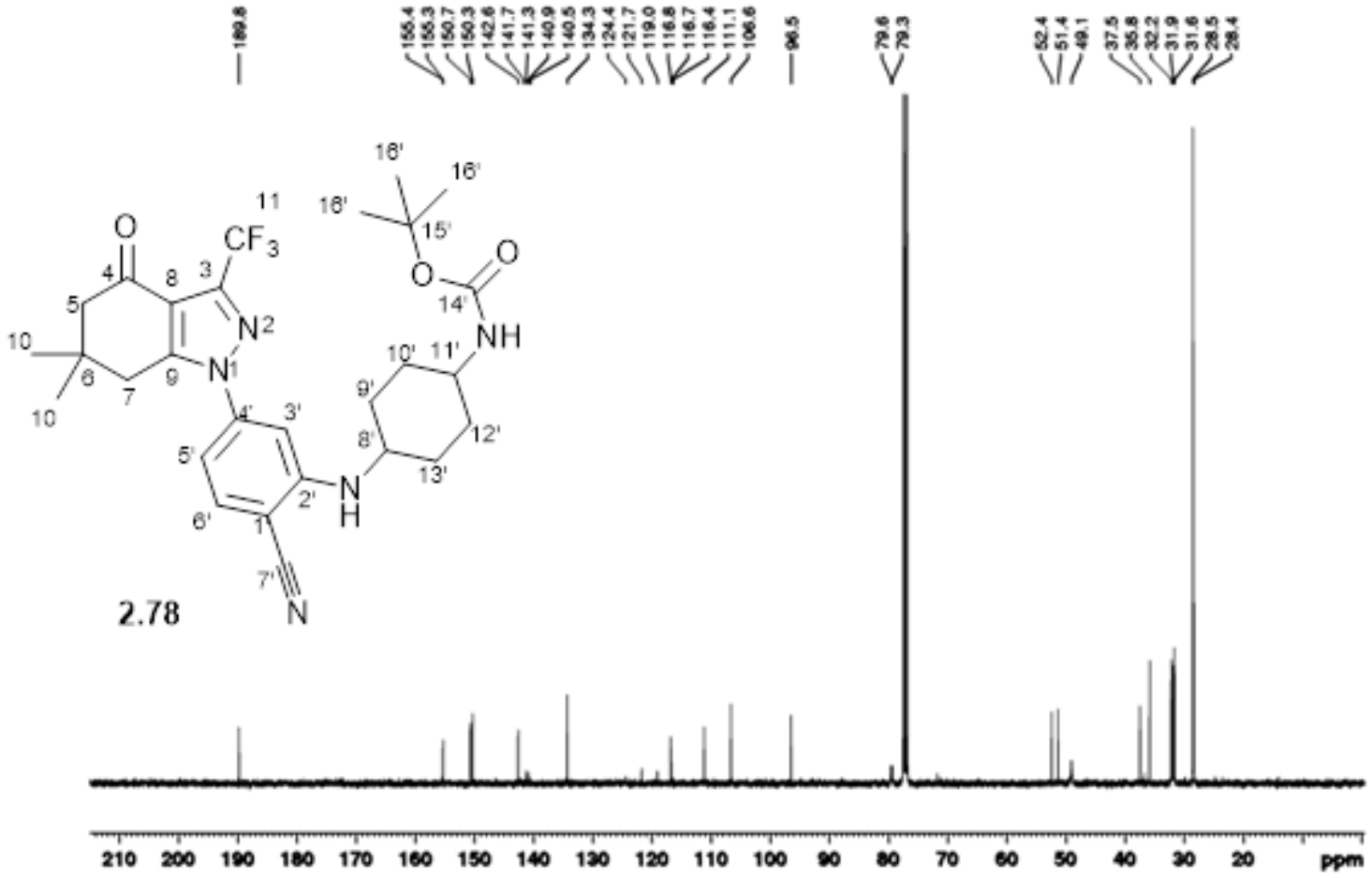
189.8
155.4
155.3
150.7
150.3
142.6
141.7
141.3
140.9
140.5
134.3
124.4
121.7
119.0
116.8
116.7
116.4
111.1
106.6
96.5
79.6
79.3
52.4
51.4
49.1
37.5
35.8
32.2
31.9
31.6
28.5
28.4
O
CF3
11
4
3
8
5
N2
N1
10
6
9
7
10
4'
3'
5'
2'
6'
1
7'
N
2.78
16'
16'
16'
15'
O
O
14'
NH
10'
11'
9'
8'
12'
13'
N
H
210
200
190
180
170
160
150
140
130
120
110
100
90
80
70
60
50
40
30
20
ppm

Appendix A1.17: ^{13}C NMR (125 MHz) spectra of *tert*-butyl(4-((2-carbamoyl-5-(6,6-dimethyl-4-oxo-3-(trifluoromethyl)-4,5,6,7-tetrahydro-1*H*-indazol-1-yl)phenyl)amino)cyclohexyl)carbamate (**2.79**) in DMSO

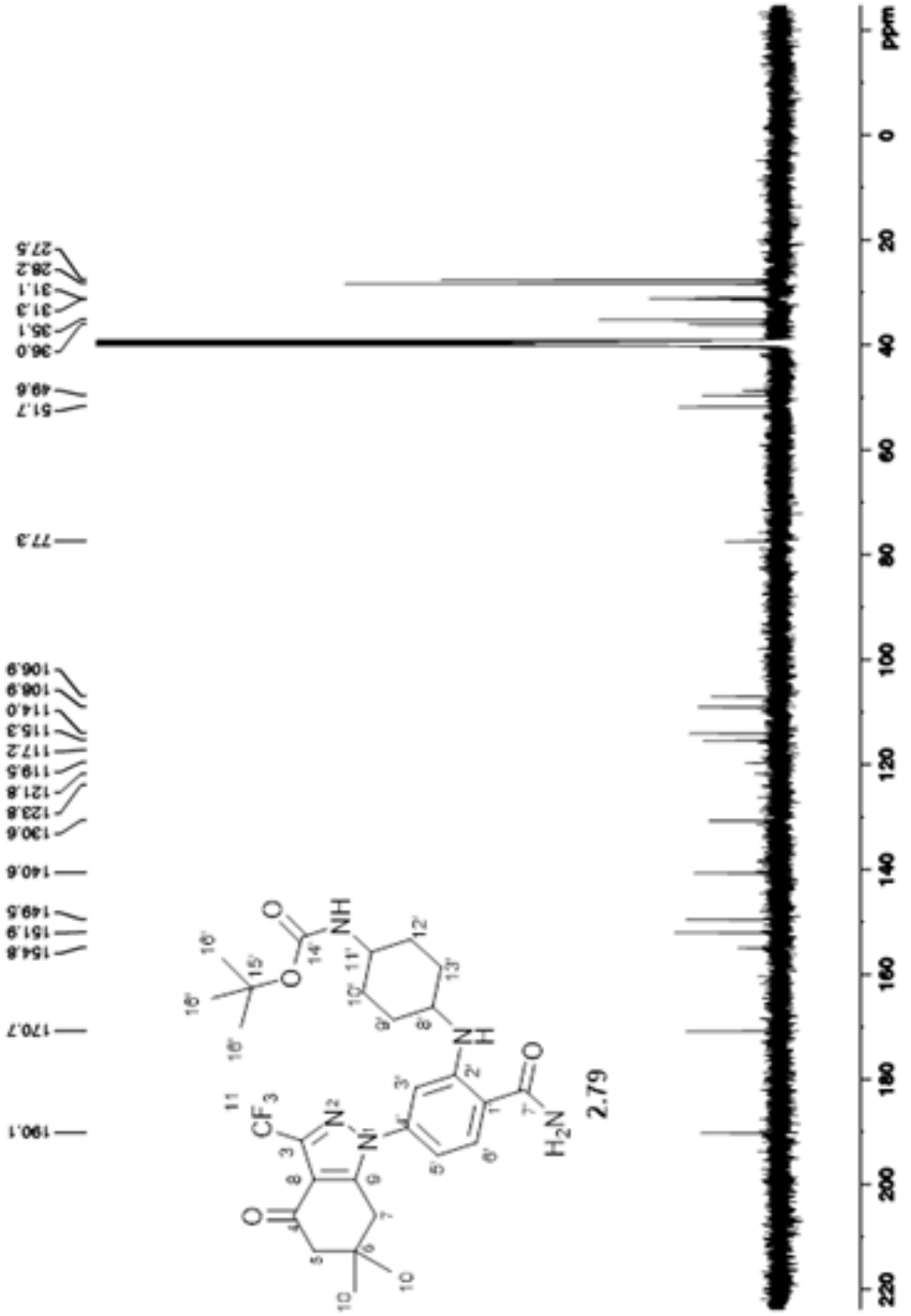

Appendix A1.18: ^{1}H NMR (400 MHz) and ^{13}C NMR (100 MHz) spectra of *tert*-butyl(4-((2-cyano-5-(3,6,6-trimethyl-4-oxo-4,5,6,7-tetrahydro-1*H*-indazol-1-yl)phenyl)amino)cyclohexyl)carbamate (**2.80**) in $CDCl_3$

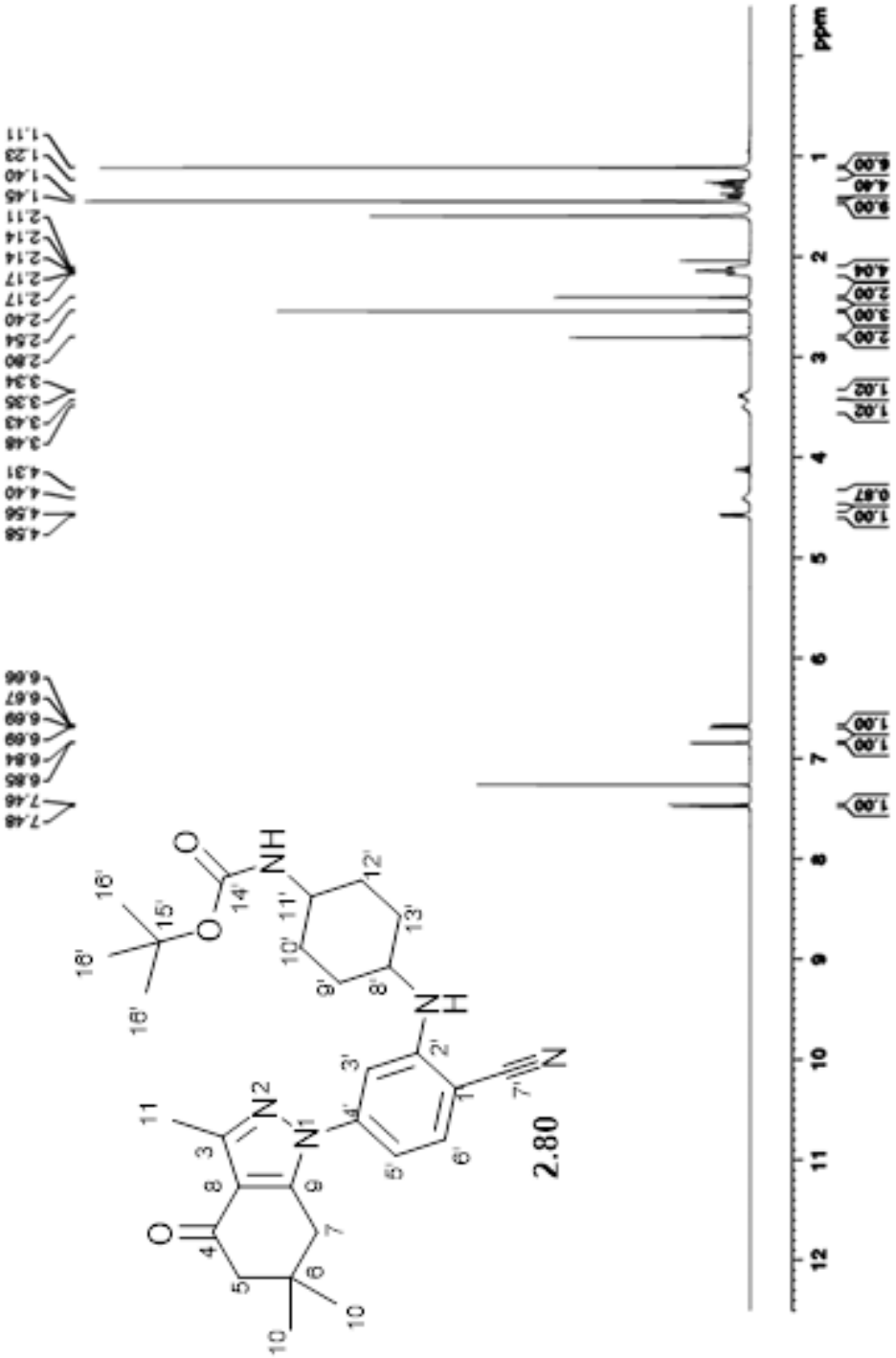

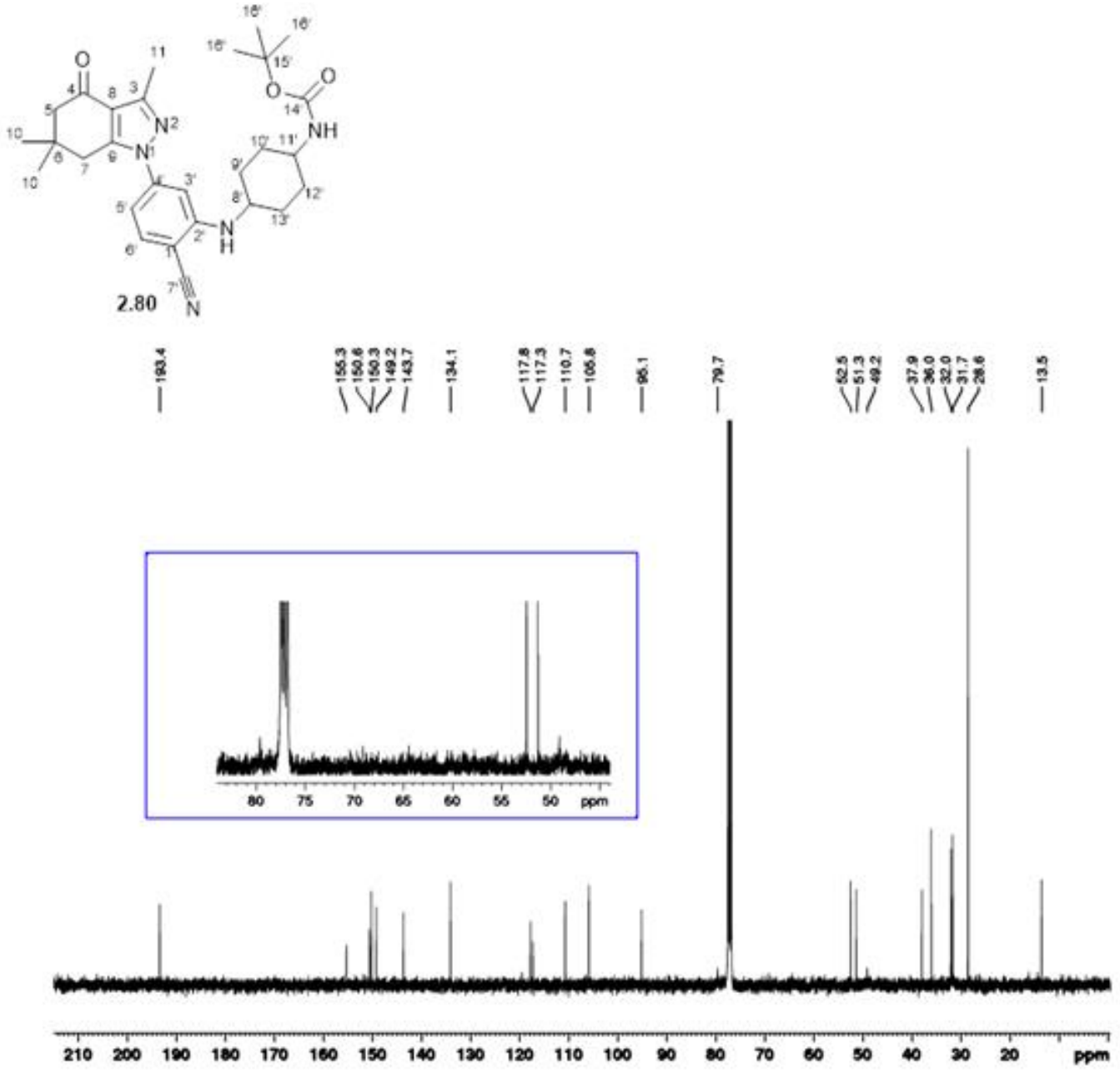
2.80
193.4
155.3
150.6
150.3
149.2
143.7
134.1
117.8
117.3
110.7
105.8
95.1
79.7
52.5
51.3
49.2
37.9
36.0
32.0
31.7
28.6
13.5
80 75 70 65 60 55 50 ppm
210 200 190 180 170 160 150 140 130 120 110 100 90 80 70 60 50 40 30 20 ppm

Appendix A1.19: ^{1}H NMR (500 MHz) and ^{13}C NMR (125 MHz) spectra of *tert*-butyl(4-((2-carbamoyl-5-(3,6,6-trimethyl-4-oxo-4,5,6,7-tetrahydro-1*H*-indazol-1-yl)phenyl)amino)cyclohexyl)carbamate (**2.81**) in $CDCl_3$

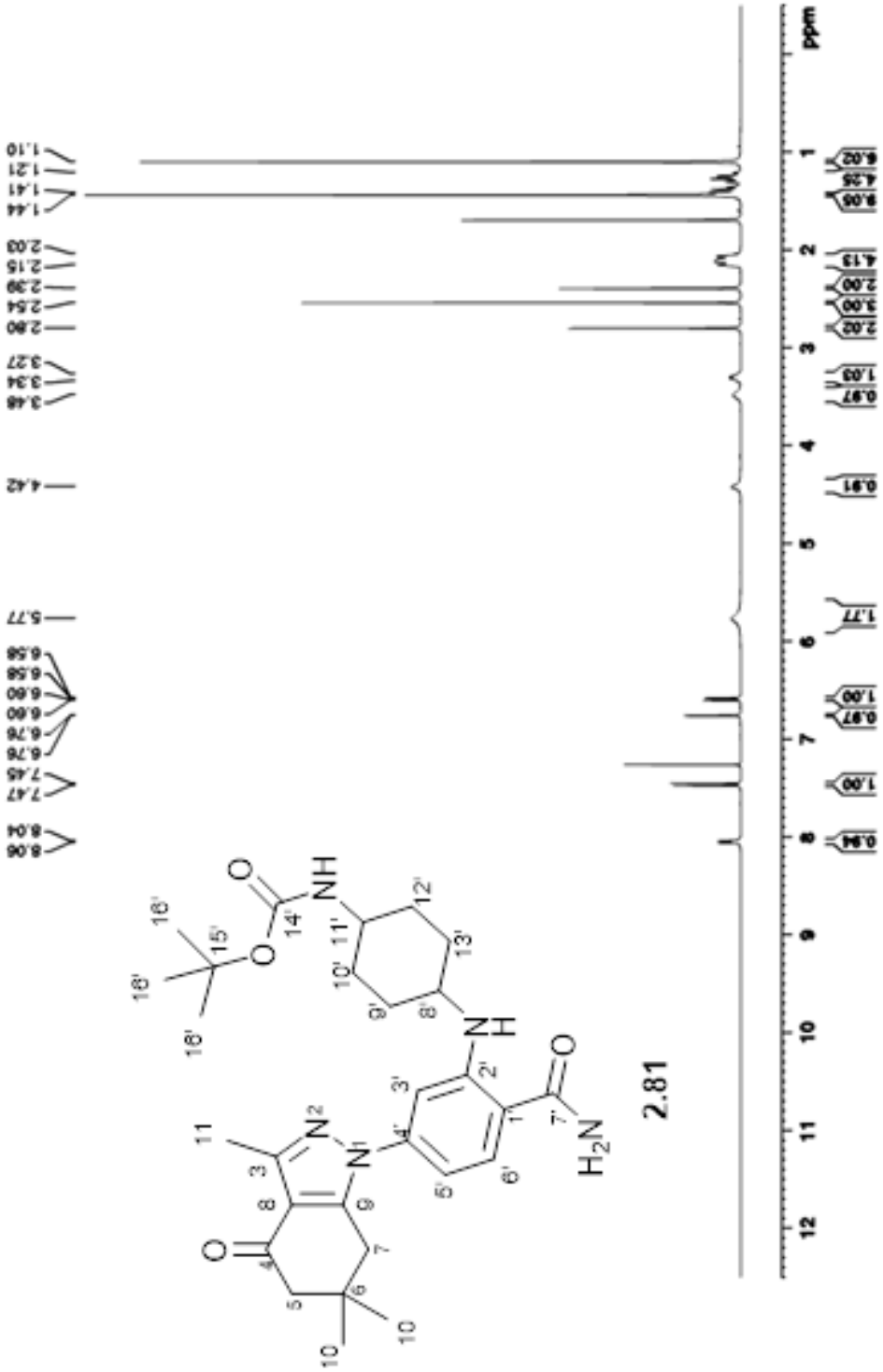

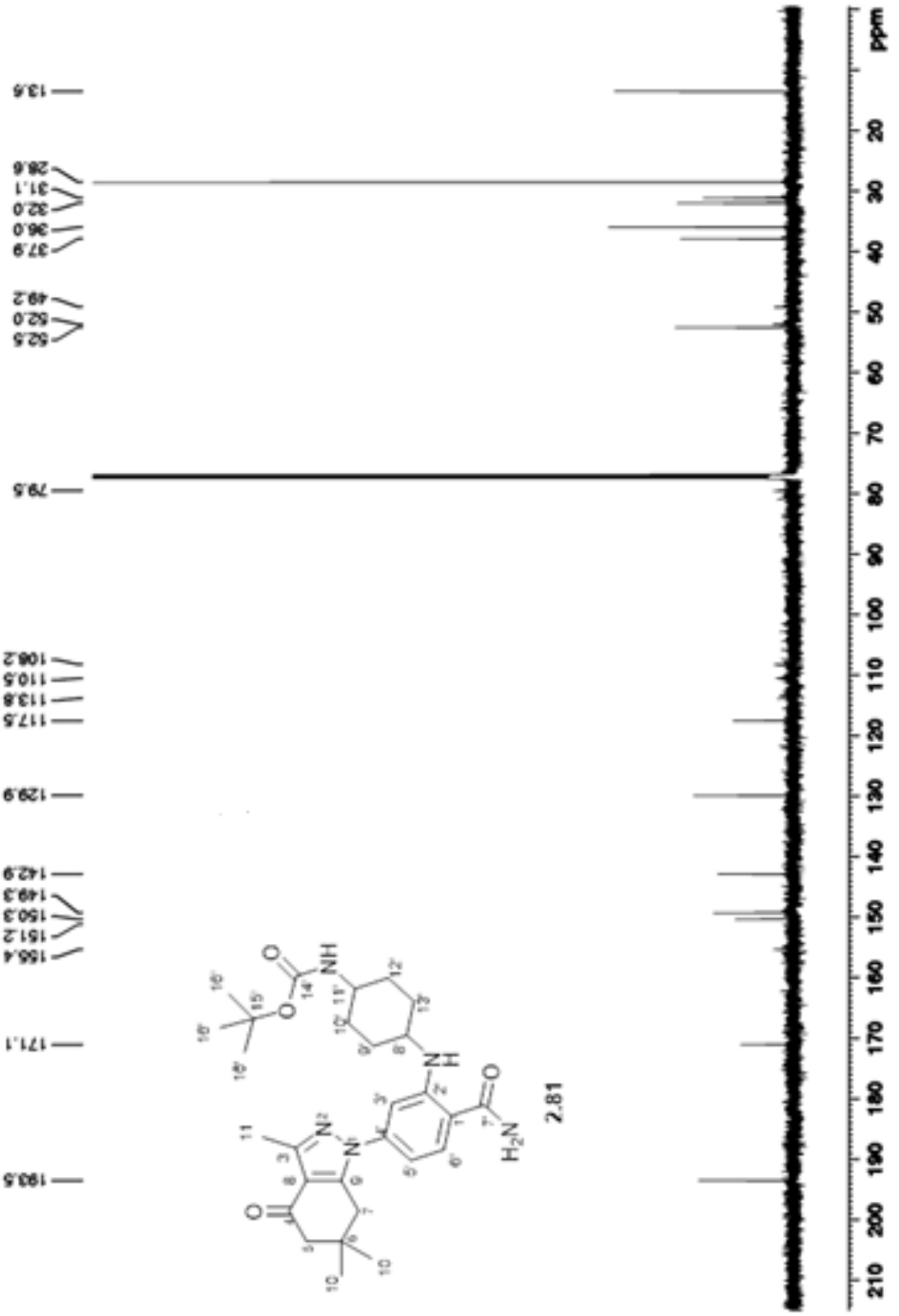
ppm
20
30
40
50
60
70
80
90
100
110
120
130
140
150
160
170
180
190
200
210
13.5
28.6
31.1
32.0
36.0
37.9
49.2
52.0
52.5
79.5
106.2
110.5
113.8
117.5
129.9
142.9
149.3
150.3
151.2
156.4
171.1
193.5
2.81